Fatty acid oxidizing enzymes in *Lobosphaera incisa*

Dissertation

For the award of the degree

"Doctor rerum naturalium"

of the Georg-August Universität Göttingen

Submitted by

Benjamin Djian

Born in

Marseille

Göttingen, 2017

Table of Contents

1. INTRODUCTION

INTRODUCTION

1.1. Some plants and algae accumulate neutral lipids under stress conditions

The primary endosymbiosis is believed to have happened between an archaebacterium and a cyanobacterium over 1.5 Billion years ago (Yoon *et al.*, 2004). It is widely accepted that this gave rise to eukaryotic algae, the first organisms to possess a cytosolic chloroplast. Shortly afterwards, a split separated red algae from green algae. The latter are estimated to be the precursor of all higher plants (Archibald, 2015). As photoautotrophic organisms, they are able to fix atmospheric CO_2, and obtain their energy from the light via photosynthesis. During day light, photons are an unlimited source of energy and H_2O as well as CO_2 are available in quasi unlimited amounts as well. With these resources as well as nitrogen, phosphate and other inorganic compounds, green algae are able to build all the biomolecules needed throughout the cell cycle. Moreover algae, like other organisms, developed ways throughout evolution to store energy and carbon in different forms such as starch and neutral lipids. The most studied phenotype is their capacity to accumulate lipids in the form of Triacylglycerol (TAG) under stress. In this regard, it was repeatedly reported that the accumulation of this neutral lipid reaches a climax during a shortage of nitrogen or phosphate (Khozin‐Goldberg *et al.*, 2002; Li *et al.*, 2014; Merchant *et al.*, 2012), two important nutrients that are not needed in the biosynthesis of neutral lipids.

From an industrial point of view, TAG is of interest as it can be used pure as 1st generation biodiesel or as 2nd generation biodiesel after transesterification. Furthermore, because photosynthetic organisms are building neutral lipids from the consumption of atmospheric CO_2, such an industrial production would be carbon neutral (Hu *et al.*, 2008). This ability of algae and plants has made them a primordial model in biotechnology (Du & Benning, 2016).

1.1.1. *Lobosphaera incisa*, a model green microalga for the accumulation of polyunsaturated fatty acids

The human population is known to face an unprecedented growth, expected to reach over 9 billion by 2050 (Godfray *et al.*, 2010; Lee, 2011; Roberts, 2011). Due to this, cultivable lands are reaching a saturation, and alternative alimentation will only be sustainable if it does not require more land (Erb *et al.*, 2016). Since microalgae can be cultivated even in a desert landscape, a high production would not be competing with plants and livestock for cultivable land. Moreover, as the primary source of very long chain poly-unsaturated fatty acids (VLC-

PUFAs), microalgae are expected to play an important role in the nutrition of an increasing human population. Indeed, VLC-PUFAs such as 20:4 (n-6) have been described to be necessary for human health, particularly during brain development (Janssen & Kiliaan, 2014).

The green alga *Lobosphaera incisa* (*L. incisa*, strain SAG 2468, formerly referred to as *Parietochloris incisa* or *Myrmecia incisa*), obtained from Ben-Gurion *University of the Negev, Israel* (and originally isolated from Mt. Tateyama, Japan), was reported to accumulate up to 77% of all acyl chains in TAG during the stationary growth phase. Moreover, TAG from *L. incisa* was reported to be composed of 47% 20:4 (n-6) (Bigogno *et al.*, 2002b). As it is an oleaginous green alga, the accumulation of starch under stress is limited, and lipid content was reported to reach 35% of dry weight after nitrogen starvation, which consists of 21 % 20:4 (n-6) acyl chains alone. This strain of microalgae is becoming an important model for its capacity to accumulate VLC-PUFAs under stress. Its plastidic (Tourasse *et al.*, 2015a), mitochondrial (Tourasse *et al.*, 2015b) as well as nuclear genome (Tourasse *et al.,* unpublished data) have been sequenced and protein-coding genes were predicted and annotated. Moreover, transcriptome of cultures grown with nitrogen supply, as well as after 12 h and 72 h of nitrogen starvation was analyzed (Tourasse *et al.,* NCBI GEO, GSE94666).

1.1.2. General model of plastidic pathways of lipid metabolism during nitrogen starvation

Pathways that oleaginous green microalgae are using to accumulate TAG under nitrogen depletion have been studied for years (Li *et al.*, 2014; Liu & Benning, 2013; Zienkiewicz *et al.*, 2016). Figure 1 represents the general model of plastidic pathways believed to be upregulated during nitrogen starvation. Mostly described in *Chlamydomonas reinhardtii* (*C. reinhardtii*), these pathways have also been shown to lead to the accumulation of TAG (Fan *et al.*, 2011). During photosynthesis, green microalgae are consuming atmospheric CO_2 and water to create glyceraldehyde-3-phosphate (G3P), a key precursor for all biomolecules in photoautotroph organisms. During shortage of nitrogen however, the carbon and energy can no longer be used for the *de-novo* synthesis of amino acids nor nucleotides, as nitrogen is needed for the formation of these biomolecules. Most of the available carbon and the energy delivered from the photosynthesis are directed into storage pathways that are not dependent on nitrogen. Green microalgae are categorized into two types depending on whether they store this energy mostly in form of neutral lipids (oleaginous) or starch (non-oleaginous).

In addition to the storage of energy, it was recently reported that the accumulation of lipids into storage was vital for photosynthetic organisms during a period of nitrogen shortage (Li *et al.*, 2012). During such a stress, the reduced cofactor nicotinamide adenine dinucleotide phosphate (NADPH) accumulates in the chloroplast stroma, since it can no longer be used in the synthesis of protein or DNA. It seems that this leads to an accumulation of electrons in the electron
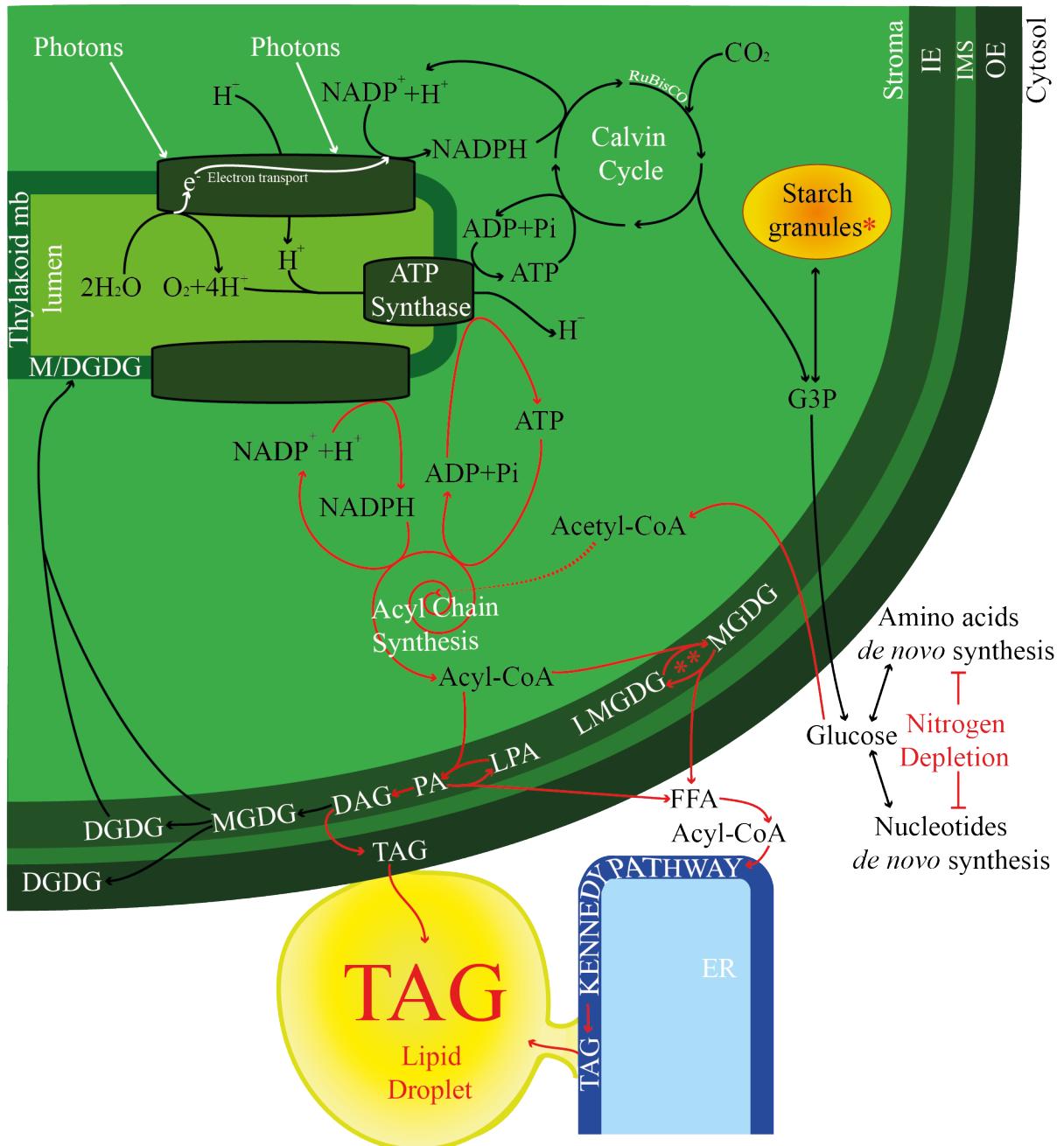
Figure 1 Simplified model of plastidic pathways of lipid metabolism in green microalgae under nitrogen depletion. The pathways depicted in red represent those favored under nitrogen depletion. ADP: adenosine diphosphate, ATP: adenosine triphosphate, NADP: nicotinamide adenine dinucleotide phosphate, CoA: coenzyme A, TAG: triacylglycerol, DAG: diacylglycerol, ER: endoplasmic reticulum, DGDG: digalactosyldiacylglycerol, MGDG: monogalactosyldiacylglycerol, LMGDG: lyso-monogalactosyldiacylglycerol, Pi-TPT: P$_i$-triose phosphate transporter, PA: phosphatidic acid, LPA: lyso-phosphatidic acid, G3P: glycerol-3-phosphate, IE: inner envelope, OE: outer envelope, IMS: inter membrane space. *The accumulation of starch is minimized in oleaginous algae such as *L. incisa*. **PGD1 protein, characterized in *C. reinhardtii* (Li *et al.*, 2012). (Du & Benning, 2016; Miesfeld, 2017; Zienkiewicz *et al.*, 2016)

transport chain, since the acceptors (NADP$^+$) are no longer available. In the thylakoid lumen, the high concentration of O_2 might become an electron acceptor and become reactive oxygen species (ROS) which are toxic for the cells. To prevent this, green microalgae are supporting the *de novo* fatty acid synthesis as an "electron sink" under nitrogen starvation.

1.1.3. Nitrogen starvation induces chloroplast degradation and quiescence

In addition to the *de novo* synthesized acyl chains, the formation of TAG was reported to depend on the conversion of acyl chains from membrane lipids, mostly the endoplasmic reticulum (ER) (Dahlqvist *et al.*, 2000) and plastidic membrane (Yoon *et al.*, 2012). In *L. incisa* for instance, extended nitrogen starvation provoked strong reduction of the chloroplast size, as well as a decrease in chlorophyll content (Merzlyak *et al.*, 2007). Similar phenomena were reported in *C. reinhardtii*, *Nannochloropsis*, as well as in higher plants during the same stress (Iwai *et al.*, 2014; Simionato *et al.*, 2013; Yang *et al.*, 2011). Because this leads to a shutdown of photosynthesis, the accumulation of TAG will eventually stop and microalgae enter quiescence. Hence at least two factors seem to explain the degradation of the chloroplast.

(i)   Since galactolipids are the most abundant lipids in plants and algae (Kalisch *et al.*, 2016), mostly localized in the chloroplast, the degradation of this organelle will provide a large pool of acyl chains to recycle in the form of TAG. A phospholipid:diacylglycerol acyltransferase (PDAT) able to accept galactolipids identified in *C. reinhardtii* was suggested to play a role in this conversion. (Yoon *et al.*, 2012).

(ii)   An MGDG lipase, the plastid galactolipid degradation 1 (PGD1, Figure 1 **), was also discovered in *C. reinhardtii* although it seems implicated in a second pathway: The PGD1 protein seems to be involved in a turnover of monogalactosyldiacylglycerol (MGDG), targeting its acyl chains *de novo* synthesized to the formation of TAG. This turnover was described to act as an "electron sink" during nitrogen starvation, since the knock out mutation *pgd1* lead to the formation of ROS, chlorosis and eventually cell death (Li *et al.*, 2012), after 7 days of nitrogen starvation. Therefore it seems that the cell survival is likely to depend on the dismantlement of the photosynthetic machinery under nitrogen starvation, as it becomes toxic under this stress.

INTRODUCTION

Finally, the degradation of the thylakoid membrane and the dismantlement of the photosynthesis machinery seems to be tightly related with the TAG accumulation, yet mechanisms involved are not fully understood. On the other hand, lipids are known to also fulfill important roles besides storage of energy, and the accumulation of TAG will never be fully understood without a clear comprehension of all aspects of lipid function.

1.2. Lipids, lead actors of cell compartmenting

Together with nucleic acids, proteins and carbohydrates, lipids are the most important biomolecules, present in all kingdoms of life. Glycerolipids are the most abundant of them, composed of a polar part (headgroup) and a non-polar part composed of 1 to 3 acyl chains. From this amphiphilic property, most glycerolipids in solution will spontaneously organize themselves into bilayers in solution, with their non-polar parts buried together, and the polar headgroup in contact with water. This behavior of lipids allows the cells to separate the environment from their inner constituents, which is a prerequisite for all living organisms. In eukaryotic cells, this compartmenting ability is also used to constitute organelles within the cell, creating an additional level of organization. The chloroplast is for instance, in higher plants and most green algae, composed of 3 different membranes: the outer envelope, inner envelope and the thylakoid membrane (Kalisch *et al.*, 2016). In these membranes, the lipid fraction is almost exclusively made of galactolipids, mostly MGDG and digalactosyldiacylglycerol (DGDG) (Kobayashi & Wada, 2016).

Within galactolipids, MGDGs are the most abundant lipids in the thylakoid membrane (above 50% of all lipids in the plastids of higher plants), yet they remain in minority compared to the high proportion of proteins (80% of the dry mass) that is suspected to be the main responsible factor for the shape of this membrane (Garab, 2014). Nevertheless, MGDGs and their unique biochemical properties were described to have a critical importance in the thylakoid membrane. This lipid class was reported to be crystalized with the PHOTOSYSTEM II (PSII) complex (Guskov *et al.*, 2009) in which it was reported to play a major role in the dimerization of this complex (Kansy *et al.*, 2014). The crystal structure of the PSI complex as well harbors an MDGD molecule (Jordan *et al.*, 2001). MGDGs were also reported to increase the efficiency of the cytochrome b6f electron transport (Yan *et al.*, 2000). They have the distinctive feature to form non-bilayer structures within membranes, and this behavior was also described to be of major importance in the xanthophyll cycles (Garab *et al.*, 2016; Schaller *et al.*, 2010). Finally, *Arabidopsis thaliana* (*A. thaliana*) galactolipid deficient mutant *mgd1-2* was reported to have dwarf and albino phenotypes, and is unable to grow in a photoautotrophic manner (Kobayashi *et al.*, 2007). The complementation with a bacterial MGDG synthase rescued the galactolipids levels, although it resulted in a slightly lower MGDG/DGDG ratio than the wild type (WT), and had abnormal thylakoid membranes (Masuda *et al.*, 2011). Altogether, former studies demonstrate the major importance of MGDG and its correct ratio with DGDG in the thylakoid membrane for the operation of photosynthesis.

1.3. Lipoxygenase, a lipid oxidizing enzyme

1.3.1. The lipoxygenase reaction

Lipoxygenases (LOXs) are non-heme iron-containing enzymes (De Groot *et al.*, 1975) catalyzing the oxidation of polyunsaturated acyl chains with at least one pentadiene system. Contrary to non-enzymatic oxidations, the oxidation of polyunsaturated acyl chains catalyzed by LOXs is regio- and stereospecific (Hamberg & Samuelsson, 1967). The LOX reaction was described to proceed in 4 steps (Figure 2) (Ivanov *et al.*, 2010).

1- A polyunsaturated acyl chain substrate enters the active site of a LOX and naturally a *bis*-allylic carbon will localize itself next to the iron(III) of the LOX. In this configuration, the non-heme iron will abstract one of the two hydrogen atom on the *bis*-allylic carbon, and get reduced from iron(III) to iron(II). Because both the proton and the electron are abstracted in a proton coupled electron transfer reaction, a free radical will be formed on the acyl chain. At room temperature and at low substrate concentration, this abstraction of hydrogen is known to be the limiting step of the LOX reaction (Glickman & Klinman, 1995).
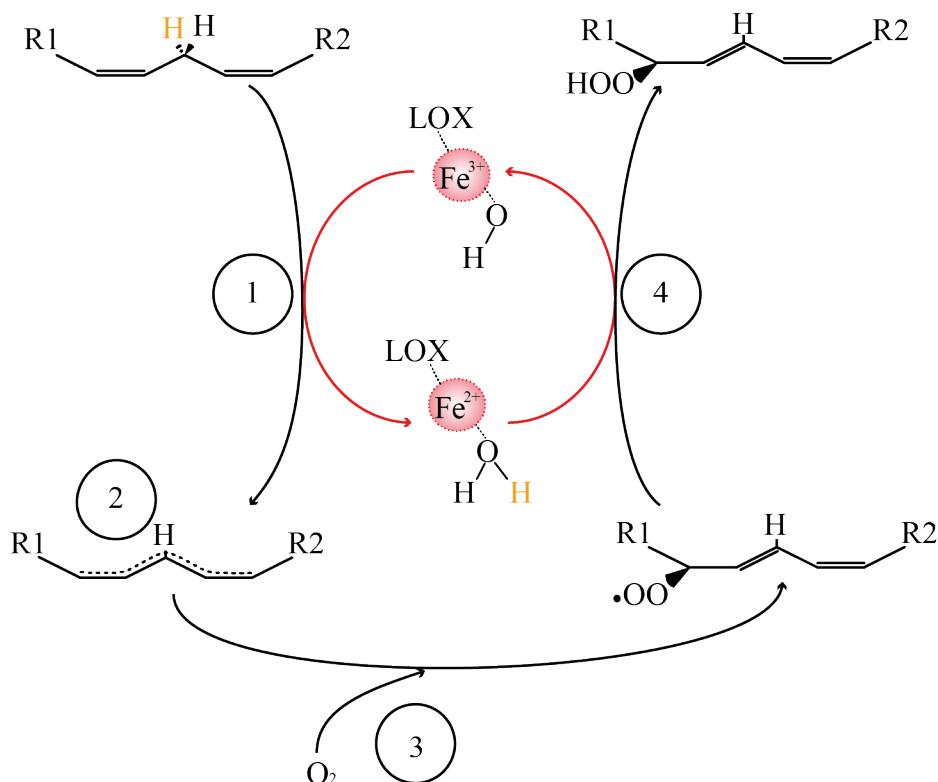
Figure 2 - The LOX reaction. Detailed representation of the four steps of the of the LOX reaction (black arrows). **1.** Hydrogen abstraction. **2.** Radical rearrangement. **3.** Oxygen insertion. **4.** Radical reduction. Included are the two states of the non-heme iron of the LOX (red arrows). The Fe^{3+} is reduced during the hydrogen abstraction into Fe^{2+}. At the end of the reaction (step 4), the iron returns to its Fe^{3+} state. (Ivanov *et al.*, 2010)

2- Because of the two double bonds on either side of the *bis*-allylic carbon atom, the free radical will delocalize over the five carbons structure (Figure 2. 2).

3- A molecule of dioxygen is activated by the free radical and forms a peroxyl radical on the acyl chain. If the oxygen is added on the [+2] or [-2] carbon atom relative to the *bis*-allylic carbon atom, the two double bonds will end up conjugated. This insertion of oxygen is believed to be a critical step in the regio- and stereospecificity of the LOX mechanism. It must be noted that LOXs seem to insert dioxygen in an antarafacial way relative to the hydrogen abstracted. This was demonstrated by the use of substrate having either Pro-*S* or Pro-*R* isotope of hydrogen on the *bis*-allylic carbon atom (Egmond *et al.*, 1972; Hamberg & Samuelsson, 1967; Rickert & Klinman, 1999).

4- The peroxyl radical is reduced, and the iron is oxidized back to its iron(III) state. Although it is believed that the hydrogen being abstracted in the first place is the same which is reducing the peroxyl group, this was never proven. Some scientists even argued that, since the oxygenation happens in an antarafacial way relative to the hydrogen being abstracted, this theory would imply a rather inconvenient rotation of the substrate inside the tight environment of the active site (Newie, 2016).

Finally, the natural LOX products from free fatty acids (FFAs) are hydroperoxides, yet since hydroperoxyl groups are rather unstable they are often reduced into hydroxyl groups (Figure 3). In laboratory experiments, a complete chemical reduction is often performed in order to
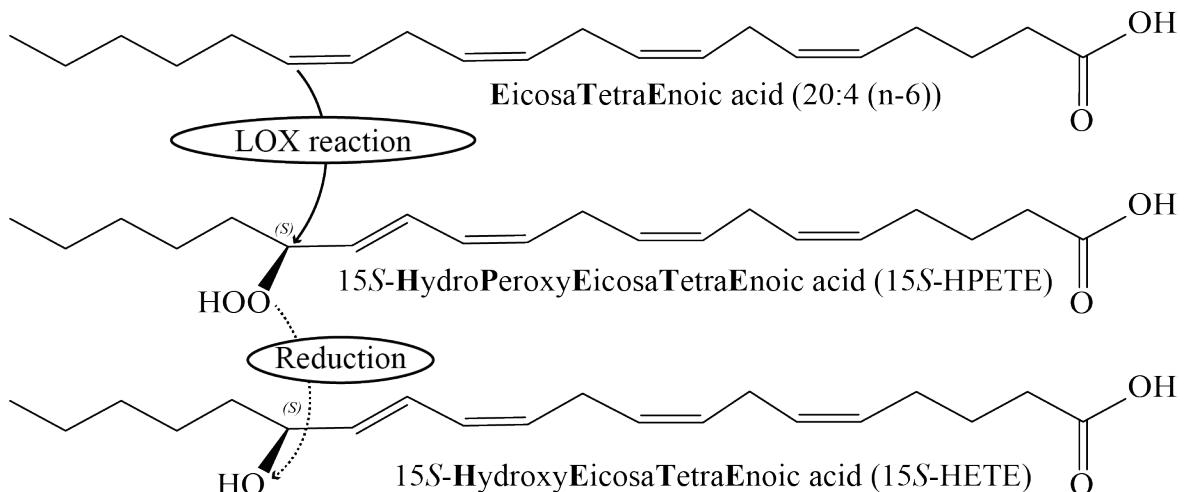
Figure 3. Example of the LOX reaction with 20:4 (n-6). As a first step, the LOX catalyzes the regio- and stereospecific oxygenation of 20:4 (n-6) into 15*S*-Hydroperoxyeicosatetraenoicacid (15*S*-HPETE). In a second step, the hydroperoxyl group will naturally be reduced into a hydroxyl group.

avoid having a hydroxide/hydroperoxide mixture, which facilitates the interpretation of the results.

1.3.2. The LOX specificity

Contrary to non-enzymatic reaction, LOXs oxidize polyunsaturated acyl chains with a high regio- and stereospecificity. Yet when one hydrogen is abstracted from the acyl chain by the non-heme iron, the dioxygen molecule could in theory be inserted at four different positions: [+2]Pro*R*, [+2]Pro*S*, [-2]Pro*R* and [-2]Pro*S* (Liavonchanka & Feussner, 2006). Decades of studies on LOX protein alignment, 3D structures, targeted mutations, and LOXs oxidation product analysis allowed to identify mechanisms that LOXs might use in order to achieve specific oxidation. Schneider *et al.* proposed four models to summarize them (Schneider *et al.*, 2007). (i) Oxygen shielding. This theory implies that when a substrate is positioned in the active site of a LOX, the tight environment around the iron shields three positions from putative oxidation. The oxidation happens specifically, since only one position remains available to the dioxygen. This hypothesis is supported by Coffa *et al.* who characterized a single alanine residue able to block the insertion of molecular oxygen to the carbon [-2] (Coffa & Brash, 2004). After mutating this residue into a smaller glycine, the LOX lost its specificity, as both positions became available to oxygenation. (ii) Oxygen channel. Since the active site of the LOX is buried inside the enzyme, an access to oxygen must exist in order to allow oxidation at a stable rate. This theory would also explain why the oxygen insertion in LOXs is antarafacial, relatively to the hydrogen being abstracted. On the other hand, years after the structural data of numerous LOXs are available, clear characterization of an oxygen channel is still missing and is still subject to debate nowadays (Collazo & Klinman, 2016; Kalms *et al.*, 2017). (iii) Radical localization. This theory is based on the fact that torsions inside the pentadiene can influence the thermodynamic favorability of the carbon atoms [+2] and [-2] to hold a radical. Since this radical is responsible for the activation of the molecular oxygen, torsions inside the pentadiene provoked by the LOX could influence the likelihood of the radical to be at one position, hence influence the final position of the peroxyl group. (iv) Radical trapping. This theory is based on the fact that even after insertion of molecular oxygen on the acyl chain, this peroxyl radical is highly unstable, and might still undergo β-fragmentation, until it is reduced in to a hydroperoxyl group. Therefore in theory the specificity from the LOX could come from a hydrogen donor, terminating the reaction on the appropriate carbon atom.

These four theories are explaining the specific oxidation after that a hydrogen was abstracted from a specific *bis*-allylic carbon atom. Yet in the case of acyl chains having more than one pentadiene, LOXs must also be able to abstract the hydrogen from a specific carbon atom in order to achieve specific oxidation. With such substrates, two additional mechanisms might influence the selection of a pentadiene (Figure 4). (I) Substrate orientation. Most LOX are believed to accept the acyl chains by their methyl end (Tail-first). Yet it is also accepted that a FFA substrate can, in certain conditions, penetrate the LOX substrate channel by their carboxyl end (Head-first) (Hornung *et al.*, 1999). Since the LOX oxidation is happening in an antarafacial way relative to the hydrogen abstracted, a different insertion of the substrate into the LOX substrate channel would *de facto* modify the end product considerably, as the hydrogen being abstracted would be on the opposite face of the substrate (Figure 4A). Along with the size of the substrate channel allowing a bulky carboxyl group to enter the active site, it was proposed in some plant LOXs that a basic residue in the bottom of the substrate channel could favor the substrate orientation (Browner *et al.*, 1998; Hornung *et al.*, 2008). (II) Substrate frameshift. In order to achieve regiospecificity, a LOX must implicate the same pentadiene in all reactions. Hence it was hypothesized that the acyl chain is inserted with a certain depth inside the substrate channel, in order to present the same *bis*-allylic carbon atom to the catalytic metal (Figure 4B). Sloane *et al* described two bulky residues located at the bottom of the substrate channel of some LOXs, preventing the acyl chain to penetrate deeper and be oxidized non-specifically (Sloane *et al.*, 1991).
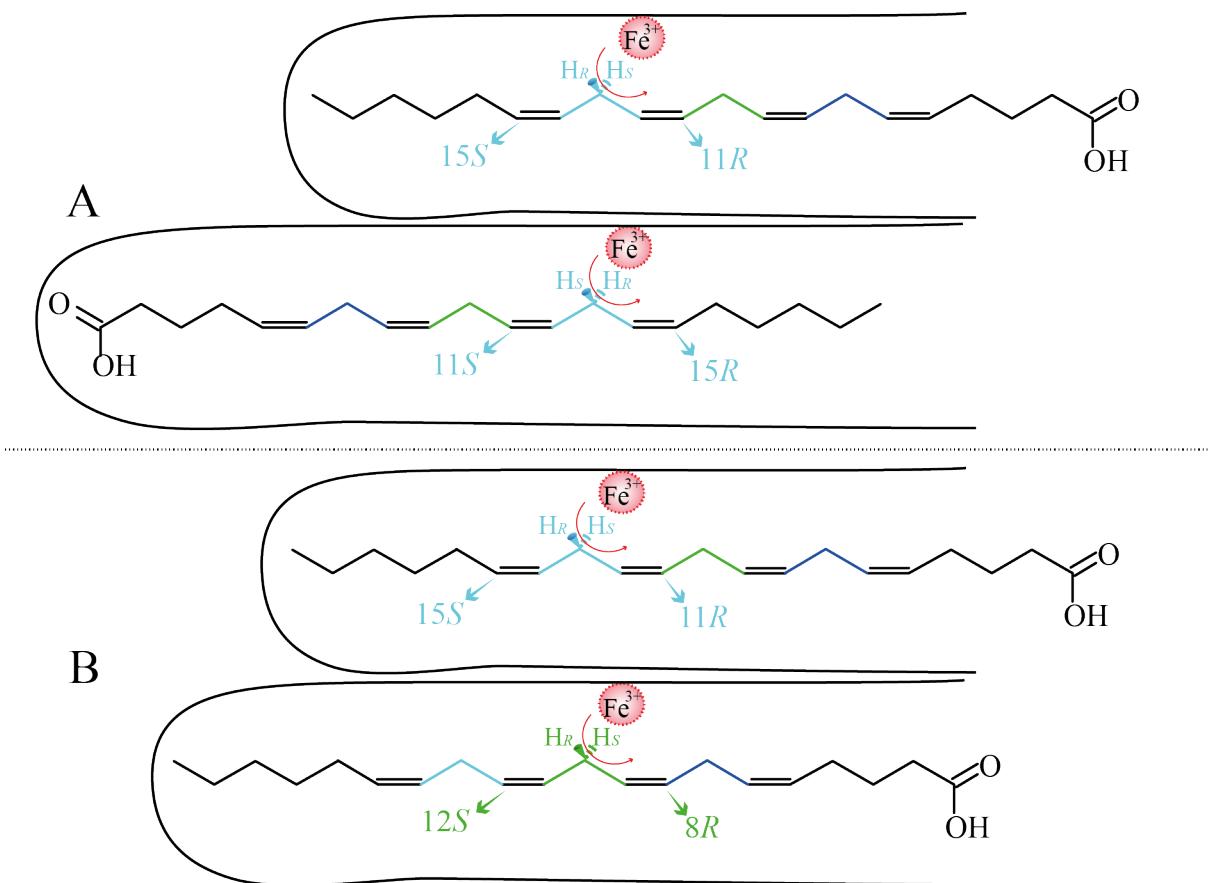
Figure 4. The selected pentadiene system affects the LOX specificity. **A.** Substrate orientation. Whether the FFA is inserted by its carboxyl group first (Head-first) or by its methyl end first (Tail-first) will influence the hydrogen being abstracted (Pro-*S* or Pro-*R*). This also influences the direction from which the oxygen in inserted on the acyl chain. **B.** Substrate frameshift. The depth to which the substrate is inserted into the active site will influence which pentadiene is attacked, hence the regio-specificity of the oxygenation.

Therefore with substrates having more than one pentadiene system, the LOX regio- and stereospecific oxidation cannot be explained with a single model, but rather with a combination of models.

1.3.3. Role of LOXs as signal molecules

Besides their major role in membrane formation or as energy storage, lipids are also described to have biological functions as signal molecules. After oxidation of polyunsaturated acyl chains, a wide variety of oxidation products is possible, called oxylipins. The FFA 20:4 (n-6) for instance can in theory be oxidized on 8 different carbons, each with 2 chiral configurations (Figure 5). Contrary to non-enzymatic oxidation, dioxygenases have a major importance in the specific biosynthesis of oxylipins (Andreou *et al.*, 2009). Among them, LOXs are the most ubiquitously distributed, and have been characterized to perform regio- and stereospecific oxygenation of PUFAs in a variety of organisms. LOXs have been classified according to three factors: the PUFA they will most likely oxidize in their natural environment, their regiospecificity as well as their stereospecificity. Hence in mammals, LOXs are classified according to the oxidation products they form from 20:4 (n-6), and will be classified as arachidonate 15*S*-LOX, 12*R*-LOX or 5*S*-LOX to cite a few. The different oxidation products will enter different oxylipins pathways, and will have different biological functions. In humans for instance, 5-Hydroperoxyeicasotetraenoic acid (5-HPETE) will be converted into leukotriene and induce a pro-inflammatory response (Shimizu *et al.*, 1984). The oxidation
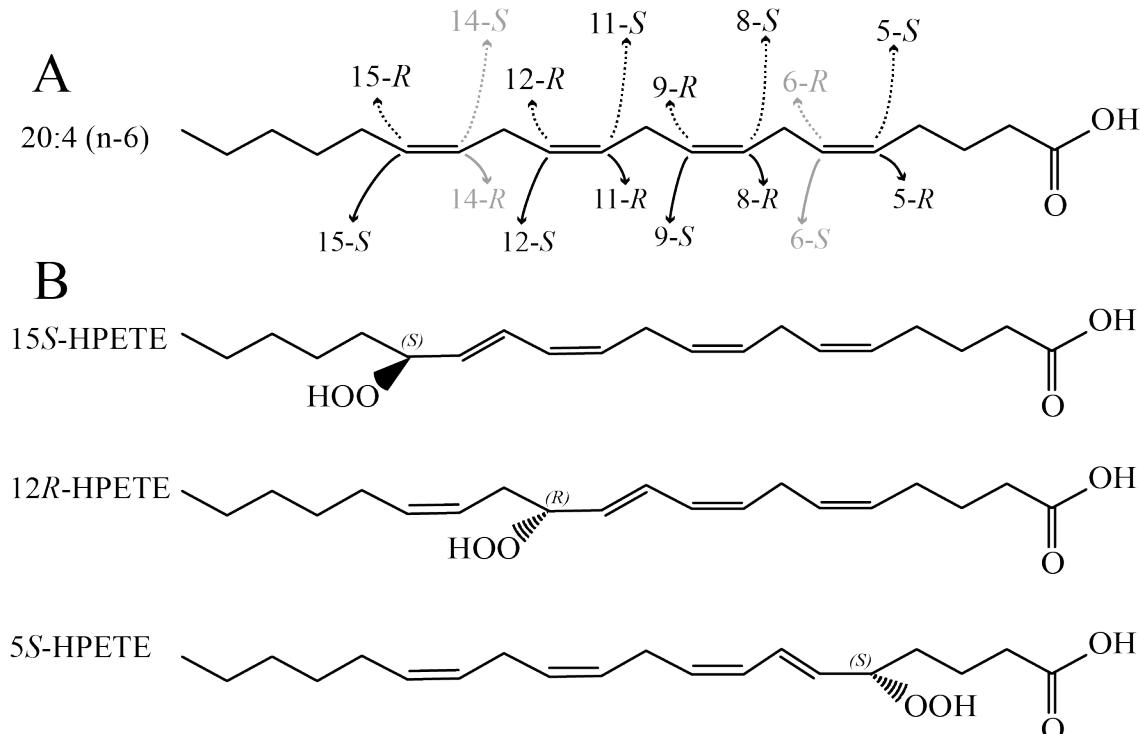
Figure 5. Oxidation products from 20:4 (n-6). **A.** The carbon atoms on 20:4 (n-6) most likely to undergo oxidation, each with *R* or *S* chiral configuration. All oxidation products possible in theory from a LOX are represented in black. The four oxidation products only possible by chemical oxidation are represented in gray. B. Examples of characterized LOX products from the FFA 20:4 (n-6).

product 12-HPETE however, was first known to be involved in the formation of platelets (Hamberg & Samuelsson, 1974). Yet a presence of 15-HPETE or 12-HPETE together with 5-HPETE leads to the formation of lipoxins, an anti-inflammatory mediator (Brash, 1999). In mammals, LOXs are known to be involved in a wide variety of signals for the regulation of blood pressure, the central nervous system, but also diabetes and the proliferation of cancer (Kühn *et al.*, 2015). The human pathogen *Pseudomonas aeruginosa* is also using LOX pathways and expresses PaLOX (15-LOX) during colonization, although the mechanism by which this LOX increases the virulence of the pathogen is still unclear (Deschamps *et al.*, 2016).

Plant LOXs were historically divided into two subgroups, those harboring a plastidic peptide signal, and those which did not. Nowadays these enzymes are usually characterized according to their regio- and stereospecificity towards 18:3 (n-3), as fatty acids with 18 carbon chains (C18) are abundant in plant cells. Notably, all chloroplastidial plant LOXs have been reported to be 13*S*-LOX, hence oxidizing 18:3 (n-3) on the 13th carbon atom. The LOX pathway in plants has been intensely studied (Andreou & Feussner, 2009; Feussner & Wasternack, 2002; Liavonchanka & Feussner, 2006). It is known to be involved in the biosynthesis of green leaf
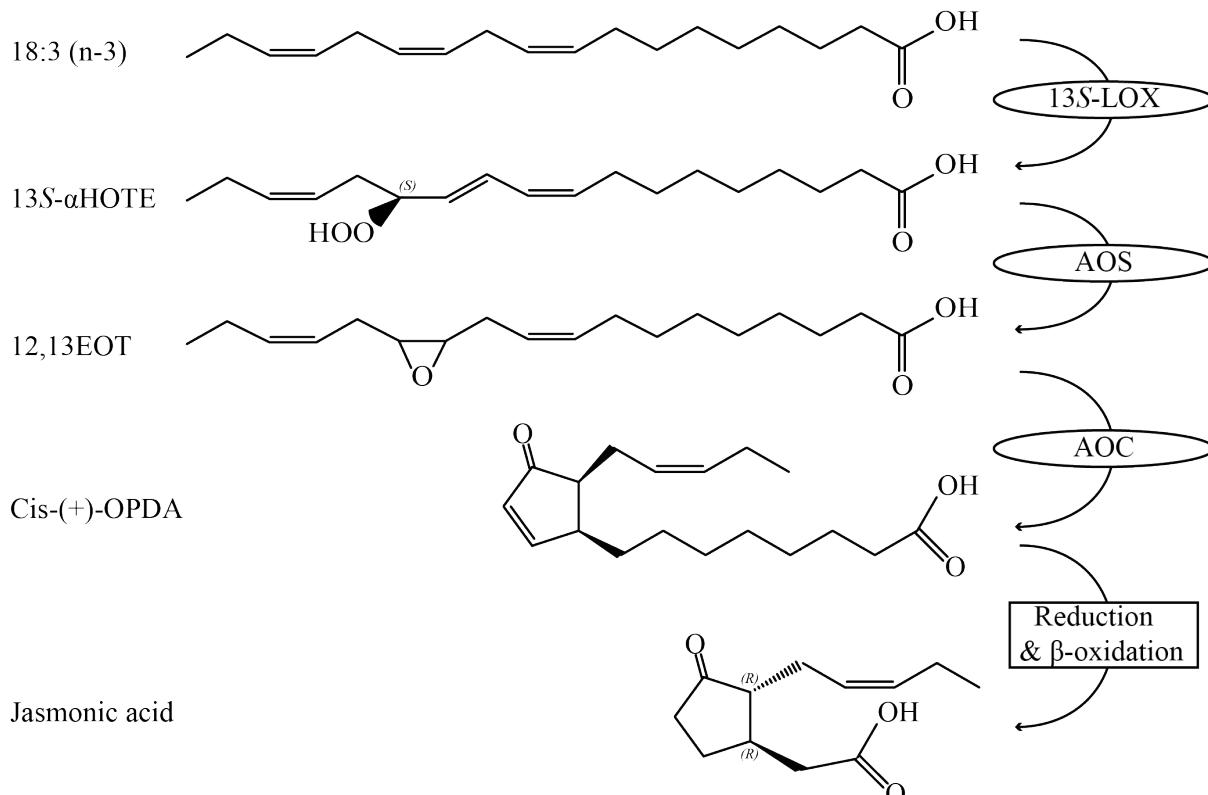
Figure 6. Jasmonic acid (JA) pathway. In the stroma of the chloroplast, the 13*S*-LOX performs an oxidation on 18:3 (n-3), producing 13*S*-Hydroperoxyoctadecatrienoic (13*S*-αHPOTE). From this, the allene oxide synthase (AOS) and allene oxide cyclase produce 12-Oxo-phytodienoic acid (OPDA). OPDA will enter the peroxisome, in which it will undergo three cycles of β-oxidation, giving rise to JA.

volatile (GLV)(Mochizuki *et al.*, 2016; Mwenda & Matsui, 2014; Shiojiri *et al.*, 2006) and divinyl ethers (Chechetkin *et al.*, 2008; Stumpe *et al.*, 2008), implicated in the plant resistance to herbivores and pathogens. Yet among all the signaling molecules originating from plant LOX reactions, the most documented is the production of the phytohormone Jasmonic acid (JA) (Figure 6). The first step is performed by a plastidic 13*S*-LOX on 18:3 (n-3), leading to 13*S*-Hydroperoxyoctadecatrienoic acid (13*S*-HPOTE) (Heitz *et al.*, 1997). This substrate is then metabolized further by an allene oxide synthase (AOS) and allene oxide cyclase (AOC), giving rise to 12-Oxo-phytodienoic acid (OPDA). OPDA is then directed to the peroxisome, and undergoes three cycles of β-oxidation, resulting in the formation of JA. In *A. thaliana*, the production of JA is involved in a wide variety of signals during development, senescence or in response to stress and was subject to numerous publications and reviews (Creelman & Mullet, 1997; Heitz *et al.*, 2016; Turner *et al.*, 2002; Wasternack & Hause, 2013). Notably in the flowers, JA was described to trigger development of the pollen, as its absence was described to result in the male sterility (Ishiguro *et al.*, 2001). Upon wounding, leaves will overexpress 13-LOXs and produce JA, resulting in an improved defense (Farmer & Ryan, 1992) against insects (McConn *et al.*, 1997) and pathogens (Staswick *et al.*, 1998).

Although the LOX pathway has been intensively studied, surprisingly little is known about plastidic LOXs, besides their regio- and stereospecificity. In *A. thaliana*, OPDA and dinor-OPDA were reported to exist in a form esterified to a galactosyl headgroup, and were named arabidopsides (Ibrahim *et al.*, 2011), opening the question whether plastidic LOX are able to perform oxidation directly on esterified acyl chains. Moreover, in *A. thaliana*, four different LOXs are known to be localized in chloroplasts: AtLOX2, AtLOX3, AtLOX4 and AtLOX6. All four of these LOXs are known to oxidize 18:3 (n-3) with the same regio- and stereospecificity. All four enzymes have been described to induce the biosynthesis of JA in different contexts, such as AtLOX3 and AtLOX4 in pollen development (Caldelari *et al.*, 2011), AtLOX2 for defense response upon wounding (Bell *et al.*, 1995) and AtLOX6 in long distance signaling (Chauvin *et al.*, 2013). Yet since they yield the same oxidation products, the reason for their different roles is not fully understood, and is still debated nowadays (Chauvin *et al.*, 2016). Finally, although numerous plastidic LOXs were reported in the scientific literature, none has ever been crystalized. It is a tacit knowledge that this class of enzyme is hard to express heterologously, a limiting factor for crystallization screens as this method is demanding high amounts of pure protein. For these reasons, a model for this class of enzymes would give

precious information in order to understand the role of different plastidic LOXs, their biochemical properties, and their individual roles in the plant LOX pathway.

1.3.4. Role of LOXs in the degradation of membranes

Some LOXs have also been shown to play an important role in the targeted membrane degradation. In rabbit reticulocytes, a 15-LOX was shown to initiate the degradation of intact mitochondria, while preserving other organelles and the plasma membrane. This process was described to be involved in the differentiation process from reticulocytes to keratinocytes (Schewe *et al.*, 1986; van Leyen *et al.*, 1998). In the mouse eye lens, another 15-LOX was reported to be responsible for the degradation of the organelles, a process necessary to make the inner eye lens transparent. In this case the degradation was not targeted to a specific membrane, but believed to be involved in an apoptotic pathway (van Leyen *et al.*, 1998). In cucumber, barley, flax and sunflower cotyledons, the degradation of the lipid body was found to be LOX dependent. Indeed, it was reported that a 13-LOX oxidize the TAG from lipid bodies, before the acyl chains are directed to an alternative β-oxidation. Plants were suggested to use this pathway during germination, before the photoautotrophic metabolism becomes a sufficient source of carbon skeletons and energy. (Feussner *et al.*, 1997; Feussner *et al.*, 2001; Gerhardt *et al.*, 2005; Meyer *et al.*, 2013; Rudolph *et al.*, 2011). In barley leaves, a 13*S*-LOX was also found upregulated during senescence, which was reported to have a role in the degradation of the plastidic membrane (Springer *et al.*, 2016).

1.4. Aims of this study

An open reading frame (ORF) sharing high identity with known plastidic LOXs has been identified in the oleaginous green alga *L. incisa* (Tourasse et al., NCBI GEO, GSE94666). The putative enzyme was named LiLOX, and would represent the first known LOX to be characterize from a green alga.

The first part of this study was to identify similarities of LiLOX with other published LOXs, as well as pointing out the uniqueness of this enzyme. In this regard, the protein sequence of LiLOX was investigated *in silico* by protein alignment and structural modeling. Throughout the study, a special focus was given on the resemblances between LiLOX and plastidic LOXs from higher plants, including the localization of LiLOX at a subcellular level.

In a second part, heterologous expression of LiLOX was performed in order to characterize it *in vitro*. As the first LOX to be characterized from a green microalga, targeted mutations were performed on this enzyme, as it might become a model for this class of LOX. Attempts to crystalize LiLOX were performed as well in the course of this work.

An important part of this work focused on the identification of the endogenous substrate of LiLOX, and the characterization of product(s) formed from this substrate(s). Finally, as LiLOX was found to be upregulated upon nitrogen starvation, this study aimed at shedding light on its role in *L. incisa* during such a stress.

2. MATERIAL

2.1. Equipment

If not otherwise acknowledged, all chemicals were obtained from Carl Roth (Karlsruhe, Germany), and Sigma-Aldrich (Munich, Germany). Solvents were purchased in HPLC and LC-MS quality from Thermo Fisher Scientific (Waltham, USA).

The following equipment was used during the course of this study.

Table 1. Equipment used in the course of this study

Machine or system	Manufacturer
1100 Series HPLC System	Agilent Technologies, Santa Clara, CA, USA
Ab Sciex 6500 QTRAP® tandem mass spectrometer	AB Sciex, Framingham, MA, USA
ÄKTAprime plus	GE Healthcare, Chalfont St Giles, UK
CARY 100 Bio UV-vis Spectrophotometer	Varian Inc., Paolo Alto, CA, USA
Centrifuge 5417 R	Eppendorf, Hamburg, Germany
Centrifuge 5810 R	Eppendorf, Hamburg, Germany
Diana documentation system	Raytest, Straubenhardt, Germany
Fluidizer	Microfluidics, Newton, MA, USA
IDA gel documentation system	Raytest, Straubenhardt, Germany
Laser Scanning Microscope 510	Carl Zeiss Microscopy GmbH, Jena, Germany
MAR345 image plate detector	Mar Research GmbH, Norderstedt, Germany
Mastercycler gradient	Eppendorf, Hamburg, Germany
Mastercycler personal	Eppendorf, Hamburg, Germany
MicroMax 007	Rigaku, Tokio, Japan
Mini-PROTEAN3 Electrophoresis System	Bio-Rad, Hercules, CA, USA
Nanodrop 2000c	Thermo Fisher Scientific, Waltham, MA, USA
Oxygraph Plus System	Hansatech Instruments, Norfolk, UK
PDS1000/He Biolistic Particle Delivery System	BioRad Laboratories GmbH, München, Germany
Sonifier Cell Disruptor B15	Branson, Danbury, CT, USA
Sterile bench Prettl Telstar Bio II A	Telstar, Woerden, Netherlands
UHPLC 1290 Infinity	Agilent Technologies, Santa Clara, CA, USA
UV-table 312 nm	Raytest, Straubenhardt, Germany

Table 2. Columns used in the course of this study.

Columns	Chromatography	Manufacturer
HiLoad 26/60 Superdex S200	SEC	GE Healthcare, USA
Superdex 200 10/300 GL	SEC	GE Healthcare, USA
HisTrap HP	IMAC	GE Healthcare, USA
EC250/2 Nucleosil C18	RP-HPLC	Macherey-Nagel, Germany
Zorbax RX-SIL	SP-HPLC	Agilent, USA
CHIRALCEL OD-H	CP-HPLC	Technologies Inc, USA
ACQUITY UPLC HSS T3	UPLC	Waters Corporation, USA
ACQUITY UPLC BEH C18	UPLC	Waters Corporation, USA

2.2. Software

Table 3. Software used in the course of this study

Software	Developer(s), Headquarters
OriginPro8.5	*OriginLab Corporation, Northampton, USA.*
Geneious R8	*Biomatters Ltd., Auckland, New Zealand*
TargetP 1.1	*(Emanuelsson et al., 2000)*
PredAlgo	*(Tardif et al., 2012)*
ChloroP	*(Emanuelsson et al., 1999)*
ChemStation	*Agilent Technologies, Santa Clara, USA*
pyMOL	*Schrödinger, LLC, New York, USA*
MassLynx	*Waters Corporation, Milford, U.S.A.*
MarVis	*(Kaever et al., 2009)*
ChemDraw	*CambridgeSofr, Waltham, USA*
Excel	*Microsoft, Redmond, USA*
Illustrator	*Adobe, San José, USA*
Mass Hunter B05.01	*Agilent Technologies, Santa Clara, USA*
Photoshop	*Adobe, San José, USA*
Cary WinUV	*Agilent Technologies, Santa Clara, USA*
Oxygraph Plus	*Hansatech Instruments Ltd, King's Lynn, UK*
Phyre2	*(Kelley et al., 2015)*

2.3. Medium, buffers and gels

L. incisa cells were grown at 25 °C in 300 mL BG11 medium (Stanier *et al.*, 1971) inside glass columns of 400 mL total volume and with an inner diameter of 3 cm. The cells were exposed to a constant light of 190 µmol photons.$m^{-2}.s^{-1}$ and the medium was supplemented by a constant flow of 1 % (v/v) CO_2, also used to distribute the cells homogeneously in the entire column. Nitrogen starvation was performed by washing and re-suspending the cells in modified BG11 media (BG11N-) without any source of nitrogen. Like described previously (Khozin-Goldberg *et al.*, 2002) $NaNO_3$ was simply removed from the media composition, and ferric citrate replaced ammonium ferric citrate.

2.3.1. Medium used for L. incisa growth

Table 4. Media recipe for 1 L Blue-green algae (BG11)

Stock solutions		Volumes
Sodium nitrate	15 g/L	100 mL
Dipotassium phosphate	4 g/L	10 mL
Magnesium sulfate	7.5 g/L	10 mL
Calcium chloride	3.6 g/L	10 mL
Citric Acid	0.6 g/L	10 mL
Ammonium Ferric citrate	0.6 g/L	10 mL
EDTA	0.1 g/L	10 mL
Sodium carbonate	2 g/L	10 mL
Trace metals	5.41 g/L	1mL
Water		Up to 1 L

Table 5. Media recipe for 1 L nitrogen free BG11 (BG11N-)

Chemical compounds		Volumes
Dipotassium phosphate	4 g/L	10 mL
Magnesium sulfate	7.5 g/L	10 mL
Calcium chloride	3.6 g/L	10 mL
Citric Acid	0.6 g/L	10 mL
Ferric citrate	0.56 g/L	10 mL
EDTA	0.1 g/L	10 mL
Sodium carbonate	2 g/L	10 mL
Metal mix-BG11	5.41 g/L	1mL
Water		Up to 1 L

Table 6. Recipe for 1L metal mix-BG11

Metals	Amount
Boric acid	2.86 g
Manganese chloride	1.81 g
Zinc sulfate	0.22 g
Sodium molybdate	0.39 g
Copper sulfate	0.08 g
Cobalt Nitrate	0.05 g
Water	Up to 1L

2.3.2. Media used for *Escherichia coli* growth

Auto-induction ZYP-5052 was used for all protein expression. Auto-induction medium is always prepared fresh. All stock solutions for this medium were autoclaved separately and stored at room temperature for up to 6 months. For all other purposes than protein expression, *Escherichia coli* (*E. coli*) cells were cultivated in LB medium.

Table 7. LB Medium

Component	Amounts
Sodium chloride	5 g
Yeast extract	10 g
Peptones	10 g
Water	Up to 1 L

Table 8. : ZYP-5052 rich medium for auto-induction

Component	Volumes
ZY medium	928 mL
1 M Magnesium sulfate	1 mL
1000x metals mix-ZYP	1 mL
50x5052	20 mL
20xNPS	50 mL
Water	up to 1L

Table 9. ZY Medium

Component	Amounts
N-Z-amine AS	10 g
Yeast extract	5 g
Water	up to 1L

MATERIAL

Table 10. 20x NPS

Salts	Amounts
Ammonium sulfate	66 g
Potassium dihydrogen phosphate	136 g
Sodium dihydrogen phosphate	142 g
Water	Up to 1L

Table 11. 50x 5052

Component	Amounts
Glycerol	250 g
Water	730 mL
Glucose	25 g
α–Lactose	100 g

Table 7.4-8: Metal mix-ZYP

Metals	Volumes
Water	36 mL
0.1 M Iron chloride	50 ml
1 M Calcium chloride	2 ml
1 M Manganese chloride	1 ml
1 M Zinc sulfate	1 ml
0.2 M Cobalt chloride	1 ml
0.1 M Copper chloride	2 ml
0.2 M Niquel chloride	1 ml
0.1 M Sodium molybdate	2 ml
0.1 M Sodium selenite	2 ml
0.1 M Boric acid	2 ml

2.3.3. Medium for agrobacterium

Table 12. YEB-Media

Component	Amounts
Meat extract	5 g
Yeast extract	1 g
Peptone	5 g
Sucrose	5 g
1 M Magnesium sulfate	2 mL

2.3.4. Sodium dodecyl sulfate-polyacrylamide gel electrophoresis (SDS-PAGE)

Table 13. SDS gel

Stocks	Staking gel	Separative gel
Final concentration of Acrylamide/Bis-acrylamide	4 %	12 %
Acrylamide/Bis-Acrylamide (Stock concentration = 30%)	1.3 mL	6.4 mL
1.5M TRIS pH 8.8	0.00 mL	4.00 mL
0.5M TRIS pH 6.8	2.50 mL	0.00 mL
Water	6.1 mL	5.5 mL
25% Amonium peroxo disulfate	0.040 mL	0.064 mL
TEMED	0.010 mL	0.016 mL
Total volume	10 mL	16 mL

2.3.5. Buffers

Table 14. SDS running buffer, for 2.5 L

Component	Amounts
TRIS/HCl, pH 8	3 g
Glycerol	14.4 mL
Sodium dodecyl sulfate (SDS)	1.0 g

Table 15. TAE buffer

Component	Final concentration
TRIS/HCl, pH 7	40 mM
Acetic acid	20 mM
Ethylenediaminetetraacetic acid (EDTA)	1 mM

Table 16. 6x Loading dye agarose gel

Component	Concentration
TRIS/acetate pH 8.5	40 mM
EDTA	100 mM
Sodium dodecyl sulfate (SDS)	0.1 % (w/v)
Glycerol	50 % (v/v)
Xylencyanol blue	0.25 % (w/v)
Bromophenol blue	0.25 % (w/v)

Table 17. IMAC Running Buffer

Component	Concentration
HEPES Buffer pH 8.4	0.02 M
Sodium chloride	0.15 M
Phenylmethylsulfonylfluorid	1 mM

Table 18. IMAC Elution Buffer

Component	Concentration
HEPES Buffer pH 8.4	0.02 M
Sodium Chloride	0.15 M
Imidazole	0.5 M

Table 19. SEC running buffer

Component	Concentration
HEPES Buffer pH 8.4	0.02 M
Sodium Chloride	0.1 M
Glycerol	2 % (v/v)

Table 20. TRIzol Buffer

Component	Volumes
Roti Phenol	3.8 mL
4 M Guanidinum thiocyanate	2 mL
4 M Ammonium thiocyanate	1 mL
3 M Sodiump acetat, pH 5,0	334 µL
Glycerin	500 µL
Water	2.366 mL

Table 21. High salt precipitation buffer

Salts	*concentration*
Sodium chloride	0.8 M
Sodium citrate	1.2 M

2.4. Consumables

Table 22. Enzymes

Enzymes	Suppliers
DNaseI	Thermo Fisher Scientific, Waltham, USA
GoTaq Polymerase	Promega Corporation, Madison, USA
Phusion Polymerase	New England Biolabs, Ipswich, USA
restriction enzymes	Thermo Fisher Scientific, Waltham, USA
RevertAid H Minus reverse transcriptase	Thermo Fisher Scientific, Waltham, USA

Table 23. Consumables

Consumables	Manufacturer
CloneJETPCR Cloning Kit	Thermo Scientific, USA
GeneRuler -50 bp DNA Ladder	Thermo Scientific, USA
GeneRuler 1 kb DA Ladder	Thermo Scientific, USA
Polystyrene cuvettes	Sarstedt, Germany
NucleoSpin Gel and PCR Clean-up	Macherey-Nagel, Germany
NucleoSpin Plasmid	Macherey-Nagel, Germany
Protino Ni-NTA Agarose	Macherey-Nagel, Germany
Roti-Mark STANDARD	Carl Roth, Germany
Spin-X® UF Concentrators	Corning, USA
TLC Silica gel 60	Merck, Germany
Unstained Protein Molecular Weight Marker	Thermo Scientific, USA

2.5. Primers and vectors

Table 24. Primers for LiLOX amplification. The five amino acids in the name of the forward primer, represent the five first amino acids from the recombinant protein sequence after translation (regardless of His-tag). MELGL: Full length LiLOX. DSVLP: LiLOX sequence without signal peptide.

Forward-MELGL	5'-GAATTCGACAGCGTGCTTCCCCATGGC-3'
Forward-DSVLP	5'-GAATTCGACAGCGTGCTTCCCCATGGC-3'
Reverse	5'-TTGCGGCCGCTTACATTGAGACGCTGGTTGGGAT 3'

Table 25. Primers for LiLOX mutations

Forward N702T/F703V	5'-ATCATCGAGGGCACCGTCACTCCTGGCCGCTATGCC-3'
Reverse N702T/F703V	5'-GCGGCCAGGAGTGACGGTGCCCTCGATGATACCACC-3'
Forward A688G	5'-CAACGTGAACTCCAACGGCCGCCAGCAGCTGATTAATG-3'
Reverse A688G	5'-TAATCAGCTGCTGGCGGCCGTTGGAGTTCACGTTGAGT-3'.
R853L Forward	5'-GGCTTCATGCCCAACCTGAGCCCGATGATCCGAAAGGC-3'
R853L Reverse	5'-TTTCGGATCATCGGGCTCAGGTTGGGCATGAAGCCTGA-3'
R853M forward	5'-GGCTTCATGCCCAACATGAGCCCGATGATCCGAAAGGC-3'
R853M Reverse	5'-TTTCGGATCATCGGGCTCATGTTGGGCATGAAGCCTGA-3'

Table 26. Vectors used in this study

Vector	Purpose	Supplier	Important feature(s)
pJET2.1/blunt	Cloning	Thermo Fisher Scientific (Waltham, MA, USA)	Ampicillin resistance
pUC18 Entry	Cloning	Dr. Ellen Hornung, University of Göttingen (Hornung *et al.*, 2005)	Ampicillin resistance
pUC18 YFP	Expression	Dr. Ellen Hornung, University of Göttingen (Hornung *et al.*, 2005)	tag-eYFP, Ampicillin resistance, 35S-promoter
pET28a	Expression	Novagen (Darmstadt, Deutschland)	T7 promoter, tag-6His, Kanamycin resistance
pCAMBIA	Expression	Dr. Ellen Hornung, University of Göttingen (Hornung *et al.*, 2005)	35S promoter, BASTA resistance, Kanamycin resistance

2.6. Strains

Table 27. Strains used in the course of this study

Specie	Strain	Obtained from
E. coli	XL1-blue	Agilent Technologies, USA
E. coli	BL21*(DE3)	NEB, USA
E. coli	DH5-α	New England Biolabs, Ipswich, USA
L. incisa	SAG 2468	Kindly provided by Dr. Inna Khozin-Goldberg, Ben-Gurion University of the Negev, Israel
A. tumefaciens	EHA 105	
A. thaliana	Columbia-0	Nottingham Arabidopsis Stock Center

2.6.1. 13LOX-knockout mutant of *A. thaliana*

Single *A. thaliana* lipoxygenase knockout (KO) plant lines were obtained from Nottingham Arabidopsis stock center (Salk lines). The AtLOX2 mutant *lox2-1* was kindly provided by Edward Farmer (Glauser *et al.*, 2009). The *lox3/4* double mutant was kindly provided by Klaus Apel (ETH, Zürich). Crossings to obtain the quadruple mutants were done by Dr. Ellen Hornung.

Table 28. Mutations in A. thaliana 13LOX-KO

LOXs	Type of Knock-out	Accession numbers
AtLOX2-KO	*lox2-1* (point mutation) (Glauser *et al.*, 2009)	At3g45140
AtLOX3-KO	Salk_062064 (TDNA insertion line)	At1g17420
AtLOX4-KO	Salk_071732 (TDNA insertion line)	At1g72520
AtLOX6-KO	Salk_08365 (TDNA insertion line)	At1g67560

2.7.Commercially available crystal screens

Table 29. Commercially available crystal screens used in the course of this study

Screen name	Compagny
Morpheus	*Molecular Dimensions Limited, Suffolk, U.K.*
Proplex	*Molecular Dimensions Limited, Suffolk, U.K.*
PGA	*Molecular Dimensions Limited, Suffolk, U.K.*
Midas MD1-59	*Molecular Dimensions Limited, Suffolk, U.K.*
JCSG+	*Molecular Dimensions Limited, Suffolk, U.K.*
Midas MD1-59 diluted	*Molecular Dimensions Limited, Suffolk, U.K.*
JBScreen PACT++HTS	*Jena Bioscience GmbH, Jena, Germany*
JB Nuc-Pro HTS S	*Jena Bioscience GmbH, Jena, Germany*
JB-1-2-4-5	*Jena Bioscience GmbH, Jena, Germany*
JB 6-7-8-10	*Jena Bioscience GmbH, Jena, Germany*
Natrix	*Hampton Research, Aliso Viejo, U.S.A.*
Ammonium Sulfate	*QIAGEN, Hilden, Germany*

3. METHODS

3.1. Molecular biology

If not mentioned otherwise, all molecular biology techniques were performed according to (Ausubel *et al.*, 1993)

3.1.1. cDNA synthesis

RNA was extracted from 50 mg of lyophilized algae cells using TRIzol buffer. cDNA was obtained using the RevertAid reverse transcriptase (RT) (Thermo Fisher Scientific, Waltham, USA) according to the manufacturers' instructions. Oligo(dT)18 was used as primers for reverse transcription.

3.1.2. Quantitative Real Time PCR (qRT-PCR)

Total cDNA freshly synthetized was used as template. In order to ensure that no mispriming occurs, resulting in the production of more than one PCR product, at first a regular PCR reaction was carried out, and analyzed on agarose gel. When a single band corresponding to the expected size was observed, the qRT-PCR reaction mixture was carried out using the Takyon No Rox SYBR MasterMix dTTP Blue (Eurogentec Biologics Division, Seraing, Belgium), according to the manufacturer's instructions. The PCR was performed in a thermocycler iQ5 qPCR cycler (BioRad Laboratories GmbH, München, Germany). Data analysis were interpreted with the iQ5 software (BioRad Laboratories GmbH, München, Germany). The qRT-PCR on LiLOX transcripts in *L. incisa* under nitrogen starvation was performed by Dr. Heike Siegler.

The protein phosphatase 2A gene (*PP2A*) was used as a reference gene in Arabidopsis, as formerly described (Czechowski *et al.*, 2005). The qPCR primers for *PP2A* were kindly provided by Anna Mueller. The Ribosomal Protein S21 (*RPS21)* was chosen as a reference gene in *L. incisa.* Both the qPCR primers for *LiLOX* and *RPS21* were kindly provided by Dr. Heike Siegler.

3.1.3. DNA amplification per polymerase chain reaction

For heterologous expression LiLOX was amplified from *L. incisa*'s cDNA, using the primers LiLOX WT. The polymerase chain reaction (PCR) reaction was performed with Phusion High Fidelity DNA polymerase (Thermo Scientific, USA).

Table 30. PCR reaxtion mixture

Volume	Stock	
1 µL	DNA	100 ng/L
1 µL	Forward Primer	10 µM
1 µL	Revers Primer	10 µM
35.5 µL	Water	
1 µL	dNTPs	10 mM each
10 µL	HF Puffer	5 X
0.5 µL	Phusion polymerase	2 U/µL
50 µL		

Table 31. Thermocycler program for DNA amplification per PCR

98 °C	5 min
94 °C	30 sec
55 °C	30 sec
72 °C	15 - 30 sec/kb
72 °C	10 min
32 cycles	

3.1.4. Targeted point mutations

Site directed mutagenesis was performed via PCR with Pfu polymerase (Thermo Scientific, USA) using the primers described in Table 25.

Table 32. Reaction mixture for targeted mutation by PCR

Volume	Stock	
1 μL	DNA	50 ng/L
1 μL	Forward Primer	10 μM
1 μL	Revers Primer	10 μM
35.5 μL	Water	
1 μL	dNTPs	10 mM each
10 μL	Pfu buffer	5 X
0.5 μL	Pfu	2.5 U/μL
50 μL		

Table 33. Thermocycler program for targeted mutation per PCR

95 °C	5 min
95 °C	30 sec
55 °C	30 sec
72 °C	2 min/kb
72 °C	10 min
18 cycles	

3.1.5. Agarose gel electrophoresis

DNA fragments obtained via PCR or after digestion were purified via electrophoresis in agarose gel (1 % (w/v)), after addition of 6 x DNA loading dye (5:1 (v/v)). The gels of agarose were submerged in TAE buffer, before samples were loaded. As standard calibration, a 1 kilobasepair GeneRuler DNA ladder (Thermo Fisher Scientific, Waltham, USA) was loaded in each gel. Voltage: 10 V/cm time of run: 30 min. After separation, the gels were submerged in in TAE buffer containing ethidium bromide for 5 min. DIANA gel documentation system (Raytest Isotopenmessgeräte GmbH, Straubenhardt, Germany) was used to visualize the DNA fragments.

3.1.6. Restriction DNA and cloning

Vectors and amplification products were cleaved using the appropriate restriction enzymes, having compatible overhangs. The DNA fragments were separated via electrophoresis agarose gel, as described in 3.1.5. The agarose gel was cut out around the fragments of DNA having the appropriate sizes, and purified with NucleoSpin Gel and PCR clean-up (Macherey-Nagel, Germany). The cleaved vectors and amplified fragments were added to the same microcentrifuge tube with the ratio 1:3. Ligase buffer and ligase were added to the mixture, and the ligation was incubated at room temperature for an hour. After an hour, 100 µL of the competent *E. coli* XL1-Blue cells were added to the mixture, and left 20 minutes on ice. After a heat chock of 45 seconds at 42 °C, the cells were incubated at 37 °C with 900 µL LB medium, and constant shaking. After 3 h of growth, the cells were plated on LB agar plates with the appropriate antibiotic, and incubated overnight at 37°C. The following morning, plates could be stored at 4 °C up to 1 month. In order to extract the vectors, positive colonies were inoculated into 5 mL of LB medium with the appropriate antibiotic, and incubated at 37 °C overnight. The following morning, the suspension was centrifuged, and the DNA was extracted using the kit NucleoSpin Plasmid (Macherey-Nagel, Germany). Cloned vectors were verified via sequencing based on (Sanger *et al.*, 1977), performed by the company GATC (Biotech, Konstanz, Germany). Sequences were then analyzed through the Geneious R8 software (Biomatters Ltd., Auckland, New Zealand).

3.1.7. Gateway cloning

In order to transform of *A. thaliana*, a first transformation in agrobacterium had to be performed. This technique requires the use of rather large vectors, which cannot be cloned with the usual ligation procedure. In order to do so, the Gateway cloning system (Thermo Fisher Scientific, Waltham, USA) was used. After the appropriate DNA fragment were inserted into pUC18 entry vectors as described in section 3.1.6, this plasmid was used in order to transfer the DNA fragment into the expression vector pCAMBIA (according to the manufacturer's instructions).

The pUC18 entry vector (10 fmol) containing the DNA fragment of interest was mixed with pCAMBIA vector (20 fmol), LR Clonase II enzyme mix (1 µL) and TRIS EDTA buffer (TE buffer) for a final volume of 10 µL. The reaction mixture was incubated at 25 °C overnight. In

order to stop the reaction, the Proteinase K was added (1 µL) and the mixture was incubated for 10 min at 37 °C. The proteinase K was inactivated by incubation at 70 °C for 10 min. The mixture was used in transformation of 100 µL competent *E. coli* DH5-α cells (New England Biolabs, Ipswich, USA). The transformation was performed with heat shock at 42°C for 45 sec, and the cells were incubated for 90 min at 37°C with constant shaking. The cells were then plated on LB agar plates containing 25 µg/mL kanamycin and incubated at 37 °C overnight. The following morning, colonies were transferred individually into a new LB plate with the same antibiotic and a second plate containing carbenicillin. The following morning, only colonies that grew on kanamycin but not on carbenicillin were used in colony PCR (see section 2.5.4).

3.2. Co-expression in onion cells and fluorescence microscopy

3.2.1. Transformation of epithelial onion cells

The transformation of epithelial onion cells and the confocal microscopic analysis was performed under the guidance of Dr. Till Ischebeck. The fluorescent proteins enhanced yellow fluorescent protein (eYFP) and enhanced cyan fluorescent protein (eCFP) were used to tag the proteins of interest, allowing them to be visualized by fluorescence microscopy later on. The two vectors pUC18-LiLOX-YFP and pCAT-ACP-CFP (Fulda *et al.*, 2002) were used for transformation. 10 mg of gold particles (1 µm diameter, from BioRad Laboratories GmbH, (München, Germany) were washed repeatedly with ethanol. After resuspending them in sterile bidistilled water, 0.2 mg of the particles were mixed with 8 µg of highly concentrated vector, for a maximum volume of 55 µL. After vigorous agitation, 50 µL of CaCl2 (2.5 M) and 20 µL of spermidine (0.1 M) were added to precipitate the DNA, allowing its coating onto the gold particles. After thorough mixing and three washing steps with ethanol, the freshly coated particles were resuspended in 60 µL ethanol. Particles were directly shot at the epidermis of freshly prepared onion (Allium cepa) layers using a PDS1000/He Biolistic Particle Delivery System (BioRad Laboratories GmbH, München, Germany) according to the manufacturer's instructions. For each bombardment, 20 µL of particle suspension as well as rupture discs (max pressure: 1350 pounds per square inch (psi)) were used in vacuum (28 inches of mercury). The onion freshly shot were placed in a petri dish with wet tissues to avoid dryness, and kept in the dark overnight at room temperature. The next morning, the single layers of epithelial cells were collected with using a forceps, and placed on a glass slide (Carl Roth GmbH & Co. KG, Karlsruhe, Germany) for analysis.

3.2.2. Confocal microscopy

A Laser Scanning Microscope 510 (Carl Zeiss Microscopy GmbH, Jena, Germany) was used to analyze the heterologously expressed proteins in epithelial onion cells. eCFP and eYFP were sequentially scanned. eCFP was excited with a 458 nm laser and an HFT 458 major beam splitter and images recorded via a band pass filter of 470-500 nm. eYFP was excited with a 488 nm laser line and an HFT 488/543 major beam splitter and a band pass of 505-550 nm was applied.

3.3. LiLOX recombinant expression in *E. coli* and purification

3.3.1. Affinity chromatography

At each steps of the purification, 200 µL of the eluate were collected in an individual microcentrifuge tube, and stored on ice before protein electrophoresis. 5 mL preculture was cultivated overnight from a single colony of *E. coli* BL21 Star (ThemoFisher scientific) freshly transformed with LiLOX-pET28. The following morning, the preculture was transferred to 1 L auto-induction ZY-medium (Studier, 2005), distributed in two flasks of 2 L each. The cells were grown at 37 °C for 2 h 30 minutes, then kept at 16 °C during 42 h, with constant shaking of 200 rotation per minute (rpm). The cells were then harvested via centriguation (4000 RPM, 20 min), transferred to conical centrifuge tubes and re-suspended in 10 % (w/v) *Running buffer*. 1 to 5 mg of lysozyme and 1 to 5 mg of desoxy-ribonuclease were added to each tube which were incubated on ice for 1 h 30 min. Further lysis was performed using a Fluidizer B12-04DJC/M3 (Parker Watts) at 60 PSI. The lysate was centrifuged at 10 000 x g for 10 min. For purification, immobilized metal affinity chromatography (IMAC) was performed using a nickel column HisTrap HP (GE healthcare, USA) either with an ÄKTAFPLC or an ÄKTAPrime system (GE healthcare, USA). At all steps of the chromatography, the absorbance was recorded at 280 nm. The column was rinsed with 4 times column volumes (CV) of running buffer, then 4 times CV with 5 % Elution Buffer. The supernatant of the *E. coli* cell lysate was loaded to the column. After a first washing step with 5 % elution buffer in order to remove loosely bound protein, the protein of interest was finally eluted and fractionated with 50 % Elution Buffer. Fractions with a high protein content corresponding to LiLOX were pooled and concentrated via Spin-X UF Concentrators (Corning, USA) to a maximal volume of 2 mL.

3.3.2. Size exclusion chromatography

Size Exclusion Chromatography (SEC) was performed by applying 2 mL of purified protein, obtained as described in section 3.3.1, on an HiLoad 26/60 Superdex 200 column equilibrated in gel filtration buffer beforehand. The protein was eluted with a constant flow rate of 1 mL/min. The absorbance was constantly recorded at 280 nm.

3.3.3. Protein analysis by polyacrylamide gel electrophoresis

In order to estimate the purity of the recombinant protein, a protein electrophoresis was performed in 12% acrylamide/Bis-acrylamide gel. Briefly, the different protein fractions from the section 3.3 were mixed with denaturing buffer (1:5 (v/v)), and individually loaded in the pockets of the acrylamide/Bis-acrylamide gel. The gels were placed in the BioRad system (Hercules, CA, USA), and electrophoresis was performed with a current of 30 mA per gel in the electrophoresis chamber (power supply E838, Consort, Turnhout, Belgium) for 30 min, or until the bromophenol blue reached the bottom of the gel.

Proteins were stained by immersion in a solution of Coommassie Brilliant Blue dye for 60 min and subsequently destained in ethanol 40 % (v/v) and acetic acid 10 % (v/v).

3.3.4. Bradford assay

Protein concentration was measured by Bradford assay (Bradford, 1976). Briefly, the protein fractions were incubated in a spectrophotometric cuvette with 1 mL of Bradford-reagent (35 g Serva Blue G in 25 mL EtOH, 50 ml 85 % (v/v) phosphoric acid, H_20 *ad* 500 mL) and vortexed. After 20 minutes of incubation in darkness, the mixtures were vortexed again, before the absorbance was measured at 595 nm. Along with the samples, 1 mL pure Bradford-reagent was used as blank, and different concentrations of bovine serum albumin (BSA) were used as calibration. Once properly labeled, the proteins were stored at -80°C until use. On average, 40 mg of pure LiLOX were harvested from 1 L of cell culture.

3.4. Protein Biochemistry

3.4.1. Thermal shift assay

A thermal shift assay was performed with the assistance of Dr. Achim Dickmanns (Department of Molecular Structural Biology, University of Göttingen, Germany) according to a previously published method (Ericsson *et al.*, 2006). The protein freshly purified in a low concentrated buffer (0.02M) was mixed with different buffer solutions (0.1 M) and the fluorescent dye Sypro Orange (0.05M) at a ratio of 8:1:1 (v/v/v) in a 96 well plate. The plate was then centrifuged briefly to remove putative air bubble, and analyzed in a CFX96 real-time PCR cycler (BioRad, Germany). A heat gradient was applied to the plate from 20°C to 95 °C, with an increase of 1 K every 30 sec, while fluorescence was recorded at 570 nm. The MaxFit-software (Department for Cryo Electron Microscopy, Max Planck Institute for Biophysical Chemistry, Göttingen, Germany) was used to analyze the data.

3.4.2. Kinetic assay measured by spectrophotometry

When not stated otherwise, LiLOX reactions were performed in Bis-TRIS Propane buffer pH 7.5 at 30 °C. The reaction was started by the addition of 1 µg enzyme purified according to 3.3.1 and 3.3.2. Lipoxygenase reactions were quantified by recording the formation of conjugated double bonds by measuring the absorbance increase at 234 nm ($\varepsilon = 2.5 \times 10^4$ M-1 cm-1) using a spectrophotometer CARY 100 Bio (Varian). Unless specified otherwise, all kinetic reactions were measured in 1 mL final volumes of 20 mM Bis-TRIS propane buffer pH 7.5 at 30 °C. Reactions were started by adding 1 µg of pure LiLOX. To determine optimum pH, LiLOX activity was measured with the same concentration of FFA (100 µM) at a pH varying from 5.5 to 9.5. To determine K_M and V_{max}, analysis was performed at optimal pH while the concentration of 18:2 (n-6), 18:3 (n-3) and 20:4 (n-6) varied from 10 mM to 100 mM. Activity of LiLOX in methanol containing buffer was measured using five different concentrations of methanol varying from 0 to 20 % (v/v).

3.4.3. LOX reaction with complex lipids

Solubilization of complex lipids could be reached in two different manners, according to the subsequent detection technique used. 100 µM of pure lipid species were solubilized in 20 mM Bis-TRIS propane buffer using a final concentration of 0.1 % (w/v) sodium deoxycholate. 5 µg

of pure LiLOX were added to start the reaction. The reactions were observed via the spectrophotometer, recording the formation of conjugated double bonds at 234 nm. Alternatively, lipids could be solubilized in 20 mM Bis-TRIS propane buffer pH 7.5 with 10 % methanol.

3.4.4. LOX *Ex-vivo* reaction assay

The combined extraction phases obtained as described in section 3.5.1 were dissolved in 0.5 mL 20 mM Bis-TRIS propane buffer, vortexed for 10 min and solubilized further by incubating in an ultrasonic water bath for 10 min. The dissolved extracts were centrifuged at 1500 x g for 10 min. The supernatants of all samples were split into two identical aliquots of 0.2 mL and transferred to reaction vials. 2 µg of LiLOX were added to one of the two aliquots. The second aliquot (without enzyme) was used as negative control. All reaction vials were incubated for 1 h at room temperature. The reaction was stopped by adding 50 µL of acetonitrile. After 10 min of centrifugation at 1500 x g, the supernatant was directly used for measurement as described in section 3.7.7.

3.4.5. Kinetic assay measured by ultra-performance liquid chromatography

In the reaction mixtures 0.1 % sodium deoxycholate was replaced by 10 % methanol, and the reactions were started by the addition of 5 µL of LiLOX. All three reactions were performed with different enzyme preparations. The three reactions were stopped at a different time point after reaction (10 min, 30 min and 60 min) by diluting with methanol (1:1 v/v). A fourth mixture was prepared in parallel without addition of enzyme as negative control. Measurements were performed by ultra-performance liquid chromatography-electrospray ionization-time of flight-mass spectrometry (UPLC-ESI-TOF-MS). The analysis was performed as described in section 3.7.6 and 3.7.8.

3.5. Lipid purification

3.5.1. Extraction of *L. incisa* metabolome

To identify natural substrates of *L. incisa* for the LiLOX activity a non-targeted *ex vivo* metabolome approach was performed. Therefore a two-phase methyl-*tert*-butylether (MTBE) extraction modified from (Matyash *et al.*, 2008) was used to generate the total metabolite extract. Six parallel extractions of 20 mg lyophilized algae material each (normal growth conditions) were used. To three of the six extractions, 250 µg FFA 18:2 (n-6) and 250 µg FFA 20:4 (n-6) was added before starting the MTBE extraction for use as internal standards.

3.5.2. Total lipid extraction from *L. incisa*

0.5 g of dried cells were ground with mortar and pestle. To prevent any deterioration of the lipids during this step, the cells were homogenized under constant cooling with liquid nitrogen. The cell powder was resuspended in 10 mL of isopropanol, previously heated at 80 °C, and then transferred into a glass tube. To prevent any potential lipase activity the material was incubated at 80 °C for 2 minutes. All isopropanol was dried under nitrogen stream, resuspended in 10 mL chloroform:methanol 1:1 (v/v). To get the maximum amount of lipid in the nonpolar phase, the mixture was shaken during 4 hours at 4 °C. The tube was centrifuged 5 minutes at 1000 x *g*. The supernatant was stored at 4 °C, and the pellet resuspended in 15 mL chloroform:methanol 2:1 (v/v). The mixture was then shaken over-night at 4 °C, centrifuged for 5 minutes at 1000 g, and the supernatant was combined with the previous supernatant. In order to separate polar from nonpolar phase, 10 mL of saturated solution of sodium chloride were added to the combined fractions, which was then centrifuged for 1 minute at 1000 g. The chloroform fraction (lower) was collected and dried until the volume reach approximately 1 mL.

3.5.3. Solid phase extraction

The three major lipid classes were separated using solid phase extraction (SPE) Strata SI-1 Silica columns (Phenomenex, Torrance, California) according to the instructions from the manufacturer. Briefly: after equilibrating the column with 1mL chloroform, 1 mL of total lipid extract from the section 3.5.2 was loaded. Neutral lipids were eluted with 14 mL of chloroform, glycolipids with 15 mL of acetone/2-propanol (9:1; v/v) and finally phospholipids with 15 mL of methanol/acetic acid (9:1; v/v). The three fractions were dried under a stream of nitrogen and resolved either in 200 µL of chloroform for further purification by thin layer

chromatography (TLC), or in 200 µL ethanol with argon on top of the solution for storage at -20°C.

3.5.4.   Thin Layer Chromatography

The different lipid extracted from *L. incisa* as described in sections 3.5.2 and 3.5.3 were separated on a silica gel 60 plate (Merck, Darmstadt, Germany). Different solvents were used for the separation of the different lipid classes. After applying 200 µL of the pure lipid fraction from section 3.5.3, the TLC place was placed in a developing chamber. 100 mL of solvent system were used for the separation, either chloroform:methanol (85:15; v/v) for galactolipids or chloroform:methanol:ammonium hydroxide (65:25:4; v/v/v) for phospholipids. Samples were sprayed with a solution of 8-anilinonaphthalene-1-sulfonic acid (ANS) and revealed under a UV lamp. MGDG, DGDG, GlcADG, TGDG and phosphatidylcholine (PC) were scraped out from the plate and transferred into individual glass tubes. Lipids were extracted from the Silica membrane with methanol:chloroform:water 1:1:1 (v/v/v). After the samples were vortexed for 1 min and centrifuged for 1 min at 4000 rpm, the non-polar phase was dried out under nitrogen stream. Samples were then transferred into 2 mL microcentrifuge tubes using pure ethanol. The quantity of each galactolipid fraction was estimated by weighing the dried sample, before the samples were stored at -20 °C in 200 µL 100 % ethanol under a layer of argon.

3.6. Treatments of LOX products

3.6.1. Reduction of hydroperoxides

1 mL of 100 µM hydroperoxide FFA was reduced with 100 µL of 1 % (w/v) sodium borohydride solution. After 5 to 10 minutes reduction at room temperature, 100 µL glacial acetic acid were used to stop the reduction. Lipids were extracted with pure n-hexane, transferred to a microcentrifuge tube, dried and resuspended in 100 µL n-hexane.

Hydroperoxides of complex lipids were transferred into a glass tube containing 50 mM tin(II) chloride dissolved in methanol in a ratio of 1:1 (v/v). After 10 minutes reduction, chloroform was added to the reaction in a final ratio of 1:1:1 (v/v/v). Samples were shaken vigorously to mix the solvents and were centrifuged at 1000 x g for a minute in order to separate two phases. The lower lipid containing chloroform phase was transferred into another glass tube, dried under a nitrogen stream and resuspended in 200 µL 100 % ethanol.

3.6.2. Transesterification of complex lipids

Complex lipids were solubilized in 220 µL of methanol. 110 µL of toluol were added for a final volumetric methanol/toluol ratio of 2:1. 170 µL of 0.5 M sodium methoxide in methanol was added before samples were agitated for 20 minutes at room temperature. 500 µL of saturated sodium chloride solution were added before extracting fatty acid methyl ester three times with 500 µL of n-hexane.

3.6.3. Methylation of free fatty acid

Free fatty acids were resolved in 400 µL methanol, and 6.5 µL of diazomethane. Samples were shaken for 20 minutes at room temperature. The reaction was stopped by the addition of 2 µL of 10 % acetic acid. Samples were dried under a nitrogen stream and resuspended in pure n-hexane.

3.7. Lipid analysis

During chromatography, absorbance was constantly recorded by a diode array detector (DAD) at wave lengths 220 nm, 234 nm and 268 nm.

3.7.1. Galactolipids

Galactolipids were separated on reverse phase high pressure liquid chromatography (RP-HPLC), using the column EC250/2 Nucleosil C_{18} (length 250 mm, inner diameter 4 mm, particle size 5 μm, (Macherey-Nagel, Germany). Galactolipids were separated with solvent system A: acetonitrile/water/acetic acid (50:50:0.1, v/v/v); B: acetonitrile/water/acetic acid (100:0:0.1, v/v/v). After resolving the products in solvent A, the mixture was injected on the column with a flow rate of 0.2 mL/min. The gradient used is listed below (modified method from (Ibrahim *et al.*, 2011)).

Table 34. Gradient of solvent system used for reverse phase (RP)-HPLC analysis of galactolipids

Time (min)	Solvent A	Solvent B	Flow rate
0	100 %	0 %	0.2 mL/min
10	100 %	0 %	0.2 mL/min
30	0 %	100 %	0.2 mL/min
60	0 %	100 %	0.2 mL/min
75 (post run)	100 %	0 %	0.2 mL/min

3.7.2. Fatty acid methyl esters

After transesterification, fatty acid methyl esters were dissolved in solvent system A: methanol/water/acetic acid (75:25:0.1, v/v/v) and B: methanol/water/acetic acid (100:0:0.1 v/v/v). Using the same column as described above, the separation method was as follows:

Table 35. Gradient of solvent system used for reverse phase (RP)-HPLC analysis of fatty acid methyl esters

Time (min)	Solvent A (%)	Solvent B (%)	Flow rate
0	100	0	0.18
5	100	0	0.18
20	0	100	0.36
30	0	100	0.36
35	100	0	0.36
40	100	0	0.36
46 (post run)	100	0	0.18

3.7.3. Di-hydroxyl fatty acid

In order to separate mono-hydroxyl fatty acid from di-hydroxyl fatty acids, the same column as described above was used. A mixture of methanol:water:acetic acid with a ratio of 75:25:0.1 (v/v/v) for the solvent A and ratio of 100:0:0.1 (v/v/v) for the solvent B was applied. The separation was performed according to the following gradient:

Table 36. Gradient of solvent system used for reverse phase (RP)-HPLC analysis of Di-hydroxyl free fatty acids

Time (min)	Solvent A (%)	Solvent B (%)	Flow rate
0	100	0	0.18
10	100	0	0.18
25	0	100	0.18
27	0	100	0.36
32	0	100	0.36
37	100	0	0.36
40	100	0	0.18
46	100	0	0.18

3.7.4. Straight phase-HPLC

The purified hydroxy fatty acids were analyzed on a straight phase (SP) column Zorbax RX-SIL; (150 x 2.1 mm, particle size 5 µm, Agilent, California, USA). To analyze free fatty acids, the method consists of a constant flow rate of 0.2 mL/min solvent system D containing *n*-hexane/2-propanol/trifluoroacetic acid (100:1:0.1, v/v/v). In the case of hydroxide methyl esters, the same solvent was used at a flow rate of 0.1 mL/min.

3.7.5. Chiral phase-HPLC

Purified oxidized fatty acids were further analyzed on chiral phase (CP) column CHIRALCEL OD-H (150 x 2.1 mm, Technologies Inc. Delaware, USA). Flow rate was constant at 0.1 mL/min. The solvent system ratio of *n*-hexane/2-propanol/trifluoroacetic acid differed according to the hydroxide to be analyzed: For all Hydroxyoctadecadienoic acid (HODE) and Hydroxyoctadecatrienoic acid (HOTE) analytes, solvents had a ratio of 100:5:0.02, (v/v/v), for all 8-HETE, 12-HETE and 15-HETE analytes, the ratio was 100:2:0.02, (v/v/v). For 5-HETE and 11-HETE it was 100:1:0.02, (v/v/v). All oxidized fatty acid methyl esters were analyzed on CP-HPLC using the same solvent system, *n*-hexane/2-propanol/trifluoroacetic acid in a ratio of 100:1:0.02, (v/v/v).

3.7.6. UPLC-ESI-TOF-MS

For the identification of oxidized and non-oxidized MGDG, DGDG and PC species as substrates and products of the LiLOX reaction the accurate mass information from UPLC-ESI-TOF-MS analysis was used.

<u>Analysis of oxidized and non-oxidized MGDG and DGDG species</u>

MGDG and DGDG species extracted from *L. incisa* and purified by SPE (3.5.3) and TLC (3.5.4) as well as oxidized MGDG and DGDG species extracted after incubation with LiLOX were analyzed by UPLC-ESI-TOF-MS. For UPLC an ACQUITY UPLC HSS T3 column (1.0 x 100 mm, 1.8 µm particle size, Waters Corporation, Milford, USA) was used at 40 °C with flow rate of 0.2 mL/min. The following gradient was run for sample separation: 0 – 0.5 min 40 % B, 0.5 – 6 min 40 % B to 100 % B, 6 – 12 min 100 % B, 12 – 12.1 min 100 % B to 40 % B, 12.1 – 15 min 40 % B; (solvent system A: water:formic acid (100:0.1, v/v); B:

acetonitrile:formic acid (100:0.1, v/v)). The TOF-MS analysis was performed in the negative ESI-mode as described in 3.7.7.

<u>Analysis of oxidized and non-oxidized PC species</u>

PC species extracted from *L. incisa* and purified by SPE (3.5.3) and TLC (3.5.4) as well as oxidized PC species were analyzed by UPLC-ESI-TOF-MS. For UPLC an ACQUITY UPLC BEH C18 column (1.0 x 100 mm, 1.8 μm particle size, Waters Corporation, Milford, USA) was used at 50 °C with flow rate of 0.2 mL/min. The following gradient was run for sample separation: 0 – 0.5 min 80 % B, 0.5 – 7 min 80 % B to 100 % B, 7 – 11 min 100 % B, 11 – 11.1 min 100 % B to 80 % B, 11.1 – 13 min 80 % B; (solvent system A: water:formic acid (100:0.1, v/v); B: acetonitrile:formic acid (100:0.1, v/v)). The TOF-MS analysis was performed for 13 min in the positive ESI-mode as described in 3.7.7.

3.7.7. Non-targeted metabolome analysis of the LOX reaction by UPLC-ESI-TOP-MS

For non-targeted analysis the samples were analysed by ultra-performance liquid chromatography (UPLC, ACQUITY UPLC System, Waters Corporation, Milford, USA) coupled to an electrospray ionization time-of-flight mass spectrometer (ESI-TOF-MS, LCT Premier, Waters Corporation, Milford, USA). The UPLC was equipped with an ACQUITY UPLC HSS T3 column (1.0 x 100 mm, 1.8 μm particle size, Waters Corporation, Milford, USA) and was used at 40 °C with flow rate of 0.2 mL/min. The following gradient was run for sample separation: 0 – 0.5 min 40 % B, 0.5 – 6 min 40 % B to 100 % B, 6 – 12 min 100 % B, 12 – 12.1 min 100 % B to 40 % B, 12.1 – 15 min 40 % B; (solvent system A: water:formic acid (100:0.1, v/v); B: acetonitrile:formic acid (100:0.1, v/v)).

The TOF-MS analysis was recorded in the mass range of *m/z* 85 – 1200 for positive ESI and *m/z* 50 – 1200 for negative ESI mode over a runtime of 10 min using a capillary voltage of 2700 V (positive ESI) and 2500 V for negative ESI mode, respectively. The following source parameters were used: cone voltage, 30 V; desolvation temperature, 350 °C; source temperature, 80 °C. Nitrogen was used as cone and as desolvation gas at 30 l/h and 800 l/h, respectively. The mode of dynamic range enhancement was used for data acquisition. Data were recorded by MassLynx software (MassLynx V4.1, Waters Corporation, Milford, USA)

in centroid format. Mass analyses were adjusted by applying the reference spray compound leucine-enkephaline ([M+H]$^+$ 556.2771 and the respective 2x^{13}C isotopologue ([M+H]$^+$ 558.2837) for positive ESI mode and [M-H]$^-$ 554.2615 and as well as the respective ^{13}C isotopologue ([M-H]$^-$ 555.2648) for the negative ESI mode; Sigma-Aldrich, Deisenheim, Germany) at a concentration of 0.5 µg/mL in acetonitrile:water (50:50, v/v) and a flow rate of 20 µL/min.

The raw data obtained by UPLC-TOF-MS analysis were subsequently used for data deconvolution (peak picking and peak alignment) by MarkerLynx Application Manager for MassLynx software (Waters Corporation, Milford, USA) to generate data matrixes. For peak detection, the following parameters were used: retention time range, 0.30 - 10.00 min, mass range, 50 – 1200 Da, extracted ion chromatogram window 0.03 Da. Apex track peak parameters were set to automatic. Data deconvolution led to data matrixes of 2893 features for the positive ESI-mode and 1616 features for the negative ESI-mode, respectively.

3.7.8. Data analysis by MarVis

Further data processing steps like ranking and filtering, adduct correction, merging data sets, data base search as well as clustering and visualization of the data was supported by the MarVis toolbox (Kaever *et al.*, 2015). For ranking and filtering of the features an ANOVA test was applied to obtain a subset of 1002 (positive ESI-mode) respective 422 (negative ESI-mode) high quality features with a p-value < 10^{-3}. Adduct correction was performed for the following adducts: [M+H]$^+$, [M+Na]$^+$, [M+NH$_4$]$^+$ (for positively charged ions); [M-H]$^-$, [M+CH$_2$O$_2$-H]$^-$, [M+CH$_2$O$_2$+Na-2H]$^-$ (for negatively ions). Subsequently the data sets were combined and used for automated data base search as well as for clustering and visualization by means of by means of one-dimensional self-organizing maps (1D-SOMs). The number of three clusters was used to represent 1424 features. To identify tentative LiLOX substrates and products an in-house data base was created, which includes the exact mass information of all MGDG, DGDG and PC species calculated for the acyl chains known to exist in the *L. incisa* lipid species and the derived hydroxides and hydroperoxides.

3.7.9. MS/MS fragmentation analysis UHPLC-ESI-QTOF-MS

For MS/MS fragmentation analyses LiLOX reaction products were reduced by tin(II) chloride, acidified, separated by RP-HPLC and subsequently analyzed by UHPLC-ESI-QTOF-MS. For

UHPLC, an Agilent 1290 Infinity UHPLC system (Agilent Technologies, Böblingen, Germany) equipped with an ACQUITY UPLC HSS T3 column (2.1 x 100 mm, 1.7 µm particle size, Waters Corporation, Milford, USA) was used at 40 °C with an flow rate of 1 ml/min. The UHPLC was coupled to an Agilent 6540 UH Accurate-Mass-Q-TOF mass spectrometer (Agilent Technologies, Böblingen, Germany). Same solvent systems and gradients were used as described in 3.7.7. The QTOF-MS was in negative ESI-mode with a source suitable for Agilent Dual Jet Stream Technology (Agilent Technologies, Böblingen, Germany). Source parameters were as follows: gas temperature 300 °C, gas flow 8 L/min, nebulizer pressure 35 psi, sheath gas temperature 350 °C, sheath gas flow 11 L/min, VCap 3.f kV, nozzle voltage 100 V. Collision energies from 20 eV – 40 eV were used for collision induced dissociation. For data acquisition, the MS was operated with the software Mass Hunter Workstation Acquisition (Version: B.05.01, Agilent Technologies, Böblingen, Germany). The Mass Hunter Qualitative Analysis software (Version: B.06.00, Agilent Technologies, Böblingen, Germany) was used for data analysis.

3.7.10. UPLC-nano ESI-MS/MS

Analysis of lipids by UPLC-nanoESI-MS/MS was done by Dr. Cornelia Herrfurth. UPLC-nanoESI-MS/MS molecular species analysis was performed as previously described (Tarazona *et al*., 2015), with some modifications. The analysis was started by UPLC using an ACQUITY UPLC® I-class system (Waters Corp., Milford, MA, USA) equipped with an ACQUITY UPLC® HSS T3 column (100 mm × 1 mm, 1 µm; Waters Corp., Milford, MA, USA). Aliquots of 2 µL were injected, the flow rate was 0.1 mL/min and 0.13 ml/min, respectively, and the separation temperature was 35 °C. Solvent B was tetrahydrofuran/methanol/20 mM ammonium acetate (6:3:1; v/v/v) containing 0.1% (v/v) acetic acid; and solvent A was methanol/20mM ammonium acetate (3:7; v/v) containing 0.1% (v/v) acetic acid. All lipids were separated with linear binary gradients following the same scheme: start conditions (65, 80, or 100% solvent B) held for 2 min, linear increase to 100% solvent B for 8 min, 100% solvent B held for 2 min and re-equilibration to start conditions in 4 min. The start conditions were 80% solvent B for diacylglycerols (DAG), 100% solvent B for triacylglycerols (TAG) and 65% solvent B for all remaining lipid classes. For TAG, the isocratic chromatographic runs were finished after 8 min.

METHODS

Chip-based nanoelectrospray ionization was achieved with a TriVersa Nanomate (Advion, Ithaca, NY, USA) in both positive and negative ion mode with 5 μm internal diameter nozzles. The ion source was controlled with the Advion ChipSoft Manager software. By using a post-column splitter 255 nL min^{-1} of the eluent were directed to the nanoESI chip and ionization voltage was set to either 1.4 kV (TAG), 1.3 kV (DAG) or 1.23 kV (all remaining lipid classes). Molecular lipid species were detected with a 6500 QTRAP tandem mass spectrometer (AB Sciex, Framingham, MA, USA) in multiple reaction monitoring mode. All theoretically possible molecular lipid species were calculated and measured by UPLC-nano ESI-MS/MS-based method as described above on the basis of the known fatty acid profile of *L. incisa* consisting of 14:0, 16:0, 16:1, 16:2, 16:3, 18:0, 18:1, 18:2, 18:3, 20:0, 20:1, 20:2, 20:3, 20:4 and 20:5 (Bigogno *et al.*, 2002a). The oxidized fatty acid species containing one oxygen as well as two oxygens of 16:2, 16:3, 18:2 and 18:3 were additionally taken into account for calculation of the molecular species of the glycerophospholipids and glyceroglycolipids. Target precursor ions were [M+NH$_4$]$^+$ for DAG and TAG; [M-H]$^-$ for PE, PG, PS and SQDG; and [M-H+CH$_3$CO$_2$H]$^-$ for PC, MGDG, DGDG, TGDG, tetragalactosyldiacylglycerol (TeGDG) and glucuronosyldiacylglycerol (GlcADG). For diacyl and triacyl lipids, target selected reaction monitoring transitions were diagnostic for the acyl chain composition of the molecular species, either by a fatty acid-associated neutral loss in the positive mode (DAG and TAG) or by formation of fatty acyl-related fragments in the negative ion mode (glycerophospholipids and glyceroglycolipids). Dwell time was 5 ms and MS parameters were optimized to maximize detector response. The integration workflow made use of the Analyst IntelliQuan (MQII) peak-finding algorithm.

3.8. Plants

3.8.1. *A. thaliana* growth conditions

The soil was obtained from (Fruhstorfer Erde Typ T fein, Hawita Gruppe GmbH, Vechta, Germany). To prevent contamination, the soil was steamed 8 hours at 80 °C before treatment with 0.25 % (v/v) Previcur fungicide (Bayer AG, Leverkusen, Germany). *A. thaliana* seeds were placed isolated in freshly steamed soil, kept at 4 °C for 2 days and transferred to a climate chamber (York Industriekälte GmbH & Co. KG). *A. thaliana* plants were grown at 22 °C, with long day conditions (16 hours of light for 8 hours of dark) and 60 % humidity. In order to induce the growth of several inflorescence meristems for plants that were to be transformed, the first inflorescence was cut. All other plants were directly transferred to the greenhouse as they started flowering.

3.8.2. *A. thaliana* transformation

Prior to *A. thaliana* transformation, *Agrobacterium tumefaciens* (*A. tumefaciens)* had to be transformed following a modified version of (Höfgen & Willmitzer, 1988). 100 µL of competent agrobacteria were mixed with 3 µL of plasmid DNA, and left on ice for 30 minutes. The cells were frozen for 2 minutes at -80 °C, then thawed immediately at 37°C in a water bath. 800 µL LB Media were added to the cells, before incubation at 28 °C for 3 to 4 hours, with constant shaking at 200 rpm. The cells were centrifuged at 2 000 x g for 1 minute and plated on agar with kanamycin and rifampicin before incubation for 2 days at 28 °C. Single colonies were picked after 48 hours, plated on a new agar plate and incubated for 48 hours. Liquid cultures were done with these colonies. Agrobacteria were grown at 28 °C with constant shaking at 200 rpm in YEB-Medium. *Arabidopsis* plants were then transformed by flower dipping. When the plants started to flower, a freshly prepared pre-culture of Agrobacterium was transferred into 500 mL of YEB-media and incubated at 28 °C. The following morning, cells were harvested by centrifugation at 4,000 x g, and resuspended in 300 mL of 5 % sucrose and 70 µL Silwet L-77 (Momentive, USA). Flowers of *Arabidopsis* were dipped into the *A. tumefaciens* solution. After the transformation procedure plants were put under a plastic hood overnight. The plant were kept growing in the green house, and the dipping procedure was repeated after 1 week. Seeds were harvested after 4 to 6 weeks. These T_1-seeds were planted again and in order to select transformed *Arabidopsis*. Plants were sprayed with a BASTA solution. Surviving plants were transferred to pots and grown as described above. As

transformation was performed with a knock-out plant line deficient of jasmonic acid resulting in male sterility, flowering plants had to be treated with jasmonic acid to obtain seeds. Therefore flowers were sprayed daily with a solution containing 0.1 % Tween 20 (v/v) and 0.1 % methyl jasmonate.

3.8.3. Jasmonic acid extraction

In order to induce the expression of enzymes from the JA pathway (except LOX, knocked out) leaves of *A. thaliana* 13-LOX-KO were mechanically wounded using forceps. Forceps where applied three times across the midvein for each leaf. Wounded leaves were collected 2 hours after wounding and shock frozen in liquid nitrogen. For extraction of JA, the frozen leaves were crushed with a pistil and transferred to glass tubes containing 2 mL ethyl acetate, agitated at 8°C for 1 h. 2 mL of water was added in order to obtain two phases, before samples were strongly mixed and centrifuged 10 min at 4°C, 4000 RPM. Supernatant was collected, and this extraction step was repeated one more time on the remaining pellet.

3.9. Protein crystallography

Protein crystallography was performed in the department of structural biochemistry, with the kind authorization of Prof. Dr. Ralf Ficner.

3.9.1. Commercially available crystal screen

After purification of LiLOX from the SEC in HEPES buffer pH 8.4; 100 mM NaCl; 2 % glycerol, all fractions measured to have LOX activity were combined. After ensuring the purity of the fraction by SDS-PAGE, the proteins were concentrated by spin-concentrators to a final concentration of 7 µg/µL. The freshly purified protein was mixed with different buffers using commercially available crystal screens (Table 29) at a ratio of 1:1 (v/v) for a final sitting drop volume of 0.5 µL or 1:2 (v/v) for a final drop volume of 0.75 µL. In order to verify that putative crystals do not originate from salts present in the protein buffer, a buffer control was also performed on the respective plates. The microtiter plates were sealed immediately after pipetting, in order to allow vapor diffusion and the plates were incubated at 20 °C. Pictures were taken automatically after 0; 1; 3; 7; 14; 30; and 45 days to track the apparition of crystals.

3.9.2. Customized crystal screen

According to the results of commercially available crystal screens, customized crystal screens were performed. Screens were made containing one type of buffer, one type of salt, and one type of precipitant. One factor was varying from A to D, and another one from 1 to 6 as shown in Figure 7. Drop size could vary from 2 to 4 µL, sitting drop as well as hanging drop screenings were carried out.

Protein to Reservoir ratio (µL)

A	1.5:1.5	1.5:1.6	1.5:1.7	1.5:1.8	1.5:1.9	1.5:2
	8 % PEG 20,000; 0.1 M Tris pH 8.0; LiLOX concentration 10 µg/µL; Sitting drop					
B	1.5:1.5	1.6:1.6	1.7:1.7	1.8:1.8	1.9:1.9	2:2
	8 % PEG 20,000; 0.1 M Tris pH 8.0; LiLOX concentration 10 µg/µL; Sitting drop					
C	1.5:1.5	1.6:1.5	1.7:1.5	1.8:1.5	1.9:1.5	2:1.5
	8 % PEG 20,000; 0.1 M Tris pH 8.0; LiLOX concentration 10 µg/µL; Sitting drop					
D	1:1	1.1:1.1	1.2:1.2	1.3:1.3	1.4:1.4	1.5:1.5
	8 % PEG 20,000; 0.1 M Tris pH 8.0; LiLOX concentration 10 µg/µL; Sitting drop					

Figure 7. Example of optimized crystal screen. The ratio protein:reservoir varies from condition 1 to 6. From A to C, different drop sizes were performed, ranging from 2 µL to 4 µL.

4. RESULTS

Since knowledge on lipid oxidizing processes in green algae is scarce, the aim of the thesis was to analyze the available genome, transcriptome and proteome sequences of *L. incisa* for the existence of putative lipid oxidizing enzymes. As a start, the focus was on the major lipid oxidizing enzyme from flowering plants, the LOX. In the first section the identification of a putative LiLOX protein, its *in silico* analysis by protein sequence alignments, its predicted 3D structure as well as the *in vitro* characterization by enzymatic assays will be described.

4.1. Identification of a putative LOX sequence in the transcriptome of *L. incisa*

Assembly of the nuclear genome of *L. incisa* was carried out (Tourasse *et al.*, unpublished data) along with that of the mitochondrial and plastidial genomes (Tourasse *et al.*, 2015a; Tourasse *et al.*, 2015b). Protein-coding genes were predicted and annotated (as described in NCBI GEO GSE94666), revealing a potential ORF of 994 amino acid residues, identified a LOXs (accession number g6219, named LiLOX, supplemental Figure 10). In addition to the genome sequencing, the transcriptome of *L. incisa* was also investigated by the same research group, and will be mentioned in a following section 4.2.

In order to further estimate the automatic annotation of LiLOX, its protein sequence of was aligned with those of 38 characterized LOXs from *A. thaliana*, *Burkholderia thailandensis* (*B. thailandensis*), *Cyanothece sp.*, *Fusarium oxysporum* (*F. oxysporum*), *Gersemia fruticosa* (*G. fruticosa*), *Gaeumannomyces graminis* (*G. graminis*), *Glycine max* (*G. max*), *Homo sapiens* (*H. sapiens*), *Magnaporthe salvinii* (*M. salvinii*), *Nostoc punctiforme* (*N. punctiforme*), *Oryza sativa* (*O. sativa*), *Pseudomonas aeruginosa* (*P. aeruginosa*), *Plexaura homomalla* (*P. homomalla*), *Physcomitrella patens* (*P. patens*) and *Symphytum tuberosum* (*S. tuberosum*). LiLOX was found to have the highest identity with the LOXs from the moss *P. patens*, and the higher plant *A. thaliana* (Supplemental table 1).

4.1.1. Phylogenetic tree of Lipoxygenases

A phylogenetic tree confirmed a separation between plant LOXs and all other known LOX from bacteria, animals and fungi (Figure 8). The plant LOX cluster itself divided into three main clusters: plastidic LOXs, extra plastidic LOXs and moss LOXs. Although it was never characterized, the amino acid sequence of the putative LOX from *C. reinhardtii* (CrLOX) was included to the tree as a putative second green algal LOX. Interestingly, LiLOX groups closest with CrLOX.

Figure 8 Phylogenic three of Lipoxygenases based on protein sequence homology. All accession numbers were obtained from GeneBank: *A. thaliana* LOX1 (9*S*) (NP_175900.1), *A. thaliana* LOX2 (13*S*) (NP_566875.1), *A. thaliana* LOX3 (13*S*) (NP_564021.1), *A. thaliana* LOX4 (13*S*) (NP_177396.1), A. *thaliana* LOX5 (9*S*) (NP_188879.2), A. *thaliana* LOX6 (13*S*) (NP_176923.1), *B. thailandensis* (13*S*) (ABC36974), *C. reinhardtii* LOX (putative) (XP_001690882.1), *Cyanothece sp*. LOX1 (9*R*) (WP_012595715.1), *Cyanothece* sp. LOX2 (11*R*) (WP_012596348.1), *F. oxysporum* LOX (13*S*) (EXK38530), *G. fructosovora* LOX (11*R*) (AAY98506.1), *G. graminis* Mn-LOX (13*R*) (AAK81882.1), *G. max* LOX1 (13*S*) (NP_001236153.1), *G. max* LOX2 (9/13*S*) (NP_001237685.1), *G. max* LOX3 (9/13*S*) (CAA30016), *G. max* LOX4 (13*S*) (BAA03101), *H. sapiens* LOX2 (15*S*) (AAB61706.1), *H. sapiens* LOX (5*S*) (NP_000689.1), *H. sapiens* LOX (12*R*) (NP_001130.1), *H. sapiens* LOX (12*S*) (NP_000688.2), *H. sapiens* LOX (15*S*) (NP_001131.3), *M. salvinii* Mn-LOX (9*S*) (CAD61974.1), *N. punctiforme* LOX (9*R*) (WP_010994078.1), *N. punctiforme* LOX2 (13*S*) (WP_012407347.1), *O. sativa* LOX2 (13*S*) (NP_001067011.1), *O. sativa* LOX (13*S*) (EEC72668), *P. aeruginosa* LOX (15*S*) (WP_023436288.1), *P. homomalla* LOX (8*R*) (AAC47743), *P. patens* LOX1 (13*S*) (XP_001784705.1), *P. patens* LOX2 (13*S*) (ABF66648), *P. patens* LOX3 (13*S*) (XP_001785004.1), *P. patens* LOX4 (13*S*) (ABF66650.1), *P. patens* LOX5 (13*S*) (ABF66651.1), *P. patens* LOX6 (13*S*) (ABF66652.1), *P. patens* LOX7 (13*S*) (ABF66653.1), *S. tuberosum* LOX (9*S*) (NP_001275357.1), *S. tuberosum* LOX (13*S*) (NP_001274843.1), *S. tuberosum* LOX2 (13*S*) (NP_001275115.1).

4.1.2. Analysis of LiLOX putative active sites

Among all characterized LOXs, the five amino acid residues responsible for iron binding (here three histidines, one asparagine and one isoleucine) are mainly conserved. The 5th ligand however, the C-terminal isoleucine was found to be a methionine in LiLOX. Apart from this, the active site of LiLOX seemed very homologous to plant LOX (Figure 9). The Coffa (Coffa & Brash, 2004) determinant, either a valine or a glycine in all characterized LOX, was describe to influence the specificity of oxidation. In LiLOX this residue is found to be an alanine (A688), suggesting that LiLOX belongs to the group of *S*-LOXs. In contrast to other LOXs from plant and animals LiLOX harbors at the position described by Sloane (Sloane *et al.*, 1991) two bulky residues (N702; F703).
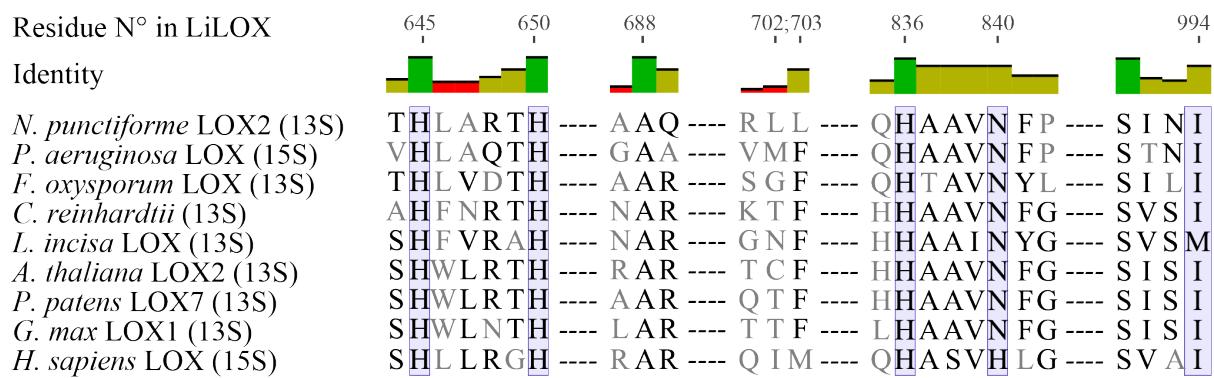
Figure 9. Alignment of relevant active site amino acid residues of LOXs. Residue numbers are those from the LiLOX sequence. The five amino acid residues responsible for iron binding are framed. For every given residue, identity represents its homology between all 13*S*-LOXs from Figure 8 used in this alignment (Green = 100 % < Gold < 50 % ≤ Red). Allignment obtained from the software Geneious, Muscle allignment with default parameters. LOXs accession numbers are as indicated in Figure 8.

RESULTS

4.1.3. General aspects of LOX domain alignment

It was formerly reported that a central domain is conserved specifically in all plant LOXs (Newcomer & Brash, 2015). SoyLOX1 for instance has a domain of 29 amino acids following the highly conserved L292, Y293, whereas the alignment displays a gap for all non-plant LOX (Figure 10). When present, this domain contains three additional residues, G296 L299 and P309, conserved in almost all known plant LOXs. Contrary to other plant LOXs, the additional domain in LiLOX was found to be composed of 116 residues following the conserved L297, Y298. Although CrLOX does not have the conserved LY residues, the same long domain composed of 136 residues was observed.

|	
1. N. punctiforme LOX1 (9R)	
2. Cyanothece LOX1 (9R)	
3. F. oxysporum LOX (13S)	
4. G. graminis Mn-LOX (13R)	
5. M. oryzae Mn-LOX (9R)	
6. C. reinhardtii	
7. L. incisa LOX (13S)	
8. O. sativa LOX2 (13S)	
9. O. sativa LOX (13S)	
10. A. thaliana LOX2 (13S)	
11. S. tuberosum LOX (13S)	
12. P. patens LOX1 (13S)	
13. P. patens LOX2 (13S)	
14. P. patens LOX7 (13S)	
15. A. thaliana LOX6 (13S)	
16. S. tuberosum LOX2 (13S)	
17. A. thaliana LOX3 (13S)	
18. A. thaliana LOX4 (13S)	
19. G. max LOX4 (13S)	
20. G. max LOX3 (9/13S)	
21. G. max LOX1 (13S)	
22. G. max LOX2 (9/13S)	
23. A. thaliana LOX5 (9S)	
24. A. thaliana LOX1 (9S)	
25. S. tuberosum LOX (9S)	
26. P. patens LOX5 (13S)	
27. P. patens LOX6 (13S)	
28. P. patens LOX3 (13S)	
29. P. patens LOX4 (13S)	
30. G. fructosovora LOX (11R)	
31. P. homomalla LOX (8R)	
32. H. sapiens LOX (12S)	
33. H. sapiens LOX (15S)	
34. H. sapiens LOX (5S)	
35. H. sapiens LOX2 (15S)	
36. H. sapiens LOX (12R)	
37. Cyanothece LOX2 (9R/11R)	
38. N. punctiforme LOX2 (13S)	
39. B. thailandensis (13S)	
40. P. aeruginosa LOX (15S)	
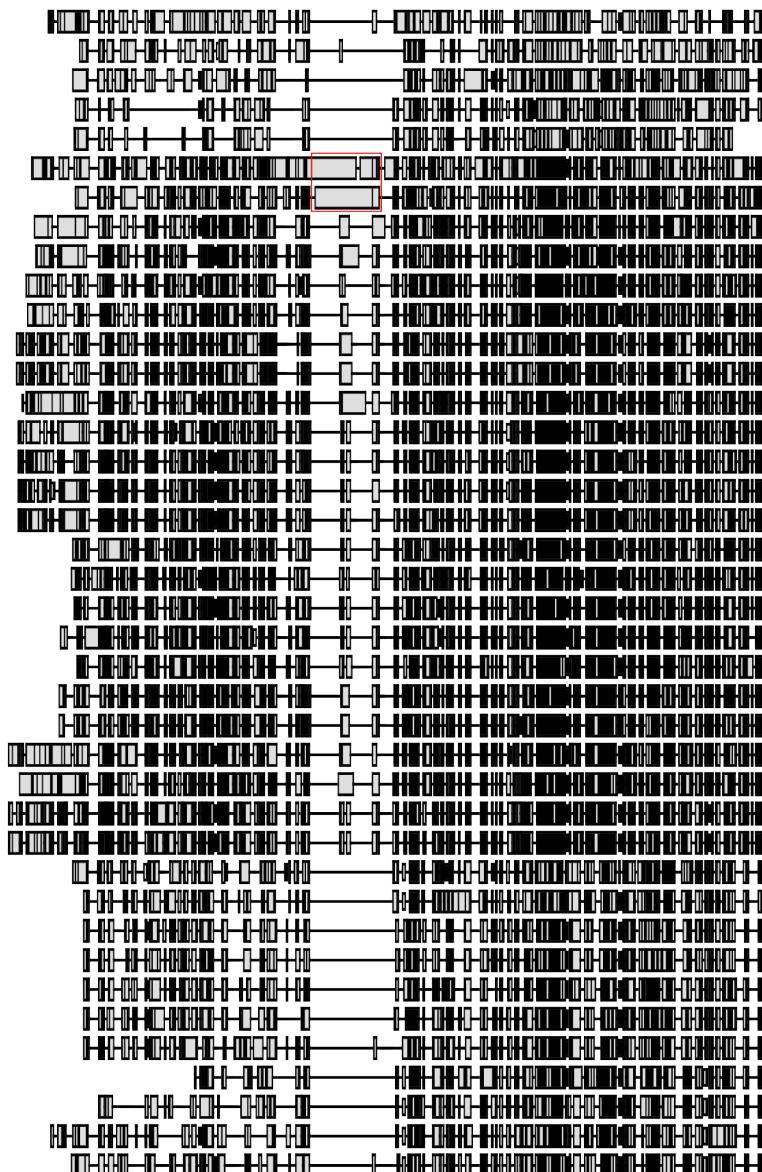
Figure 10. Allignment of 40 LOX protein sequence. Allignment obtained from the software Geneious, Muscle allignment with default parameters. LOXs accession numbers are as indicated in Figure 8.

62

4.1.4. LiLOX structure prediction

To further attest the likelihood that LiLOX is a functional LOX, its 3 dimensional structure was predicted based on the published structure of GmLOX1 (Youn *et al.*, 2006), using the online software Phyre2 (Kelley *et al.*, 2015). The predicted structure obtained was superimposed with the published crystal structure from PaLOX (Garreta *et al.*, 2013) and PhLOX (Neau *et al.*, 2014). In all cases, the five amino acid residues suspected to bind the iron were found in prefect concordance with the iron atom (Figure 11).
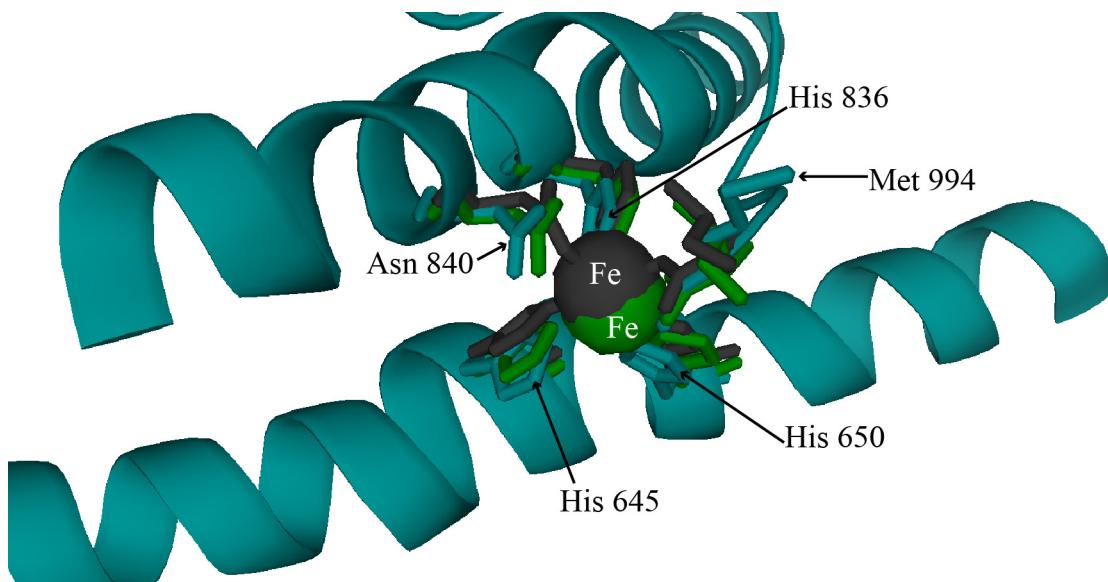
Figure 11. Structural superimposition of the predicted active site of LiLOX with *P. homomalla* LOX (PhLOX, PDB accession number: 4QWT), and *P. aeruginosa* LOX (PaLOX, PDB accession number: 5IR5). The three structures were aligned to one another by the software PyMOL. Focus was made on the two α-helices and the C-terminal region of LiLOX (cyan cartoon), harboring the residues involved in iron binding of LiLOX (cyan sticks, labeled with black arrows). Iron binding of PhLOX: green sticks and sphere, white label. Iron binding of PaLOX: Black sticks and sphere, white label.

4.2. LiLOX is found to be upregulated under nitrogen starvation.

Green algae undergo drastic lipid modifications when grown under nitrogen starvation (Khozin‑Goldberg *et al.*, 2002; Zienkiewicz *et al.*, 2016). In order to identify lead actors of this remodeling, the transcriptome of *L. incisa* cell cultures in stationary phase as well as undergoing 12 h and 72 h of nitrogen starvation was subject to investigation (Tourasse *et al.,* NCBI GEO, GSE94666). The transcripts of LiLOX were found to be accumulating 3.78 fold (log2Fold) upon 72 hours of nitrogen starvation.

Table 37. LiLOX transcript levels after 12h or 72h of nitrogen starvation with normal light (NL) or high light (HL) compared to growth in medium supplied in nitrogen (control). LiLOX accession number g6219, NCBI GEO [https://www.ncbi.nlm.nih.gov/geo], GSE94666.

Conditions compared	FoldChange	log2FoldChange
Control vs Nitrogen starvation 12h (NL)	2.08	1.06
Control vs Nitrogen starvation 72h (NL)	13.78	3.78
Control vs Nitrogen starvation 72h (HL)	10.36	3.37

This result seems to be in agreement with the identification as LOXs, since this class of enzyme are known to be highly involved in the production of signaling molecules (Feussner & Wasternack, 2002) as well as general lipid metabolism (Meyer *et al.*, 2013; Rudolph *et al.*, 2011; van Leyen *et al.*, 1998). In order to confirm this finding, *L. incisa* cells were cultivated in medium supplemented in nitrogen (BG11 medium) (until d0) before being transferred in a medium depleted in nitrogen (BG11N- medium, from d0 to d7), and transferred back to fresh BG11 medium at d7 (experiment was performed by Dr. Heike Siegler). The levels of LiLOX transcripts were measured at different time points (6 h, 1 d, 3 d, 7 d after nitrogen starvation, as well as 6 h, 1 d and 3 d after nitrogen resupply). After 3 days of nitrogen starvation, *L. incisa* accumulated LiLOX transcript 6.3 fold comparted to day 0 (Fold change, Figure 12). This level remained at its maximum during the whole period of starvation. Six hours after nitrogen resupply (day 7) the transcript level of LiLOX dropped to its level from day 0. Transcripts of LiLOX at day 8 and day 10 remained at this low level, suggesting a strong dependency to the nitrogen supply.
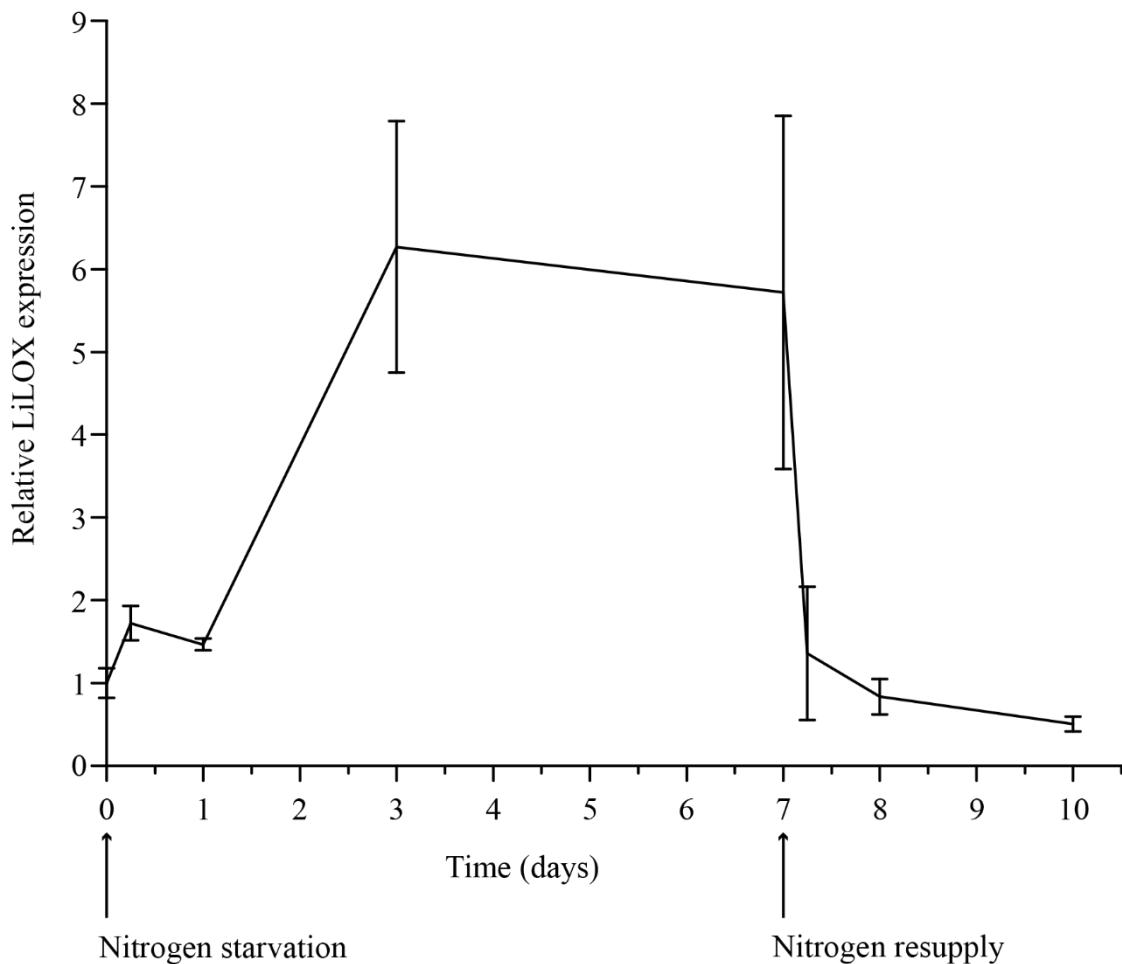
Figure 12. Time course of LiLOX transcript levels during nitrogen starvation. Real-time quantitative-PCR was performed using cDNAs from *L. incisa* grown under nitrogen depleted conditions for seven days. At day seven algae were transferred to medium containing nitrogen. Ribosomal protein S21 expression was used as standard. Expression is shown relative to time point 0 and error bars represent the standard error of the mean for three batches cultivated in parallel in a single experiment. This experiment was performed by Dr. Heike Siegler.

In addition to the transcript levels, Dr Heike Siegler performed a proteomic assay on *L. incisa* (Siegler, 2016) after 3 days of nitrogen starvation. This proteomic assay revealed six peptides covering LiLOX protein sequence (supplemental figure 10), confirming the presence of LiLOX at the protein level under this type of stress.

4.3. LiLOX localizes in the plastids of onion epithelial cells.

As LiLOX showed highest homology to plastidial LOX (Figure 8), its subcellular localization was investigated. Since attempts to transform cells of *L. incisa* with high efficiency remained unsuccessful, onion epithelial cells were chosen as model system to investigate the subcellular localization of LiLOX by confocal microscopy. The acyl carrier protein (ACP) from *A. thaliana* fused to the eCFP was chosen for co-localization, as the ACP is known to be localized in the plastid, and to harbor a plastidial signal peptide (Kunst *et al.*, 1988). As expected, the onion cells transformed with ACP-eCFP showed fluorescence signals inside small organelles, the proplastid from these onion cells (Figure 13). LiLOX fused to the yellow eYFP was found to also localize in small organelles, confirmed to be the proplastids by co-localization with the reporter ACP-eCFP (Figure 13C and D).
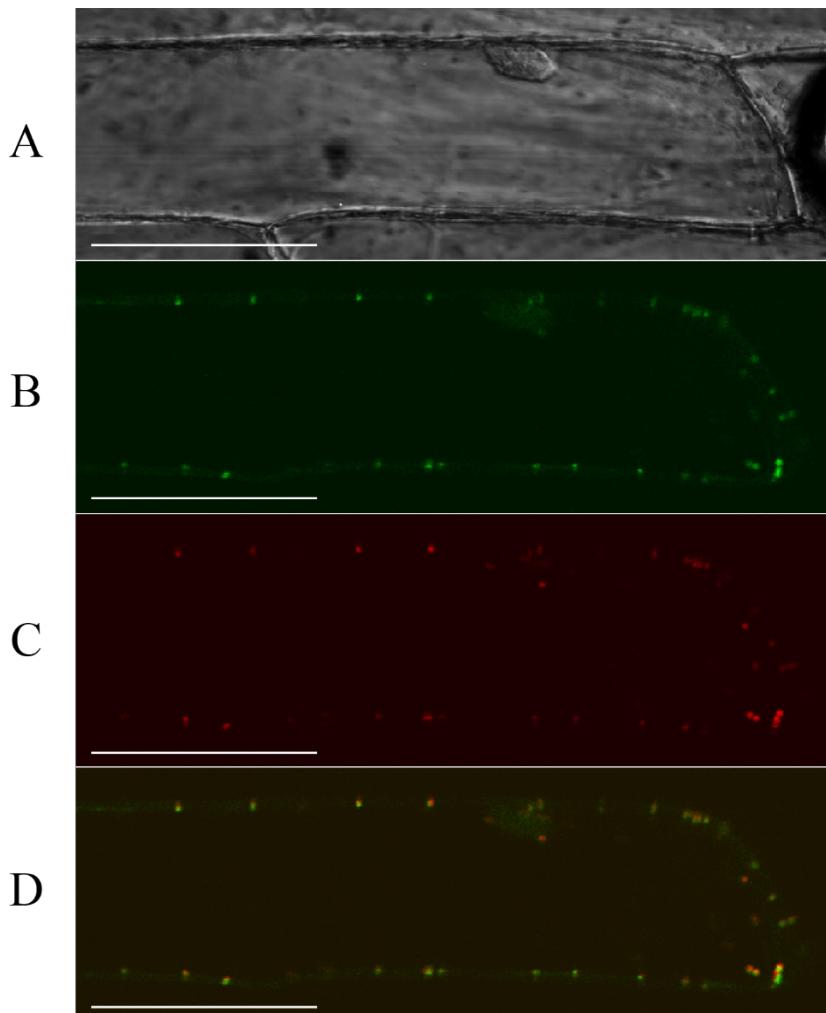
Figure 13. Subcellular localization of LiLOX yellow fluorescence fusion protein (LiLOX-eYFP). Confocal microscopy of epithelial onion cell co-transformed with LiLOX-eYFP and acyl carrier protein fused to cyan fluorescence protein (ACP-eCFP). **A.** Bright field; **B.** LiLOX-eYFP; **C.** ACP-CFP; **D.** Merged signals of LiLOX-eYFP and ACP-eCFP. All 10 cells analyzed from a single experiment showed comparable results. White Bar: 100 μm.

4.4. Heterologous expression of LiLOX

For biochemical and enzymatic characterization, large amounts of active protein were necessary. For this purpose, it was decided to express LiLOX heterologously in *E. coli*. Yet since plastidial proteins harbor a signal peptide that is cleaved during the transport into the plastid, the length of this signal peptide was predicted via the bioinformatics tool ChloroP (Emanuelsson *et al.*, 1999), supplemental Figure 10). LiLOX was cloned without the 62 amino acids corresponding to the putative signal peptide, replaced by six histidines for affinity chromatography. This version of LiLOX was used for all heterologous expressions in *E. coli* regarding protein purification.

4.4.1. LiLOX purification

For protein purification, LiLOX was usually expressed heterologously in *E. coli*, grown in auto-induction medium for 42 hours at 16°C. After a preliminary purification by immobilized metal affinity chromatography (IMAC) and size exclusion chromatography (SEC) using TRIS buffer pH 8, a thermal shift essay was performed to determine the best condition for the stability of LiLOX *in vitro*. Freshly purified LiLOX was diluted in buffer systems of different pHs, and tested for resistance to heat treatment. The presence of dye which binds all hydrophobic surfaces highlighted the protein denaturation in each samples (Ericsson *et al.*, 2006). As the HEPES buffer pH 8.4 was the condition leading to highest stability of LiLOX (data not shown), it was used as a standard buffer system for all purifications.

After heterologous expression, LiLOX represented the main protein in the lysate of *E. coli* (Figure 14B). Affinity chromatography via IMAC was used to further purify LiLOX, increasing the ratio between LiLOX and all other proteins. Furthermore, SEC allowed to remove other undesired proteins from the lysate, as well as LiLOX proteins in aggregated form. The SEC chromatogram revealed that almost all LiLOX proteins were present in the same oligomeric state, eluted around 130 mL (Figure 14A). The very low amount of aggregated protein eluting in the void volume (from 100 mL to 110 mL) confirmed the high stability of LiLOX in HEPES buffer pH 8.4. The SDS-PAGE showed that almost all of the other protein from the lysate of *E. coli* were removed by the two purification steps. Expression as well as purification of LiLOX was highly reproducible, as the SEC chromatogram and SDS-PAGE were representative for at least five independent experiments.
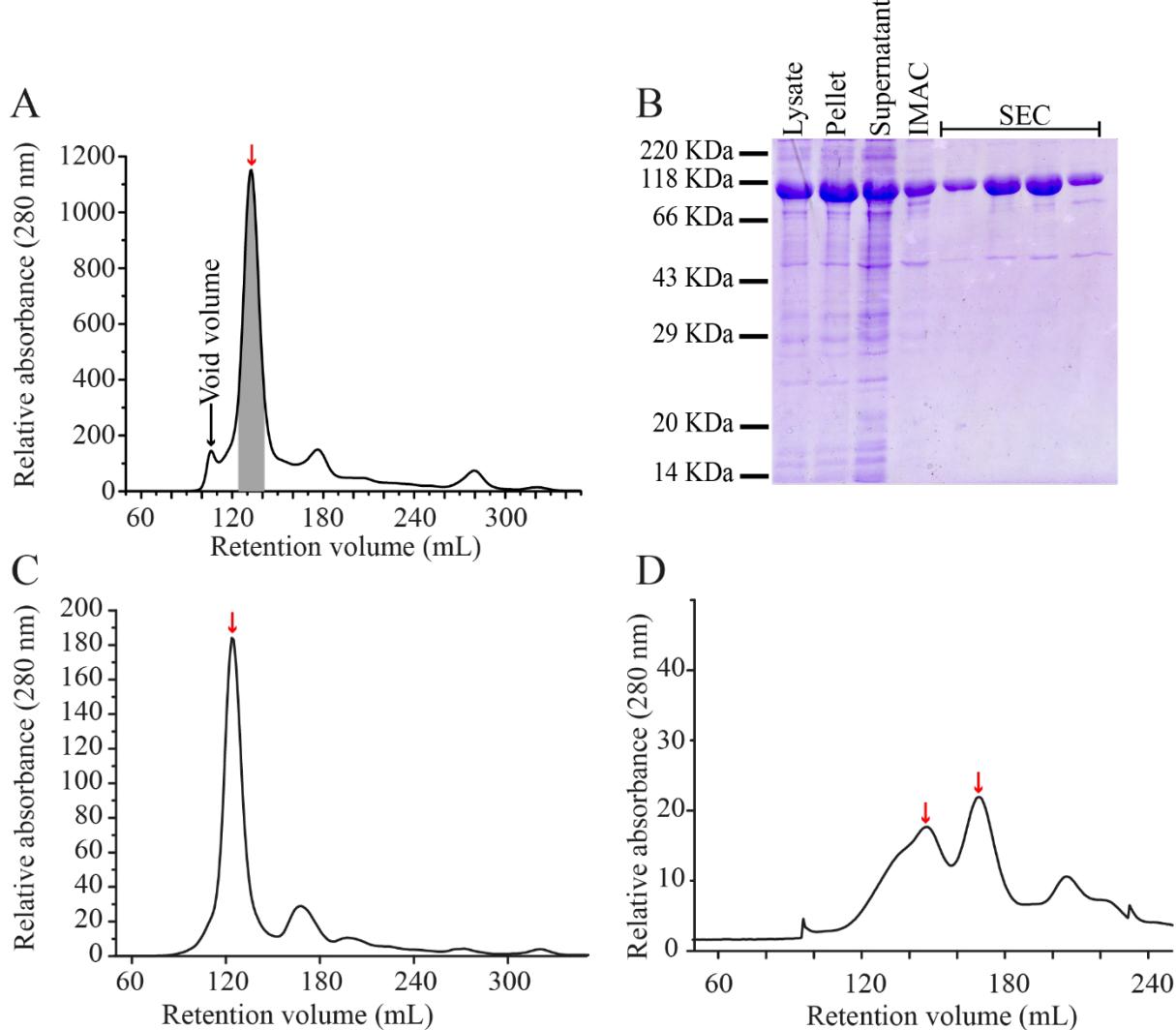
Figure 14. Purification of *L. incisa* lipoxygenase (LiLOX). LiLOX cloned without the N-terminal putative signal peptide and fused to an N-terminal His-tag was heterologously expressed in *E. coli* BL21 star cells. After expression in auto-induction medium, cells were disrupted by sonication. LiLOX was purified by Immobilized Metal Affinity Chromatography (IMAC) and size exclusion chromatography (SEC). All SEC were performed on HiLoad 26/60 Superdex S200 SEC-column (GE Healthcare, USA). The red arrows represent fractions in which LOX activity was detected. **A.** SEC in 20 mM HEPES buffer pH 8.5; 100 mM sodium chloride and 2 % glycerol. The chromatogram shows the absorption at 280 nm during elution, the grey area indicates the 4 fractions containing detectable LiLOX activity. **B.** SDS-PAGE, illustrating the proteins of the *E. coli* lysate, supernatant and pellet fractions, IMAC fraction as well as the four SEC fractions from Figure A containing LiLOX. Protein purification performed at least five times gave comparable results. **C.** SEC in 20 mM HEPES buffer pH 8.5; 500 mM sodium chloride and 10 % glycerol. **D.** SEC in 20 mM TRIS buffer pH 8; 500 mM sodium chloride and 10 % glycerol. SEC represented by Figure C and D were performed once.

As the gel filtration separates proteins according to their sizes, an analytical SEC was used to estimate the oligomeric state of LiLOX. A calibration sample containing a mixture of five proteins of known molecular weight was run through the SEC Superdex 200 10/300 GL (GE Healthcare, Germany). From their elution volume a calibration curve was determined (Supplemental Figure 1). Since LiLOX was expressed without the signal peptide and with a tag of six histidines (His-tag), its theoretical molecular weight was calculated to be 107.2 kDa,

which leads to an expected elution at 13.5 mL retention volume. As the retention volume of LiLOX was 10.0 mL, its native molecular weight was determined to be 596.8 kDa, suggesting that LiLOX protein formed preferentially oligomers.

Attempts were made in order to elute LiLOX as a monomer, using higher ionic strength and high concentration of glycerol. When using the same HEPES buffer pH 8.4 with 500mM sodium chloride and 10 % of glycerol, no difference was observed in the retention volume of the protein. Only when using TRIS Buffer pH 8 with 500 mM sodium chloride and 10 % glycerol was LOX activity was detected in fractions collected with retention volume of 145 mL and 175 mL (red arrows, Figure 14D), confirming its oligomeric state in HEPES buffer pH 8.4.

4.5. Crystallography

Although plastidial LOXs from flowering plants have been known to trigger the biosynthesis of JA for decades, very little is known about their enzymology and structure as none has been crystallized successfully. Therefore if solved, the 3D structure of such a LOX would represent a valuable information, yet remains a challenge in the field. One main limiting factor for crystallization screens of plastidial LOXs is the yield after purification following heterologous expression in *E. coli* (Dr. Ellen Hornung, personal communication). As mentioned above, LiLOX could however be purified in milligram quantities. Moreover LiLOX was shown to be plastidial, and phylogenetic analysis highlighted significant similarities in the protein sequences with plastidial plant LOXs. Altogether, LiLOX seemed to constitute a good model for this class of enzyme and its crystallization was attempted.

4.5.1. First screens

After being purified, LiLOX was stored in the gel filtration buffer, and concentrated to 7 µg of protein/µL. In order to try as many different conditions as possible, LiLOX was then tested in 12 different crystal plates and incubated at 20°C. After only 3 days, crystals of LiLOX were observed in two plates, in a surprisingly high number of conditions. Yet, despite this high number, crystals were rather small and stopped growing rapidly. None of the crystals showed a well-defined geometric shape. Moreover precipitated protein was observed in all conditions (Figure 15).
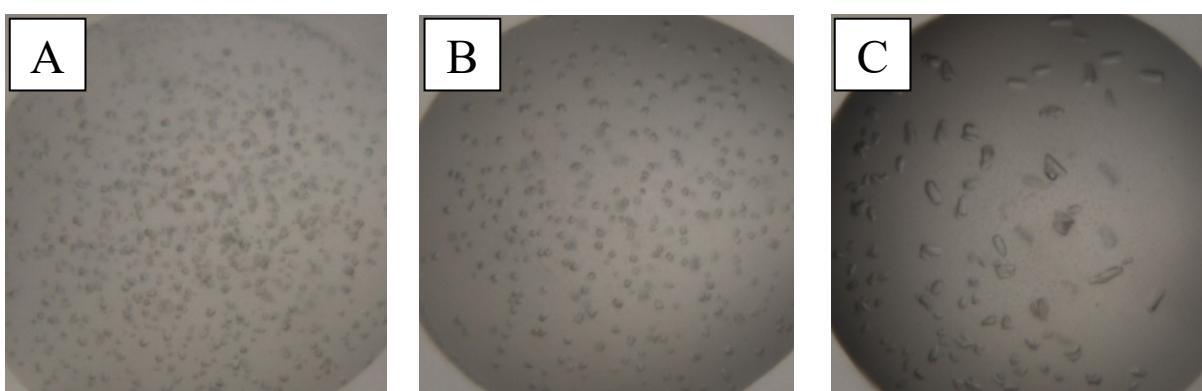
Figure 15. Three representative conditions from commercially available Morpheus (Molecular dimensions, F. Gorrec, 2009) and *ProPlex* (Molecular dimensions) crystal screen leading to crystallization of *L. incisa* lipoxygenase (LiLOX) after 3 days. **A.** 0.03 M sodium nitrate; 0.03 M disodium hydrogen phosphate; 0.03 M ammonium sulfate; 0.1 M Bicine/Trizma base pH 8.5; 10 % (w/v) PEG 8 000; 20 % (v/v) ethylene glycol (Morpheus screen, C10). **B.** 0.2 M 1,6-hexanediol; 0.2 M 1-butanol; 0.2 M (RS)-1,2-propanediol; 0.2 M 2-propanol; 0.2 M 1,4-butanediol; 0.2 M 1,3-propanediol; 0.1 M Bicine/Trizma base pH 8.5; 10 % (w/v) PEG 8 000; 20 % (v/v) ethylene glycol (Morpheus screen, D10). **C.** 0.1 M sodium chloride; 0.1 M Tris pH 8; 8 % (w/v) PEG 20 000 (*ProPlex* screen, F5).
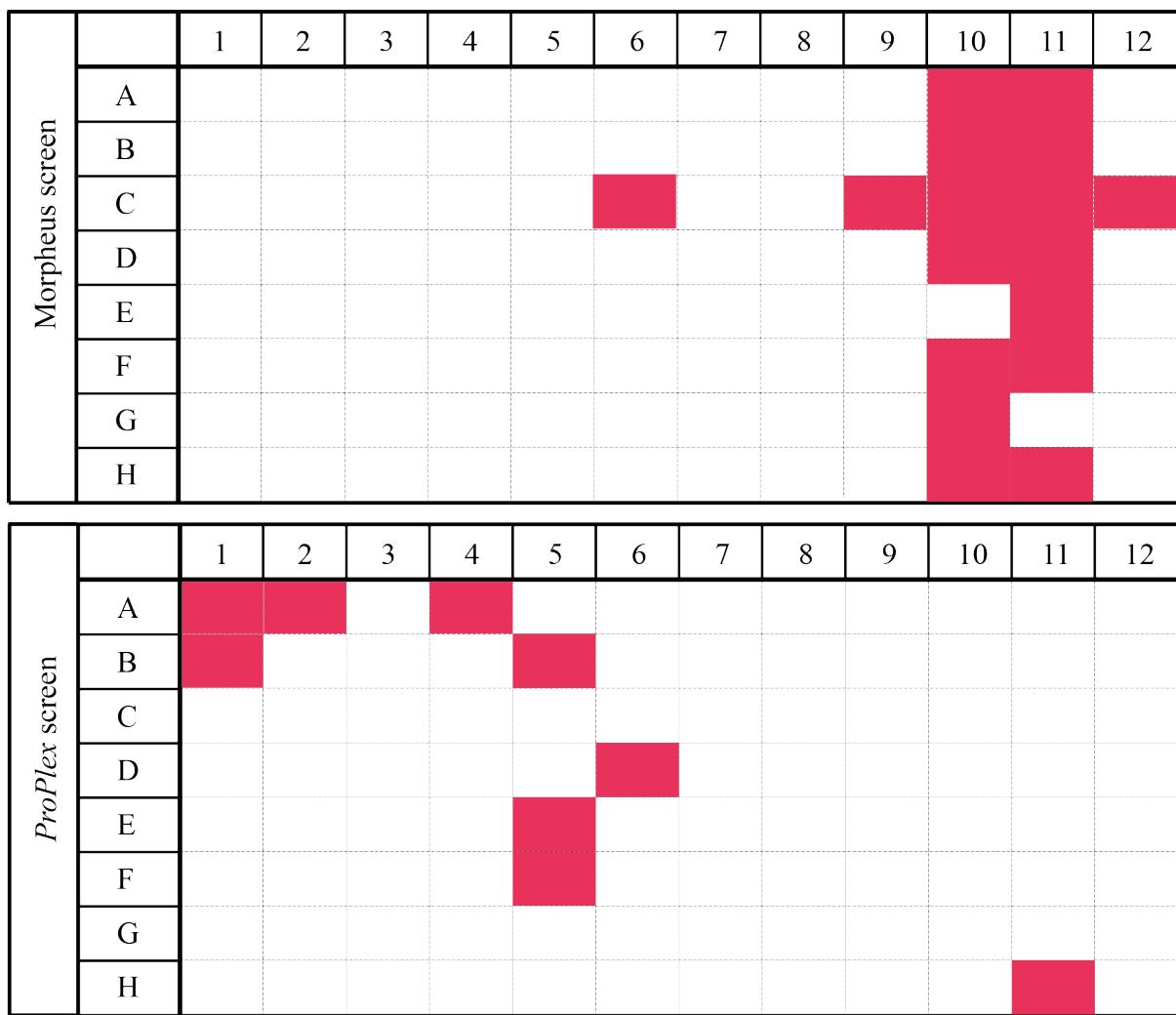
Figure 16 All conditions of the commercially available crystal screens leading to crystallization of LiLOX **A.** Morpheus (Molecular dimensions, F. Gorrec, 2009) and **B.** *ProPlex* (Molecular dimensions). Letters A to H and numbers 1 to 12 correspond to those from the corresponding commercially available screen. Red squares highlight the conditions which lead to crystallization of LiLOX after 3 days.

In order to improve the stability of the protein, the crystal integrity as well as their size, an optimization screen was performed. Conditions that lead to the best crystals were reproduced while varying slightly each parameter. The high number of positive hits (Figure 16) allowed to draw a fine picture for the ideal conditions leading to LiLOX's crystallization. Although pH of either 8 or 8.5 represented only 27 % of all conditions, 80 % of all positive hits were obtained at these pHs, all of which contained TRIS buffer. PEG also seemed to be an effective LiLOX precipitant, as 99% of the positive hits contain one form of PEG. Of course the representation of PEG is high in both of these screens (84 %), but out of 30 conditions without PEG (Figure 16B, from F7 to H12) only one led to LiLOX crystals. As observed with the Morpheus screen the additives did not seem to have a high importance, as crystals were observed in every singles lines of columns 10 and 11, each of which having a different additive.

4.5.2. Screen optimization

At this point, crystal screens were performed with fixed TRIS buffer, either pH = 8 or 8.5. Screens were varying in LiLOX concentration, PEG type, PEG concentration and drop size. Although crystals were observed in almost all tested conditions, their small size as well as a high irregularity in the crystal shapes prevented any diffraction. Irregularity could be explained as crystals were formed rather quickly, as soon as 2 hours after pipetting. Moreover, precipitated protein was observed in each drop, and nucleation was also very high (minimum 50 crystals per drop), confirming that the crystallization might be happening too fast. In order to increase ionic strength and possibly LiLOX solubility, sodium chloride was added with concentrations varying from 0 to 0.5 M, with the objective to lower the protein precipitation,
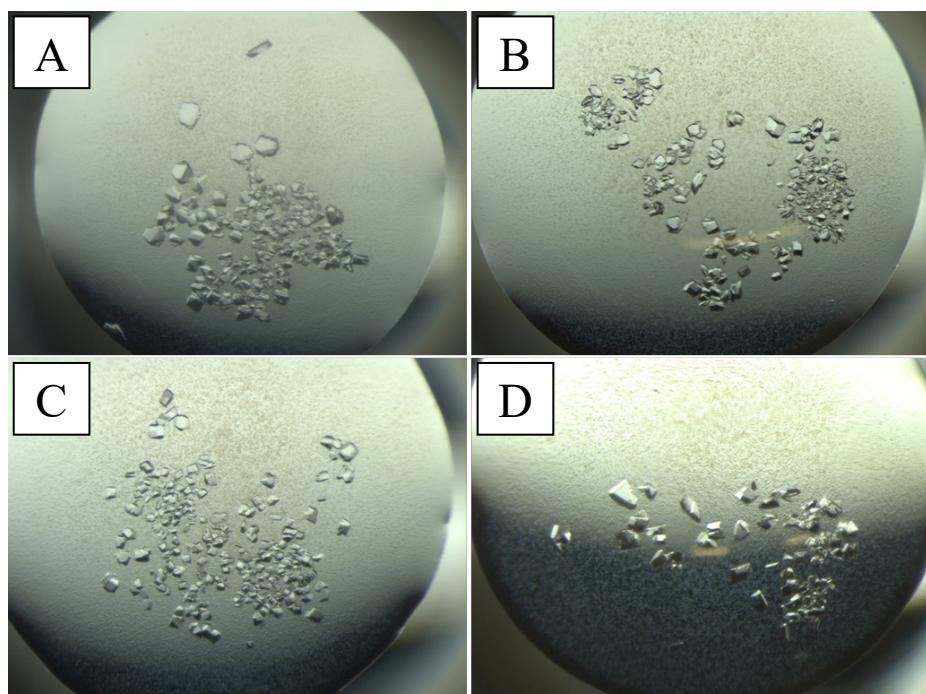
Figure 17. Crystals of LiLOX from optimized screens. **A-D.** Crystals of LiLOX grown for 2 days at 20°C, 3 µL sitting drop and vapor diffusion. Reservoir: 0.1 M TRIS pH 8; 0.1 M sodium chloride; 8 % (w/v) PEG 20 000.

lower the nucleation, and improve crystal growth. The following set of conditions was the one resulting in the best shaped crystals: 0.1 M TRIS pH 8; 0.1 M NaCl; 8 % (w/v) PEG 20 000, drop size 3 µL (Figure 17). Finally, although the general shape and size of crystals was improved, the best one ever obtained diffracted with a resolution of 4 Å, which did not allow to solve the structure of LiLOX down to the level of amino acids side chains.

4.6. Activity of LiLOX towards FFA

The LOX reaction induces the conjugation of double bonds in pentadiene systems of PUFAs. Such system will absorb light with a maximum at 234 nm, and consequently the LOX reaction can be followed spectrophotometrically by measuring the increase of absorbance at this wavelength.

4.6.1. pH optimum

Since 20:4 (n-6) is the major PUFA in *L. incisa* (Khozin‑Goldberg *et al.*, 2002), the pH optimum of LiLOX was measured recording the initial speed of the reactions with this FFA at varying pH (Figure 18). As LiLOX is known to be located in the chloroplast and suspected to be in the stroma, the optimum pH is expected to be around 8. Therefore activity was first tested with pH varying from 5.5 to 9.5. Bis-TRIS propane buffer was selected as it covers this range of pH. Moreover it does not absorb light at 234 nm, contrary to the regular Bis-TRIS buffer. In Bis-TRIS propane buffer, LiLOX was measured to have the highest activity at pH 7.5 towards 20:4 (n-6). From this point on all LiLOX reactions *in vitro* were measured in Bis-TRIS propane buffer, at pH 7.5.
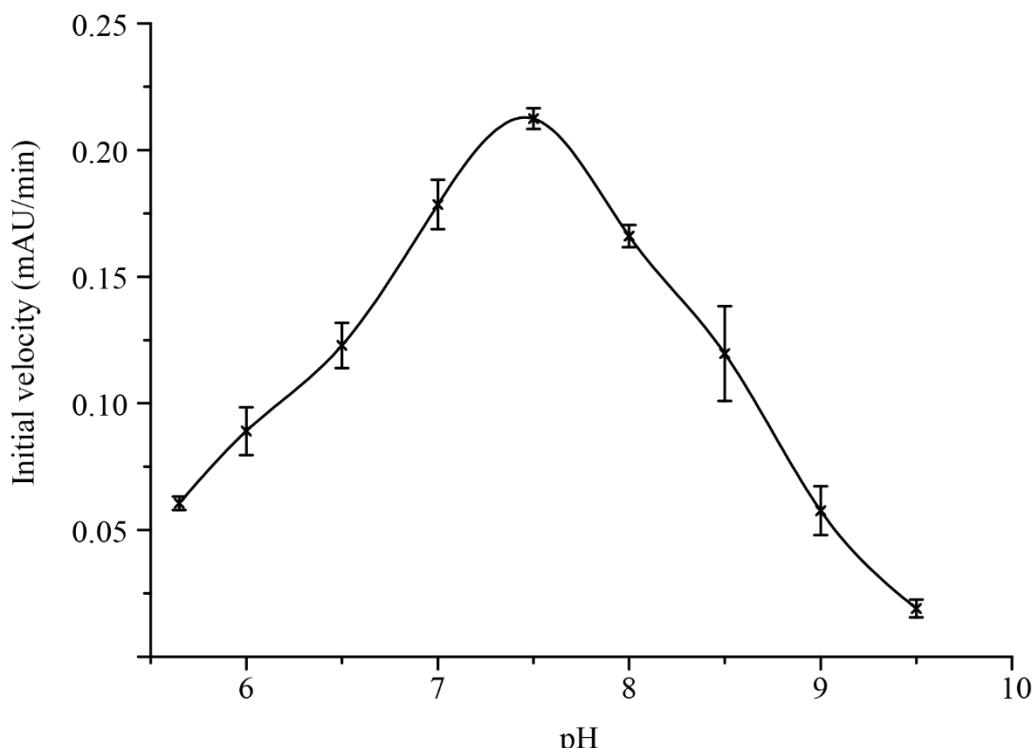
Figure 18. Optimum pH of LiLOX. The free fatty acid 20:4 (n-6) was used as substrate at a concentration of 100 μM. 20 mM Bis-TRIS propane was used as buffer. 1 μg of pure LiLOX was used for determine the initial slope of the LiLOX activity at a given pH. The reaction was detected as increase of absorbance at 234 nm. Error bars represent the standard deviation of three replicates.

4.6.2. Kinetic parameters

All LOXs are known to oxidize the pentadiene system of polyunsaturated FFA. Yet a great variability of polyunsaturated FFA exists in term of chain length as well as degree and position of unsaturation. To determine the kinetic parameters of LiLOX, polyunsaturated acyl chains present endogenously in *L. incisa* were chosen as substrates in the form of FFA.

Due to a sigmoidal shape (Figure 19) the kinetic measurements of LiLOX with 18:3 (n-3) did not fit the Michaelis-Menten equation. Such a shape suggested a cooperative behavior of enzyme subunits (Monod *et al.*, 1965; Weiss, 1997) and seems to confirm the oligomeric state of LiLOX found by SEC Figure 14. This sigmoidal shape was obtained with three independent enzyme preparations. Instead of the Michaelis-Menten equation, the Hill equation was used to determine the kinetic parameters of LiLOX with all substrates (both equations are shown in supplemental Figure 2).The calculation of kinetic parameters revealed that LiLOX has the highest turnover rate ($k$cat) towards 18:3 (n-3) (Figure 19, Table 38), which is more than twice as high as the $k$cat for 18:2 (n-6). Despite such a high turnover rate, the affinity of LiLOX towards 18:3 (n-3) was found to be the lowest of all tested FFA with a K_M of 55.5 µM, four times higher than with 20:4 (n-6). Nevertheless, the catalytic efficiency ($k$cat/K_M) was found by far the highest with 18:3 (n-3), confirming the preference of LiLOX towards this substrate. The reaction of LiLOX with the FFA 16:3 (n-3) was surprising, as it fitted neither Michaelis-Mentens nor the Hill equation. With a 16:3 (n-3) concentration between 0 µM and 100 µM, the reaction rate of LiLOX was almost not detected, yet it increased with substrate concentration above 100 µM despite the formation of micelles. Nevertheless, this result suggested a very low affinity of LiLOX for this substrate. In presence of both FFA belonging to the group of n-6 PUFAs, LiLOX did not seem to display a strong cooperative behavior, as the Hill coefficient was below 2. With these two substrates, the affinity of LiLOX was also found to be higher and the turnover lower than with 18:3 (n-3). Finally, as LiLOX was found to oxidize all tested FFAs, further investigations were performed in order to determine the oxidation products of LiLOX.
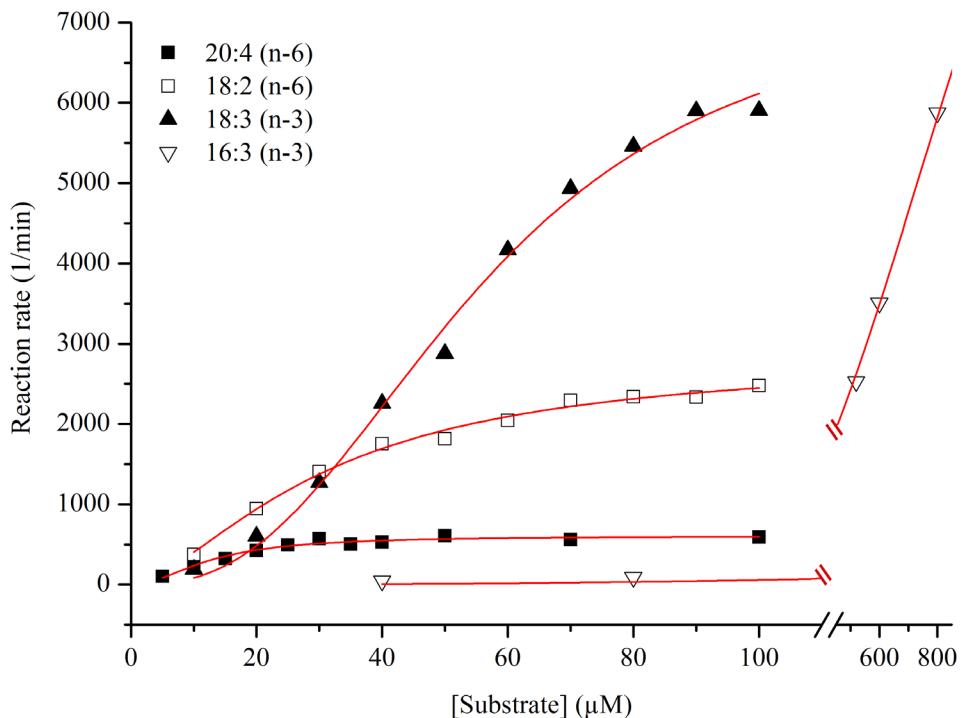
Figure 19. Kinetic plots for polyunsaturated free fatty acids (PUFAs) conversion by LiLOX. The FFAs 20:4 (n-6), 18:2 (n-6), 18:3 (n-3), and 16:3 (n-3) were used as substrate at a concentration from 10 µM to 100 µM (respective 800 µM for 16:3 (n-3)). 20 mM Bis-TRIS propane was used as buffer pH 7.5, 1 µg of pure LiLOX was used to determine the initial slope of LiLOX activity at a given substrate concentration. The reaction was detected as increase of absorbance at 234 nm at 30 °C. For the PUFA 18:3 (n-3), each point represents the mean value of three reactions. Each reaction was performed with different enzyme preparations. For the PUFAs 18:2 (n-6) and 20:4 (n-6), each point represent the mean value of 2 replicates.

Table 38. Overview of the kinetic parameters for PUFAs conversion by LiLOX. The FFAs 20:4 (n-6), 18:2 (n-6), 18:3 (n-3) and 16:3 (n-3) were used as substrate at a concentration from 10 to 100 µM (respective 800 µM for 16:3 (n-3)). 20 mM Bis-TRIS propane was used as buffer. 1 µg of purified LiLOX was used to determine the initial slope of the LiLOX activity at a given substrate concentration. The reaction was detected as increase of absorbance at 234 nm at 30 °C. All kinetic parameters were determined using the software tool OriginPro8.5. Data derived from the analysis shown in Figure 19.

	$k$cat (min^{-1})	Standard deviation	K_M (µM)	Standard deviation	$k$cat/K_M (µM^{-1}.min^{-1})	Hill coefficient	Standard deviation
16:3 (n-3)	Did not fit the Hill equation						
18:2 (n-6)	**2834.92**	157.67	**31.16**	2.78	**90.98**	**1.58**	0.16
18:3 (n-3)	**7432.84**	574.41	**55.55**	4.10	**133.80**	**2.61**	0.28
20:4 (n-6)	**606.06**	27.25	**12.64**	1.1	**47.95**	**1.96**	0.31

4.7. Analysis of LiLOX products by HPLC

Although the natural LOX products are hydroperoxides, they were chemically reduced to their more stable hydroxide forms before being analyzed. Since during a LOX reaction, different regioisomers and stereoisomers may be possible, the final hydroxides obtained were sequentially analyzed by HPLC. The SP-HPLC was used to separate and purify all regioisomers derived from a substrate. Absorbance was recorded at 202 nm and 234 nm, in order to detect the FFA substrate and hydroxide products respectively.

Thereby it was determined that LiLOX oxidized the FFAs 20:4 (n-6), 18:3 (n-3), 18:3 (n-6), 18:2 (n-6) and 16:3 (n-3) preferentially into 15-hydroperoxyeicosatetraenoic acid (15-HPETE), 13-αhydroperoxyoctadecatrienoic acid (13-αHPOTE), 13-γhydroperoxyoctadecatrienoic acid (13-γHPOTE), 13-hydroperoxyoctadecadienoic acid (13-HPODE) and 11-hydroperoxyhexadecatrienoic acid (11-HPHTE), respectively (Figure 20, Table 39). These results suggested a dioxygen insertion into the fatty acid backbone counting from the methyl end since LiLOX oxidized all FFA preferentially at the n-6 position.

All major products observed on SP-HPLC were collected and run on CP-HPLC to determine their chiral configuration. Analysis by CP-HPLC revealed that all LiLOX products had *S* configurations, proving that oxidations were due to the enzymatic activity of LiLOX, since non-enzymatic oxidation would lead to a racemic mixture. Furthermore, this finding is also consistent with the fact that the different FFAs are all inserted the same way in the active site with their methyl end first, as the oxygen is likely to be inserted from the same direction (Figure 21) and confirms the prediction made via the Coffa position (Figure 9). Altogether, these results showed that LiLOX is a linoleate 13*S*-LOX and an arachidonate 15*S*-LOX.
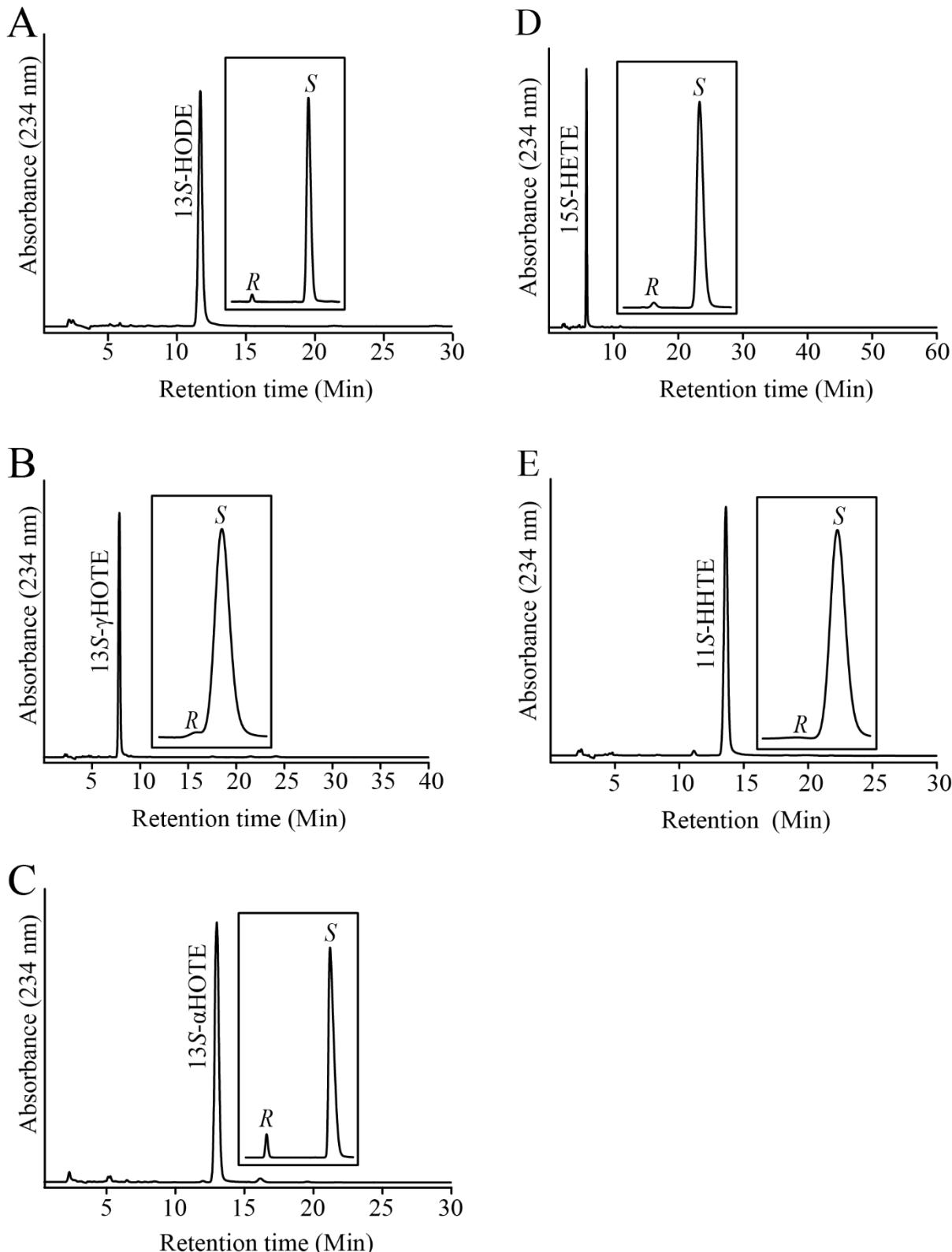
Figure 20- Identification of product regioisomers and stereoisomers of LiLOX products. The reaction mixture contained 1 µg of purified LiLOX in 20 mM Bis-TRIS propane buffer pH 7.5 and 100 µM of FFA. Reactions took place for 1 h at room temperature with open tubes. Products were reduced by sodium borohydride for 10 minutes at room temperature. **A-E.** SP-HPLC chromatogram of LiLOX products derived from the following FFA acid substrates: **A.** 18:2 (n-6); **B.** 18:3 (n-6); **C.** 18:3 (n-3); **D.** 20:4 (n-6); **E.** 16:3 (n-3). Results shown are representative for three experiments. Each experiments was performed with different enzyme preparations. For each main product, the respective chromatogram of the Chiral Phase CP-HPLC is represented in the corresponding box, representative of one measurement. Stereoisomers 11*R*-HHTE/11*S*-HHTE and 11*R*-HHDE/11*S*-HHDE were self-assigned. All LiLOX products were detected at 234 nm.

Table 39. Products formed by LiLOX activity from PUFAs. The reaction mixture contained 1 µg of purified LiLOX in 20 mM Bis-TRIS propane buffer pH 7.5 and 100 µM of FFA. Reactions took place for 1 h at room temperature with open tubes. Products were reduced by sodium borohydride for 10 minutes at room temperature. Analyzed and purified by straight phase (SP)-HPLC, results representative for three experiments. Each experiments was performed with different enzyme preparations. Finally stereoisomers were analyzed by chiral phase CP-HPLC, results representative a single measurement. HHTE: hydroxyhexadecatrienoic acid, HETE: hydroxyeicosatetraenoic acid; HODE: hydroxyoctadecadienoic acid; HOTE: hydroxyoctadecatrienoic acid.

Substrat	Position Specificity (Chiral conformation)					
16:3 (n-3)	11-HHTE	7-HHTE	14-HHTE	10-HHTE		
	97.9 (100 % *S*)	2.1				
18:2 (n-6)	13-HODE	9-HODE				
	98.5 (97.9 % *S*)	1.5				
18:3 (n-3)	13-HOTE	12-HOTE	16-HOTE	09-HOTE		
	96.4 (100 % *S*)	3.6				
18:3 (n-6)	13-HOTE	10-HOTE	09-HOTE	06-HOTE		
	98.4 (97.8 % *S*)	0.6	0.9			
20:4 (n-6)	15-HETE	12-HETE	11-HETE	8-HETE	9-HETE	5-HETE
	99.4 (97.8 % *S*)	0.2	0.4			
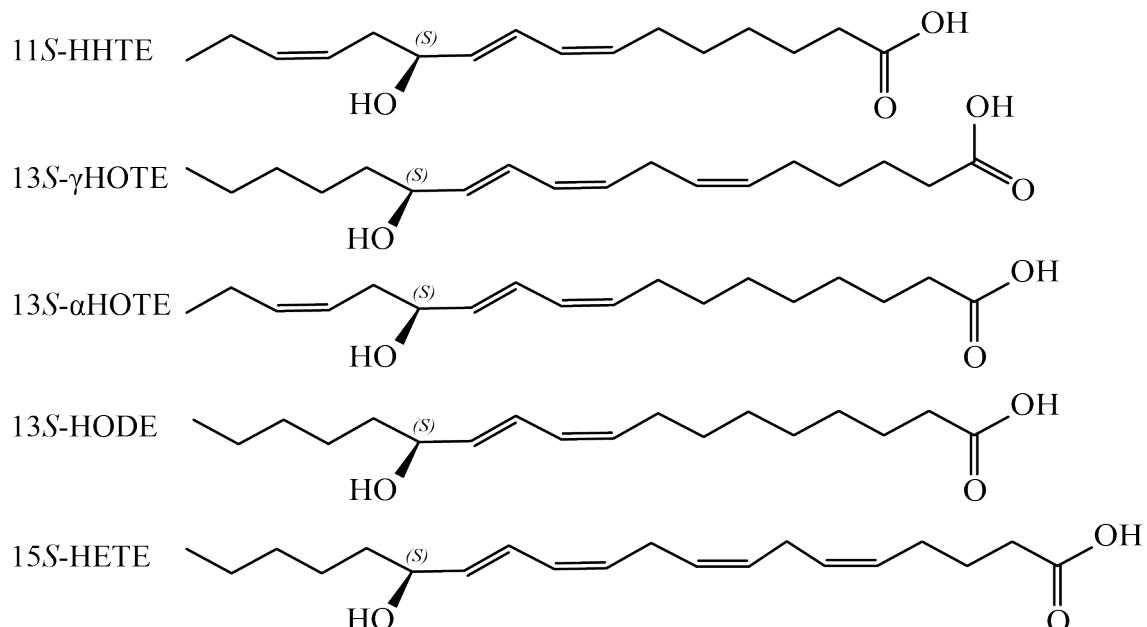
Figure 21. Formulas of the reduced LiLOX products.

The aims of the above sections were to characterize LiLOX *in silico* by protein sequence alignments and predicted 3D structure as well as *in vitro* by enzymatic assay monitored via spectrophotometer or HPLC. Although these data gave first valuable hints, nothing is yet

known on the endogenous role of LiLOX. Knowing the endogenous substrate of this enzyme would be an additional valuable information in this regard. Kinetic parameters gave a hint regarding the chain length and the degree of unsaturation preferred by LiLOX. However since FFAs are known to be present in very low quantities in the natural environment of LiLOX, the aim of the following experiments was to shed light on the favorite endogenous substrate of LiLOX.

4.8. LiLOX used on *L. incisa* lysate shows oxidation towards complex lipids.

To search for natural substrates present in *L. incisa* cells a so-called *ex vivo* non-targeted metabolome approach was performed together with Dr. Kirstin Feussner. The idea of the approach is to bring the heterologously expressed and purified enzyme back to its natural metabolite environment thereby identifying endogenous substrates via their respective products. In order to do so, *L. incisa* cells were cultivated with nitrogen (BG11 medium) for two days, a condition in which the expression level of LiLOX has been described to be very low (Figure 12). Therefore the putative substrates of LiLOX should occur in high amounts under this condition. Next the metabolites of *L. incisa* had to be extracted by two-phase extraction according to (Matyash *et al.*, 2008). Metabolites solved in the polar as well as in the non-polar extraction phase were combined and the semi-dry pellets were resolved in 20 mM Bis-TRIS propane buffer and incubated for 1 h, either with 5 µg of pure LiLOX or without enzyme (as negative control). As a positive control, the metabolite assay was performed with addition of 18:2 and 20:4 to the extracts. Therefore, the experimental setup consisted of four different conditions, two with LiLOX and two without LiLOX, each of them in 3 technical replicates. Samples treated with LiLOX were expected to be depleted in substrate(s), and to accumulate its product(s), contrary to the samples not treated with LiLOX to which they are compared.

After the LOX reaction, a non-targeted metabolome fingerprinting workflow was performed in positive and negative ionization mode without any further metabolite extraction. Data preprocessing steps provided big data matrixes, further processed by ranking, filtering, adduct correction, data merging and automated data base search with the software tool MarVis (Kaever *et al.*, 2015). Finally 1424 high quality features with a pVal $<10^{-3}$ were selected for clustering by one-dimensional self-organizing maps (1D-SOMs, Figure 22). The number of three clusters were used to present the data. Cluster one represents features for putative products, as it shows high intensities exclusively in the two conditions where LiLOX was present in the assay. On the other hand, cluster three represents features for putative substrates, present only in the two conditions in which no LiLOX was added. In cluster two, features of rather low signal intensity are summarized, which seemed to be impurities of the added FFA.
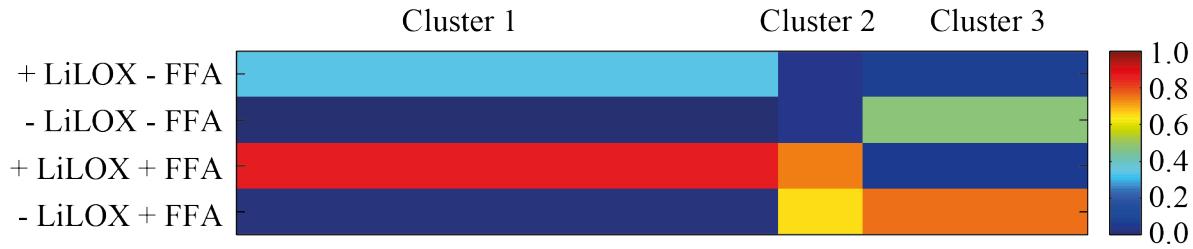
Figure 22. Non-targeted search for substrates and products of LiLOX. Total metabolite extract of *L. incisa* grown for 2 days in BG11 medium has been obtained by two-phase extraction according to Matyash *et al*. (2008). Metabolites of both phases were resolved in 20 mM Bis-TRIS propane buffer pH 7.5 and incubated for 1 h with 2 μg of pure LiLOX or without enzyme. As positive control the same assays was performed adding FFAs 20:4 (n-6) and 18:2 (n-6) as known LiLOX substrates. Non-targeted metabolome analysis by LC-MS analysis was performed in positive and negative ionization mode. 1424 features with a pVal < 10^{-3} were selected for clustering by one-dimensional self-organizing maps (1D-SOMs). **Cluster 1** represents features for putative products, while **cluster 3** represents features for putative substrates. The experiment was performed with three technical repetition. Non-targeted LC-MS analysis were performed by Dr. Kirstin Feussner.

4.8.1. Galactolipids

In the search for the endogenous substrates, a special focus was made on galactolipids, especially MGDG and DGDG as their fatty acid moieties are known to be highly unsaturated in *L. incisa* (Bigogno *et al.*, 2002a). They are also the most abundant lipids in chloroplasts, which makes MGDG and DGDG interesting substrate candidates for the plastidic LiLOX.
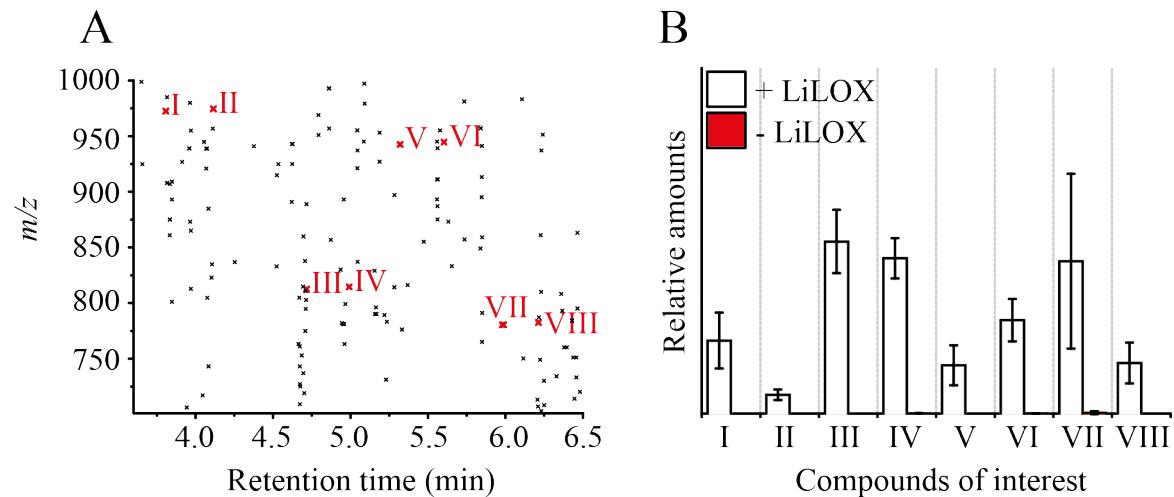
Figure 23 Oxidized galactolipids are tentative products of the *L. incisa* lipoxygenase (LiLOX) reaction. Total metabolite extract of *L. incisa* grown for 2 days in BG11 medium has been obtained by two-phase extraction according to Matyash, *et al.* (2008). Metabolites of both phases were resolved in 20 mM Bis-TRIS propane buffer pH 7.5 and incubated for 1 h either with 2 μg of pure LiLOX or without enzyme. Non-targeted metabolome analysis by LC-MS analysis was performed. Features related to oxidized galactolipid species could be tentatively identified by exact mass information. **A**. Retention time/mass plane shows signals representing all 1424 features. Features in red represent candidates for oxidized galactolipid species (Table 4). **B.** Bar diagram showing the relative amounts of the 8 features related to oxidized galactolipids detected in the reaction mixture with enzyme (white) and without enzyme (red), summarized in Table 40. Error bars represent the standard deviations of three reaction replicates. Non-targeted LC-MS analysis were performed by Dr. Kirstin Feussner.

Table 40- Oxidized galactolipids tentatively identified as products of the LiLOX reaction. Total metabolite extract of *L. incisa* grown for 2 days under normal conditions has been obtained by two-phase extraction according to Matyash et al. (2008). Metabolites of both phases were resolved in 20 mM Bis-TRIS propane buffer and incubated for 1 h either with 2 µg of pure LiLOX or without enzyme. Non-targeted metabolomics analysis by LC-MS analysis was performed. Features related to oxidized LiMGDG, and LiDGDG identified as LiLOX products and their corresponding substrates are shown. The following nomenclature has been used: Number of carbon atoms for combined acyl chains: number of double bonds for both acyl chains; number of additional oxygen atoms in both acyl chains-lipid class.

	RT (min)	Accurate mass (Da)	Identified LiLOX product (put. identity)	Corresponding LiLOX substrate
I	3.81	972.5284	34:6;4-DGDG $C_{49}H_{80}O_{19}$	34:6-DGDG $C_{49}H_{80}O_{15}$
II	4.11	974.5454	34:5;4-DGDG $C_{49}H_{82}O_{19}$	34:5-DGDG $C_{49}H_{82}O_{15}$
III	4.72	812.4936	34:5;4-MGDG $C_{43}H_{72}O_{14}$	34:5-MGDG $C_{43}H_{72}O_{10}$
IV	4.99	814.5071	34:4;4-MGDG $C_{43}H_{74}O_{14}$	34:4-MGDG $C_{43}H_{74}O_{10}$
V	5.32	942.5542	34:5;2-DGDG $C_{49}H_{82}O_{17}$	34:5-DGDG $C_{49}H_{82}O_{15}$
VI	5.60	944.5678	34:4;2-DGDG $C_{49}H_{84}O_{17}$	34:4-DGDG $C_{49}H_{84}O_{15}$
VII	5.98	780.5033	34:5;2-MGDG $C_{43}H_{72}O_{12}$	34:5-MGDG $C_{43}H_{72}O_{10}$
VIII	6.21	782.519	34:4;2-MGDG $C_{43}H_{74}O_{12}$	34:4-MGDG $C_{43}H_{74}O_{10}$

From the 1428 features of interest, 8 were identified to be directly related to MGDG or DGDG (Figure 23, Table 40). Features I, II, V and VI were identified as derived from DGDG substrates, with acyl chains composed of 34 carbons with 4 to 6 double bonds. Similarly, features III, IV, VII and VIII were identified as derived from MGDG substrates with acyl chains of 34 carbon atoms, harboring 4 or 5 unsaturations. Features I, II, III and IV would have 4 additional oxygens in the acyl chains, possibly 1 hydroperoxyl group on each acyl chain. Compounds V, VI, VII and VIII have 2 additional oxygens, probably 1 hydroxyl group on each acyl chain, or 1 hydroperoxyl group on 1 acyl chain. The retention time and the m/z ratio of features I to VIII were summarized in Table 40. It was determined that two putative compounds which only differed by 1 double bond had a retention time varying always by 0.3 min. Moreover, compound pairs II / III and V / VII have most likely the same acyl chains, but having different

headgroups, DGDG and MGDG, respectively. The difference in retention time between the two pairs was 0.601 min and 0.660 min, respectively, DGDG eluting before MGDG. Furthermore, retention time variations between putative hydroperoxides and hydroxides, may be around 1.2 min for comparable compound pairs (II and V, or III and VII), whereby hydroperoxides eluted before hydroxides.

It must be stressed that all features from I to VIII were observed almost only in the samples following a LiLOX reaction (Figure 23B). The control samples without LiLOX reaction are represented in red in the bar diagram, but are barely visible as these compounds accumulated in very low amounts in these samples. Altogether the accurate masses of these compounds seemed to be concordant with their retention time and the abundancy which seems to confirm the nature of these compounds. Surprisingly, neither the corresponding MGDG nor DGDG molecular species representing the substrates were detected in the 1424 features of interest, but could be identified in the features with a p-value above 0.001. Nevertheless, galactolipids seemed to be good candidates for LiLOX endogenous substrates for LiLOX, and were therefore studied further.

4.8.2. Phosphatidylcholine

In the 1424 compounds, oxidized molecular species with either two or four additional oxygen atoms were also identified among the phosphatidylcholines (PCs) although fewer than among the galactolipids (Figure 24, Table 41). For this reason, an additional focus was on phospholipids. Interestingly features XII and XIII were putatively identified as a PC substrate and its corresponding oxidized product. The putatively oxidized substrate (feature XIII) was found to be eluted 0.9 minutes earlier than the putative substrate (feature XII). Moreover, feature XII was only observed in samples to which no recombinant LiLOX was added, whereas feature XIII was only observed in samples to which the enzyme was added.
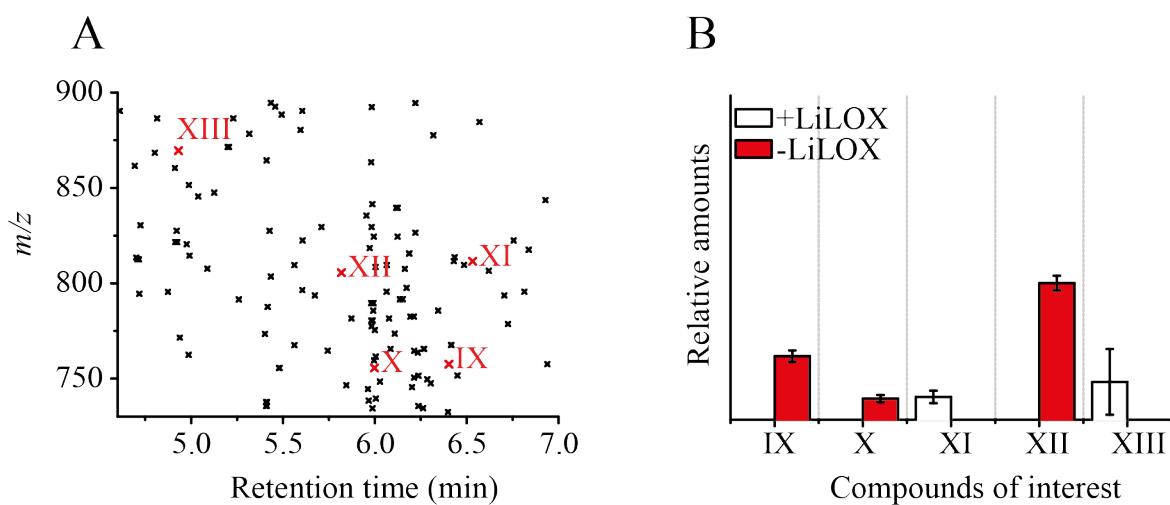
Figure 24- Oxidized phosphatidylcholines (PCs) are tentative products of the LiLOX reaction. Total metabolite extract of *L. incisa* grown for 2 days under normal conditions has been obtained by two-phase extraction according to Matyash et al. (2008). Metabolites of both phases were resolved in 20 mM Bis-TRIS propane buffer pH 7.5 and incubated for 1 h with 2 µg of pure LiLOX or without enzyme. Non-targeted metabolomics analysis by LC-MS was performed. Features related to oxidized PC (by exact mass information) could be identified. **A**. Retention time/mass plane shows signals representing all 1424 features. Features represented in red are candidates for oxidized PCs (see Table 4). **B.** The bar diagram shows relative amounts of 5 features related to PCs detected in the reaction mixture with enzyme (white color) and without enzyme (red color). Error bars represent the standard deviations of three reaction replicates. Non-targeted LC-MS analysis were performed by Dr. Kirstin Feussner.

Table 41. Oxidized PCs tentatively identified as products of the LiLOX reaction. Total metabolite extract of *L. incisa* grown for 2 days under normal conditions has been obtained by two-phase extraction according to (Matyash et al., 2008). Metabolites of both phases were resolved in 20 mM Bis-TRIS propane buffer pH 7.5 and incubated for 1 h with 2 μg of pure LiLOX and without enzyme. Non-targeted metabolomics analysis by LC-MS was performed. Features related to PCs of *L. incisa* identified as LiLOX or products and the corresponding substrates are shown. The following nomenclature has been used: number of carbon atom for both acyl chains: number of double bonds for both acyl chains; number of additional oxygen atom in both acyl chains-lipid class.

	RT (min)	Accurate mass (Da)	Identified LiLOX product and substrate (put. identity)	Corresponding LiLOX substrate
IX	6.40	757.5621	34:2-PC $C_{42}H_{80}NO_8P$	
X	6.00	755.5465	34:3-PC $C_{42}H_{78}NO_8P$	
XI	6.53	811.53634	36:5;2-PC $C_{44}H_{78}NO_{10}P$	36:5-PC $C_{44}H_{78}NO_8P$
XII	5.82	805.56216	38:6-PC $C_{46}H_{80}NO_8P$	
XIII	4.93	869.5382	38:6;4-PC $C_{46}H_{80}NO_{12}P$	38:6-PC $C_{46}H_{80}NO_8P$

4.9. Extraction and analysis of complex lipids from *L. incisa*

From the non-targeted ex vivo approach we obtained hints that 34:5-MGDG, 34:4-MGDG, 34:6-DGDG, 34:5-DGDG, 34:4-DGDG, 34:2-PC, 34:3-PC, 36:5-PC and 38:6-PC could be *in vivo* substrates of LiLOX. In order to confirm that MGDG, DGDG, and PC are indeed substrates of LiLOX, these three classes of complex lipid were purified from *L. incisa* grown for 2 days in BG11 medium. After lipid extraction by chloroform:methanol (1:1 (v/v), then 2:1 (v/v)), galactolipids and phospholipids were separated by SPE. TLC allowed to further purify each lipid class. The amounts of the lipid class obtained after purification were determined by weighing the dried compounds. Finally the quality of the enriched MGDG, DGDG, and PC fraction from *L. incisa* (LiMGDG, LiDGDG, and LiPC) as well as their specific composition was analyzed by LC-MS (Figure 25, Figure 26 and Figure 27). Altogether, three apparent molecular species of LiMGDG, nine apparent molecular species of LiPC and ten apparent molecular species of LiDGDG were detected, summarized in Table 42.

Table 42. Summary of all apparent molecular species of LiMGDG, LiDGDG as well as LiPC. Lipids were purified from *L. incisa* grown for 2 days in BG11 medium after a total lipid extraction, lipid class separation by SPE followed by TLC.

Apparent species of	34 carbons acyl chains (C16 + C18)	36 carbons acyl chains (C18 + C18 or C16 + C20)	38 carbons chains (C18 + C20)
LiMGDG	34:4 34:5 34:6		
LiDGDG	34:2 34:3 34:4 34:5 34:6	36:4 36:5 36:6	38:6 38:7
LiPC	34:1 34:2	36:2 36:3 36:4 36:5	38:5 38:6 38:7

Figure 25A, Figure 26A and Figure 27A show the total ion chromatograms (TICs) for LiMGDG, LiDGDG and LiPC respectively. Figure 25B, Figure 26B and Figure 27B represent

extracted ion chromatograms (EICs) for each lipid species of the respective lipid class. The three LiMGDGs with 34 carbons chain length eluted as distinct signals with retention times of 6.6 min, 7.2 min and 7.6 min (Figure 25). Although the LiDGDG and the LiPC fractions are composed of nine and ten species respectively, the LC-gradient applied allowed to identify the more polar species with highly unsaturated acyl chains (36:6-DGDG, RT 6.1 min and 38:7-PC, RT 4.1 min) as well as rather non polar species with saturated acyl chains (34:2-DGDG, RT 7.5 min and 34:1-PC, RT 6.7 min). The last four peaks from the LiPC fraction are broader compared to the others, since the gradient of acetonitrile had already reached 100%. In summary, the LC-MS analysis from the three *L. incisa* lipid classes confirmed a good purity of each of the lipid fractions.

The purified LiMGDG, LiDGDG, and LiPC lipid fractions were used as specific substrates from *L. incisa* for further characterization of the substrate specificity of LiLOX.
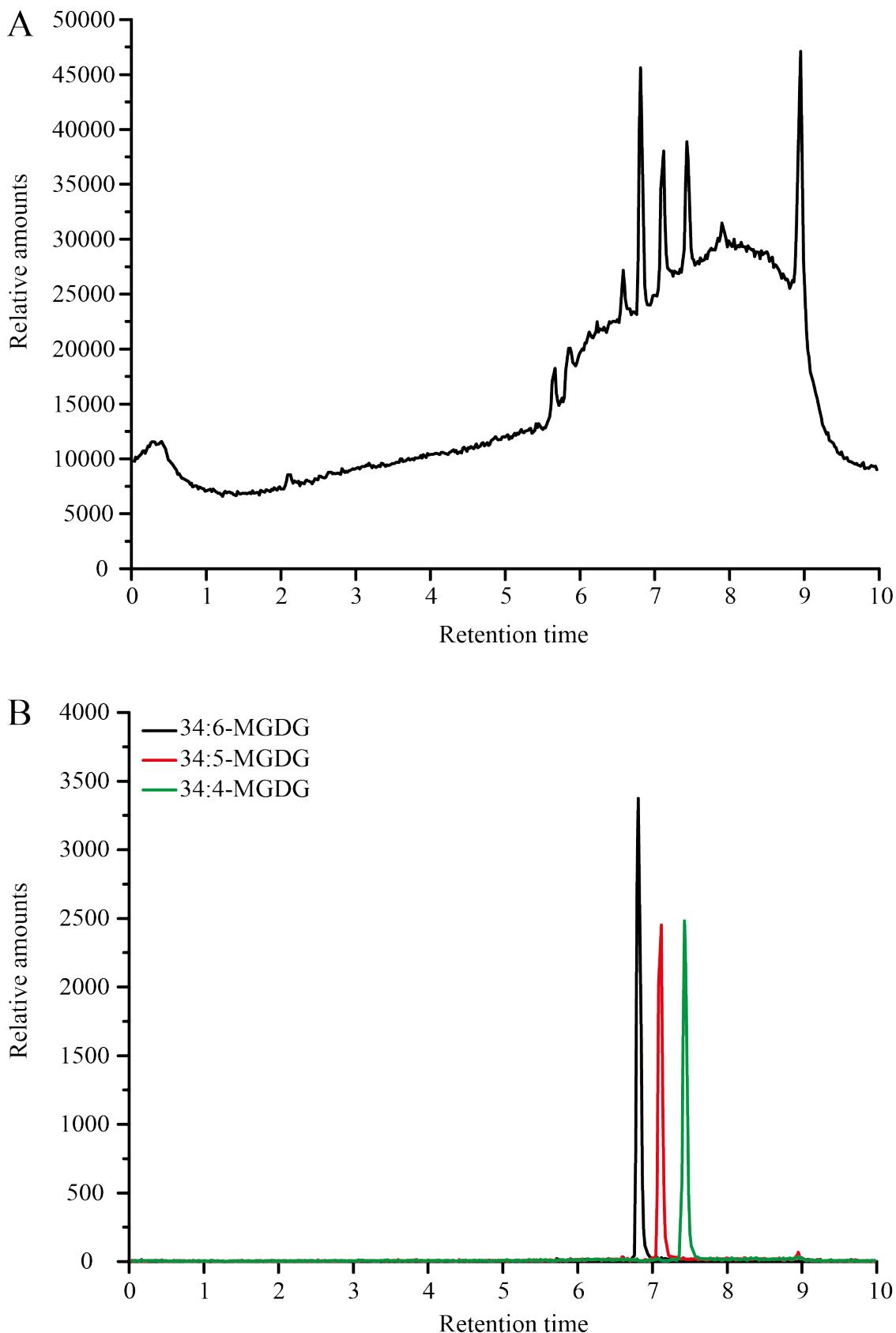
Figure 25. Analysis of *L. incisa* LiMGDG molecular species by LC-MS. LiMGDG was purified from *L. incisa* grown for 2 days in BG11 medium. After a total lipid extraction, lipid class separation by SPE followed by TLC were performed. Apparent species of LiMGDG were determined by LC-MS analysis. **A.** Total ion chromatogram of the LiMGDG fraction. **B.** Extracted ion chromatograms for the indicated LiMGDG species. Results representative for three lipid extraction from the same algae cultures. The LC-MS analysis was performed by Dr. Kirstin Feussner.
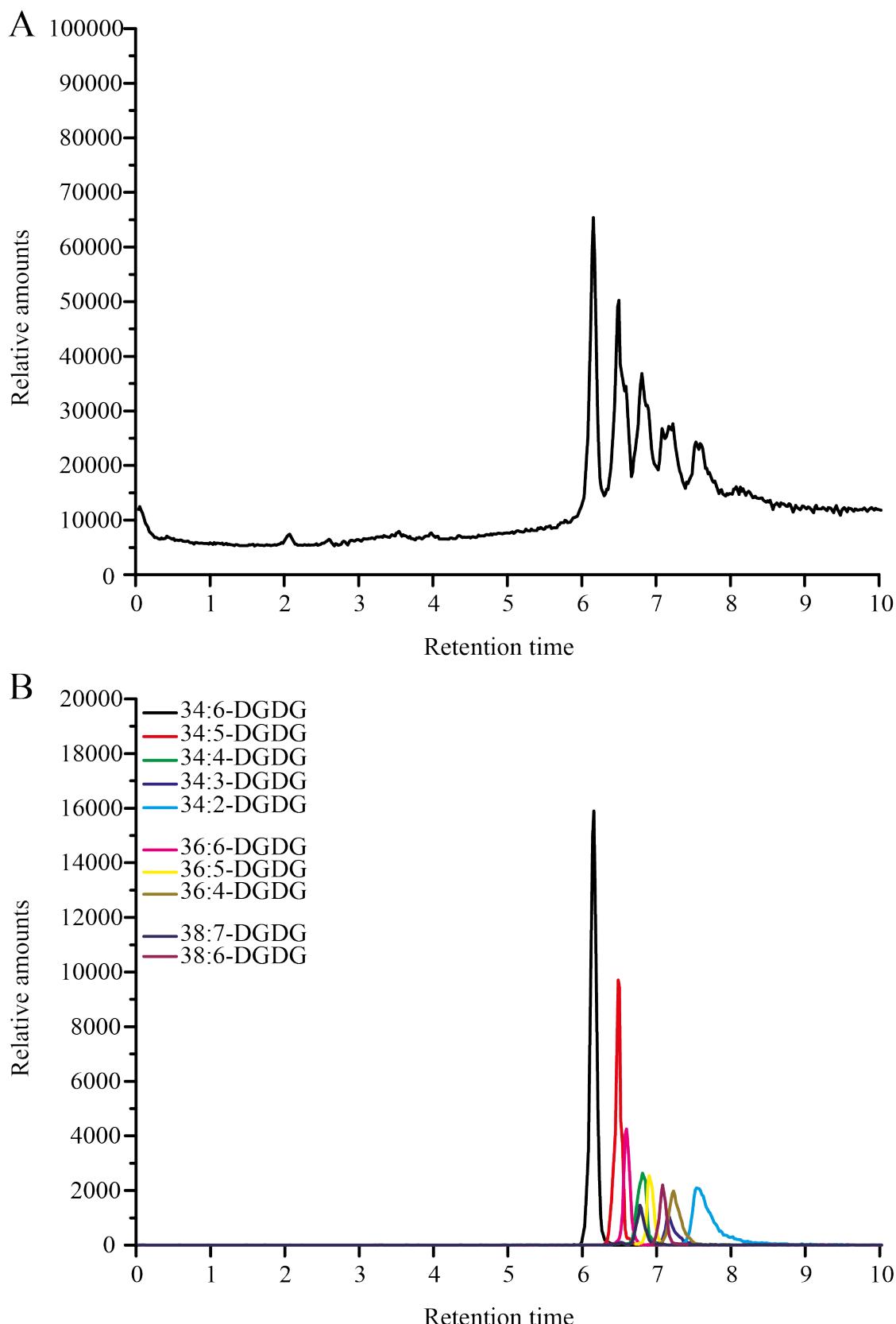
Figure 26. Analysis of LiDGDG species by LC-MS. LiDGDG was purified from *L. incisa* grown for 2 days in BG11 medium. After a total lipid extraction, lipid class separation by SPE and TLC were performed. Apparent species of LiDGDG were determined by LC-MS analysis. **A.** Total ion chromatogram of LiDGDG fraction. **B.** Extracted ion chromatograms for the indicated LiDGDG species. Result representative for one out of one lipid purification. The LC-MS analysis was performed by Dr. Kirstin Feussner.
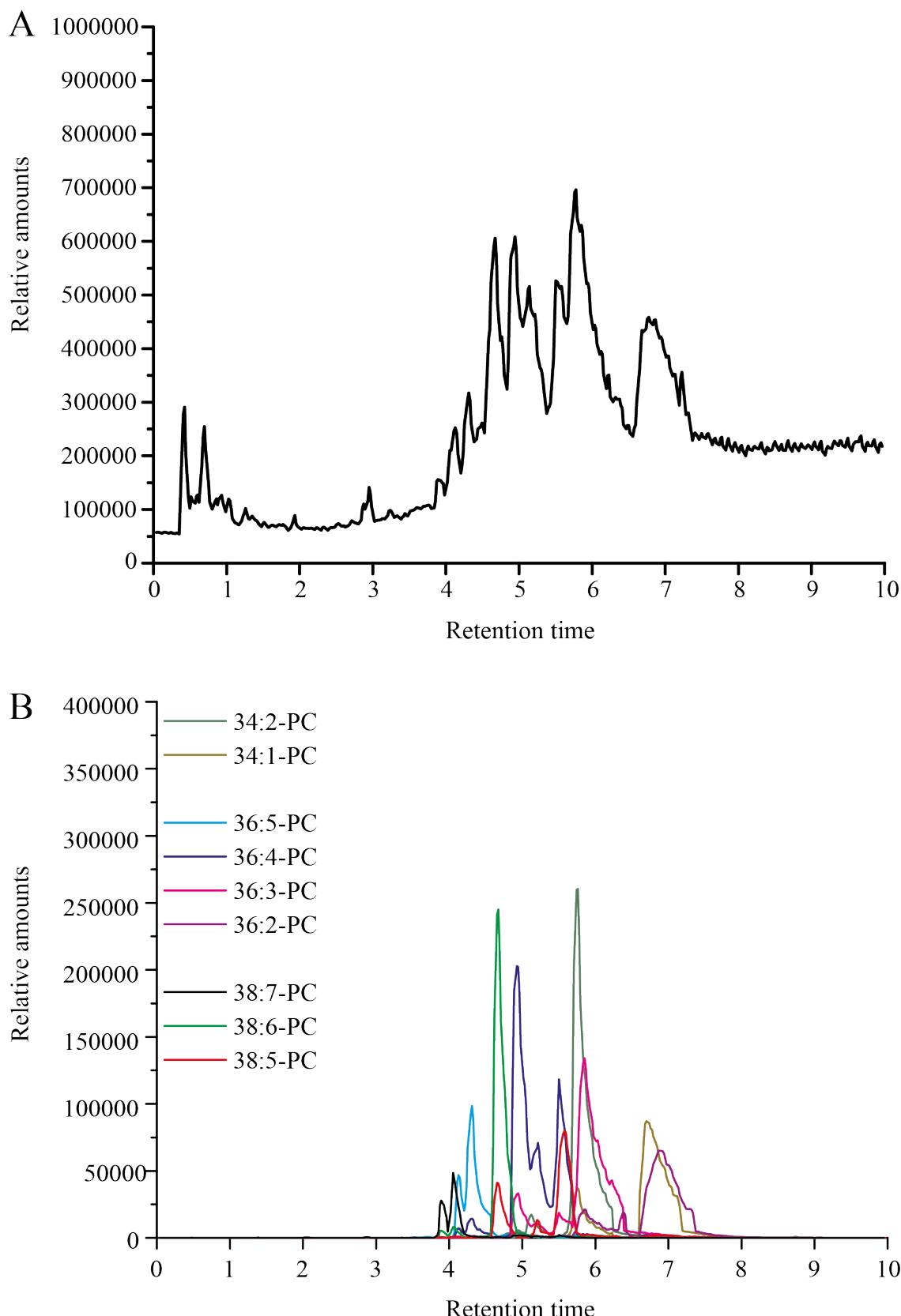
Figure 27. Analysis of LiPC molecular species by LC-MS. LiPC was purified from *L. incisa* grown for 2 days in BG11 medium. After a total lipid extraction, lipid class separation by SPE followed by TLC were performed. Apparent species of LiPC were determined by LC-MS analysis. **A.** Total ion chromatogram of LiPC fraction. **B.** extracted ion chromatograms for the indicated LiPC species. Results representative for three lipid extraction from the same algae cultures. The LC-MS analysis was performed by Dr. Kirstin Feussner.

4.10. LiLOX showed activity towards purified complex lipid fractions

From the non-targeted *ex vivo* approach we obtained hints that LiMGDG, LiDGDG and LiPC could be *in vivo* substrates of LiLOX. In order to estimate which lipids of *L. incisa* are likely to be the preferred substrates of LiLOX, kinetic *in vitro* measurements were performed. As complex lipids are poorly soluble in the so far used Bis-TRIS propane buffer, no LOX activity was detectable without addition of detergent. Yet since the detergent affects hydrophobic interactions, it most likely also affected the activity of LiLOX itself. In order to compare our data with data from the literature, we used the in this field well established detergent sodium deoxycholate (Brash *et al.*, 1987; Murray & Brash, 1988). The three FFAs 18:3 (n-3), 18:2 (n-6) and 20:4 (n-6) dissolved with 0.1 % (w/v) sodium deoxycholate were used as positive controls. Because LiLOX showed 20 % of remaining activity in presence of 0.1 % sodium deoxycholate, in order to obtain products in the detection range of the spectrophotometer, 5 µg of LiLOX was used for each measurement instead of 1 µg without detergent. In presence of detergent, enzymatic measurements did not fit the Hill equation in a range of substrate concentration below 500µM. At higher substrate concentrations, absorbance was detected at 280 nm signaling the formation of ketodienes instead of hydroperoxides, suggesting that molecular oxygen became a limiting factor of the reaction. Since $k$cat and K_M could not be determined in these conditions, all activities were measured by spectrophotometric assay with fixed substrate concentrations of 100 µM. LiLOX was determined to be active for all tested substrates, including the purified complex lipids.

LiLOX activity towards all three FFAs was determined to be the fastest with 18:3 (n-3) and the slowest with 20:4 (n-6), confirming the previously measured kinetic parameters without detergents in section 4.6.2, and 18:3 (n-6) was designated as reference substrate. After measuring the reaction rate of LiLOX for all substrates by spectrophotometric assay, the data were expressed as percentage relative to the activity of LiLOX towards 18:3 (n-3). The activity of LiLOX towards 18:2 (n-6) and 20:4 (n-6) was respectively 42 % and 9.8 % (Figure 28B) concordant with the kinetic parameters measured without detergent. As expected, the activity of LiLOX was slower with complex lipids than with FFAs.

LiLOX showed a clear preference towards LiMGDG *in vitro*, having a reaction rate 5 and 9 times faster than with LiDGDG and LiPC, respectively. Notably, the time course of LiLOX oxidizing LiMGDG seemed to be different than with all other lipids. Indeed, the lag phase seemed to last for more than 1 minute, in contrast to all other substrates were the reaction reached maximum velocity after no more than 5 to 10 seconds. This shape was observed in all

three technical replicates with LiMGDG as substrate. Therefore, LiMGDG was studied from this point on with thorough focus and compared to the other lipid classes.
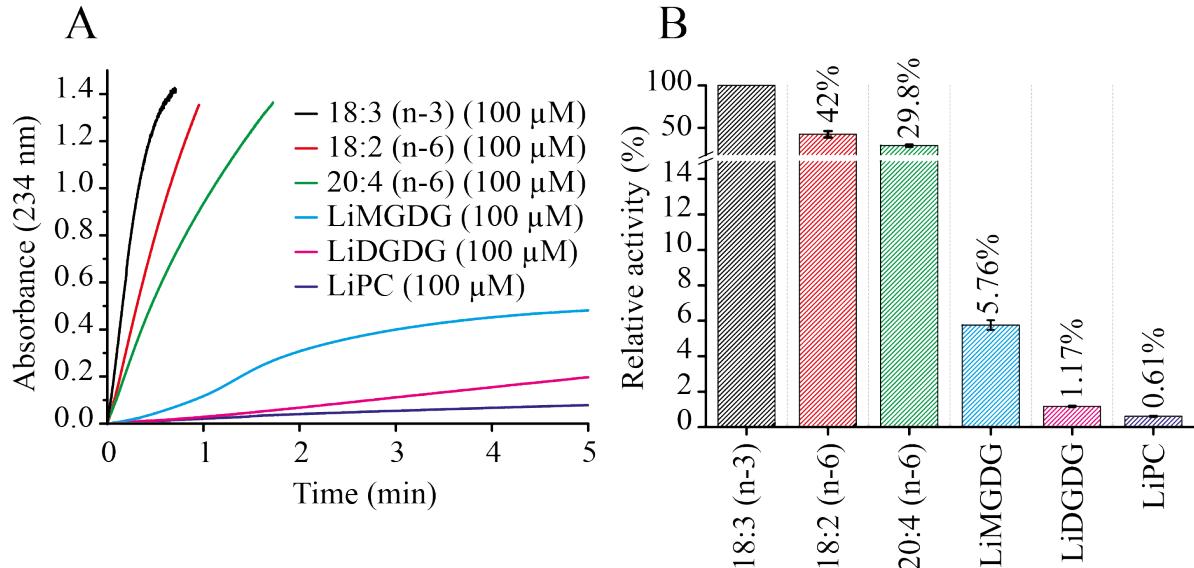
Figure 28. Comparaison of the conversion of FFAs and complex lipids by LiLOX. FFA (20:4 (n-6), 18:2 (n-6), 18:3 (n-6)) and LiMGDG, DGDG as well as PC purified from *L. incisa* cultures were used as substrate at a concentration of 100 µM. 20 mM Bis-TRIS propane pH 7.5 with 0.1 % sodium deoxycholate was used as buffer. **A.** Initial velocity of LiLOX with 100 µM of each lipid, recorded as the increase of absorbance at 234 nm. **B.** Activity of LiLOX relative to 18:3 (n-3), in which error bars represent the standard deviation of 3 reaction. Each reaction was performed with the same enzyme preparations.

4.11.   Product analysis of the LiLOX reaction with complex lipid

To further characterize LiLOX, the oxidation reaction it catalyzed on complex lipids was further analyzed. Yet the three lipids classes MGDG, DGDG and PC are all composed of two acyl chains with a great variability as seen in section 4.9, which called for different levels of analysis. Firstly, the number of oxidized lipid species for a given lipid class was investigated by LC- diode array detector (DAD) and LC-MS. Secondly, the number of acyl chains oxidized for a given lipid specie was determined by LC-MS and LC-MS[2]. Finally, the position of the oxidation in a given acyl chain and its chiral configuration were characterized after transesterification of the acyl chain by RP-HPLC, SP-HPLC and CP-HPLC.

It must be remembered that LOXs add hydroperoxyl groups on acyl chains that are highly unstable *in vitro* and will naturally be reduced to a hydroxyl group. Yet a mixture of hydroperoxide and hydroxide groups would create another level of complexity during the analysis. To prevent this, hydroperoxides formed by the LiLOX reaction were chemically reduced into the more stable hydroxides by $SnCl_2$, whenever it was possible to do so.

4.11.1. MGDG

Since LiMGDG was expected to be the natural substrate of LiLOX, the different oxidation products were analyzed individually after a first purification using RP-HPLC. The LiLOX oxidation product mixture resulting from the incubation with LiMGDGs showed six distinct peaks on the RP-HPLC, all having a maximum absorbance at either 234 nm or 236 nm (I to VI, Figure 29A). Their retention times were up to 20 min shorter than those of the LiMGDG substrates. Moreover, since none of these six peaks were observed in absence of the LiLOX reaction, they were considered to represent at least 6 oxidized LiMGDG products. The compounds were collected individually from the RP-HPLC column and injected on UPLC coupled to quadrupole (Q)-TOF-MS to obtain further structural information (Figure 29B, C and D). The exact masses of the ions of all products allowed to deduce their sum formula. Peaks I, II and III represented *m/z* values corresponding to the respective LiMGDG species 34:6, 34:5, 34:4 with two additional oxygens (34:6;2, 34:5;2 and 34:4;2), suggesting an oxidation on both acyl chains. Fragmentation analysis of compound I by MS[2] targeting the mass of 34:6;2-MGDG revealed fragments with *m/z* values 293.2137 expected for a HOTE-residue and 265.1828 expected for a Hydroxyhexadecatrienoic acid (HHTE)-residue. Similarly, fragmentation analysis targeting the mass of 34:5;2-MGDG and 34:4;2-MGDG revealed

signals for a HHTE-residue (*m/z*: 265.182), Hydroxyhexadecadienoic acid (HHDE)-residue (*m/z*: 267.1981), HOTE-residue (*m/z*: 293.214) and HODE-residue (*m/z*: 295.2286) in the case of compound II and signals for both a HHDE-residue (*m/z*: 267.1804) and HOTE-residue (*m/z*: 295.2273) in case of compound III.
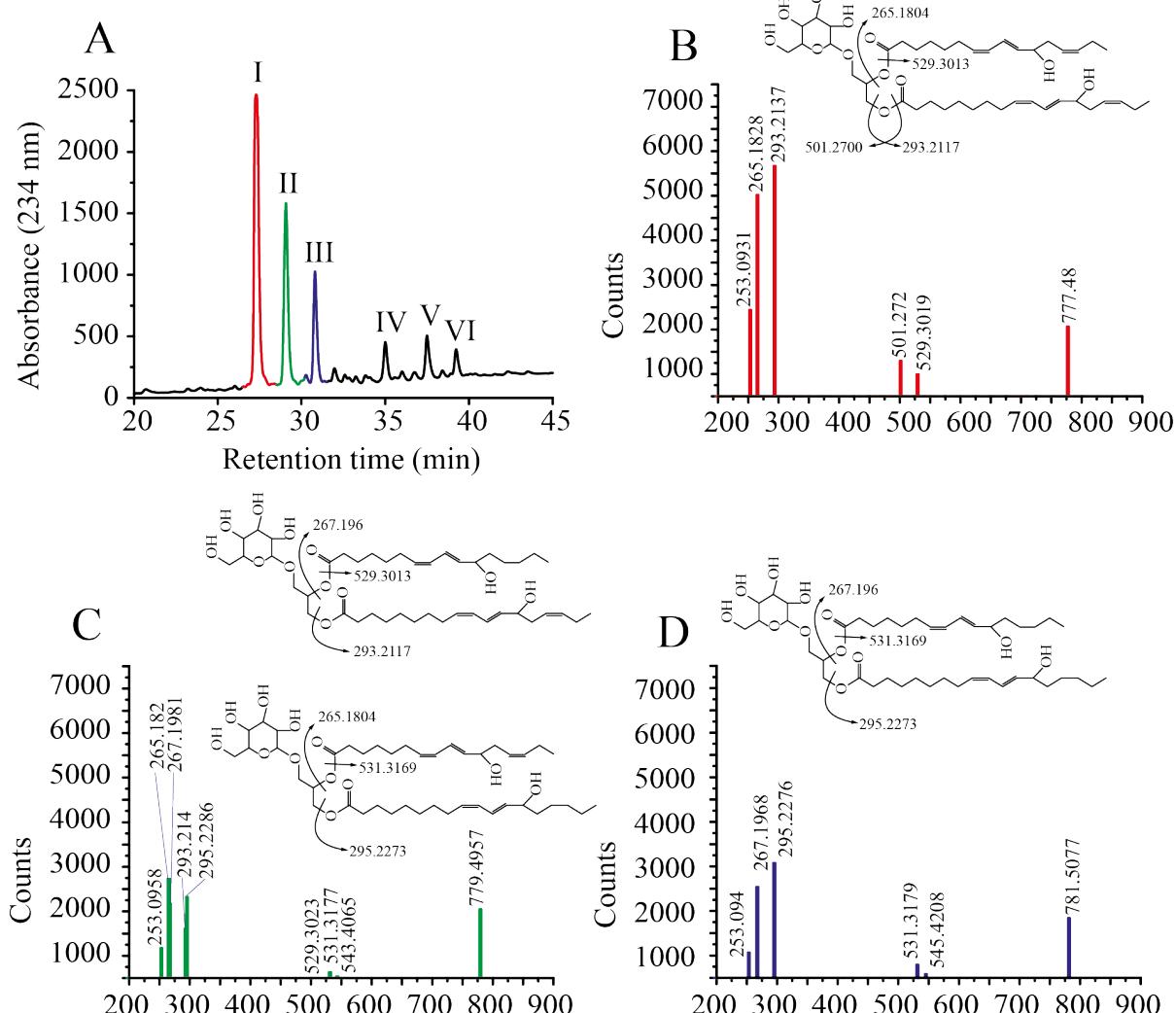
Figure 29. Identification of LiLOX products derived from LiMGDG. LiMGDG was purified from *L. incisa* grown for 2 days in BG11 medium after a total lipid extraction, lipid class separation by SPE followed by TLC. 20 mM Bis-TRIS propane pH 7.5 with 0.1 % (w/v) sodium deoxycholate was used as buffer for LiLOX reaction with LiMGDG. Products were reduced by SnCl₂, and separated by RP-HPLC. **A.** RP-HPLC chromatogram of total LiMGDG products catalyzed by LiLOX. The products separated by RP-HPLC (I to VI) were collected and analyzed by LC-MSMS. **B-D.** Fragment spectra of LiMGDG oxidation products for: **B.** 34:6;2-MGDG, **C.** 34:5;2-MGDG and **D.** 34:6;2-MGDG. Data shown represent a single experiment. The LC-MSMS analysis was performed by Dr. Kirstin Feussner.

Peaks IV, V and VI eluted up to 10 minutes earlier than the peaks of non-oxidzed LiMGDG substrates, and were found to have masses corresponding to the MGDG molecules 34:6, 34:5 and 34:4 respectively harboring one additional oxygen each (supplemental figure 3). Fragmentation of compound IV by MS^2 revealed fragments corresponding to a HOTE-residue

and a 16:3-residue. Peak V was a compound mixture since a HOTE-residue, HODE-residue as well as 16:3 and 16:2 were detected among other fragments. Fragmentation of compound VI by MS^2 displayed fragments corresponding to a HODE-residue and a 16:2 residue. It should be stressed that within the four mono-oxidized compounds (from peaks IV, V and VI) only the C18 acyl chains were oxidized. In addition it must be stressed that the molecules drawn in Figure 29B, C and D compounds I, II and III respectively are tentative since the absolute position of the hydroxyl group cannot be determined by this approach. However, the hydroxyl groups were placed in position n-6 as this was for the preferred position in case of the FFA. The elucidation of the absolute configuration was subject to further analysis by HPLC:

After transesterification of compounds I II and III, the resulting acyl methyl-esters were separated by a second run on RP-HPLC. From the compounds I, II and III, two, four and two peaks respectively were eluted (Figure 30B, C and D). The resulting products from compound I were named I.I and I.II, from compound II were named II.I, II.II, II.III and II.IV, and the products from compound III were named III.I and III.II. Analysis of the retention times of these products confirmed the results found by MS^2: Compound I was composed of HHTE and HOTE, compound II was composed of a mixture of HHTE, HOTE, HHDE and HODE and compound III was composed of HHDE and HODE. The identity of the methyl-esters was confirmed by authentic standards. All eight were collected separately from the RP-HPLC and were analyzed sequentially on SP-HPLC in order to separate the different regioisomers, and on CP-HPLC in order to separate the stereoisomers The SP-HPLC chromatograms from peaks II.I, II.II, II.III and II.IV, revealed one major regioisomer for each oxidized acyl chain methyl-ester (Figure 30E, F, G, H). For all peaks, the retention times corresponded to the acyl chains being oxidized on the carbon atom n-6. The CP-HPLC chromatograms revealed an *S* configuration for all analyzed compounds (Figure 30E, F, G, H, in the respective boxes). Analyses of compounds I.I, I.II, III.I, and III.II gave similar results, all summarized in Table 43.
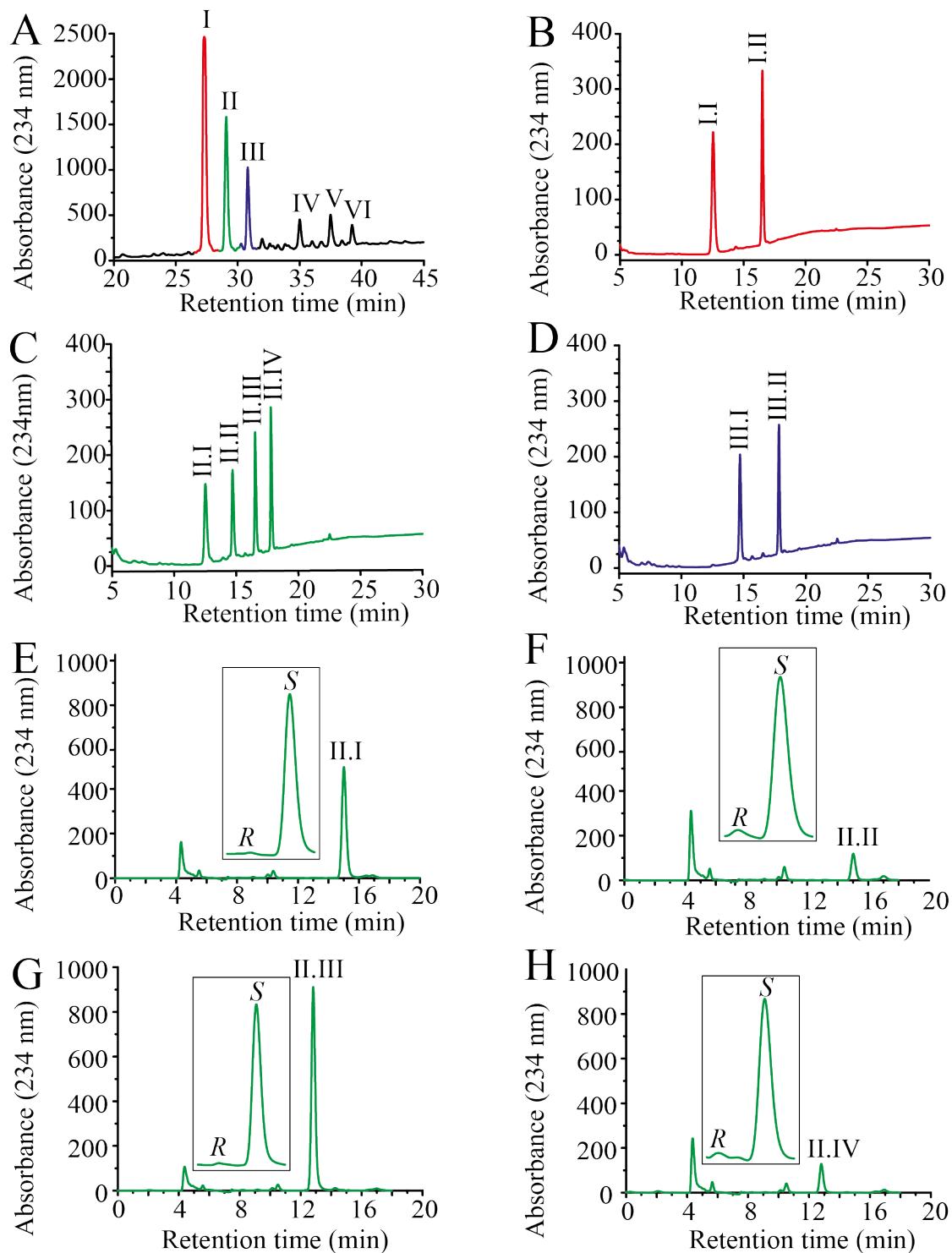
Figure 30. Structural identification of oxidized LiMGDG produced by LiLOX. LiMGDG was purified from *L. incisa* grown for 2 days in BG11 medium after a total lipid extraction, lipid class separation by SPE followed by TLC. 20 mM Bis-TRIS propane pH 7.5 with 0.1 % (w/v) sodium deoxycholate was used as buffer for LiLOX reaction with LiMGDG. Products were reduced by SnCl$_2$, and sequentially analyzed. **A.** RP-HPLC chromatogram from LiMGDGs oxidized by LiLOX, which is representative of three independent reactions. **B-C.** RP-HPLC chromatograms from collected and transesterified compounds which are representative of three independent reactions. **B.** I. **C.** II. **D.** III. **E-H.** SP-HPLC chromatograms from the four products transesterified from compound II (II.I; II.II; II.III; II.IV), which are representative of three reactions. All reactions were performed with three different enzyme preparations. CP-HPLC chromatograms are represented in each corresponding box, representative of one measurement. All products were detected at 234 nm.

Since LiDGDG and LiPC were composed of a greater variability of lipid species, the oxidation products of LiLOX had to be analyzed as a mixture of different lipid species.

4.11.2. DGDG

A first purification step by RP-HPLC was performed in order to eliminate all traces of SnCl$_2$, used during the reduction step, from the mixture as they could damage the equipment of the MS. After this purification, the LiDGDGs oxidized by LiLOX were analyzed by LC-MS. This analysis revealed the masses corresponding to the apparent DGDG species 34:5, 34:5, 34:4, 36:4, 36:5, 36:6, 38:6 and 38:7 with two additional oxygen atoms (Figure 31). Only the species that may have been derived from 34:2-DGDG, and 34:3-DGDG were not detected to be oxidized. After transesterification of the oxidized LiDGDGs, the resulting acyl methyl-esters were sequentially analyzed by RP-HPLC, SP-HPLC, and CP-HPLC. Notably, HODE (42.2 %) and HOTE (28.4 %) were found to be the most abundant acyl chains in the methyl-ester fraction. Moreover, as observed for LiMGDG, all acyl chains were found to be oxidized at the
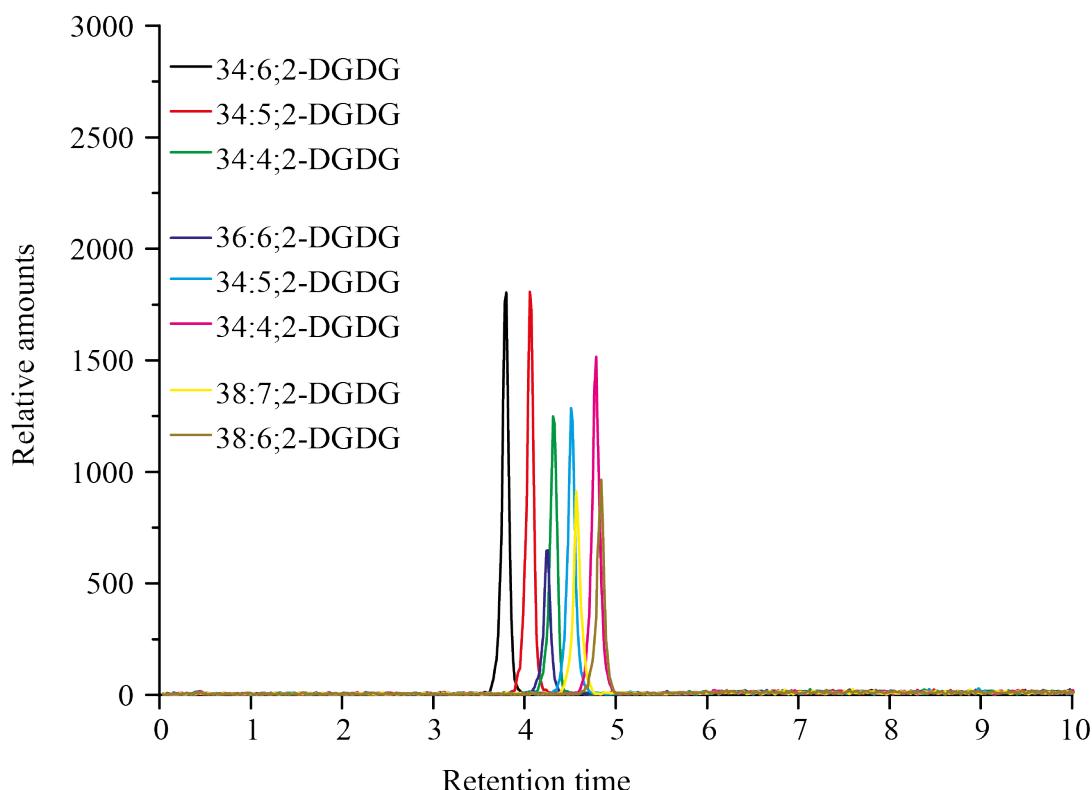
Figure 31. Identification of oxidized LiDGDG molecular species formed by LiLOX activity. LiDGDG was purified from *L. incisa* grown for 2 days in BG11 medium after a total lipid extraction, lipid class separation by SPE followed by TLC. 20 mM Bis-TRIS propane with 0.1 % (w/v) sodium deoxycholate was used as buffer for LiLOX reaction with LiDGDG. Products were reduced by SnCl$_2$, purified on RP-HPLC and apparent species of LiDGDG were determined by LC-MS analysis. The extracted ion chromatograms for the indicated oxidized LiDGDG species are shown. Data shown represent a single experiment. The LC-MS analysis was performed by Dr. Kirstin Feussner.

corresponding carbon n-6 with *S* configuration (results are summarized in Table 43 and in the supplemental figure 5).

4.11.3. PC

All species of oxidized LiPC could not be purified by RP-HPLC, therefore, the reduction step was abandoned before analysis of this lipid class by LC-MS, as all traces of $SnCl_2$ could not be removed from the mixture. The LiPC fraction oxidized by LiLOX was analyzed by LC-MS (Figure 32). The masses of 4 apparent PC species: 36:5, 36:4, 38:7 and 38:6 with 4 additional oxygens were detected, suggesting one hydroperoxide on each acyl chain. Moreover, the feature corresponding to the species 36:4-PC was also detected with two additional oxygens. Finally, no oxidation products of the species 34:2-PC, 34:1-PC, 36:2-PC, 36:3-PC and 38:5-PC were detected.

After reduction by $SnCl_2$, the total LiPC mixture oxidized by LiLOX was transesterified and sequentially analyzed by RP-HPLC, SP-HPLC, CP-HPLC. Notably, from the LiPC fraction
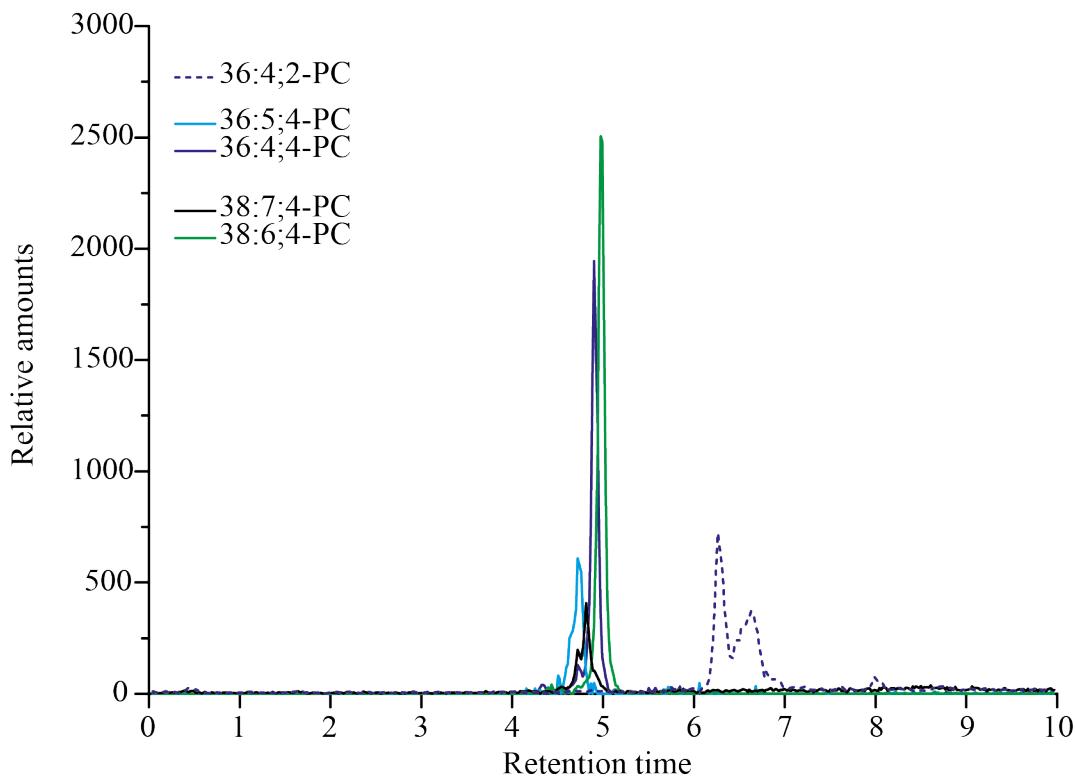
Figure 32. Identification of oxidized LiPC molecular species formed by LiLOX activity. LiPC was purified from *L. incisa* grown for 2 days in BG11 medium after a total lipid extraction, lipid class separation by SPE followed by TLC. 20 mM Bis-TRIS propane with 10 % (v/v) methanol was used as buffer for the LiLOX reaction with LiPC. Apparent species of LiPC were determined by LC-MS analysis. The extracted ion chromatograms for the indicated oxidized LiPC species are shown. Two experiments analyzed showed comparable results. The LC-MS analysis was performed by Dr. Kirstin Feussner.

oxidized by LiLOX, no oxidized acyl chain with 16 carbon atoms was detected, suggesting that oxidized PC species with 36 carbons and 38 carbons acyl chains are composed of 18 carbons and 20 carbons acyl chains exclusively. This result was confirmed by the very high proportion of HODE (59.4 %) and HETE (27.5 %) as well as by the occurrence of αHOTE (6 %) and γHOTE (7.3 %). Finally, as observed for LiLOX oxidation products with LiMGDG and LiDGDG, all acyl chains were found to be oxidized on the carbon atom n-6 with *S* configuration. These results are summarized in Table 43 and supplemental figure 6.

4.11.4. GlcADGs and TriGDG

In addition to MGDG and DGDG, apparent species of glucuronosyldiacylglycerol (GlcADG) and trigalactosyldiacylglycerol (TriGDG) were observed from the galactolipid fraction of *L.incisa.* Although they could never be purified from one another, these two lipid species have also been found to be accepted by LiLOX as substrate (Figure 33).
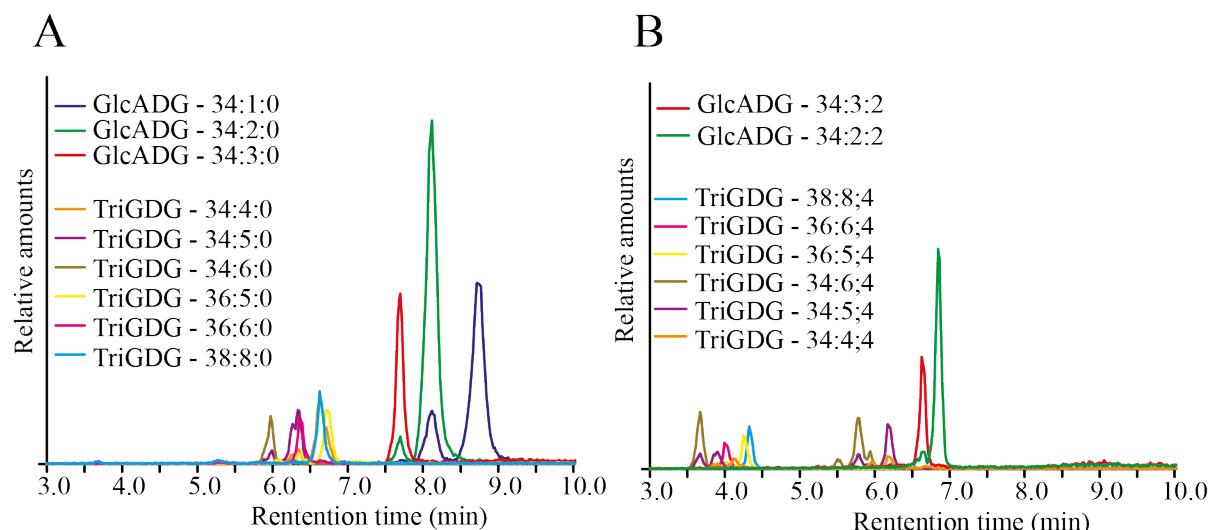
Figure 33. Identification of non-oxidized and oxidized glucuronosyldiacylglycerol (LiGlcADG) and trigalactosyldiacylglycerol (LiTGDG) molecular species formed by LiLOX activity. LiGlcADG and LiTGDG were purified from *L. incisa* grown for 2 days in BG11 medium after a total lipid extraction, lipid class separation by SPE followed by TLC. 20 mM Bis-TRIS propane with 10 % (v/v) methanol was used as buffer for the LiLOX reaction with LiPC. Apparent species of LiGlcADG and LiTGDG were determined by LC-MS analysis. **A.** The extracted ion chromatograms for the indicated LiGlcADG and LiTGDG species are shown. B**.** The extracted ion chromatograms for the indicated oxidized LiGlcADG and oxidized LiTGDG species are shown. Data shown represent a single experiment. The LC-MS analysis was performed by Dr. Kirstin Feussner.

Table 43. Products of LiLOX activity on complex lipids LiMGDG, LiDGDG and LiPC were purified from *L. incisa* grown for 2 days in BG11 medium. After a total lipid extraction, lipid class separation by SPE followed by TLC was performed. 20 mM Bis-TRIS propane with 0.1 % (w/v) sodium deoxycholate was used as buffer for the LiLOX reaction. Products were reduced by SnCl$_2$, transesterified and analyzed sequentially by RP-HPLC, SP-HPLC and CP-HPLC. The fraction of oxidized acyl chains within a given lipid class (analyzed by RP-HPLC) are shown in red. The major regioisomer for each acyl chain (analyzed by SP-HPLC) is shown in blue. The chiral configuration was measured for all major regioisomers and is shown in brackets. Stereochemistry for HHTE-Me and HHDE-Me was only tentatively assigned, since no standards were available. HHTE: hydroxy hexadecatrienoic acid, HETE: hydroxy eicosatetraenoic acid; HODE: hydroxy octadecadienoic acid; HOTE: hydroxy octadecatrienoic acid; nd: not determined.

		HHTE	HHDE	HOTE	HODE	HETE
MGDG	**34:4;2**	0 %	7.9 % 11-HHDE: 81.4 % (92.2 % *S*) 07-HHDE: 18.6 % All trans: 0 %	0%	7.1 % 13-HODE: 96.1 % (100 % *S*) 09-HODE: 3.9 % All trans: 0 %	0 %
	34:5;2	8.1 % 11-HHTE: 97.6 % (100 % *S*) 07-HHTE: 0 % 10-HHTE: 0 % 14-HHTE: 0 % All trans: 2.4 %	6.5% 11-HHDE: 83.1 % (98.1 % *S*) 07-HHDE: 0 % All trans: 16.9 %	7.2 % (α) 13-HOTE: 98.5 % (98 % *S*) 09-HOTE: 0 % 12-HOTE: 0 % 16-HOTE: 0 % 13-All trans: 1.5 %	7.7 % 13-HODE: 98.2 % (96.6 % *S*) 09-HODE: 0 % 13-All trans: 1.8 %	0 %
	34:6;2	28.5 % 11-HHTE: 87.6 % (87.9 % *S*) 07-HHTE: 0 % 10-HHTE: 0 % 14-HHTE: 0 % All trans: 12.4 %	0 %	26.9 % (α) 13-HOTE: 86 % (97.4 % *S*) 09-HOTE: 0% 12-HOTE: 0% 16-HOTE: 11.6% 13-All trans: 2.4%	0 %	0 %
DGDG mixture		9.10 % 11-HHTE: 100 % (87.6 % *S*) 10-HHTE: 0 % 07-HHTE: 0 % 14-HHTE: 0 % All trans: 0 %	12.90 % 11-HHDE: 98.1 % (96.8 % *S*) 07-HHDE: 0.8 % All trans: 1 %	28.40 % (α) 13-HOTE: 99.3 % (13*S*-αHOTE: nd) (13*S*-γHOTE: nd) 16-αHOTE: 0 % 12-αHOTE: 0 % 09-HOTE: 0 % 10-γHOTE: 0 % 6-γHOTE: 0 % 13-All trans: 0.7 %	42.20 % 13-HODE: 95.9 % (98.9 % *S*) 09-HODE: 2.5 % 13-All trans: 1.5 % 9-All trans: 0 %	7.40 % 15-HETE: 100 % (87.1 % *S*) 10-HETE: 0 % 11-HETE: 0 % 12-HETE: 0 % 08-HETE: 0 % 05-HETE: 0 % All trans: 0 %
PC mixture		0 %	0 %	6 % α & 7.3 % γ 13-HOTE: 91.1 % (13*S*-αHOTE: nd) (13*S*-γHOTE: nd) 16-αHOTE: 7.4 % 12-αHOTE: 0.7 % 09-HOTE: 0 % 10-γHOTE: 0 % 6-γHOTE: 0 % All trans: 0.8 %	59.40 % 13-HODE: 93.1 % (87 % *S*) 09-HODE: 2.3 % 13-All trans: 1.7 % 9-All trans: 2.9 %	27.50 % 15-HETE: 100 % (87.3 % *S*) 10-HETE: 0 % 11-HETE: 0 % 12-HETE: 0 % 08-HETE: 0 % 05-HETE: 0 % All trans: 0 %

4.12. Oxidized LiMGDG molecular species harboring a conjugated diene system do not seem to be the final LiLOX product.

When the enzymatic activity of LiLOX towards LiMGDG was recorded photometrically, a two-step reaction was observed. Under the described conditions, a first reaction step ranged from 0 to 10 minutes leading to the formation of products harboring a conjugated double bond system (Figure 34A). After 10 minutes however a second phase of the reaction was observed, as the absorption at 234 nm started to drop again (Figure 34B), suggesting that also the amount of the oxidation products with a conjugated double bound system decreased in the reaction mixture. This finding suggested that the LiLOX reaction with LiMGDG did not stop after all acyl chains were oxidized, but that they are further metabolized, leading to the loss of the chromophore. When analyzed in more detail, no additional or new formation of a chromophore absorbing in the range from 200 nm to 800 nm was observed (supplemental Figure 8).
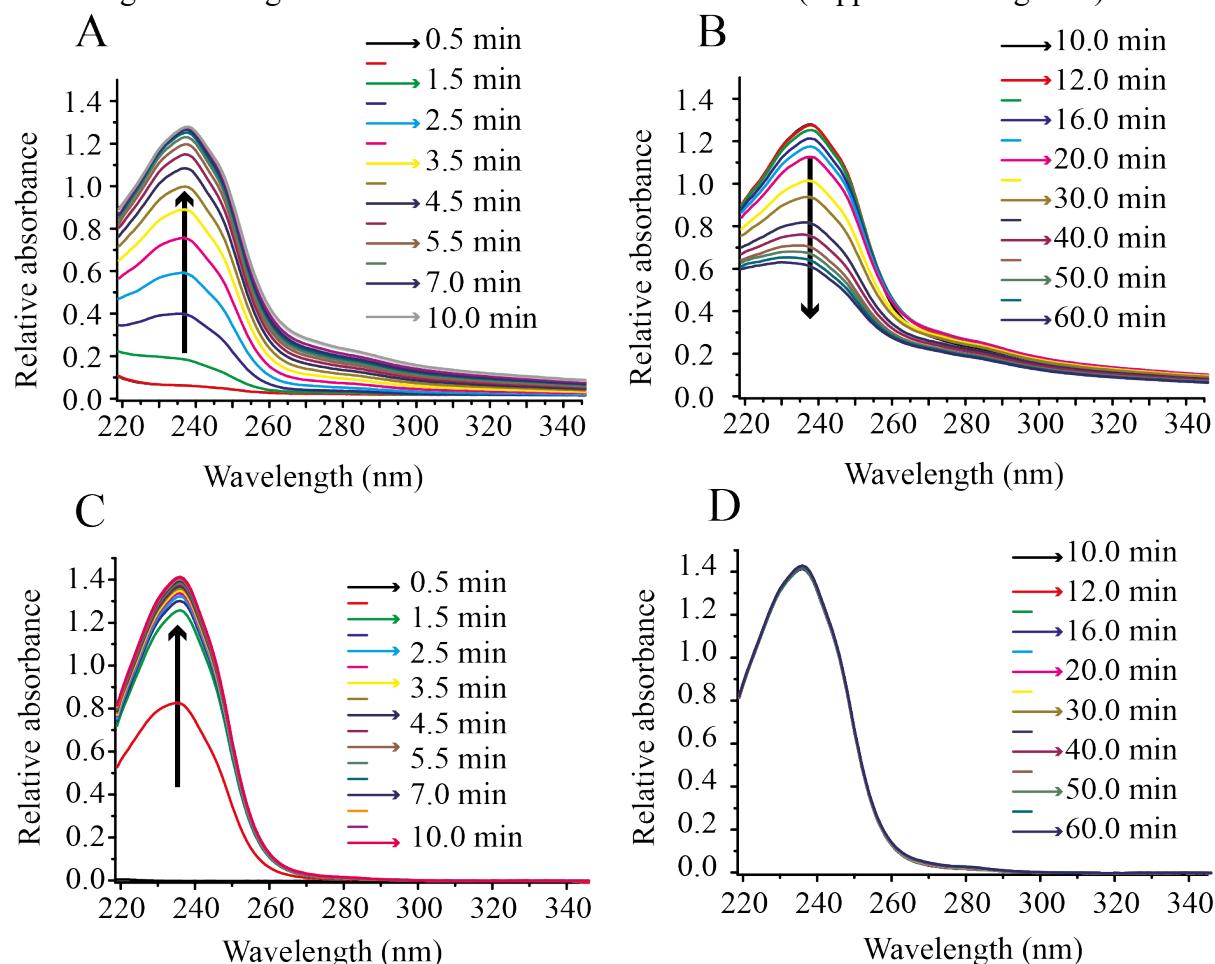
Figure 34. Time course of LiLOX catalysis with LiMGDG in comparison to FFA. LiMGDG was purified from *L. incisa* grown for 2 days in BG11 medium. After a total lipid extraction, lipid class separation by SPE followed by TLC was performed. 20 mM Bis-TRIS propane pH 7.5 with 0.1 % (w/v) sodium deoxycholate was used as buffer for the LiLOX reaction with LiMGDG or the FFA 18:3 (n-3). The baseline level is established after addition of LiLOX. **A.** LiLOX reaction with LiMGDG (0 to 10 min). **B.** LiLOX reaction with LiMGDG (10 to 60 min). **C.** LiLOX reaction with 18:3 (n-3) (0 to 10 min). **D.** LiLOX reaction with 18:3 (n-3) (10 to 60 min). All reactions were followed by changes in absorbance at 234 nm at 30 °C. Results shown are representative for three experiments. Each experiments was performed with different enzyme preparations.

In order to clarify whether this reaction is specific to complex lipids, a similar reaction was performed with 18:3 (n-3). With this FFA, the amount of oxidized FFAs with a conjugated double bond system increased as the LOX reaction proceeded shown by the increasing absorbance at 234 nm. The amount of oxidized FFA reached a plateau after 10 minutes, but did not decrease, as the absorbance stayed at its maximal level for as long as it was measured (Figure 34C, D). As the second phase of the reaction was not observed for FFA, and seemed to be specific for complex lipids, it must be next analyzed whether the oxidized LiMGDG species are further metabolized by LiLOX. In this regard, mass spectrometric analysis was chosen to measure the levels of oxidized LiMGDGs species at different time points of the reaction and to search for follow up products of these hydroperoxides. LiMGDGs are insoluble in aqueous solution and detergents were used for their solubilization in order to allow a reaction with LiLOX *in vitro*. In order to follow the metabolism of LiMGDG by LiLOX in more detail, our metabolomic workflow was applied next. However, samples containing detergent are not appropriate for LC-MS, as they are known to affect MS analysis and in case of the previous experiments the detergent in all samples was removed by RP-HPLC before further MS analysis. Therefore, LiMGDGs had to be solubilized in a different way, though preserving the activity of LiLOX.

4.12.1. Methanol used to solubilize MGDG

As lipids are known to have a higher solubility in the presence of organic solvents, methanol was tested as candidate for this matter. First of all, the integrity of LiLOX in presence of 0 to 20 % (v/v) methanol was estimated by the photometric assay with the FFA 18:2 (n-6) (Supplemental Figure 7A) and the presence of organic solvent indeed affected the activity of LiLOX. Yet, LiLOX was measured to have 33 % of its remaining activity in the presence 10 % of methanol in the reaction assay. However, addition of 10 % (v/v) methanol was enough to solubilize LiMGDG for following the LiLOX reaction (Supplemental Figure 7B). Due to the reduced enzymatic activity in presence of methanol, 5 µg of LiLOX had to be used for each measurements in order to obtain products in the detection range of the spectrophotometer. However, when LiMGDG was oxidized by LiLOX in presence of methanol, a similar two-phase reaction was observed (Supplemental Figure 7C).

4.13.   Kinetic analysis of LiLOX oxidation products

Different time points of the LiLOX reaction with LiMGDG were analyzed, measuring the presence and the relative amounts of substrates and products present in the reaction mixture at the given time point. As very little was known about the chemical structure and the physicochemical properties of the putative final products of lipid peroxidation catalyzed by LiLOX with LiMGDGs, the reduction of hydroperoxides with $SnCl_2$ was abandoned for this protocol. Indeed any extra reaction had to be prevented as it could have been misinterpreted as one of the reactions from LiLOX. In addition to that, lipid extraction with chloroform/methanol was also omitted in order not to introduce a bias or to lose the putative final product. Thus, LiMGDG was dissolved in buffer with 10 % (v/v) methanol and 5 µg LiLOX. After different time point of reaction (10 min, 30 min, 60 min) the reaction was stopped by dilution with
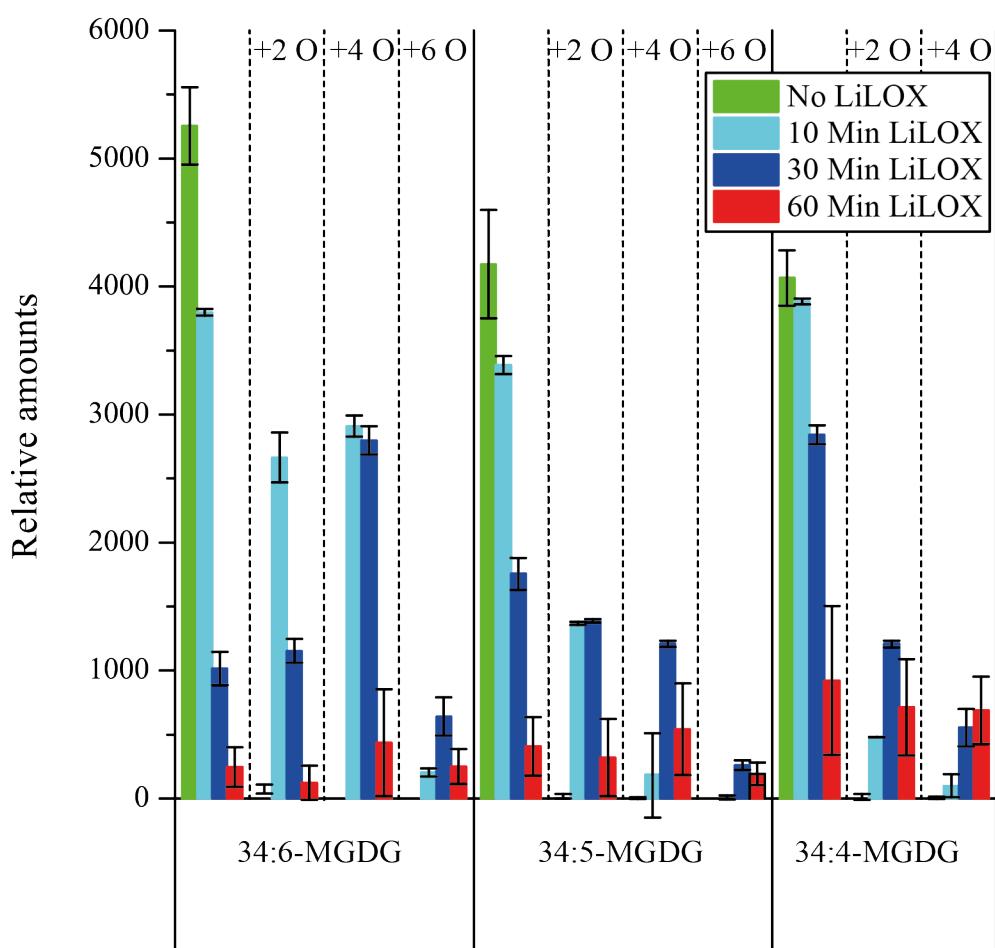
Figure 35. Identification of early and late LiLOX products from LiMGDG. LiMGDG was purified from *L. incisa* grown for 2 days in BG11 medium after a total lipid extraction, lipid class separation by SPE followed by TLC. 20 mM Bis-TRIS propane with 10 % (v/v) methanol was used as buffer for the LiLOX reaction with LiMGDG. The reactions were started with the addition of 5 µL of LiLOX and were stopped at a different time point after reaction (10 min, 30 min and 60 min) by dilution with methanol (1:1 v/v). The height of the mass signal of the indicated LiMGDGs and their corresponding oxidized species with two (+2O), four (+4O) or six oxygens (+6O) are shown as relative amounts. Error bars represent the standard deviation of three experiments. Each experiments was performed with different enzyme preparations. The LC-MS/MS analysis was performed by Dr. Kirstin Feussner.

methanol inactivating the enzyme (1:1, v/v) and the reaction mixtures were analyzed by LC-MS (Figure 35).

Without enzyme (Figure 35, green bars), the expected substrates (34:6-MGDG, 34:5-MGDG, 34:4-MGDG) were detected by exact mass analysis. As the reaction proceeded, the signals corresponding to the substrates were decreased by 28 %; 19 % and 4 % respectively already after 10 minutes (Figure 35, light blue bars). The rapid oxidation of the substrate 34:6-MGDG seemed to confirm that LiLOX had a preference for n-3 acyl chains. At the same time, the signal corresponding to 34:6-MGDG with two oxygens (+2O) (one hydroperoxyl group on one acyl chain) increased and reached already a maximum level at 10 minutes. It was followed by the signal corresponding to 34:6-MGDG with four oxygens (+4O) (one hydroperoxyl group on each acyl chain) at 30 minutes, suggesting that the oxidation of the two acyl chains by LiLOX happened in a two-step reaction. As revealed by the photometric assay, the signals for all products with two hydroperoxyl groups (+4O) started to be metabolized as well after 30 minutes (Figure 35). After 60 minutes, 34:6-MGDG and 34:5-MGDG the corresponding products with a single hydroperoxyl group (+2O) as well as products with two hydroperoxyl groups (+4O) were barely detected anymore in the reaction mixture. Interestingly, the 34:4-MGDG-derived products had a slightly slower kinetic. Similar results were obtained after extraction of putative products with chloroform:methanol prior to analysis.

Under these conditions, only two new products were detected: 34:6;6-MGDG and 34:5;6-MGDG (+6O). Both products were detected already at 10 minutes and reached a maximum at 30 minutes and both seemed to be degraded as well 60 minutes after reaction. In order to better understand the LiLOX reaction the structure of the MGDG molecules with 6 additional oxygens (34:6;6-MGDG, 34:5;6-MGDG) was solved by analyzing the product mixture by LC-MSMS. However, the structure of these two MGDG species with 6 additional oxygens could not be resolved until now. In order to identify additional metabolites of the oxidized MGDG molecules, the data sets were first analyzed for the occurrence of the potential fragments of the corresponding hydroperoxides and in a second step by using the untargeted MarVis workflow. By neither of the two strategies additional metabolites formed by the LiLOX reaction could be identified.

4.14. Plastidic lipids from *L. incisa* are degraded after nitrogen starvation

In the previous chapters, it was demonstrated that LiLOX catalyzed *in vitro* the oxidation of PUFAs that are esterified to MGDG molecules and to a lesser extend to DGDG and PC. It was also shown in the course of this study that *L. incisa* accumulates LiLOX transcripts up to six fold under nitrogen starvation (section 4.2). Moreover, LiLOX was proven to harbor a signal peptide that targets it in the chloroplasts (section 4.3), giving another hint that MGDGs are its endogenous substrate as they are the most abundant lipid class in these organelles. In order to prove that complex lipids, and especially MGDGs are the endogenous substrate of LiLOX, a lipidomics analysis focusing on LOX products was performed on *L. incisa* cell extracts. In order to detect LiLOX activity, *L. incisa* cells were grown in BG11N- medium (without
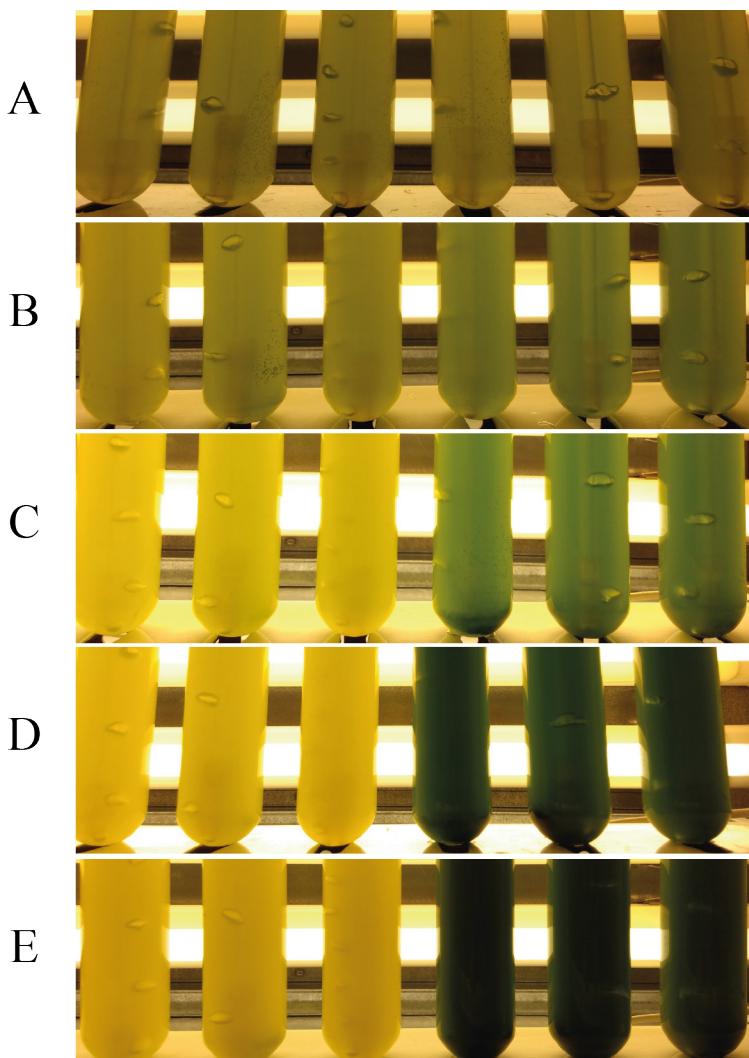
Figure 36. Effect of nitrogen starvation on *L. incisa*. The cells were grown at 25 °C in 300 mL BG11 medium, under constant irradiation with 190 μmol photons.m^{-2}.s^{-1} and aerated with an additional flow of 1 % CO_2. The three columns on the left are replicates of *L. incisa* cells grown in BG11N- medium. The three column on the right are replicates of *L. incisa* cells grown in BG11 medium. **A-E.** Pictures of the cells at five time points of growth. **A.** day zero. **B.** day one. **C.** day two. **D.** day five. **E.** day seven.

nitrogen supply) as well as BG11 medium (with nitrogen supply) as negative control. To ensure the presence of LiLOX in the cells, samples were collected after five and seven days for each condition. The analysis of 10 lipid classes by UPLC nanoESI QTRAP measurement was performed by Dr. Cornelia Herrfurth. A special focus was given to lipid compounds including MGDGs, DGDGs, and PCs identified in section 4.11, as substrates of LiLOX and the corresponding oxidation products. Since *L. incisa* is known to accumulate TAG under nitrogen starvation, this lipid class was also analyzed to ensure the proper starvation of the algae in BG11N- medium. Notably, the cultures of *L. incisa* grown in BG11N- turned yellow two days after nitrogen starvation, and this phenotype was amplified throughout the seven days of growth (Figure 36). The control cells grown in BG11 medium showed a green color that kept getting darker from day 0 to day 7.

Five days after nitrogen starvation, the levels of the two galactolipids MGDG and DGDG were observed to be lowered compared to the cells grown with nitrogen supply (Figure 37), suggesting a degradation of the chloroplast. The levels of the PC, phosphatidylethanolamine (PE) and phosphatidylglycerol (PG) however were not found to be affected by the nitrogen starvation, confirming that plastidic lipids are mostly affected under this stress. As it was expected, the TAG content was increased after five days of nitrogen starvation, confirming the accumulation of neutral lipids.

Despite the strong decrease of MGDG, DGDG, and PC molecules in *L. incisa* cells after nitrogen depletion, no lipid molecular species were detected with 1; 2; 3 nor with 4 additional oxygen atoms. This result was observed for all lipid classes analyzed, regardless of the nitrogen content in which the cells were grown or of the time point of the measurement suggesting the absence of endogenous LiLOX oxidation products. However, the detected molecular species in all three lipid classes confirmed the data obtained before in chapters 4.9 (Supplemental figure 4).
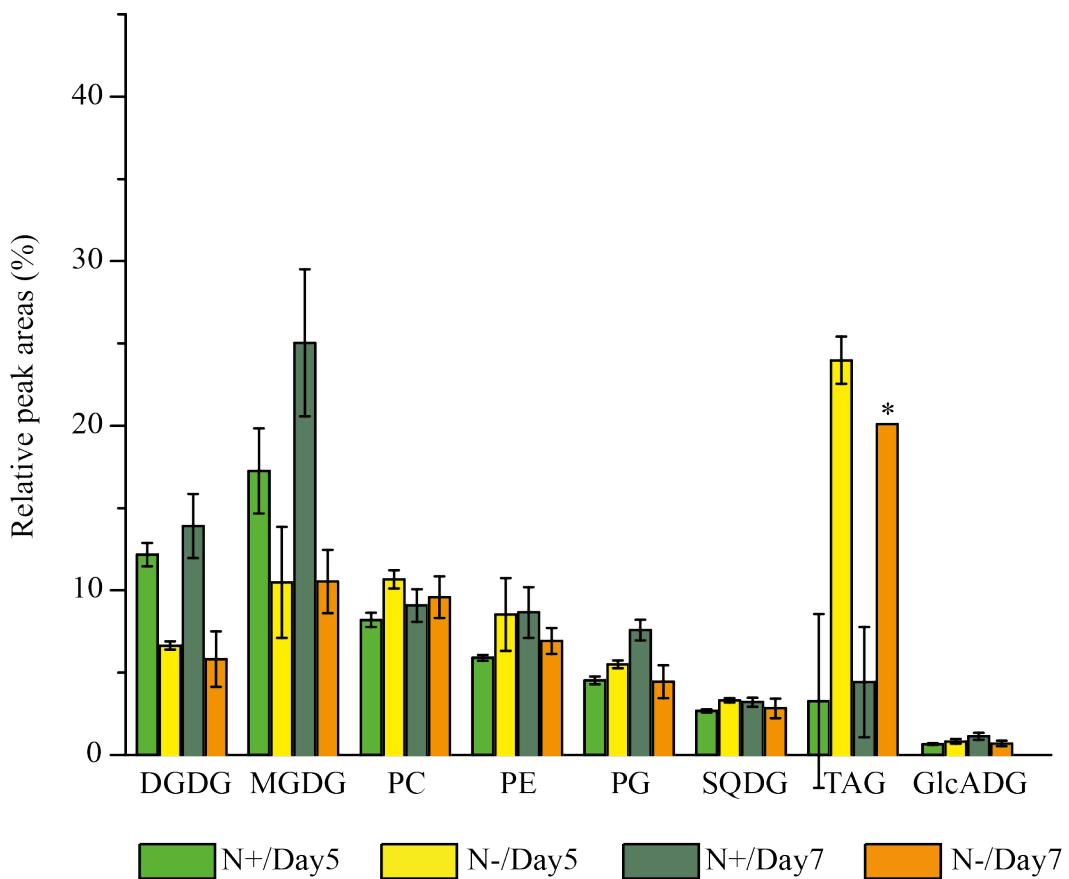
Figure 37. Analysis of complex lipids of *L. incisa* grown in BG11 medium (N+) and BG11N- medium (N-). After total lipid extraction the lipid species were analyzed by a multiple reaction monitoring (MRM) based LC-MS method. For each lipid class, the proportion relative to the total lipid measured is shown. Error bars represent the standard error of the mean of three *L. incisa* batches cultivated in parallel in a single experiment. The standard deviation of TAG levels at seven days after nitrogen starvation was not included, as the mean of two replicates are represented. The light and dark green bars represent the relative amount of lipids of the indicated lipid class of *L. incisa* grown for five respective seven days in BG11 medium. The yellow and orange bars represent the relative amount of lipids of the indicated lipid class of *L. incisa* grown for five respective seven days in BG11N- medium. The LC-MS analysis was performed by Dr. Cornelia Herrfurth.

4.15. LiLOX may be able to rescue the jasmonic acid pathway in wounded leaves of an *A. thaliana* 13-LOX-mutant.

Since in flowering plants the major function of plastidic 13*S*-LOXs is to catalyze the first oxidation step triggering the production of JA, the corresponding quadruple mutant from *A. thaliana* in which all genes encoding plastidic 13-LOXs are inactivated, is deficient in JA. Since JA is involved in regulating the pollen development, these mutants are male sterile. Therefore this mutant is a valuable tool to investigate the ability of LiLOX to rescue the JA pathway in *A. thaliana* by following this phenotype, and in particular the production of silique in the resulting transgenic plants. As expected, *A. thaliana* wildtype (WT) produced high amounts of siliques contrary to the 13-LOX KO mutant which presented few and small siliques, which were empty of seeds. Therefore, this mutant was transformed with the cDNA encoding
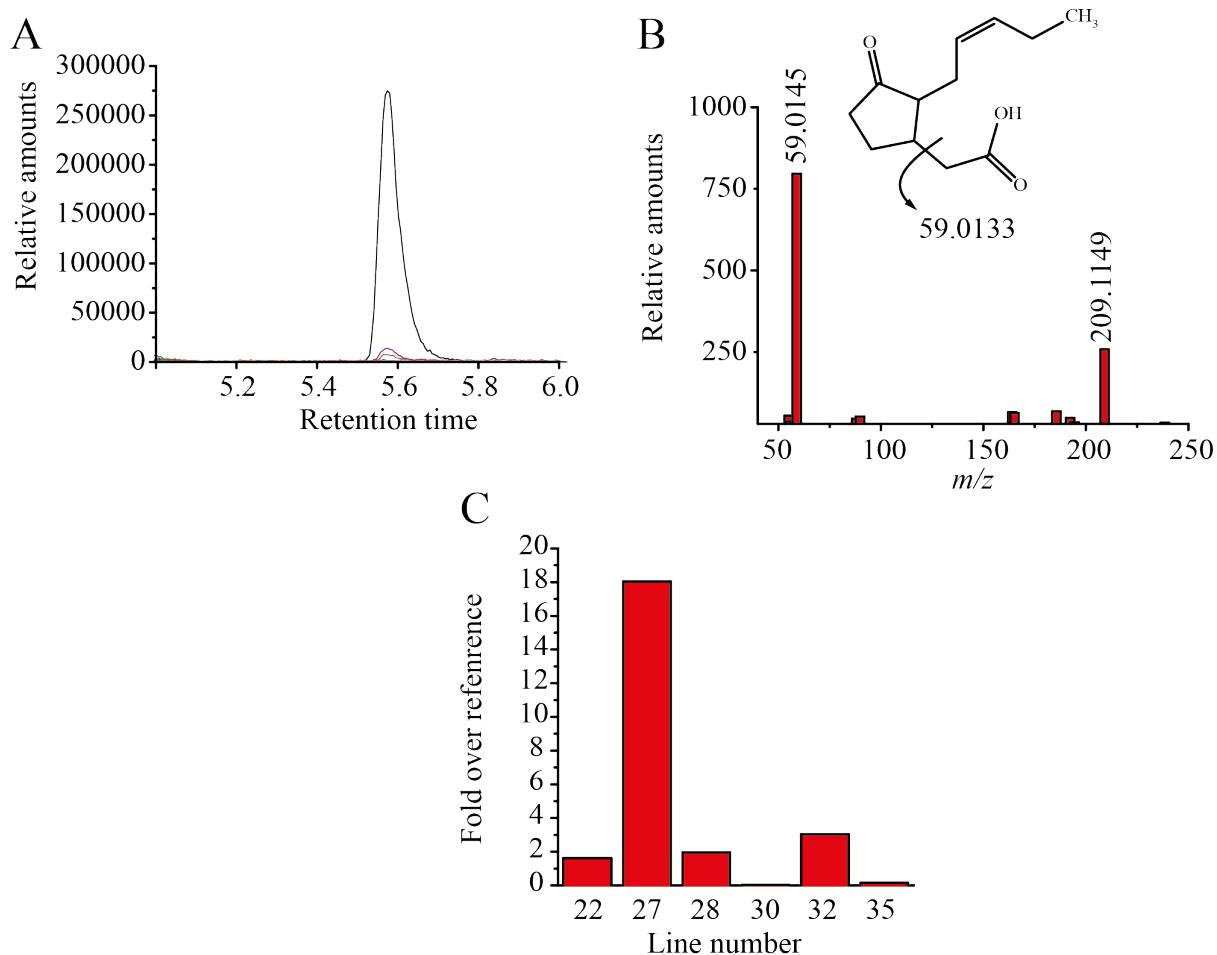
Figure 38. JA levels in 13-LOX KO lines of *A. thaliana* complemented with LiLOX. Leaves of 3 week old wild type plants, 13-LOX-KO lines and 13-LOX-KO lines complemented with 35S::LiLOX were wounded with forceps, harvested 2 h after wounding, extracted by ethyl acetate and analyzed by LC-MS. **A.** Extracted ion chromatograms for JA (*m/z* 209.1173) for 19 lines of 13-LOX-KO plants, one WT line and 17 lines complemented with 35S::LiLOX are shown. The main peak in black represents the JA-signal of the WT line. The 13-LOX-KO line showed no signal, while two of the 17 lines complemented with LiLOX (27 and 32) showed a very low, but significant JA-signal. **B.** The identity of JA in the two complemented lines was confirmed by its fragmentation pattern by LC-MSMS. **C.** Real time quantitative PCR measurement of LiLOX transcript in *A. thaliana* leaves of 13-LOX-KO lines complemented with LiLOX. Data shown represent a single experiment. The LC-MS analysis was performed by Dimitrij Rekther.

LiLOX under the control of a constitutive promoter. However, even after screening 40 independent transformants, it seemed that LiLOX was not able to rescue its phenotype. Yet, the 13-LOX-KO *A. thaliana* plants transformed with AtLOX4 under the 35S promotor as positive control were found to produce a high number of siliques harboring intact seeds, just as WT plants (performed by Dr. Ellen Hornung, data not shown). Although the developmental phenotype was not rescued, further investigations were performed in order to determine whether LiLOX was able to complement the JA pathway in other organs such as leaves, since the expression of the used promoter may have been insufficient only in the siliques. As the plants are sterile, they were sprayed with methyl-JA for two weeks in order to obtain and collect the seeds.

Next the wound-induced JA formation was tested in leaves. Three weeks after sowing of the resulting seeds, leaves were wounded to induce the JA pathway. Two hours after wounding, leaves were collected in order to perform lipid extraction by ethyl acetate, before analyzing JA levels by LC-MS (Figure 38A). While the WT plant clearly showed detectable levels of JA, the phytohormone was not detectable in the 13-LOX-KO. Two lines (line 27 and line 32), out of 40 transformed with LiLOX displayed detectable JA levels in the wounded leaves. The identity of JA in the two positive transformed lines was confirmed by MS/MS, as revealed by the characteristic fragment of *m/z* 59.0133 (Figure 38B). Although these two complemented plant lines showed JA levels being much lower than the WT, it was demonstrated that LiLOX may be able to complement at least the JA biosynthesis in *A. thaliana* leaves. In addition to the JA levels in the 13-LOX-KO plant lines complemented with LiLOX, the transcript levels in these lines were investigated. The protein phosphatase 2A (PP2A) was used as a reference gene. The two lines which showed detectable levels of JA upon wounding in leaves (lines 27 and 32) were selected for analysis, as well as four other lines chosen randomly as negative controls (Figure 38C). As a result, the JA producing lines showed the highest levels of LiLOX mRNA, being up to 18 fold over the reference gene suggesting a proper expression of the protein in *A. thaliana* plant leaves. However, it should be pointed out, that these experiments shall be regarded as being preliminary and need to be repeated in an independent experiment.

4.16.   LiLOX Mutations

As described above LiLOX is the first plastidic LOX that can be expressed heterologously in large quantities leading to a pure and stable enzyme. These properties together with its so far not described substrate specificity against glycolipids, makes it well suited for a more detailed characterization of its reaction mechanism being representative for this class of enzymes. As it is the case for most LOXs, the putative substrate channel in the predicted structure of LiLOX is composed of four α-helices, including an "arched helix" Figure 39A (Newcomer & Brash, 2015). In order to better estimate the active site of this predicted structure, the model of LiLOX was superimposed with PaLOX ((Garreta *et al.*, 2013), PDB accession number PDB: 5IR5) and PhLOX ((Neau *et al.*, 2014), PDB accession number: 4QWT).

Since these two published structures were co-crystalized with a substrate inside their active site, the position of the two acyl chains may reveal the predicted structure of the active site of LiLOX. The Figure 39B highlights 4 amino acids within the putative active site of LiLOX that may be relevant for activity. At the position of the Sloane determinants, LiLOX harbors an asparagine (N702) and a phenylalanine (F703). At the position of the Coffa site, an alanine (A688) is present. Relative to the residue A688, the iron binding residues are located at the opposite side of the putative channel.
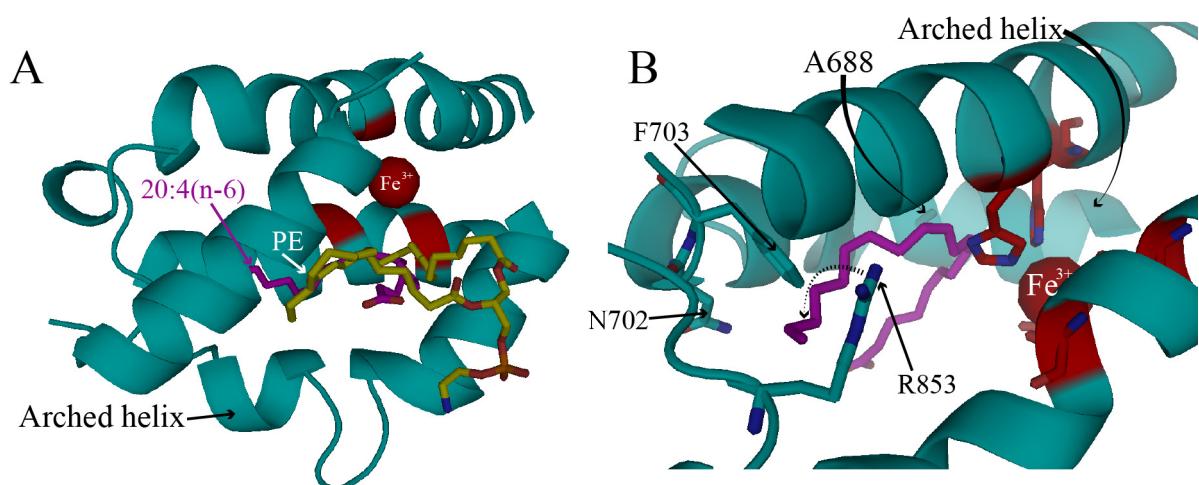
Figure 39. Superimposition of the predicted LiLOX structure with experimentally solved ones of *P. aeruginosa* LOX (PaLOX, PDB accession number: 5IR5) and *P. homomalla* LOX (PhLOX, PDB accession number: 4QWT). All three structures were aligned to one another by the software PyMOL. Helices from the predicted LiLOX structure (cyan cartoon) and the residues involved in the iron coordination (red) are shown. The substrate 20:4 (n-6) (pink sticks) from the 4QWT structure as well as the phosphatidylethanolamine substrate (yellow sticks) and the iron atom (red sphere) from the 5IR5 structure are represented. The arched helix from LiLOX was labeled to visualize the different orientation on both figures. **A.** α-helices of LiLOX forming the putative active site. **B.** Putative active site of LiLOX with 4 highlighted relevant residues (blue sticks). Because the residue A688 is not visible on this representation, the arrow point to the carbonyl group from the peptide bond.

4.16.1. Analysis of the reaction mechanism guiding the positional specificity of LiLOX by active site mutations

As LiLOX is the first plastidic LOX to be characterized, the model for the LOX regio-specificity was tested by mutating the Sloane determinant (Sloane *et al.*, 1991). These two bulky residues N702 and F703 at the end of the putative substrate-binding channel were mutated into a smaller threonine and a valine respectively. Contrary to LiLOX-WT which has a strong specificity for introducing dioxygen in the n-6 position of the fatty acid substrate, hence only producing 15*S*-HETE from 20:4 (n-6), the mutant N702T/F703V lost its specificity since it produced a mixture out of 5-HETE, 11*S*-HETE, 12*S*-HETE and 8*S*-HETE as well as the original 15*S*-HETE (Figure 40). The low amount of 5-HETE produced was found to be
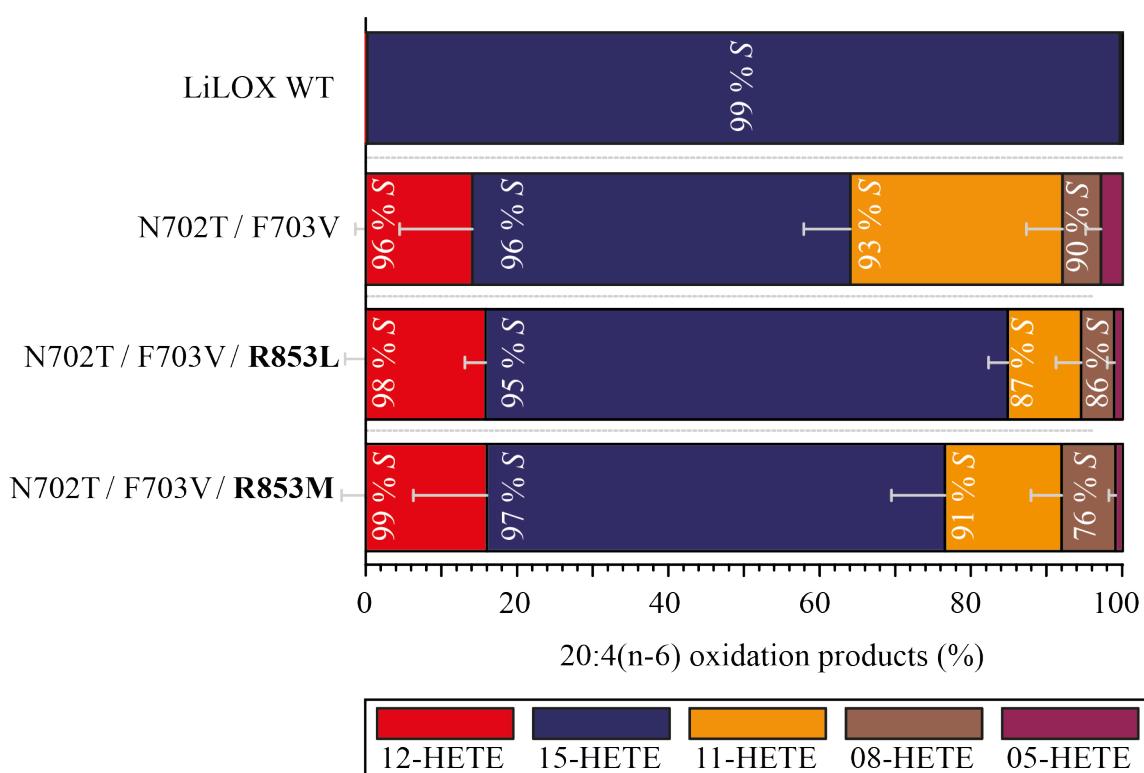
Figure 40. Comparison of oxidation products of LiLOX-WT with those of the LiLOX N702T/F703V mutant, LiLOX N702T/F703V/R853M mutant and LiLOX N702T/F703V/R853L mutant with 20:4 (n-6). Reactions were performed at pH 7.5 and products identified by SP-HPLC. 20 mM Bis-TRIS propane pH 7.5 was used as buffer with 100 µM of 20:4 (n-6). Each bar represents the amount of an oxidation product relative to the others (%). The error bars represent the standard deviations of the box on its right, for three experiments. Each experiments was performed with different enzyme preparations. The ratio of the two stereoisomers of each compound was determined by CP-HPLC and the result is given in each box, representative of one measurement.

racemic and considered to be at least a minor product or the result of auto-oxidation. As the 11-HETE formed by the LiLOX N702T/F703V mutant was found to be an *S* isomer, this phenomenon was attributed to an inverse orientation of the substrate in the active site (Head-to-tail). Since the Head-to-tail orientation was first attributed to an arginine at the bottom of the substrate-Binding channel, the so-called Hornung determinant (Hornung *et al.*, 2008), the

arginine R853 was mutated either into a methionine or a leucine. When compared to the LiLOX N702T/F703V mutant, the 15S-HETE/11S-HETE ratio of both mutants was found to be increased. Nevertheless, all mutants were found to be able to produce 12S-HETE, 11S-HETE and 8S-HETE despite the absence of a charged arginine residue at the bottom of the putative substrate channel. In summary, these data support the model of a tail-first orientation of the substrate in the active site, but a head-to-tail orientation may be possible when the Hornung determinant gets accessible for the substrate. Since this property seems to be a prominent feature of plant LOXs, these data support the phylogenetic analysis (Figure 8) that plastidic LOXs are closer related to extra-plastidic LOXs than to LOX enzymes from other genera.

4.16.2. Effect of pH on the position specificity

In case that the head-to-tail orientation is indeed guided by an arginine residue at the bottom of the substrate-binding channel, this orientation should be affected by the pH of the reaction buffer. This was found to be indeed the case. The pH of the reaction buffer affected the positional specificity of all mutants, but not of the WT, since here the arginine has according to our model no contact with the substrate. As expected, in the mutant N702T/F703V the ratio between 15S-HETE and 11S-HETE was found to be most influenced by the variation of the pH. While 15S-HETE was the major product at basic pH (58% at pH 8.0), 11S-HETE became the major product (62%) at pH 6.5 (Figure 42, supplemental figure 11). When it could be measured, the stereochemistry was not found to be affected by the variations of the pH. This pH effect was still present in the triple mutants, but less pronounced (Figure 42). It must be stressed that even though the overall activity of the mutant N702T/F703V was lowered compared to LiLOX-WT, its optimum pH was not affected (Figure 41).

In contrast to previous findings however (Hornung *et al.*, 2008), the pH effect was most likely based rather on steric than an ionic parameters. In case of a preferred ionic mechanism, the inverse orientation (11S-HETE formation) would be the preferred one in more alkaline conditions. Since the opposite was observed, it is more likely that only a protonated substrate can penetrate the active site in an inverse orientation in case of the mutants that seem to have an enlarged active site cavity.
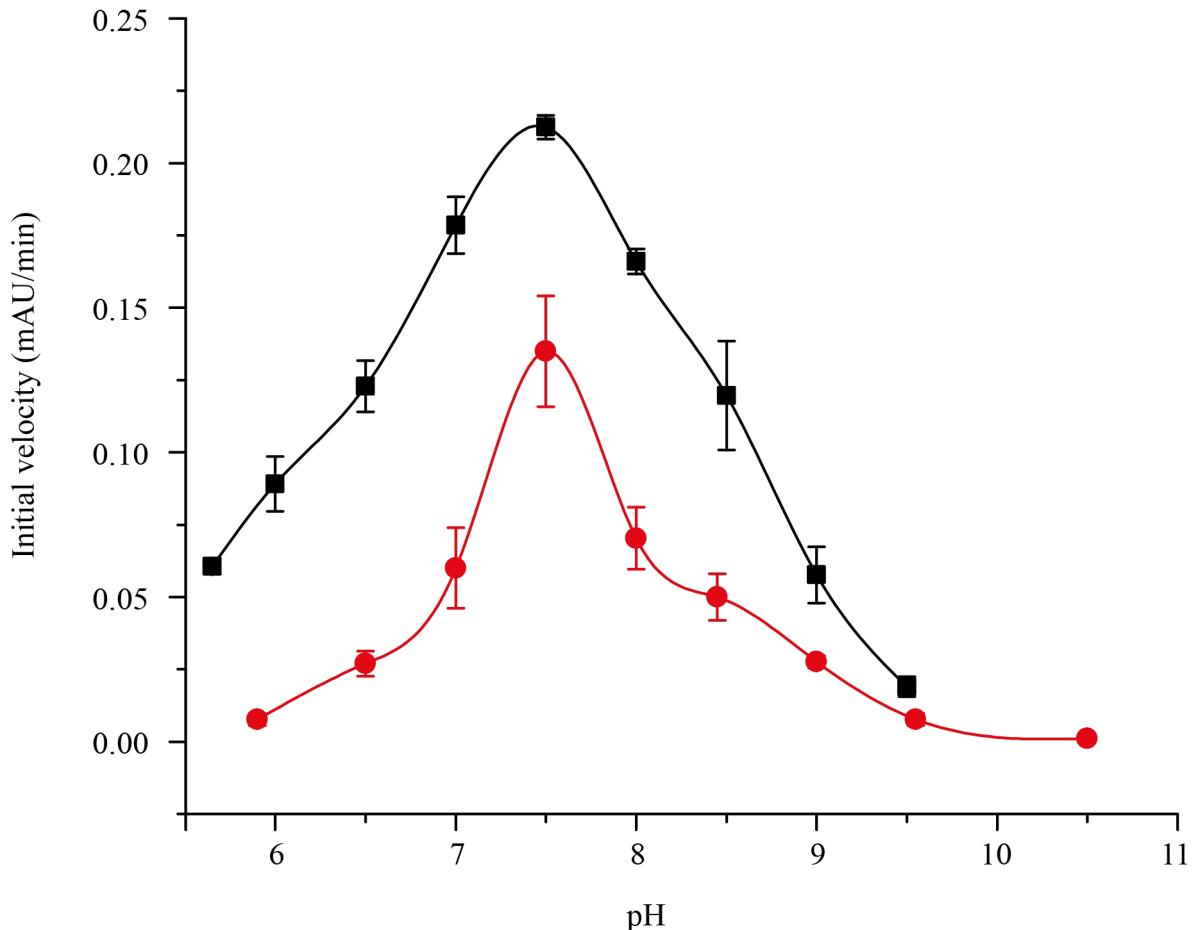
Figure 41. Spectrophotometric measurement of the pH optimum of LiLOX (black squares) and its N702T/F703V mutant (red dots). 20:4 (n-6) was used as substrate at a concentration of 100 μM. 20 mM Bis-TRIS propane was used as buffer. 1 μg of pure LiLOX WT and 2 μ of pure LiLOX N702T/F703V mutant were used to determine the initial slope of the LOX activity at a given pH. The reaction was detected as increase of absorbance at 234 nm. Error bars represent the standard deviation for three reactions. All three reactions were performed with the same enzyme preparation.
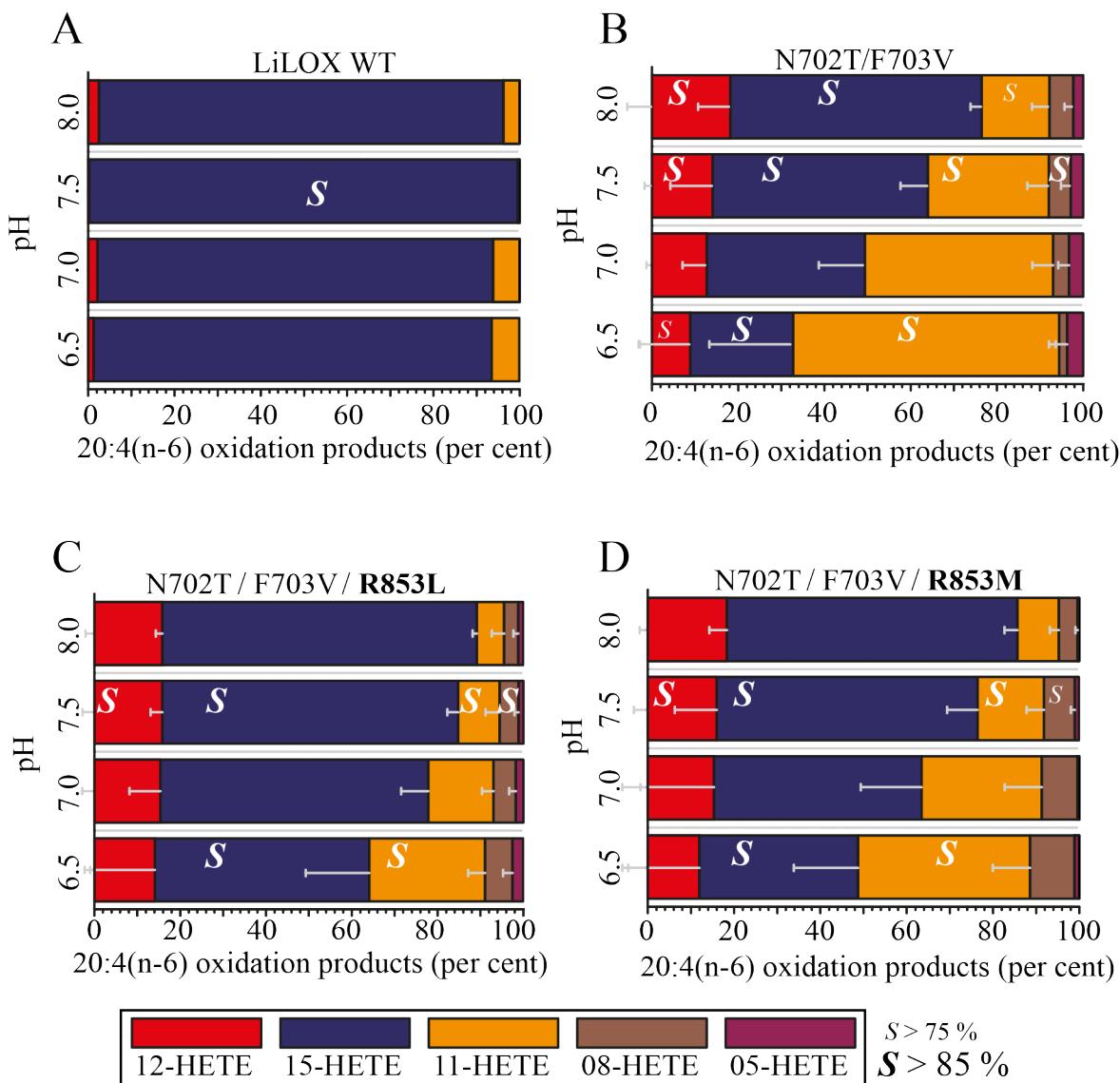
Figure 42. Effect of the pH on the oxidation products of LiLOX WT and mutants with 20:4 (n-6). Reaction products were identified by SP-HPLC. 20 mM Bis-TRIS propane was used as buffer for all reactions with 100 μM of FFA 20:4 (n-6). Each bar represent the amount of an oxidation product relative to the others (%).The error bars represent the standard deviations of the box on its right, for three experiments. Each experiments was performed with different enzyme preparations. The ratio of the two stereoisomers of each compound was determined by CP-HPLC and the result is given in each box, representative of one measurement. **A.** LiLOX WT **B.** LiLOX N702T/F703V **C.** LiLOX N702T/F703V/R853L **D.** LiLOX N702T/F703VR853M

4.16.3. Di-HETE formation

The model of inverse substrate orientation in the mutants was even further supported by the following observation. When recording the product formation of N702T/F703V on the photometer, the characteristic peak for a conjugated triene, with maximum absorbance at 271 nm, was observed as soon as 3 minutes into the reaction (Figure 43A). After 10 minutes, the signal measured at 234 nm was starting to decrease, meanwhile the peak at 271 nm kept increasing. After derivatization and analysis by gas chromatography (GC)-MS/MS, this

compound was confirmed to be 8,15-Di-HETE (Figure 43B). This product was also measured to be produced in higher abundance, as much as 8 times more, when the reaction took place in acidic conditions (Figure 43C). Similar results were observed with the mutants N702T/F703V/R853L and N702T/F703V/R853M.
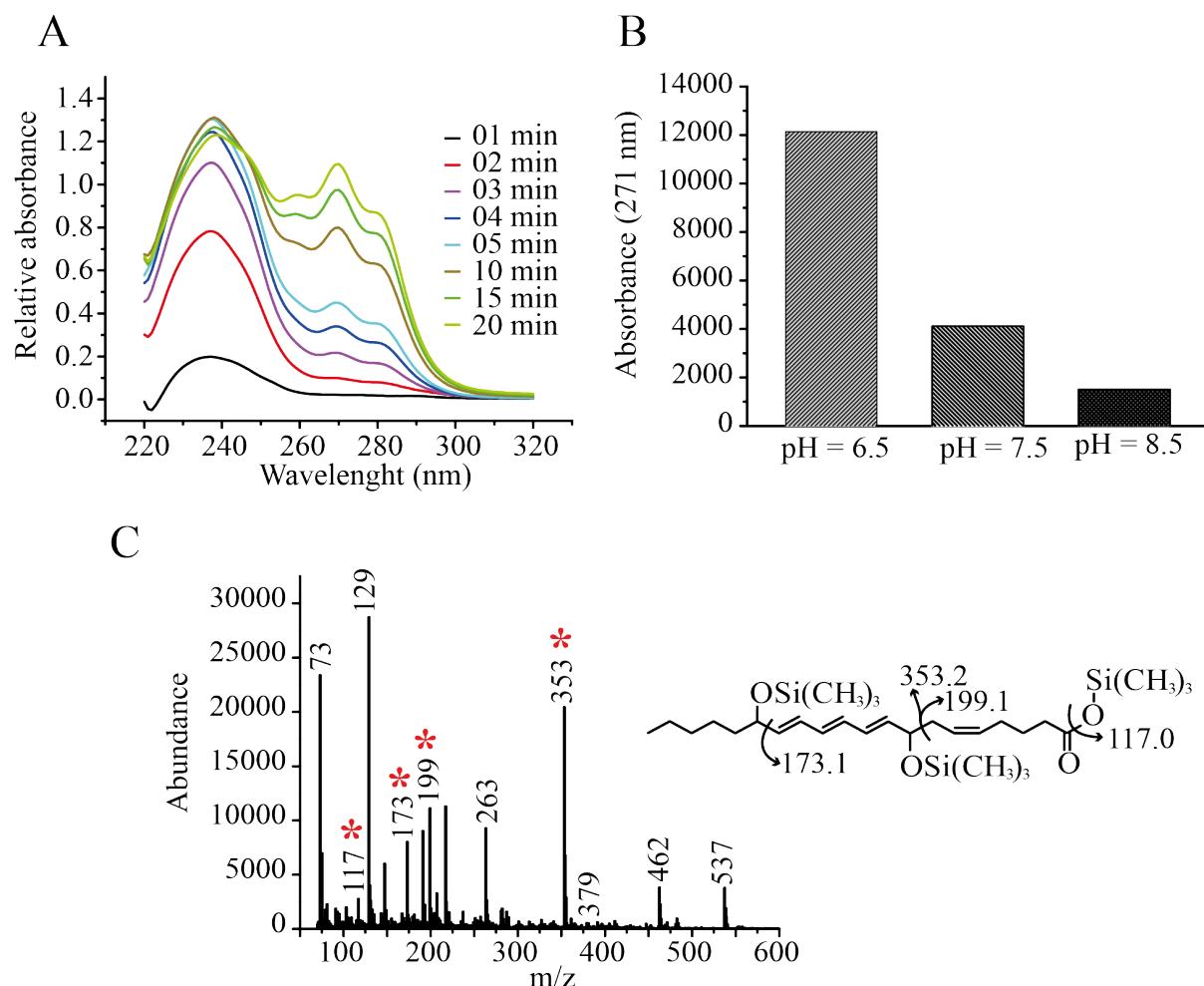
Figure 43. Di-HETE formation by the *L. incisa* LOX mutant N702T/F703V with the free fatty acid 20:4 (n-6). 20 mM Bis-TRIS propane was used as buffer, and 100 µM of 20:4 (n-6) was incubated for 1 h with 1 µg of pure LiLOX N702T/F703V mutant. Results were obtained from a single experiment. **A.** Kinetic measurement by spectrophotometer, recording the reaction from 220 nm to 330 nm, from 0 to 20 minutes. The baseline level is established after addition of LiLOX. **B.** Abundance of Di-HETE at different pHs, represented by integrated peaks from the RP-HPLC. **C.** Fragmentation of the expected Di-HETE by GC-MS/MS. The GC-MS/MS analysis was performed by Dr. Till Ischebeck. Data shown represent a single experiment.

5. DISCUSSION

5.1. LiLOX, a model for plastidic LOXs

Knowledge on the underlying biochemical processes of lipid oxidation in green algae is scarce. Therefore, the aim of the thesis was to close this gap by searching the genome of the green alga *L. incisa* for a LOX, being the major lipid-oxidizing enzyme in plants, and analyzing it on a transcript and protein level. Indeed in the course of this study, the protein sequence of LiLOX was found. It shares a high identity with plastidic LOXs from higher plants. This seems to be in concordance with the widely accepted theory that green algae are precursors of higher plants (Yoon *et al.*, 2004). Moreover, a putative LOX reported from genomic data of another green alga, *C. reinhardtii* (Merchant *et al.*, 2007), groups close to LiLOX and plastidic plant LOXs (Figure 8, supplemental Table 1). In addition, cyanobacteria are accepted to be the evolutionary precursors of plastids (de Alda *et al.*, 2014). However, LOXs from this phylum are much more diverse (Andreou *et al.*, 2009): for example the two LOXs characterized from the cyanobacterium *Cyanothece* SP.PCC8801, CspLOX1 and CspLOX2, seem to be different from other algal and plant LOXs, including LiLOX. Yet this might be easily explained by the variety of cyanobacteria, and the evolutionary distance between *Cyanothece* SP.PCC8801 and the one from which eukaryotic plastids evolved (de Alda *et al.*, 2014). Nevertheless, even if its origins are unknown, it seems that LiLOX and plastidic plant LOXs share a common ancestor, based on evolutionary data and by their sequence homology. Besides the sequence homologies, this study demonstrated that LiLOX has a similar pH optimum, positional specificity and stereo specificity as all characterized plastidic LOXs (Liavonchanka & Feussner, 2006). It was also shown that LiLOX harbors a plastidic N-terminal signal peptide that targeted it to the proplastids of onion cells.

Furthermore, four LOXs targeted to the chloroplasts have been characterized from the flowering plant *A. thaliana*, all known to be responsible for the first reaction of a cascade leading to the biosynthesis of JA, as mentioned in the section 1.3.3 (Farmer & Ryan, 1992). It was formerly reported that knock out mutations in two of these LOXs (AtLOX3 and AtLOX4) prevents the production of JA in the flower, leading to male sterility (Caldelari *et al.*, 2011). AtLOX2, AtLOX6 as well as the other enzymes from the JA cascade were reported to be highly upregulated at early stages of wounding (Bell *et al.*, 1995; Chauvin *et al.*, 2013) and are believed to be responsible for most of the JA production under this stress.

Preliminary data from the present study may suggest that the complementation of *A. thaliana* 13-LOX-KO by LiLOX under a constitutive promotor was able to rescue the biosynthesis of JA in the wounded leaves. The two positive plant lines that complemented this phenotype in

one out of two experiments were also those showing the highest accumulation of LiLOX transcripts, suggesting again the involvement in the recombinant enzyme. Although the level of JA was most likely not sufficient in the pollen to rescue the male fertility, this experiment suggests that *A. thaliana* might be able to express an active form of LiLOX, despite the evolutionary distance between the two organisms.

All these findings are in agreement with the hypothesis that LiLOX and plastidic LOXs in vascular plants share a common ancestor. Yet, contrary to the later plastidic LOXs, LiLOX could be expressed heterologously in milligram quantities. After purification in two steps, LiLOX was found to be active *in vitro* and conditions leading to its crystallization were even reported. Altogether, this study highlights the fact that LiLOX is a very suitable model to study plastidic LOXs.

5.2. LiLOX and mutants

As the biochemical properties of any plastidic LOXs were so far never investigated in detail, the biochemical properties of LiLOX were analyzed in the course of these studies. Besides the substrate specificity, its regio and stereochemical properties as well as its kinetic parameters were recorded. In addition, mutational studies were performed on LiLOX to test whether either one of the existing models to explain LOX regio- and stereospecificity (section 1.3.2) could be applied to this class of enzyme. After a specific hydrogen was abstracted from a *bis*-allylic carbon, four models exist to describe LOX regiospecificity (Schneider *et al.*, 2007): (i) steric shielding, (ii) oxygen channeling, (iii) peroxyl radical trapping and (iv) radical localization 1.3.2. These four mechanisms involve the active site of the LOX, in the close environment of the iron. This environment is believed to be quite tight around the acyl chain substrate, and mutations performed on an amino acid residue increasing, even slightly, the diameter of the channel in this region was often described to decrease the LOX reaction rate drastically or resulted in inactive enzymes (Coffa & Brash, 2004; Newie, 2016). However in the course of this study, mutations were only attempted at the bottom of the substrate channel from LiLOX, based on its predicted structure.

In the case of substrates with more than one pentadiene, additionally to the four models explaining the LOX specific oxidation, two factors might influence the specific selection of one pentadiene system. Firstly, the substrate orientation inside a LOX substrate channel might affect the selection of the *bis*-allylic carbon, especially in the case of 15-LOX and 5-LOX. In addition, an inverted orientation of the substrate must switch the side of the substrate from which the hydrogen is removed, and the side from which the oxygen is inserted. In the case of esterified acyl chains, the substrate orientation is not subject to much debate. Since the carboxyl end (head) is *de facto* linked to a bulky headgroup, its penetration into the LOX active site is very unlikely. Moreover, as LiLOX was found to oxidize acyl chains with the same regiospecificity regardless of whether they are linked to a head group or not, this strongly suggests that the substrate always penetrates the active site with its methyl end (tail) first as it
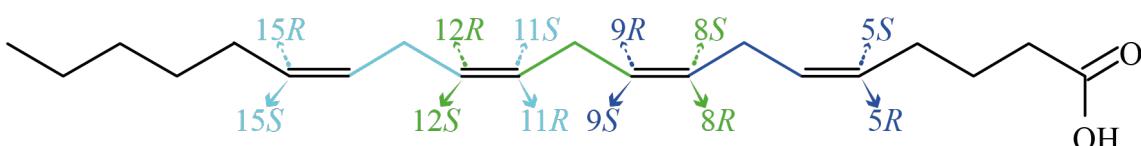
Figure 44. All possible LOX oxidation products from 20:4 (n-6). The colors highlight the three *bis*-allylic carbon groups present in this FFA. Four oxidation products are possible after one hydrogen has been abstracted from a *bis*-allylic carbon atom, depicted in the corresponding color. The representations of two stereoisomers are differentiated according to their loation either above the fatty acid (behind the plane) or below (above the plane).

was found to happen with all tested acyl chains including FFAs. In addition to this simple model of either tail-first or head-first orientation, regiospecificity of fatty acids has to take into account not only the substrate orientation, but also a frame shift between alternative pentadiene systems within the same orientation (Schneider *et al.*, 2007). Therefore, the regiospecificity of oxidation on these substrates can only be explained by combining two or more models.

Since 15*S*-HETE was found to be the only LiLOX product from 20:4 (n-6), it seems that the iron of LiLOX performs the hydrogen abstraction on the 13th carbon, and that the dioxygen molecules are directed in [+2] (Figure 44). As none of the 12th nor 9th carbons are oxidized, frameshift of the substrate or a yet unknown oxygen channel seems to play a role in product formation. Moreover, the fatty acid slides in and aligns around the iron with the pentadiene system being closest to the methyl end of the fatty acid. This suggests in addition that the Sloane determinant (Figure 39, Figure 45) blocks the fatty acid from penetrating deeper into the active site. This is supported by the fact that the mutations N702T/F703V, expected to enlarge the bottom of the LiLOX substrate channel, leading to a modified LiLOX product composition. The ability of LiLOX N702T/F703V mutant to produce 12*S*-HPETE suggests that 20:4 (n-6) could penetrate deeper into the channel, allowing hydrogen abstraction on its 10th carbon (Figure 45 B$_2$). Yet in addition to 12*S*-HPETE and 15*S*-HPETE, other products were formed by this mutant: 11*S*-HPETE, and 8*S*-HPETE. The most probable theory to explain these oxidation products is an inversed orientation of the substrate inside the substrate channel of LiLOX (Head-first orientation) (Hornung *et al.*, 1999).

Indeed, contrary to complex lipids, the carboxyl group of a FFA is not esterified, and could in theory penetrate first inside the LOX substrate channel. Moreover, only with such an orientation of the substrate could the dioxygen molecule be inserted in an antarafacial way to the positions pro8*S* and pro11*S*. In addition, a head-first orientation would be consistent with the reduced size of amino acid residues 702 and 703, allowing a bulky carboxyl group to penetrate the bottom of the substrate channel (Figure 45 B$_3$).

Furthermore, it has been discussed that a charged residue at the bottom of the LOX substrate channel could be stabilized by a salt bridge between the carboxyl group of the FFA with a basic arginine residue, hence favoring this substrate orientation at basic pH (Browner *et al.*, 1998; Hornung *et al.*, 1999). It should be pointed out that this model, suggesting to bury a charged substrate in the hydrophobic substrate channel of LOXs, was always discussed controversially (Browner *et al.*, 1998). However, in the predicted structure of LiLOX a charged arginine (R853)

was indeed found to be localized at the bottom of the substrate channel supporting this model. In order to confirm its involvement in an inverse head-first substrate alignment, this arginine was mutated into a leucine (similar size, non-polar, non-charged) and a methionine (similar
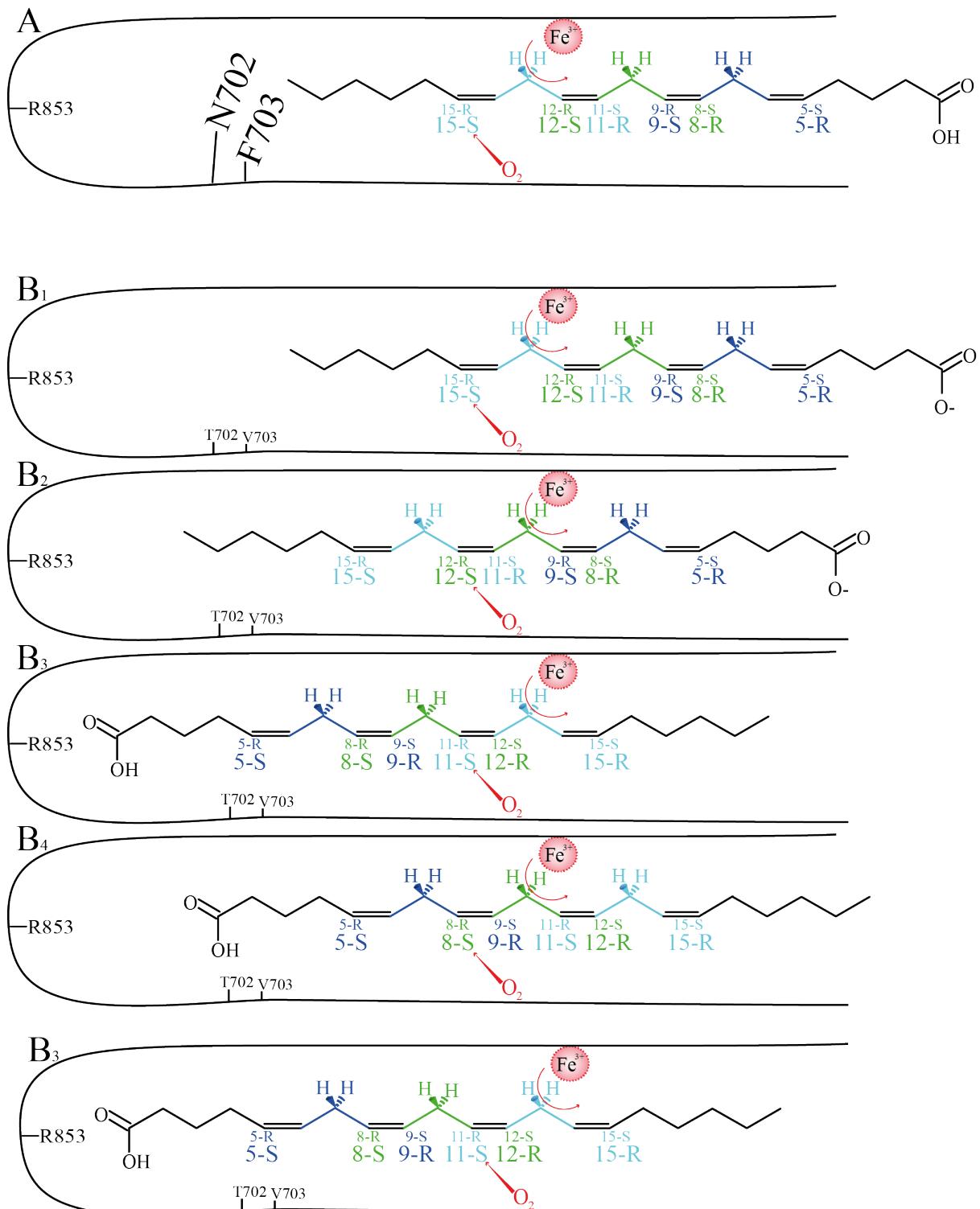
Figure 45. Models to explain the oxidation products formed in the substrate channel of LiLOX and its mutants, assuming that the direction of the molecular oxygen (red) is not affected by the mutations. The colors highlight the three *bis*-allylic carbon groups present in this FFA. Four oxidation products are possible after one hydrogen has been is being abstracted on a *bis*-allylic carbon atom, depicted in the corresponding color. The representations of two putative stereoisomers are differentiated by the size of the font, small (behind the plane) or big (above the plane). **A.** 20:4 (n-6) oxidation products by wildtype LiLOX. **B₁₋₄.** Four different 20:4 (n-6) oxidation products by the LiLOX N702T/F703V mutant.

size, polar, non-charged). As a result, the ratio 15*S*-HPETE/11*S*-HPETE was found to be higher than in the LiLOX N702T/F703V mutant. Yet, both mutants LiLOX N702T/F703V/R853L and LiLOX N702T/F703V/R853M were found to be able to produce 11*S*-HPETE and 8*S*-HPETE despite the absence of a charged residue at the bottom of the pocket. This highly suggests that 20:4(n-6) can align in an inverse orientation in the active site channel of LiLOX even without the assistance from a charged residue at the bottom of the substrate channel.

Additionally, the pH was found to have no effect on the positional specificity of WT LiLOX, but had a strong influence on all mutants. At acidic pH in particular, highly favored positional isomers were 11*S* and 8*S*-HPETE, hence the head-first orientation. Coffa *et al*. attributed this effect to the protonation of the carboxyl group at acidic pH. Once protonated, the carboxyl group becomes non-charged, less polar and therefore more likely to penetrate the highly non-polar substrate channel (Coffa *et al*., 2005b). The observed pKa of FFAs, between 7 and 8 depending on the concentration would be in agreement with this theory (Glickman & Klinman, 1995). In contrast to what was proposed earlier (Browner *et al*., 1998), this theory would limit the role of the R853, initially believed to form a salt bridge with the carboxyl group of the FFA.

Yet when mutated, the absence of R853 does have an effect on the 15*S*-HETE/11*S*-HETE ratio (Figure 42). This phenomenon, observed by Hornung *et al*. (Hornung *et al*., 2008), is in contrast to the initial model that the pH alone affects the positional specificity (Gardner, 1989; Veldink *et al*., 1972) and suggests rather another role for the residue R853. At basic pH, the FFA was shown to have a strong preference for the tail-first orientation. However when protonated, the substrate loses this preference, and penetrates the substrate channel in both orientations. If it happens to be inserted head-first, the residue R853 may only play a role in stabilizing the carboxyl group of the FFA via polar interactions. This would increase the likelihood of a hydrogen abstraction at the carbon 13 or 10 and an oxidation at the positions pro11*S* or pro8*S* respectively. This theory may also explain the difference in the oxidation products between the mutant LiLOX N702T/F703V/R853L and LiLOX N702T/F703V/R853M, since the non-polar leucine would be unable to have polar interactions with the carboxyl group of the FFA.

The head-first orientation is further supported by the formation of 15,8-Di-HPETE catalyzed by these mutants. This product was already discussed in the same context before (Coffa *et al*., 2005a), and is the result of a reaction whereby the substrate is being oxidized twice, in tail-first orientation at position pro15*S*, and in head-first orientation at the position pro8*S*. The fact that the 8,15-Di-HPETE product is observed in higher abundance at acidic pH supports the

hypothesis that in the case of LiLOX an inverse substrate alignment in the active site is more likely to happen when the FFA is protonated.

5.3. LiLOX is the first LOX shown to metabolize MGDG

A major finding of this thesis was that LiLOX was *in vitro* not only able to oxidize FFAs, but in addition it was found to be able to accept acyl chains esterified not only to PC but also MGDG and DGDG. While it is widely accepted that certain LOXs metabolize phospholipids under physiological conditions, results obtained in this study provide first evidence that LiLOX accepts in addition glycolipids such as MGDG and DGDG which may even serve as endogenous substrates.

5.3.1. The stroma of photosynthetically active chloroplasts has a pH optimum that is optimal for LiLOX activity

After transient expression in onion cells, LiLOX was found to be targeted to their plastids, clearly suggesting the presence of a plastidial N-terminal signal peptide. Even though onion epithelial cells have only plastids and no fully developed chloroplasts, this organelle is well described to be functionally similar to other plastid forms, including chloroplasts (Pogson *et al.*, 2015). Furthermore, LiLOX has high sequence identities with plastidic LOXs from vascular plants and shares their regiospecificity for substrate oxidation. This, together with the fact that algae seem to be the first organisms to ever possess a cytoplasmic plastid, leads to the model that they serve as the evolutionary ancestor of vascular plants and it seems very likely that the plastidial LOXs in both types of organism fulfill similar physiological functions. Within the plastid, LOXs are found to be located in the stroma (Blée & Joyard, 1996; Liavonchanka & Feussner, 2006). The pH optimum of LiLOX (pH 7.5) would be in agreement with a location inside the stroma, since its pH is neutral (≈7.0 - 7.2) during the night, and increases slightly (≈7.8 - 8.0) during the day when photosynthesis takes place (Robinson, 1985; Tikhonov, 2012).

5.3.2. LiLOX and its galactolipid substrates are specifically found in the same organelle, the chloroplasts

Chloroplasts have been described to harbor a very high variety of different lipid classes such as MGDGs, DGDGs, TriGDG, PCs, PEs, PGs, sulfoquinovosyldiacylglycerols (SQDGs), Glucuronosyldiacylglycerols (GlcADGs), the most abundant of which are galactolipids, in particular MGDG and DGDG (Kobayashi & Wada, 2016). As saturated acyl chains cannot be

oxidized by LiLOX, the hypothesis that SQDG and/or PG, which are highly saturated lipids in *L. incisa* (Bigogno *et al.*, 2002a), are the natural substrate of LiLOX seems rather unlikely. Moreover, as it is assumed that LiLOX is targeted to the stroma of plastids, the enzyme would therefore be in contact with the inner envelope of the plastid and in case of chloroplasts with the thylakoid membranes. These two membranes were described to be almost exclusively composed of MGDG and DGDG in plants (Kobayashi, 2016). Besides being the main component of the thylakoid membrane and the inner plastid envelope, MGDG and DGDG are described to be highly unsaturated in *L. incisa* (Bigogno *et al.*, 2002a), which was confirmed in this study (Table 42). Indeed, all acyl chains of MGDG were found to harbor at least one pentadiene system and only two species of DGDG out of 10 have acyl chains harboring fewer than 4 double bonds. Since they are the most abundant lipid classes accessible from the stroma of the chloroplast, and as they are highly unsaturated, the two galactolipids MGDG and DGDG represent the best candidates for being the natural substrates of LiLOX.

5.3.3. All MGDG species of *L. incisa* were found to be oxidized by LiLOX *in vitro*

Besides their subcellular localization, plant LOXs were found to accept complex lipids as substrates such as phospholipids (Banthiya *et al.*, 2016; Garreta *et al.*, 2013), MGDG and DGDG (Ibrahim *et al.*, 2011; Nakashima *et al.*, 2011). However, it should be pointed out that except for LOX2 from *Arabidopsis*, experimental evidence showing specifically which plastidic LOX metabolizes glycolipids is still missing (Mochizuki *et al.*, 2016). This study shows for the first time direct experimental evidence that a purified recombinant LOX oxidizes MGDG and DGDG *in vitro*. After product analysis, all molecular species of MGDG purified from *L. incisa* were found to be oxidized by LiLOX on both acyl chains (in red, Table 44). A similar result was observed for 8 out of 10 LiDGDG molecular species, whereas only 4 LiPC molecular species out of 9 were accepted as substrate by LiLOX (in red, Table 44). Even if part of these results can be explained by the saturation level of these lipid classes, it cannot be the only explanation. Indeed, the PC molecules 34:2, 36:3, and 38:5 were not found to be oxidized at all although these species in *L. incisa* were found to have at least one pentadiene system (Supplemental Figure 4).

Table 44. Summary of all apparent molecular species of LiMGDG, LiDGDG as well as LiPC accepted by LiLOX as substrate. Lipids were purified from *L. incisa* grown for 2 days in BG11 medium after a total lipid extraction, lipid class separation by SPE followed by TLC. All species found to be oxidized by LiLOX on both acyl chains are depicted in red. *The PC species 36:4 is the only one that was observed with either 2 oxygens or 4 additional oxygens.

Apparent species of	34 carbons acyl chains (C16 + C18)	36 carbons acyl chains (C18 + C18 or C16 + C20)	38 carbons chains (C18 + C20)
MGDG	34:4 34:5 34:6		
DGDG	34:2 34:3 34:4 34:5 34:6	36:4 36:5 36:6	38:6 38:7
PC	34:1 34:2	36:2 36:3 36:4* 36:5	38:5 38:6 38:7

5.3.1. MGDG is the complex lipid that is most readily turned over by LiLOX

In order to compare the activity of LiLOX towards complex lipids, the oxidation kinetics were followed with MGDG, DGDG and PC. Since the attempts to measure the kinetic parameters in the presence of detergents fitted neither the Michaelis–Menten nor the Hill equation, reaction rates were measured for all substrates at the same concentration (Figure 28). Under these conditions, MGDG was found to be oxidized 4.9 times faster than DGDG, and 9.4 times faster than PC *in vitro*. Three factors might explain this phenomenon: (i) It must be noted that in the case of complex lipids that were prepared from fresh cultures, the LOX reaction might not be stoichiometric, since the desaturation degree in the different lipid classes was not the same, as seen in Table 44. Nevertheless, as half of the acyl chains from LiPC were found to be accepted by LiLOX, the different degree of saturation of this lipid class cannot explain alone such a high difference in reaction rate. (ii) The solubility of each lipid class in the reaction mixture might also affect the reaction rate. As DGDG harbors two galactosyl head groups instead of one in case of MGDG, this lipid class is expected to be more polar than MGDG and therefore may be

better soluble in the reaction buffer. Despite this, LiDGDG was found to be oxidized by LiLOX 4.9 times slower than MGDG. Therefore another factor must be taken into account explaining the high rate at which LiLOX oxidizes MGDG: (iii) Amino acid residues located at the entrance of the LiLOX substrate channel might stabilize the headgroup of MGDG, influencing the overall turnover. The latter factor can be regarded as the most likely explanation for the observed substrate preference for complex lipids.

5.3.2. The entrance of the LiLOX substrate channel might preferentially stabilize the binding of MGDG

Lipid classes with different headgroups have very different biochemical properties, in terms of bulkiness, charge and polarity. Therefore it seems reasonable that certain amino acid residues react differently towards lipids having different types of headgroups. Headgroups of phospholipids are rather small and may harbor two charges: the negatively charged phosphate group, and the positively charged amine (PE) or choline group (PC). The headgroup of MGDG is much bigger and not charged, harboring many alcohol groups that could take part in hydrogen bonding with surrounding polar amino acids or water molecules. As the crystal
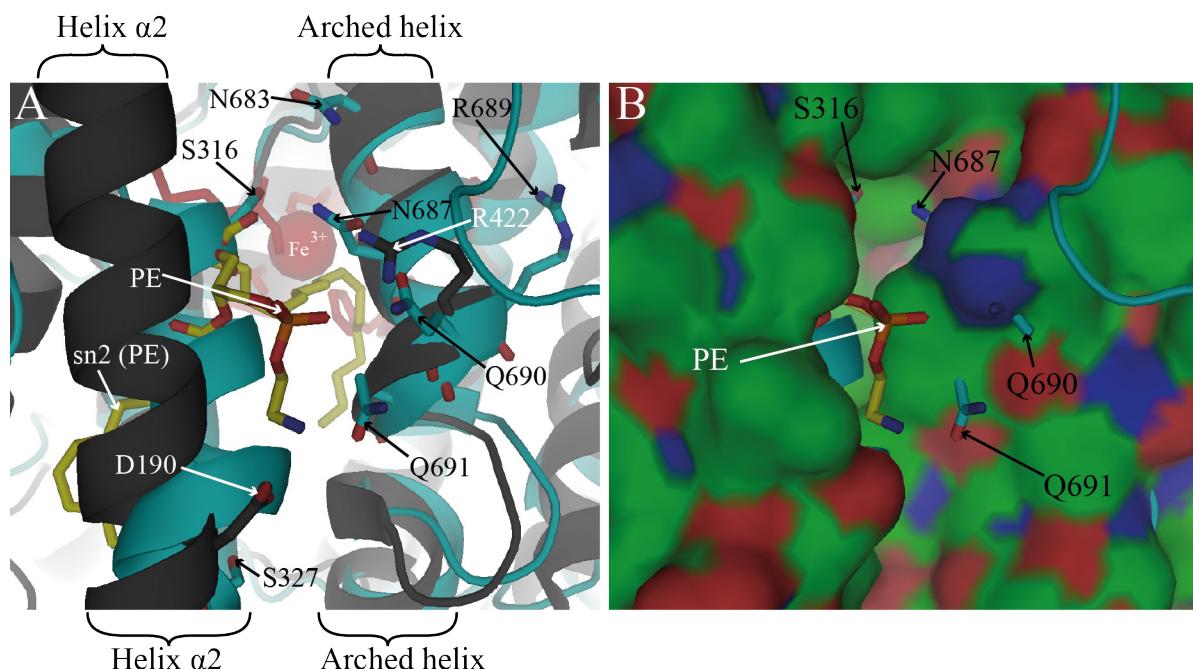
Figure 46. Superimposition of the modeled structure of LiLOX (black labels) and PaLOX (white labels, PDB accession number: 5IR5). Shown is the entrance of the substrate channel. **A.** The modeled structure of LiLOX is depicted as cyan cartoon and sticks. PaLOX is depicted as black cartoon and sticks, the substrate PE in yellow sticks and the iron as red sphere. **B.** The surface of PaLOX and the substrate PE with which it was co-crystalized are represented, highlighting the entrance of the substrate channel. Four residues from the predicted structure of LiLOX are pointing outside, shown in cyan with black labels.

structure of PaLOX has been obtained containing PE in the active site (Garreta *et al.*, 2013), this structure was superimposed to the predicted structure of LiLOX using the software PyMOL.

In analyzing these structural data, *Banthiya et al.* describe two amino acid residues from PaLOX that are stabilizing the PE headgroup (Banthiya *et al.*, 2016). D190 stabilizes the positively charged amine group and R422 stabilizes the negatively charged phosphate group by most likely forming salt bridges (Figure 46A, black residues, white labels). When the predicted LiLOX structure (cyan) is superimposed to this protein (black), it can be observed that the α-helix number 2 (α2) is not perfectly positioned, as it superposes with the PE substrate. Yet the homologous helix from the GmLOX1 was described to be very fluctuant (Bradshaw & Gaffney, 2014) and is likely to be "pushed" away from the arched helix, opening the active site when a substrate is present. Nevertheless, in the crystal structure of PaLOX, the n-8 carbon of the *sn1* acyl chain from PE is located next to the iron atom, as it has been predicted to be the case for LiLOX (Figure 21). Moreover, the five iron ligands in the predicted LiLOX structure were shown to be in concordance with the iron atom from PaLOX. Also the shown two alpha helices from both PaLOX and LiLOX were found in concordance. These two last observations suggest that the distances of the iron position to the entrance of the substrate channel is about the same in both PaLOX and LiLOX. Therefore the model for LiLOX may be valid enough to derive predictions about interactions that could happen with a lipid headgroup at the entrance of the putative substrate channel of LiLOX.

Contrary to PaLOX, no positively charged residues are observed on this part of the arched helix, forming part of the entrance of the pocket, which could stabilize a negatively charged phosphate group. Homologous to the R422 in PaLOX could be R689 in LiLOX. Although this residue seems to be highly conserved among LOXs (Supplemental Figure 9), it may be too far away from the entrance in the LiLOX model and may rather form a salt bridge with the highly conserved E654 as it was observed in the structure of PhLOX (Neau *et al.*, 2014). It is therefore unlikely to directly interact with a substrate's headgroup, thus rendering a stabilization of a phosphate head group unlikely. Instead, of this arginine, two asparagine and two glutamine residues were found on the arched helix of LiLOX, facing the entrance of the channel on the model: N683, N687, Q690 and Q691 (Figure 46A, cyan residues). These amide groups may have a strong C=O dipole and a weaker N-H dipole, both being susceptible to act as hydrogen bond acceptors, possibly for one of the alcohol groups of the galactosyl headgroup of either MGDG or DGDG. Similarly, no acidic residue homologous to D190 found in PaLOX was observed on the helix α2 of LiLOX. Instead this helix is rather non-polar, being rich in leucine

residues, and has two serine residues S316 and S327 pointing towards the entrance of the pocket. Serines have a primary alcohol on their side chains, also being able to form polar interactions with a galactosyl headgroup.

All the previous hypotheses correspond to interactions of LiLOX with a lipid species harboring 18 carbon acyl chains. In the case of a lipid species with an acyl chain of 16 carbons, a deeper penetration of the substrate will be required in order to align the n-8 carbon with the iron atom of LiLOX. In such a scenario, the headgroup can no longer be aligned with the residues S316, S327, N683, N687, Q690 and Q691. This less favorable penetration of the lipid in the substrate channel might explain why acyl chains of 16 carbons are oxidized at a slower rate than those acyl chains having 18 carbons, as revealed in the course of this study (Supplemental Figure 3, Figure 35).

Finally, since the hydrogen bonds can be weak (10 to 30kJ/mol) compared to salt bridges (20 to 80kJ/mol) (Miesfeld, 2017), it is difficult to find solid evidence supporting the observed specificity of LiLOX for a galactosyl headgroup. Nevertheless, the absence of residues being homologous to D190 and R422 in PaLOX seems to be in line with the poor affinity of LiLOX for phospholipid substrates.

Altogether, the subcellular localization of LiLOX together with its homology to other plastidic LOXs and its measured pH optimum suggest that LiLOX is located in the stroma of *L. incisa's* chloroplasts. The fact that MGDGs are known to be the main lipid class in this organelle, as well as its overall degree of desaturation make this lipid a good candidate for LiLOX natural substrate. Furthermore, *in vitro* analysis of LiLOX products with different complex lipids and the comparison of the overall LiLOX turnover with different lipid classes seem to support these hypotheses. Finally, the analysis of the predicted three dimensional structure of LiLOX seems to be in agreement with all these findings. As an outlook, mutations on any of the four residues N683, 687, Q690, Q691 into positively charged arginines and either of the two serines S316, S327 in negatively charged aspartates could give additional valuable results. If these mutations increase significantly the affinity of LiLOX for phospholipids and decrease its affinity for galactolipids, it would be a valuable hint that this region is responsible for the substrate binding and that they can determine preference for a given lipid class.

5.4. End product of the LiLOX reaction

In the course of this study, lipidomics analysis was performed on *L. incisa*, in order to find endogenous LiLOX products. The relative concentrations of plastidic lipids such as MGDG and DGDG were found to be significantly lowered after nitrogen starvation. Nevertheless, no LiLOX products could be detected in the analysis. One factor seems to be the main reason explaining why LiLOX oxidation products were not detected endogenously in *L. incisa*. LiLOX was shown to be able to convert MGDG further than the initial hydroperoxides by two independent methods. This mirrors very likely the endogenous situation. In fact, the catalysis of MGDG turnover by LiLOX recorded *in vitro* on the spectrophotometer clearly shows that methylene interrupted dienes are being converted into conjugated dienes during a first part of the reaction, due to the oxidation by LiLOX. Yet this chromophore having a maximum absorbance at 234 nm is degraded during a second part of the reaction (Figure 34, Figure 35). Because the new product(s) were not detected photometrically, it must have lost its chromophore and formation of a new chromophore was never observed (supplemental figure 8). Since the spectrophotometric measurements are limited by the absorbance of the final products, a non-targeted analysis by LC-MS was performed as another method (Section 4.13). A special focus was made concerning markers that have already been described as end products of LOX and non-LOX reactions in the literature and that affect the conjugated diene system.

Firstly, PpLOX1 and tomloxC were reported to have a lyase activity, cleaving the hydroperoxide products after the hydroperoxyl group (Senger *et al.*, 2005; Shen *et al.*, 2014) (Figure 47; 1). Secondly, a number of LOXs were reported to harbor a peroxidase activity metabolizing 13*S*-HPOTE into 13-ketooctadecadienoic acid (KOTE). Although both would affect the absorbance at 234 nm, these reactions would lead to the formation of (9Z,11E)-13-oxo-trideca-9,11-dienoic acid and 13-KOTE respectively, both of which harbor a conjugated dienone (Figure 47; 2) having a maximum absorbance around 280 nm. Such an increase of the absorbance at 280 nm was barely observed during LiLOX reactions with MGDG. Thirdly, eLOX3, 12*R*-LOX and FoxLOX were also described to metabolize 13*S*-HPOTE into epoxy alcohols (Brodhun *et al.*, 2013; Yu *et al.*, 2003). Although the corresponding epoxy alcohols have only one remaining double bond as a chromophore, they are almost not detectable by UV/vis-spectroscopy. However, these three enzymes were reported to produce epoxy alcohols always together with keto-fatty acids, and the formation of the latter was never observed with LiLOX. Fourthly, MpLOX7 was reported to have HPL activity (Tawfik *et al.*, 2017) as it was

shown to be able to form 13-HPOTE, and cleave it to form C6 aldehydes as well as the respective oxo-fatty acids (Figure 47; 4).

As shown in Figure 35, all MGDG substrates and hydroperoxide products were detected by LC-MS. Besides them, none of the compounds mentioned in Figure 47 were detected after the LiLOX reaction with MGDG. Raw data analyzed by the untargeted MarVis workflow, highlighting compounds only at late stages of the reaction did not put in evidence any new LiLOX products. This could be explained by the limitations of the LC/MS measurements. Firstly, in order to separate the compounds for analysis, the mass spectrometry is coupled with a liquid chromatography step, which is limited by the polarity of the compounds in the solvent

Chemical formula: $C_{43}H_{70}O_{14}$
Exact mass: 810.4766

① 3-Pentan-1-ol + (9Z,11E)-13-oxo-trideca-9,11-dienoic acid

② 13-KOTE

③ Epoxy alcohol

④ 3-Hexanal + (9Z)-12-oxododec-9-enoic acid (traumatine)
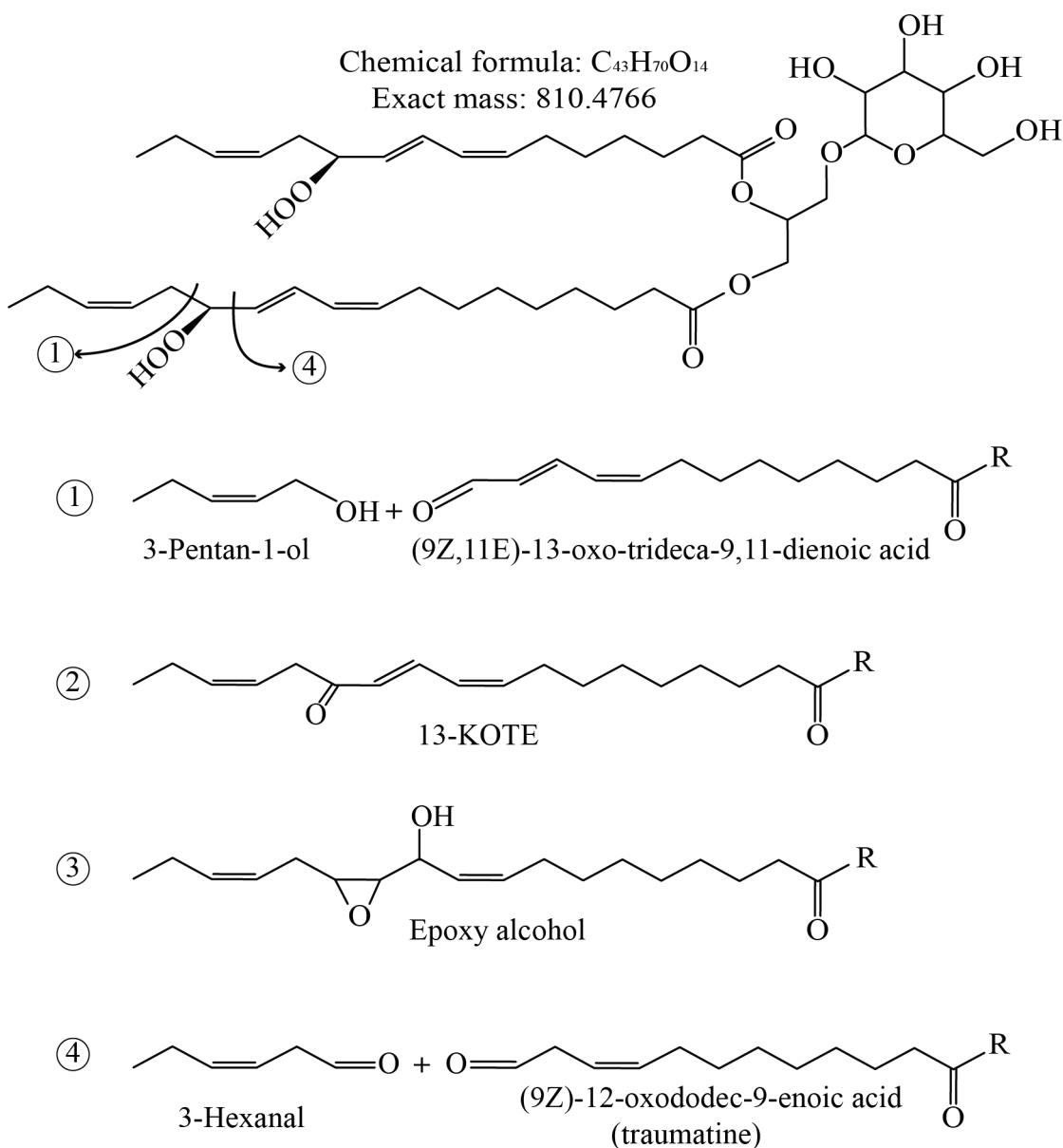
Figure 47. Putative conversions of an MGDG molecule oxidized by LiLOX. The molecules from 1 to 4 represent end products resulting from the activity of specific LOXs.

and their affinity to the column. In the case of a very non-polar end product, the compounds might not be soluble in the reaction mixture, or not be eluted by the gradient of organic solvents. Yet this seems rather unlikely, as the headgroup of MGDG is very polar. Moreover, any cleavage of the acyl chain would be expected to make the new product more polar than the substrate, hence eluting earlier. Secondly, in order to be detected by mass spectrometry, the compounds have to be ionized either positively or negatively. If the newly formed compounds cannot be ionized in either mode, their detection by this method will be nearly impossible. This hypothesis does not seem reasonable, knowing that MGDG substrates were ionized negatively, most likely on their galactosyl headgroup. Yet, any LiLOX modification on these substrates is expected to happen on the acyl chain, not on the galactosyl headgroup, which would still be ionized. Thirdly, the detection could also be limited by the detection range from 0 to 1200 Dalton. Since di-hydroperoxide-MGDGs have an exact mass between 810.476 Dalton and 814.508 Dalton, it seems unlikely that the new products have a molecular masses higher than the detection range. Fourthly, the new products may have undergone polymerization thus escaping extraction or separation during analysis.

Because the new product(s) were not detected by neither UV/vis spectroscopy nor mass spectrometry, they must have exhausted the limits of both methods, which also gives information about their nature. The conjugated diene absorbing light at 234 nm must be affected by LiLOX after all acyl chains have been oxidized. Moreover, either the solubility, the ionization capacity or the exact mass of the oxidized MGDGs are strongly modified, leading to the loss of the markers after 1 h of reaction.

The fact that MGDG substrates were detected after LiLOX reaction with 6 additional oxygen atoms, suggests that LiLOX might perform an additional reaction adding 2 oxygens after both acyl chains have been oxidized. A reaction of purified 13*S*-HOTE/11*S*-HHTE-MGDG with LiLOX, recorded by HPLC with an oxygen electrode, could confirm an addition of oxygen, since new molecules of dioxygen must be consumed during the reaction. Nevertheless, even these compounds do not seem to be the final LiLOX products, as their markers decrease between 30 minutes and 60 minutes. Moreover, the hypothesis that these MGDG molecules with 6 additional oxygen atoms are formed from MGDG through non-enzymatic oxidation, used as substrate by LiLOX, cannot be excluded. Nevertheless, the end product of LiLOX reaction with MGDG is a key to understanding the role of this enzyme in *L. incisa* and should be considered a priority in the further analysis of LiLOX.

5.5. Speculations about the role of LiLOX in *L. incisa*, and conclusion

This study reports on the first LOX to be characterized from green algae: LiLOX, a plastidic 13*S*-LOX being able to use complex lipids as substrates, showing a preference towards MGDG. Contrary to *A. thaliana*, in which 13*S*-LOXs are known to be the first step in a cascade leading to the formation of JA (1.3.3), a similar pathway was yet not described in green algae. Yet besides their role as signaling enzymes, some LOXs have also been reported to initiate the degradation of organelle membranes (1.3.4). LiLOX is proposed to have a similar role, degrading chloroplast membranes upon nitrogen starvation in *L. incisa*. LiLOX was shown to be overexpressed 6 fold under nitrogen starvation, a condition well described in green algae to lead to chloroplast degradation and the accumulation of TAG in lipid bodies. This process most likely relies on transacylating reactions thereby transferring fatty acids from galactolipids to storage lipids such as TAG (Khozin-Goldberg *et al.*, 2002; Zienkiewicz *et al.*, 2016). This scenario is supported by the observation that a PDAT, supposed actor of the TAG formation in *L. incisa*, was recently described to be up-regulated 3 fold under the same conditions, most likely transferring acyl moieties from phospholipids into TAG molecules (Liu *et al.*, 2016). Yet although TAG accumulation was first believed to be a storage mechanism, it is now also known to play a major role as electron sink when the energy from photosynthesis can no longer be used for the usual DNA and protein synthesis (Hu *et al.*, 2008). Indeed, in *C. reinhardtii* the PGD1 protein was described to be involved in a pathway leading to TAG formation mostly from *de novo* acyl chain synthesis. The KO mutant *pgd1* was described to accumulate significantly less TAG, showed signs of chlorosis 7 days after nitrogen starvation and eventually cell death. As the artificial inhibition of the electron transport of the photosynthesis apparatus prevented chlorosis and cell death in this mutant, the toxicity was imputed by the authors to reactive oxygen species formed by the accumulation of electrons in the thylakoid membrane (Li *et al.*, 2012). Therefore, the function of LiLOX may be rather to target excess fatty acids to degradation for energy production by oxidizing them while they are bound to complex lipids during stress.

Along with the TAG accumulation, nitrogen starvation lead to a change of color of *L. incisa* from green to yellow, suggesting a degradation of chloroplasts. This observation is in accordance with the strong degradation of plastidic lipids such as MGDG and DGDG (Figure 37). Moreover, some LOXs have been reported to be involved in programmed organelle degradation. In mammalians for instance, the 15*S*-LOX from rabbit reticulocytes was reported to be responsible for the selective degradation of mitochondrial membranes during

differentiation, initiating the degradation of these organelles (Schewe *et al.*, 1975; van Leyen *et al.*, 1998). In cucumber, barley, flax and sunflower, a LOX was reported to be necessary for the oxygenation of TAG and degradation of lipid bodies during germination (Feussner *et al.*, 1998; Kindl, 1997). This LOX was suggested to be a lead actor of an alternative β-oxidation pathway during germination in these plants, before the photoautotrophic pathway becomes a sufficient source of carbon skeletons and energy (Gerhardt *et al.*, 2005; Meyer *et al.*, 2013; Rudolph *et al.*, 2011). In barley leaves, a 13-LOX was reported to be the major actor of the chloroplast degradation during leave senescence (Springer *et al.*, 2016). This present study proposes that a similar role may be the case for LiLOX in the plastid membrane degradation during nitrogen depletion. Altogether, the degradation of chloroplast membranes during nitrogen starvation might have different purposes (Zienkiewicz *et al.*, 2016). Firstly, aborting photosynthesis, as its energy cannot be used for the protein or DNA synthesis, and preventing an increase of the reduction pressure inside the chloroplast. Secondly, to trigger the recycling of acyl chains from membrane lipid into TAG, by allowing access of lipases to the plastidic membrane. Thirdly, creating holes in the plastidic envelope in order to recycle the machinery from the chloroplast until nitrogen repletion. Fourthly, the oxidized acyl chains could undergo an alternative β-oxidation, described in plant cotyledons, and provide energy for the cell (Meyer *et al.*, 2013). Fifthly, as LOXs were mostly described for their role in signal transduction (Andreou *et al.*, 2009; Brash, 1999; Feussner & Wasternack, 2002; Liavonchanka & Feussner, 2006) the degradation of chloroplastidial membrane could also be the first step of oxidation leading to signaling molecules (Wasternack & Hause, 2013).

Since nitrogen depletion was the only stress condition tested in *L. incisa* in the course of this study, the regulation of LiLOX transcript levels under other conditions would be interesting for future experiments. Special focus could be made on conditions known for chloroplast degradation in some green algae such as heat stress (Legeret *et al.*, 2016), iron depletion (Urzica *et al.*, 2013) and zinc depletion (Kropat *et al.*, 2011). Interestingly, these three conditions were also reported to increase TAG levels in *C. reinhardtii*. In the same organism, heat stress was also reported to induce overexpression of the putative CrLOX, increase the level of TAG and decrease the levels of galactolipids (Legeret *et al.*, 2016).

A recent patent application reported that in *C. reinhardtii* starch degradation (STD1)-KO was reported to show overexpression of CrLOX transcript (6 log fold)(Schulz-Raffelt *et al.*, 2017) suggesting a negative regulation of CrLOX from STD1. The galactolipid MGDG was measured to be degraded faster than in the WT after nitrogen starvation, although no effect was observed

on DGDG. Oxidized MGDG species were also measured up to 18 fold higher than in the WT, after 6 days of nitrogen starvation. Finally, STD1 mutant was also reported to accumulate more TAG than the WT under nitrogen starvation, effect abolished in the WT as well as in *std1* after supplementation of the media with a LOX inhibitor.

Finally, LiLOX was described to be targeted to the plastid of an oleaginous green alga, suspected to have a preference for MGDG. It was also shown to be highly upregulated under nitrogen starvation, conditions leading to the galactolipid degradation and accumulation of neutral lipids. Altogether, this study proposes that LiLOX is playing a role in the plastid degradation during nitrogen starvation. Therefore scientists trying to understand the relation between the TAG accumulation and degradation of plastid in green algae under stress conditions can no longer ignore plastidic 13*S*-LOXs.

Abstract

Green microalgae are a model in biotechnology because of their capacity to accumulate neutral lipids, as part of a general lipid remodeling mechanism under stress. The species *L. incisa* is of special interest for its unique TAG acyl chain composition, especially 20 (n-6) that can reach up to 21 % of dry weight after nitrogen starvation. In order to identify lead actors of this remodeling, special focus was put on lipid oxidizing processes, which have been described to be of major importance in flowering plants. Investigation of the available genome, transcriptome and proteome of *L. incisa* allowed the identification of a putative LOX, which so far has not been studied in green microalgae.

The identification as a LOX was first confirmed *in silico*, by alignments and 3D structure prediction. The heterologous expression of LiLOX in *E. coli* was achieved in mg quantities, allowing further characterization of the LOX via enzymatic assays *in vitro*. Throughout the study, LiLOX was found to be a good model to study plastidic plant LOXs, as it shares highest identity with this class of enzymes and was found to have identical regio- and stereospecificity. This hypothesis was further confirmed by the localization of LiLOX in plastids, investigated via transient expression in epithelial onion cells. In order to further characterize this class of enzymes, mutational studies and attempts at crystallizations were performed and are presented in this thesis.

An important part of this work focused on identification of the endogenous substrate of LiLOX. In this regards, an *ex vivo* enzymatic assay, coupled with non-targeted analysis via mass spectrometry allowed the identification of MGDG, DGDG and PC as three substrate candidates, later confirmed via *in vitro* assays. Further investigation revealed that LiLOX has preferences towards the lipid class MGDG, which seems in agreement with its localization in the galactolipid rich plastid.

Altogether, this study shows the first characterization of plastidic LOX from green algae, showing preference for MGDGs. Finally, this study targeted the role of LiLOX in the general lipid remodeling taking place in *L. incisa* during nitrogen starvation. Since this remodeling is accompanied with the degradation of the plastidic membrane, the involvement of LiLOX in this process was discussed.

6. CITATIONS

Andreou, A., Brodhun, F. & Feussner, I. (2009). Biosynthesis of oxylipins in non-mammals. *Prog Lipid Res* 48, 148-170.

Andreou, A. & Feussner, I. (2009). Lipoxygenases - Structure and reaction mechanism. *Phytochemistry* 70, 1504-1510.

Archibald, J. M. (2015). Endosymbiosis and Eukaryotic Cell Evolution. *Curr Biol* 25, R911-921.

Ausubel, F. M., Brent, R. E., Kingston, D. D., Seidmann, J. R., Smith, J. A. & Struhl, K. (1993). Current Protocolls in Molecular Biology. New York: Green Publishing Associates and John Wiley and Sons Inc.

Banthiya, S., Kalms, J., Galemou Yoga, E., Ivanov, I., Carpena, X., Hamberg, M., Kuhn, H. & Scheerer, P. (2016). Structural and functional basis of phospholipid oxygenase activity of bacterial lipoxygenase from *Pseudomonas aeruginosa*. *Biochim Biophys Acta* 1861, 1681-1692.

Bell, E., Creelman, R. A. & Mullet, J. E. (1995). A chloroplast lipoxygenase is required for wound-induced jasmonic acid accumulation in *Arabidopsis*. *Proc Natl Acad Sci USA* 92, 8675-8679.

Bigogno, C., Khozin-Goldberg, I., Adlerstein, D. & Cohen, Z. (2002a). Biosynthesis of arachidonic acid in the oleaginous microalga *Parietochloris incisa* (*Chlorophyceae*): radiolabeling studies. *Lipids* 37, 209-216.

Bigogno, C., Khozin-Goldberg, I., Boussiba, S., Vonshak, A. & Cohen, Z. (2002b). Lipid and fatty acid composition of the green oleaginous alga *Parietochloris incisa*, the richest plant source of arachidonic acid. *Phytochemistry* 60, 497-503.

Blée, E. & Joyard, J. (1996). Envelope membranes from spinach chloroplasts are a site of metabolism of fatty acid hydroperoxides. *Plant Physiol* 110, 445-454.

Bradford, M. M. (1976). A rapid and sensitive method for the quantitation of microgram quantities of proteins utilizing the principle of protein-dye binding. *Anal Biochem* 72, 248-254.

Bradshaw, M. D. & Gaffney, B. J. (2014). Fluctuations of an exposed Ï€-helix involved in lipoxygenase substrate recognition. *Biochemistry*.

Brash, A. R., Ingram, C. D. & Harris, T. M. (1987). Analysis of a specific oxygenation reaction of soybean lipoxygenase-1 with fatty acids esterified in phospholipids. *Biochemistry* 26, 5465-5471.

Brash, A. R. (1999). Lipoxygenases: Occurrence, functions, catalysis, and acquisition of substrate. *J Biol Chem* 274, 23679-23682.

Brodhun, F., Cristobal-Sarramian, A., Zabel, S., Newie, J., Hamberg, M. & Feussner, I. (2013). An iron 13*S*-lipoxygenase with an a-linolenic acid specific hydroperoxidase activity from *Fusarium oxysporum*. *PLoS ONE* 8, e64919.

Browner, M. F., Gillmor, S. A. & Fletterick, R. (1998). Burying a charge. *Nat Struct Biol* 5, 179.

Caldelari, D., Wang, G., Farmer, E. & Dong, X. (2011). Arabidopsis *lox3 lox4* double mutants are male sterile and defective in global proliferative arrest. *Plant Mol Biol* 75, 25-33.

Chauvin, A., Caldelari, D., Wolfender, J. L. & Farmer, E. E. (2013). Four 13-lipoxygenases contribute to rapid jasmonate synthesis in wounded Arabidopsis thaliana leaves: a role

for lipoxygenase 6 in responses to long-distance wound signals. *New Phytol* 197, 566-575.

Chauvin, A., Lenglet, A., Wolfender, J. L. & Farmer, E. E. (2016). Paired Hierarchical Organization of 13-Lipoxygenases in *Arabidopsis*. *Plants (Basel)* 5.

Chechetkin, I. R., Blufard, A., Hamberg, M. & Grechkin, A. N. (2008). A lipoxygenase-divinyl ether synthase pathway in flax (*Linum usitatissimum* L.) leaves. *Phytochemistry* 69, 2008-2015.

Coffa, G. & Brash, A. R. (2004). A single active site residue directs oxygenation stereospecificity in lipoxygenases: Stereocontrol is linked to the position of oxygenation. *Proc Natl Acad Sci USA* 101, 15579-15584.

Coffa, G., Imber, A. N., Maguire, B. C., Laxmikanthan, G., Schneider, C., Gaffney, B. J. & Brash, A. R. (2005a). On the Relationships of Substrate Orientation, Hydrogen Abstraction, and Product Stereochemistry in Single and Double Dioxygenations by Soybean Lipoxygenase-1 and Its Ala542Gly Mutant. *J Biol Chem* 280, 38756-38766.

Coffa, G., Schneider, C. & Brash, A. R. (2005b). A comprehensive model of positional and stereo control in lipoxygenases. *Biochem Biophys Res Commun* 338, 87-92.

Collazo, L. & Klinman, J. P. (2016). Control of the position of oxygen delivery in soybean lipoxygenase-1 by amino acid side chains within a gas migration channel. *J Biol Chem* 291, 9052-9059.

Creelman, R. A. & Mullet, J. E. (1997). Biosynthesis and action of jasmonates in plants. *Ann Rev Plant Physiol Plant Mol Biol* 48, 355-381.

Czechowski, T., Stitt, M., Altmann, T., Udvardi, M. K. & Scheible, W. R. (2005). Genome-wide identification and testing of superior reference genes for transcript normalization in *Arabidopsis*. *Plant Physiol* 139, 5-17.

Dahlqvist, A., Stahl, U., Lenman, M., Banas, A., Lee, M., Sandager, L., Ronne, H. & Stymne, S. (2000). Phospholipid:diacylglycerol acyltransferase: An enzyme that catalyzes the acyl-CoA-independent formation of triacylglycerol in yeast and plants. *Proc Natl Acad Sci USA* 97, 6487-6492.

de Alda, J. A. G. O., Esteban, R., Diago, M. L. & Houmard, J. (2014). The plastid ancestor originated among one of the major cyanobacterial lineages. *Nature Communications* 5.

De Groot, J. J. M. C., Veldink, G. A., Vliegenthart, J. F. G., Boldingh, J., Wever, R. & Van Gelder, B. F. (1975). Demonstration by EPR spectroscopy of the functional role of iron in soybean lipoxygenases-1. *Biochim Biophys Acta* 377, 71-79.

Deschamps, J. D., Ogunsola, A. F., Jameson, J. B., 2nd & other authors (2016). Biochemical and cellular characterization and inhibitor discovery of *Pseudomonas aeruginosa* 15-Lipoxygenase. *Biochemistry* 55, 3329-3340.

Du, Z. Y. & Benning, C. (2016). Triacylglycerol accumulation in photosynthetic cells in plants and algae. *Subcell Biochem* 86, 179-205.

Egmond, M. R., Vliegenthart, J. F. G. & Boldingh, J. (1972). Stereospecificity of the hydrogen abstraction at carbon atom n-8 in the oxygenation of linoleic acid by lipoxygenases from corn germs and soya beans. *Biochem Biophys Res Commun* 48, 1055-1060.

Emanuelsson, O., Nielsen, H. & Von Heijne, G. (1999). ChloroP, a neural network-based method for predicting chloroplast transit peptides and their cleavage sites. *Protein Science* 8, 978-984.

Emanuelsson, O., Nielsen, H., Brunak, S. & von Heijne, G. (2000). Predicting subcellular localization of proteins based on their N-terminal amino acid sequence. *J Mol Biol* 300, 1005-1016.

Erb, K. H., Lauk, C., Kastner, T., Mayer, A., Theurl, M. C. & Haberl, H. (2016). Exploring the biophysical option space for feeding the world without deforestation. *Nat Commun* 7, 11382.

Ericsson, U. B., Hallberg, B. M., DeTitta, G. T., Dekker, N. & Nordlund, P. (2006). Thermofluor-based high-throughput stability optimization of proteins for structural studies. *Anal Biochem* 357, 289-298.

Fan, J., Andre, C. & Xu, C. (2011). A chloroplast pathway for the de novo biosynthesis of triacylglycerol in *Chlamydomonas reinhardtii*. *FEBS Lett* 585, 1985-1991.

Farmer, E. E. & Ryan, C. A. (1992). Octadecanoid precursors of jasmonic acid activate the synthesis of wound-inducible proteinase inhibitors. *Plant Cell* 4, 129-134.

Feussner, I., Kühn, H. & Wasternack, C. (1997). Do specific linoleate 13-lipoxygenases initiate β-oxidation? *FEBS Lett* 406, 1-5.

Feussner, I., Bachmann, A., Höhne, M. & Kindl, H. (1998). All three acyl moieties of trilinolein are efficiently oxygenated by recombinant His-tagged lipid body lipoxygenase *in vitro*. *FEBS Lett* 431, 433-436.

Feussner, I., Kühn, H. & Wasternack, C. (2001). The lipoxygenase dependent degradation of storage lipids. *Trends Plant Sci* 6, 268-273.

Feussner, I. & Wasternack, C. (2002). The lipoxygenase pathway. *Annu Rev Plant Biol* 53, 275-297.

Fulda, M., Shockey, J., Werber, M., Wolter, F. P. & Heinz, E. (2002). Two long-chain acyl-CoA synthetases from *Arabidopsis thaliana* involved in peroxisomal fatty acid β-oxidation. *Plant J* 32, 93-103.

Garab, G. (2014). Hierarchical organization and structural flexibility of thylakoid membranes. *Biochim Biophys Acta* 1837, 481-494.

Garab, G., Ughy, B. & Goss, R. (2016). Role of MGDG and non-bilayer lipid phases in the structure and dynamics of chloroplast thylakoid membranes. *Subcell Biochem* 86, 127-157.

Gardner, H. W. (1989). Soybean lipoxygenase-1 enzymatically forms both 9(*S*)- and 13(*S*)-hydroperoxides from linoleic acid by a pH-dependent mechanism. *Biochim Biophys Acta* 1001, 274-281.

Garreta, A., Val-Moraes, S. P., Garcia-Fernandez, Q. & other authors (2013). Structure and interaction with phospholipids of a prokaryotic lipoxygenase from *Pseudomonas aeruginosa*. *FASEB J* 27, 4811-4821.

Gerhardt, B., Fischer, K., Balkenhohl, T. J., Pohnert, G., Kühn, H., Wasternack, C. & Feussner, I. (2005). Lipoxygenase-mediated metabolism of storage lipids in germinating sunflower cotyledons and β-oxidation of (9*Z*,11*E*,13*S*)-13-hydroxy-octadeca-9,11-dienoic acid by the cotyledonary glyoxysomes. *Planta* 220, 919-930.

Glauser, G., Dubugnon, L., Mousavi, S. A. R., Rudaz, S., Wolfender, J.-L. & Farmer, E. E. (2009). Velocity estimates for signal propagation leading to systemic jasmonic acid accumulation in wounded Arabidopsis. *J Biol Chem* 284, 34506-34513.

Glickman, M. H. & Klinman, J. P. (1995). Nature of rate-limiting steps in the soybean lipoxygenase-1 reaction. *Biochemistry* 34, 14077-14092.

Godfray, H. C., Beddington, J. R., Crute, I. R. & other authors (2010). Food security: the challenge of feeding 9 billion people. *Science* 327, 812-818.

Guskov, A., Kern, J., Gabdulkhakov, A., Broser, M., Zouni, A. & Saenger, W. (2009). Cyanobacterial photosystem II at 2.9-A resolution and the role of quinones, lipids, channels and chloride. *Nat Struct Mol Biol* 16, 334-342.

Hamberg, M. & Samuelsson, B. (1967). On the specificitiy of the oxygenation of unsaturated fatty acids catalyzed by soybean lipoxidase. *J Biol Chem* 242, 5329-5335.

Hamberg, M. & Samuelsson, B. (1974). Prostaglandin endoperoxides. Novel transformations of arachidonic acid in human platelets. *Proc Natl Acad Sci USA* 71, 3400-3404.

Heitz, T., Bergey, D. R. & Ryan, C. A. (1997). A gene encoding a chloroplast-targeted lipoxygenase in tomato leaves is transiently induced by wounding, systemin, and methyl jasmonate. *Plant Physiol* 114, 1085-1093.

Heitz, T., Smirnova, E., Widemann, E., Aubert, Y., Pinot, F. & Menard, R. (2016). The rise and fall of jasmonate biological activities. *Subcell Biochem* 86, 405-426.

Höfgen, R. & Willmitzer, L. (1988). Storage of competent cells for agrobacterium transformation. *Nucleic Acids Res* 16, 9877.

Hornung, E., Walther, M., Kühn, H. & Feussner, I. (1999). Conversion of cucumber linoleate 13-lipoxygenase to a 9-lipoxygenating species by site-directed mutagenesis. *Proc Natl Acad Sci USA* 96, 4192-4197.

Hornung, E., Krueger, C., Pernstich, C., Gipmans, M., Porzel, A. & Feussner, I. (2005). Production of (10E,12Z)-conjugated linoleic acid in yeast and tobacco seeds. *Biochim Biophys Acta* 1738, 105-114.

Hornung, E., Kunze, S., Liavonchanka, A., Zimmermann, G., Kuhn, D., Fritsche, K., Renz, A., Kühn, H. & Feussner, I. (2008). Identification of an amino acid determinant of pH regiospecificity in a seed lipoxygenase from *Momordica charantia*. *Phytochemistry* 69, 2774-2780.

Hu, Q., Sommerfeld, M., Jarvis, E., Ghirardi, M., Posewitz, M., Seibert, M. & Darzins, A. (2008). Microalgal triacylglycerols as feedstocks for biofuel production: perspectives and advances. *Plant J* 54, 621-639.

Ibrahim, A., Schütz, A.-L., Galano, J.-M., Herrfurth, C., Feussner, K., Durand, T., Brodhun, F. & Feussner, I. (2011). The alphabet of galactolipids in *Arabidopsis thaliana*. *Front Plant Sci* 2, 95.

Ishiguro, S., Kawai-Oda, A., Ueda, J., Nishida, I. & Okada, K. (2001). The DEFECTIVE IN ANTHER DEHISCENCE gene encodes a novel phospholipase A_1 catalyzing the initial step of jasmonic acid biosynthesis, which synchronizes pollen maturation, anther dehiscence, and flower opening in *Arabidopsis*. *Plant Cell* 13, 2191-2209.

Ivanov, I., Heydeck, D., Hofheinz, K., Roffeis, J., O'Donnell, V. B., Kuhn, H. & Walther, M. (2010). Molecular enzymology of lipoxygenases. *Arch Biochem Biophys* 503, 161-174.

Iwai, M., Ikeda, K., Shimojima, M. & Ohta, H. (2014). Enhancement of extraplastidic oil synthesis in Chlamydomonas reinhardtii using a type-2 diacylglycerol acyltransferase with a phosphorus starvation–inducible promoter. *Plant Biotechnol J* 12, 808-819.

Janssen, C. I. & Kiliaan, A. J. (2014). Long-chain polyunsaturated fatty acids (LCPUFA) from genesis to senescence: the influence of LCPUFA on neural development, aging, and neurodegeneration. *Prog Lipid Res* 53, 1-17.

Jordan, P., Fromme, P., Witt, H. T., Klukas, O., Saenger, W. & Krauss, N. (2001). Three-dimensional structure of cyanobacterial photosystem I at 2.5 A resolution. *Nature* 411, 909-917.

Kaever, A., Lingner, T., Feussner, K., Göbel, C., Feussner, I. & Meinicke, P. (2009). MarVis: a tool for clustering and visualization of metabolic biomarkers. *BMC Bioinformatics* 10, 92.

Kaever, A., Landesfeind, M., Feussner, K., Mosblech, A., Heilmann, I., Morgenstern, B., Feussner, I. & Meinicke, P. (2015). MarVis-Pathway: integrative and exploratory pathway analysis of non-targeted metabolomics data. *Metabolomics* 11, 764-777.

Kalisch, B., Dormann, P. & Holzl, G. (2016). DGDG and glycolipids in plants and algae. *Subcell Biochem* 86, 51-83.

Kalms, J., Banthiya, S., Galemou Yoga, E., Hamberg, M., Holzhutter, H. G., Kuhn, H. & Scheerer, P. (2017). The crystal structure of *Pseudomonas aeruginosa* lipoxygenase Ala420Gly mutant explains the improved oxygen affinity and the altered reaction specificity. *Biochim Biophys Acta* 1862, 463-473.

Kansy, M., Wilhelm, C. & Goss, R. (2014). Influence of thylakoid membrane lipids on the structure and function of the plant photosystem II core complex. *Planta* 240, 781-796.

Kelley, L. A., Mezulis, S., Yates, C. M., Wass, M. N. & Sternberg, M. J. (2015). The Phyre2 web portal for protein modeling, prediction and analysis. *Nat Protoc* 10, 845-858.

Khozin-Goldberg, I., Bigogno, C., Shrestha, P. & Cohen, Z. (2002). Nitrogen starvation induces the accumulation of arachidonic acid in the freshwater green alga *Parietochloris incisa* (*Trebuxiophyceae*). *J Phycol* 38, 991-994.

Khozin‐Goldberg, I., Bigogno, C., Shrestha, P. & Cohen, Z. (2002). Nitrogen starvation induces the accumulation of arachidonic acid in the freshwater green alga parietochloris incisa (trebuxiophyceae). *J Phycol* 38, 991-994.

Kindl, H. (1997). The oxygen-dependent modification of triacylglycerols and phospholipids, the different way of initiating lipid body mobilization. *Z Naturforsch* 52c, 1-8.

Kobayashi, K., Kondo, M., Fukuda, H., Nishimura, M. & Ohta, H. (2007). Galactolipid synthesis in chloroplast inner envelope is essential for proper thylakoid biogenesis, photosynthesis, and embryogenesis. *Proc Natl Acad Sci USA* 104, 17216-17221.

Kobayashi, K. (2016). Role of membrane glycerolipids in photosynthesis, thylakoid biogenesis and chloroplast development. *J Plant Res* 129, 565-580.

Kobayashi, K. & Wada, H. (2016). Role of lipids in chloroplast biogenesis. *Subcell Biochem* 86, 103-125.

Kropat, J., Hong-Hermesdorf, A., Casero, D., Ent, P., Castruita, M., Pellegrini, M., Merchant, S. S. & Malasarn, D. (2011). A revised mineral nutrient supplement increases biomass and growth rate in *Chlamydomonas reinhardtii*. *Plant J* 66, 770-780.

Kühn, H., Banthiya, S. & van Leyen, K. (2015). Mammalian lipoxygenases and their biological relevance. *Biochim Biophys Acta* 1851, 308-330.

Kunst, L., Browse, J. & Somerville, C. (1988). Altered Regulation of Lipid Biosynthesis in a Mutant of *Arabidopsis* Deficient in Chloroplast Glycerol-3-Phosphate Acyltransferase Activity. *Proc Natl Acad Sci USA* 85, 4143-4147.

Lee, R. (2011). The outlook for population growth. *Science* 333, 569-573.

Legeret, B., Schulz-Raffelt, M., Nguyen, H. M., Auroy, P., Beisson, F., Peltier, G., Blanc, G. & Li-Beisson, Y. (2016). Lipidomic and transcriptomic analyses of *Chlamydomonas reinhardtii* under heat stress unveil a direct route for the conversion of membrane lipids into storage lipids. *Plant Cell Environ* 39, 834-847.

Li, J., Han, D., Wang, D. & other authors (2014). Choreography of Transcriptomes and Lipidomes of Nannochloropsis Reveals the Mechanisms of Oil Synthesis in Microalgae. *Plant Cell* 26, 1645-1665.

Li, X., Moellering, E. R., Liu, B., Johnny, C., Fedewa, M., Sears, B. B., Kuo, M.-H. & Benning, C. (2012). A galactoglycerolipid lipase is required for triacylglycerol accumulation and survival following nitrogen deprivation in *Chlamydomonas reinhardtii*. *Plant Cell* 24, 4670-4686.

Liavonchanka, A. & Feussner, I. (2006). Lipoxygenases: Occurrence, functions and catalysis. *J Plant Physiol* 163, 348-357.

Liu, B. & Benning, C. (2013). Lipid metabolism in microalgae distinguishes itself. *Current Opinion in Biotechnology* 24, 300-309.

Liu, X. Y., Ouyang, L. L. & Zhou, Z. G. (2016). Phospholipid: diacylglycerol acyltransferase contributes to the conversion of membrane lipids into triacylglycerol in *Myrmecia incisa* during the nitrogen starvation stress. *Sci Rep* 6, 26610.

Masuda, S., Harada, J., Yokono, M. & other authors (2011). A monogalactosyldiacylglycerol synthase found in the green sulfur bacterium *chlorobaculum tepidum* reveals important roles for galactolipids in photosynthesis. *Plant Cell* 23, 2644-2658.

Matyash, V., Liebisch, G., Kurzchalia, T. V., Shevchenko, A. & Schwudke, D. (2008). Lipid extraction by methyl-tert-butyl ether for high-throughput lipidomics. *J Lipid Res* 49, 1137-1146.

McConn, M., Creelman, R. A., Bell, E., Mullet, J. E. & Browse, J. (1997). Jasmonate is essential for insect defense *Arabidopsis*. *Proc Natl Acad Sci USA* 94, 5473-5477.

Merchant, S. S., Prochnik, S. E., Vallon, O. & other authors (2007). The Chlamydomonas genome reveals the evolution of key animal and plant functions. *Science* 318, 245-250.

Merchant, S. S., Kropat, J., Liu, B., Shaw, J. & Warakanont, J. (2012). TAG, you're it! *Chlamydomonas* as a reference organism for understanding algal triacylglycerol accumulation. *Curr Opin Biotechnol* 23, 352-363.

Merzlyak, M. N., Chivkunova, O. B., Gorelova, O. A., Reshetnikova, I. V., Solovchenko, A. E., Khozin-Goldberg, I. & Cohen, Z. (2007). Effect of nitrogen starvation on optical properties, pigments, and arachidonic acid content of the unicellular green alga *parietochloris incisa* (Trebouxiophyceae, Chlorophyta). *J Phycol* 43, 833-843.

Meyer, D., Herrfurth, C., Brodhun, F. & Feussner, I. (2013). Degradation of lipoxygenase-derived oxylipins by glyoxysomes from sunflower and cucumber cotyledons. *BMC Plant Biol* 13, 177.

Miesfeld, R. L., McEvoy, Megan M. (2017). Biochemistry, International Student edn. **9780393977264**

Mochizuki, S., Sugimoto, K., Koeduka, T. & Matsui, K. (2016). *Arabidopsis* lipoxygenase 2 is essential for formation of green leaf volatiles and five-carbon volatiles. *FEBS Lett* 590, 1017-1027.

Monod, J., Wyman, J. & Changeux, J. P. (1965). On the Nature of Allosteric Transitions: A Plausible Model. *J Mol Biol* 12, 88-118.

Murray, J. J. & Brash, A. R. (1988). Rabbit reticulocyte lipoxygenase catalyzes specific 12(*S*) and 15(*S*) oxygenation of arachidonoyl-phosphatidylcholine. *Arch Biochem Biophys* 265, 514-523.

Mwenda, C. M. & Matsui, K. (2014). The importance of lipoxygenase control in the production of green leaf volatiles by lipase-dependent and independent pathways. *Plant Biotechnology* 31, 445-452.

Nakashima, A., Iijima, Y., Aoki, K., Shibata, D., Sugimoto, K., Takabayashi, J. & Matsui, K. (2011). Monogalactosyl diacylglycerol is a substrate for lipoxygenase: its implications for oxylipin formation directly from lipids. *Journal of Plant Interactions* 6, 93-97.

Neau, D. B., Bender, G., Boeglin, W. E., Bartlett, S. G., Brash, A. R. & Newcomer, M. E. (2014). Crystal structure of a lipoxygenase in complex with substrate: the arachidonic acid-binding site of 8R-lipoxygenase. *J Biol Chem* 289, 31905-31913.

Newcomer, M. E. & Brash, A. R. (2015). The structural basis for specificity in lipoxygenase catalysis. *Protein Science* 24, 298-309.

Newie, J. (2016).Characterization of Lipoxygenases from *Cyanothece* sp. In Plant Biochemistry. Göttingen: Georg-August Universität Göttingen.

Pogson, B. J., Ganguly, D. & Albrecht-Borth, V. (2015). Insights into chloroplast biogenesis and development. *Bba-Bioenergetics* 1847, 1017-1024.

Rickert, K. W. & Klinman, J. P. (1999). Nature of hydrogen transfer in soybean lipoxygenase 1: Separation of primary and secondary isotope effects. *Biochemistry* 38, 12218-12228.

Roberts, L. (2011). 9 billion? *Science* 333, 540-543.

Robinson, S. P. (1985). The Involvement of Stromal ATP in Maintaining the Ph Gradient across the Chloroplast Envelope in the Light. *Biochim Biophys Acta* 806, 187-194.

Rudolph, M., Schlereth, A., Körner, M., Feussner, K., Berndt, E., Melzer, M., Hornung, E. & Feussner, I. (2011). The lipoxygenase-dependent oxygenation of lipid body membranes is promoted by a patatin-type phospholipase in cucumber cotyledons. *J Exp Bot* 62, 749-760.

Sanger, F., Nicklen, S. & Coulson, A. R. (1977). DNA sequencing with chain-terminating inhibitors. *Proc Natl Acad Sci USA* 74, 5463-5467.

Schaller, S., Latowski, D., Jemiola-Rzeminska, M., Wilhelm, C., Strzalka, K. & Goss, R. (2010). The main thylakoid membrane lipid monogalactosyldiacylglycerol (MGDG) promotes the de-epoxidation of violaxanthin associated with the light-harvesting complex of photosystem II (LHCII). *Biochim Biophys Acta* 1797, 414-424.

Schewe, T., Halangk, W., Hiebsch, C. & Rapoport, S. M. (1975). A lipoxygenases in rabbit reticulocytes which attacks phospholipids and intact mitochondria. *FEBS Lett* 60, 149-152.

Schewe, T., Rapaport, S. M. & Kühn, H. (1986). Enzymology and physiology of reticulocyte lipoxygenase: comparison with other lipoxygenases. *Adv Enzymo Mol Biol* 58, 191-272.

Schneider, C., Pratt, D. A., Porter, N. A. & Brash, A. R. (2007). Control of oxygenation in lipoxygenase and cyclooxygenase catalysis. *Chem Biol* 14, 473-488.

Schulz-Raffelt, M., Chochois, V., Li-Beisson, Y. & Peltier, G. (2017).Green microalgae lacking a functional DYRKP-1 gene, for use for increased production of feedstock. United States: Commissariat à l'énergie atomique et aux énergies alternatives (Paris, FR).

Senger, T., Wichard, T., Kunze, S., Göbel, C., Lerchl, J., Pohnert, G. & Feussner, I. (2005). A multifunctional lipoxygenase with fatty acid hydroperoxide cleaving activity from the moss *Physcomitrella patens*. *J Biol Chem* 280, 7588-7596.

Shen, J., Tieman, D., Jones, J. B., Taylor, M. G., Schmelz, E., Huffaker, A., Bies, D., Chen, K. & Klee, H. J. (2014). A 13-lipoxygenase, TomloxC, is essential for synthesis of C5 flavour volatiles in tomato. *J Exp Bot* 65, 419-428.

Shimizu, T., Radmark, O. & Samuelsson, B. (1984). Enzyme with dual lipoxygenase activities catalyzes leukotriene A4 synthesis from arachidonic acid. *Proc Natl Acad Sci USA* 81, 689-693.

Shiojiri, K., Kishimoto, K., Ozawa, R. & other authors (2006). Changing green leaf volatile biosynthesis in plants: An approach for improving plant resistance against both herbivores and pathogens. *Proc Natl Acad Sci USA* 103, 16672-16676.

Siegler, H. (2016).Biogenesis of lipid bodies in *Lobosphaera incisa*. In Plant Biochemistry. Göttingen: Georg-August Universität Göttingen.

Simionato, D., Block, M. A., La Rocca, N., Jouhet, J., Marechal, E., Finazzi, G. & Morosinotto, T. (2013). The Response of *Nannochloropsis* gaditana to Nitrogen Starvation Includes De Novo Biosynthesis of Triacylglycerols, a Decrease of Chloroplast Galactolipids, and Reorganization of the Photosynthetic Apparatus. *Eukaryot Cell* 12, 665-676.

Sloane, D. L., Leung, R., Craik, C. S. & Sigal, E. (1991). A primary determinant for lipoxygenase positional specificity. *Nature* 354, 149-152.

Springer, A., Kang, C., Rustgi, S., von Wettstein, D., Reinbothe, C., Pollmann, S. & Reinbothe, S. (2016). Programmed chloroplast destruction during leaf senescence involves 13-lipoxygenase (13-LOX). *Proc Natl Acad Sci USA* 113, 3383-3388.

Stanier, R., Kunisawa, R., Mandel, M. & Cohen-Bazire, G. (1971). Purification and properties of unicellular blue-green algae (order *Chroococcales*). *Bacteriological reviews* 35, 171.

Staswick, P. E., Yuen, G. Y. & Lehman, C. C. (1998). Jasmonate signaling mutants of *Arabidopsis* are susceptible to the soil fungus *Pythium irregulare*. *Plant J* 15, 747-754.

Studier, F. W. (2005). Protein production by auto-induction in high-density shaking cultures. *Protein Expr Purif* 41, 207-234.

Stumpe, M., Carsjens, J.-G., Göbel, C. & Feussner, I. (2008). Divinyl ether synthesis in garlic bulbs. *J Exp Bot* 59, 907-915.

Tardif, M., Atteia, A., Specht, M. & other authors (2012). PredAlgo: A new subcellular localization prediction tool dedicated to green algae. *Molecular Biology and Evolution* 29, 3625-3639.

Tawfik, M. M., Yamato, K. T., Kohchi, T., Koeduka, T. & Matsui, K. (2017). n-Hexanal and (Z)-3-hexenal are generated from arachidonic acid and linolenic acid by a lipoxygenase in *Marchantia polymorpha* L. *Biosci Biotechnol Biochem*, 1-8.

Tikhonov, A. N. (2012). Energetic and regulatory role of proton potential in chloroplasts. *Biochemistry (Mosc)* 77, 956-974.

Tourasse, N. J., Barbi, T., Waterhouse, J. C., Shtaida, N., Leu, S., Boussiba, S., Purton, S. & Vallon, O. (2015a). The complete sequence of the chloroplast genome of the green microalga *Lobosphaera (Parietochloris) incisa*. *Mitochondrial DNA* 0, 1-3.

Tourasse, N. J., Shtaida, N., Khozin-Goldberg, I., Boussiba, S. & Vallon, O. (2015b). The complete mitochondrial genome sequence of the green microalga *Lobosphaera (Parietochloris) incisa* reveals a new type of palindromic repetitive repeat. *BMC Genomics* 16, 580.

Turner, J. G., Ellis, C. & Devoto, A. (2002). The jasmonate signal pathway. *Plant Cell* 14 Suppl, S153-164.

Urzica, E. I., Vieler, A., Hong-Hermesdorf, A. & other authors (2013). Remodeling of Membrane Lipids in Iron-starved *Chlamydomonas*. *J Biol Chem* 288, 30246-30258.

van Leyen, K., Duvoisin, R. M., Engelhardt, H. & Wiedmann, M. (1998). A function for lipoxygenase in programmed organelle degradation. *Nature* 395, 392-395.

Veldink, G., Garssen, G. J., Vliegenthart, J. F. G. & Boldingh, J. (1972). Positional specificity of corn germ lipoxygenase as a function of pH. *Biochem Biophys Res Commun* 47, 22-26.

Wasternack, C. & Hause, B. (2013). Jasmonates: biosynthesis, perception, signal transduction and action in plant stress response, growth and development. An update to the 2007 review in Annals of Botany. *Ann Bot* 111, 1021-1058.

Weiss, J. N. (1997). The Hill equation revisited: uses and misuses. *FASEB J* 11, 835-841.

Yan, J. S., Mao, D. Z., Chen, H., Kuang, T. Y. & Li, L. B. (2000). Effects of membrane lipids on the electron transfer activity of cytochrome b(6)f complex from spinach. *Acta Bot Sin* 42, 1267-1270.

Yang, Y., Yu, X., Song, L. & An, C. (2011). ABI4 Activates DGAT1 Expression in *Arabidopsis* Seedlings during Nitrogen Deficiency. *Plant Physiol* 156, 873-883.

Yoon, H. S., Hackett, J. D., Ciniglia, C., Pinto, G. & Bhattacharya, D. (2004). A molecular timeline for the origin of photosynthetic eukaryotes. *Mol Biol Evol* 21, 809-818.

Yoon, K., Han, D., Li, Y., Sommerfeld, M. & Hu, Q. (2012). Phospholipid:Diacylglycerol Acyltransferase Is a Multifunctional Enzyme Involved in Membrane Lipid Turnover and Degradation While Synthesizing Triacylglycerol in the Unicellular Green Microalga *Chlamydomonas reinhardtii*. *Plant Cell* 24, 3708-3724.

Youn, B., Sellhorn, G. E., Mirchel, R. J., Gaffney, B. J., Grimes, H. D. & Kang, C. (2006). Crystal structures of vegetative soybean lipoxygenase VLX-B and VLX-D, and comparisons with seed isoforms LOX-1 and LOX-3. *Proteins* 65, 1008-1020.

Yu, Z., Schneider, C., Boeglin, W. E., Marnett, L. J. & Brash, A. R. (2003). The lipoxygenase gene ALOXE3 implicated in skin differentiation encodes a hydroperoxide isomerase. *Proc Natl Acad Sci USA* 100, 9162-9167.

Zienkiewicz, K., Du, Z. Y., Ma, W., Vollheyde, K. & Benning, C. (2016). Stress-induced neutral lipid biosynthesis in microalgae - Molecular, cellular and physiological insights. *Biochim Biophys Acta* 1861, 1269-1281.

The one-letter code was used for amino acids.

TAG	Triacylglycerol
VLC-PUFAs	Very long chain poly unsaturated fatty acid
L. incisa	*Lobosphaera incisa*
C. reinhardtii	*Chlamydomonas reinhardtii*
G3P	Glyceraldehyde-3-phosphate
NADPH	Nicotinamide adenine dinucleotide phosphate
ER	Endoplasmic reticulum
MGDG	Monogalactosyldiacylglycerol
PDAT	Phospholipid:diacylglycerol acyltransferases
PGD1	PLASTID GALACTOLIPID DEGRADATION 1
ROS	Reactive oxygen species
DGDG	Digalactosyldiacylglycerol
PSII	Photosystem II
A. thaliana	*Arabidopsis thaliana*
LOX	Lipoxygenase
FFAs	Free fatty acids
JA	Jasmonic acid
AOC	Allene oxide cyclase
OPDA	12-oxo Phytodienoic acid
ORF	Open reading frame
BG11N-	Blue green algae media
E. coli	*Escherichia coli*
SDS-PAGE	Sodium dodecyl sulfate polyacrylamide gel electrophoresis
KO	Knockout
PCR	Polymerase chain reaction
eYFP	enhanced yellow fluorescent protein
eCFP	Enhanced cyan fluorescent protein
RPM	Rotation per minute

IMAC	Immobilized metal affinity chromatography
CV	Column volume
SEC	Size exclusion chromatography
BSA	Bovine serum albumin
LC-MS	Liquide chromatography mass spectrometry
UPLC	Ultra-high performance liquid chromatography
TOF	Time of flight
MTBE	Methyl-*tert*-butylether
TLC	Thin layer chromatography
PC	phosphatidylcholine
RP	Reverse phase
HPLC	High performance liquid chromatography
SP	Straight phase
CP	Chiral phase
H(P)ODE	Hydro(pero)xyoctadecadienoic acid
H(P)OTE	Hydro(pero)xyoctadecatrienoic acid
H(P)ETE	Hydro(pero)xyeicosatetraenoic acid
SPE	Solid phase extraction
A. tumefaciens	*Agrobacterium tumefaciens*
1D-SOM	One dimensional self-organizing map
TIC	Total ion chromatogram
EIC	Extracted ion chromatogram
H(P)HTE	Hydro(pero)xyhexadecatrienoic acid
H(P)HDE	Hydro(pero)xyhexadecadienoic acid
PE	Phosphatidylethanolamine
PG	Phosphatidylglycerol
MRM	Multiple reaction monitoring
WT	Wildtype
GC	Gas chromatography

8. SUPLEMENTAL DATA

Supplemental Table 1. Protein sequence identities of LiLOX with 39 characterized LOX, performed by the software Geneious, using Muscle alignment with the default parameters.

Lipoxygenase	Identity shared with LiLOX (%)
P. patens LOX7 (13S)	32.60 %
P. patens LOX6 (13S)	31.60 %
A. thaliana LOX6 (13S)	31.50 %
A. thaliana LOX3 (13S)	31.30 %
P. patens LOX5 (13S)	31 %
A. thaliana LOX4 (13S)	30.90 %
O. sativa LOX (13S)	30.50 %
S. tuberosum LOX2 (13S)	30.40 %
A. thaliana LOX5 (9S)	29.80 %
P. patens LOX4 (13S)	29.60 %
G. max LOX1 (13S)	29.50 %
A. thaliana LOX2 (13S)	29.30 %
S. tuberosum LOX (9S)	29.30 %
G. max LOX2 (9/13S)	29.20 %
A. thaliana LOX1 (9S)	28.90 %
P. patens LOX3 (13S)	28.9 %
G. max LOX3 (9/13S)	28.8 %
S. tuberosum LOX (13S)	28.7 %
O. sativa LOX2 (13S)	28.2 %
C. reinhardtii (13S)	28 %
P. patens LOX2 (13S)	27.6 %
G. max LOX4 (13S)	27.5 %
P. patens LOX1 (13S)	27.4 %
Cyanothece LOX2 (9R/11R)	18.2 %
H. sapiens LOX (12S)	17.6 %
H. sapiens LOX (15S)	17.4 %
H. sapiens LOX (5S)	17 %
H. sapiens LOX (12R)	16.6 %
H. sapiens LOX2 (15S)	16.4 %
N. punctiforme LOX2 (13S)	16.4 %
P. homomalla LOX (8R)	16 %
B. thailandensis (13S)	15.9 %
G. fructosovora LOX (11R)	15.7 %
P. aeruginosa LOX (15S)	15.7 %
G. graminis Mn-LOX (13R)	13.6 %
F. oxysporum LOX (13S)	13.1 %
M. oryzae Mn-LOX (9R)	12.9 %
Cyanothece LOX1 (9R)	11.3 %
N. punctiforme LOX1 (9R)	10 %

A

Thyroglobulin
(670000 g/mol)

γ-globulin
(158000 g/mol)

Ovalbumin
(44000 g/mol)

Myoglobin
(17000 g/mol)

Vitamin B12
(1350 g/mol)

C

B

$$y = -0.21989x + 7.97256$$
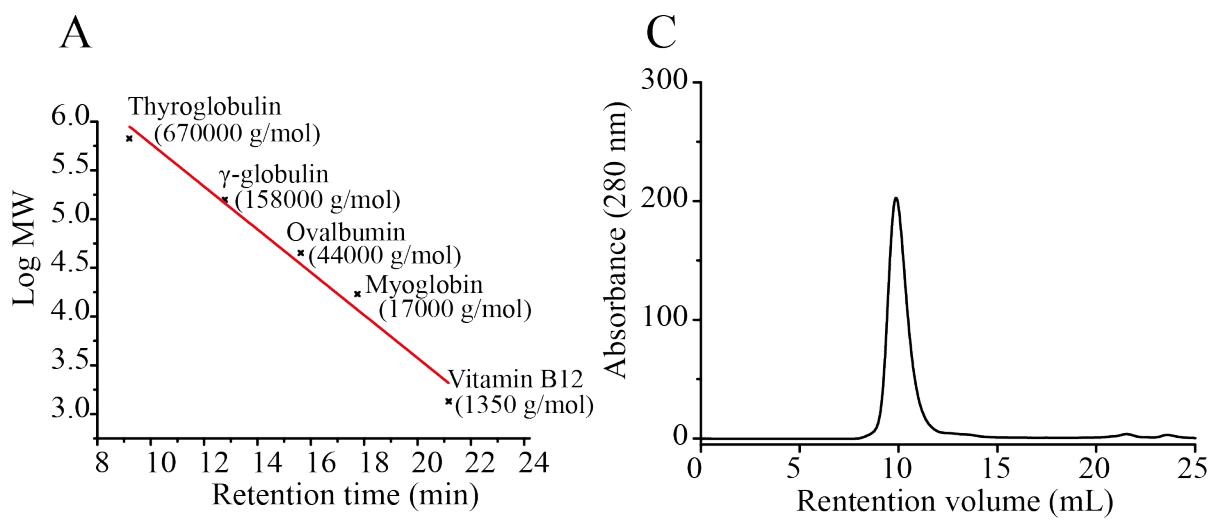
Supplemental Figure 1. Calibration of analytical size exclusion chromatography (SEC). **A.** Calibration curve performed from a mixture of gel filtration standard Gel Filtration Standard #1511901 (Bio-Rad, Germany) according to the manufacturer's instructions, on Superdex 200 10/300 GL (GE Healthcare, USA). **B.** Equation derived from the calibration curve. **C.** LiLOX purified on analytical SEC, in 20 mM HEPES buffer pH 8.4, 100 mM NaCl, 10 % (v/v) glycerol, on Superdex 200 10/300 GL (GE Healthcare, USA). Data shown represent a single experiment.

Michaelis-Menten	Hill
$$V = \dfrac{V_{max} \times [S]}{(K_M) + [S]}$$	$$V = \dfrac{V_{max} \times [S]^n}{(K_M)^n + [S]^n}$$

V   = Reaction rate
V_{max} = Maximum reaction rate
[S]   = Substrate concentration
K_M = Michaelis constant
n   = Hill coefficient

Supplemental figure 2. The Hill equation was used for the determination of all kinetic parameters, using the software OriginPro8.5.
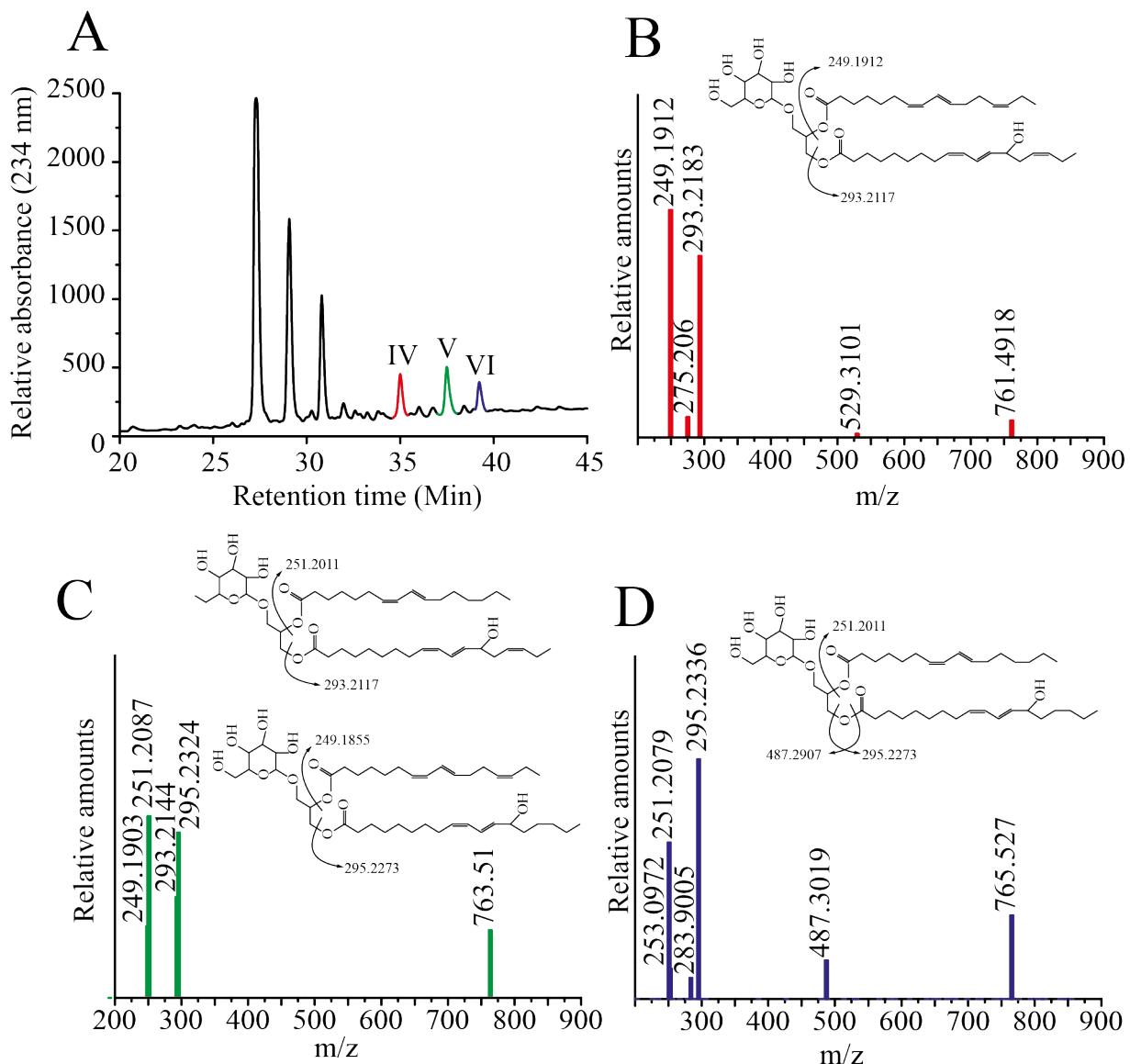
Supplemental Figure 3 Identification of *L. incisa* lipoxygenase (LiLOX) products, derived from *L. incisa* monogalactosyldiacylglycerol species (LiMGDG). LiMGDG was purified from *L. incisa* grown for 2 days in BG11 medium after a total lipid extraction, lipid class separation by solid phase extraction (SPE) and thin layer chromatography (TLC). 20 mM Bis-TRIS propane pH 7.5 with 0.1 % sodium deoxycholate was used as buffer for LiLOX reaction with LiMGDG. Products were reduced by SnCl$_2$, and separated by reversed phase (RP)-HPLC. **A.** RP-HPLC chromatogram of total LiMGDG products catalyzed by LiLOX. The products separated by RP-HPLC (I to VI) were collected and analyzed by LC-MSMS. **B-D.** Fragment spectra of LiMGDG oxidation products for: **B.** 34:6;1-MGDG, **C.** 34:5;1-MGDG and **D.** 34:6;1-MGDG. The LC-MSMS analysis was performed by Dr. Kirstin Feussner. Data shown represent a single experiment.
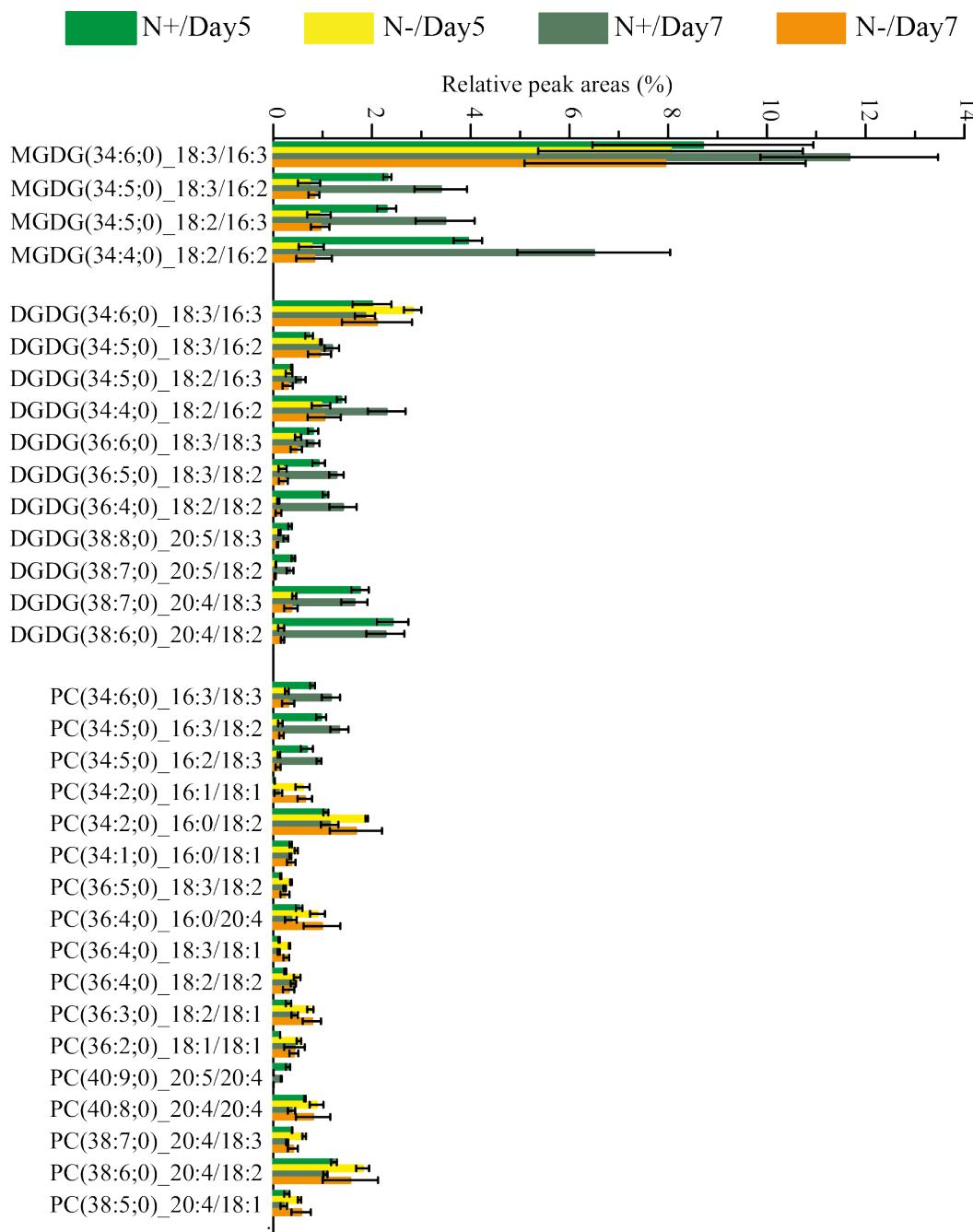
Supplemental figure 4. Analysis of complex lipids of *L. incisa* grown in BG11 medium (N+) and BG11N- medium (N-). After total lipid extraction the lipid species were analyzed by a multiple reaction monitoring (MRM) based LC-MS method. For each molecular lipid specie, the proportion relative to the total lipid measured is shown. Error bars represent the standard error of the mean of three *L. incisa* batches cultivated in parallel in a single experiment. The light and dark green bars represent the relative amount of lipids of the indicated lipid class of *L. incisa* grown for five respective seven days in BG11 medium. The yellow and orange bars represent the relative amount of lipids of the indicated lipid class of *L. incisa* grown for five respective seven days in BG11N- medium. Migalactosyldiacylglycerols (MGDGs), Digalactosyldiacylglycerols (DGDGs), Phosphatidylcholines (PCs). Error bars represent the standard error of the mean of three *L. incisa* batches cultivated in parallel in a single experiment. The LC-MS analysis was performed by Dr. Cornelia Herrfurth.
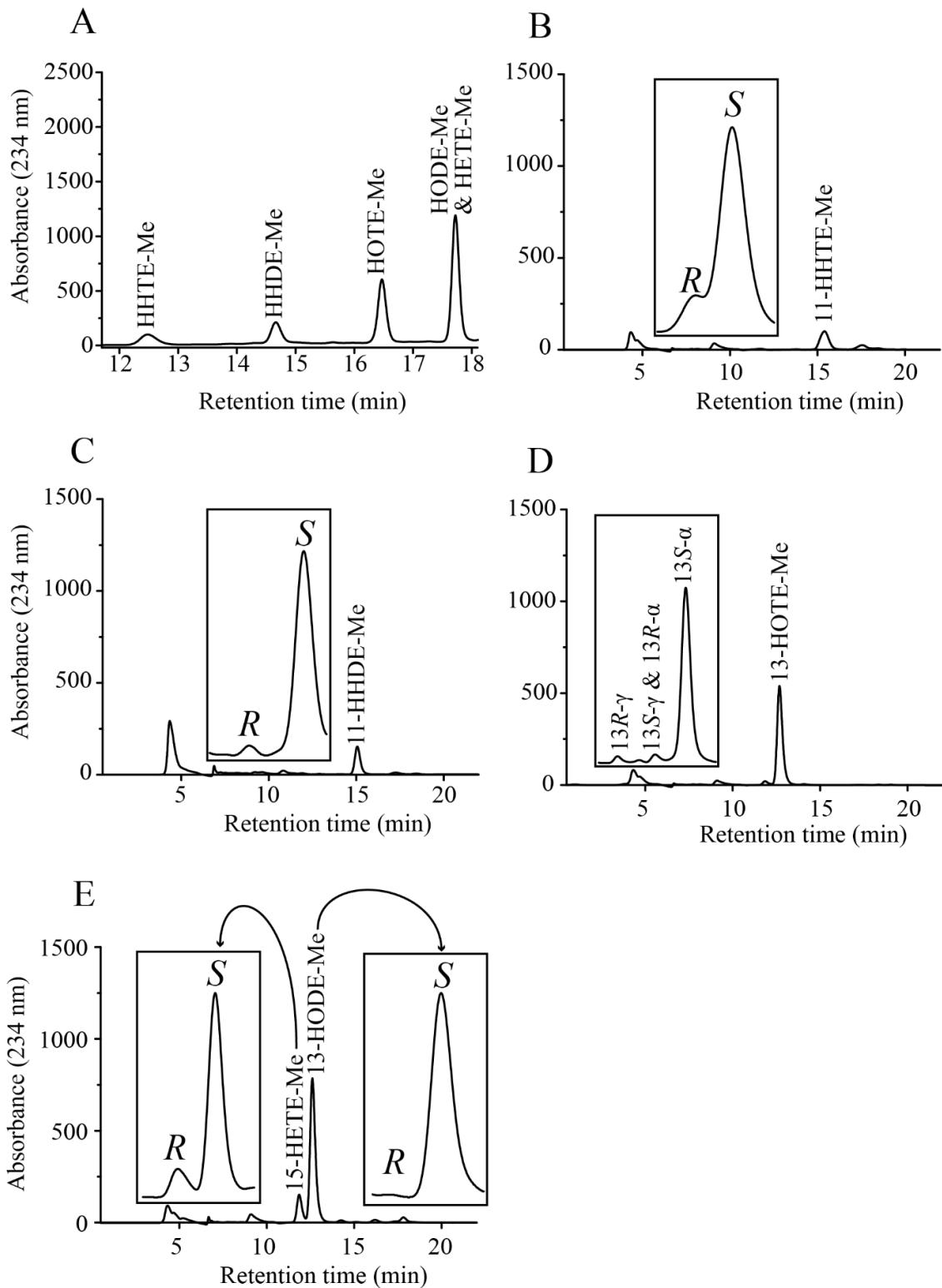
Supplemental figure 5. Identification of Methylester hydroxy fatty acid from *L. incisa* lipoxygenase (LiLOX) products, derived from *L. incisa* digalactosyldiacylglycerol species (LiDGDG). LiDGDG was purified from *L. incisa* grown for 2 days in BG11 medium after a total lipid extraction, lipid class separation by solid phase extraction (SPE) and thin layer chromatography (TLC). 20 mM Bis-TRIS propane pH 7.5 with 0.1 % sodium deoxycholate was used as buffer for LiLOX reaction with LiDGDG. Products were reduced by SnCl$_2$ and transesterified by sodium methoxide before analysis by **A.** Reverse phase (RP) HPLC. **B-E.** Straight phase (SP)-HPLC of each regioisomer. The box represent the CP-HPLC chromatogram for separation of both stereoisomers from a single regioisomer. **B.** All HHTE-Me. **C.** All HHDE-Me. **D.** All HOTE-Me. **E.** All HODE-Me & 15-HETE-Me. Data shown represent a single experiment.
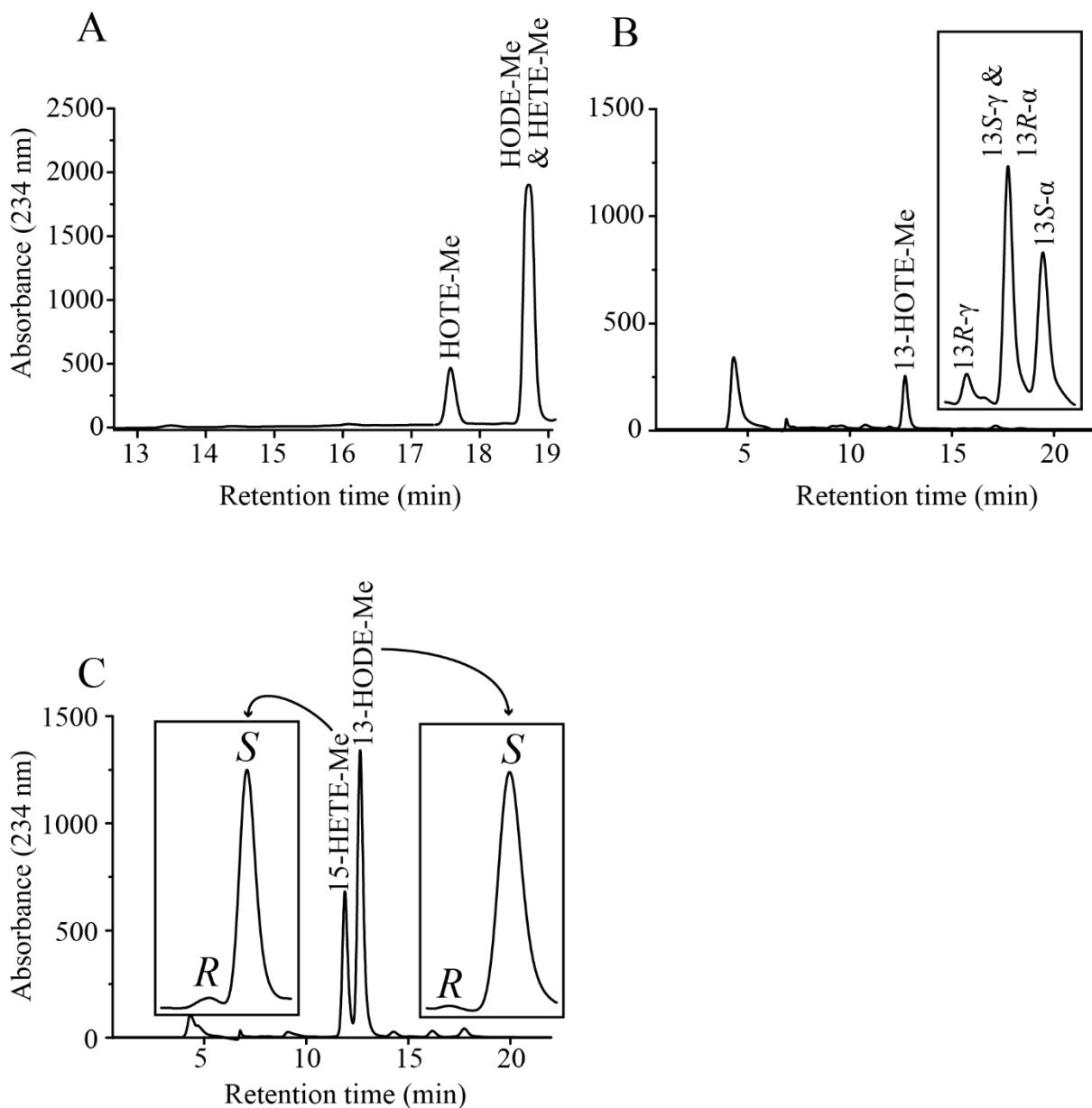
Supplemental figure 6. Identification of Methylester hydroxy fatty acid from *L. incisa* lipoxygenase (LiLOX) products, derived from *L. incisa* phosphadidylcholine species (LiPC). LiPC was purified from *L. incisa* grown for 2 days in BG11 medium after a total lipid extraction, lipid class separation by solid phase extraction (SPE) and thin layer chromatography (TLC). 20 mM Bis-TRIS propane pH 7.5 with 0.1 % sodium deoxycholate was used as buffer for LiLOX reaction with LiPC. Products were reduced by $SnCl_2$ and transesterified by sodium methoxide before analysis by **A.** Reverse phase (RP) HPLC. **B-C.** Straight phase (SP)-HPLC of each regioisomer. The box represent the CP-HPLC chromatogram for separation of both stereoisomers from a single regioisomer. **B.** All HOTE-Me. **C.** All HODE-Me & 15-HETE-Me. Data shown represent a single experiment.
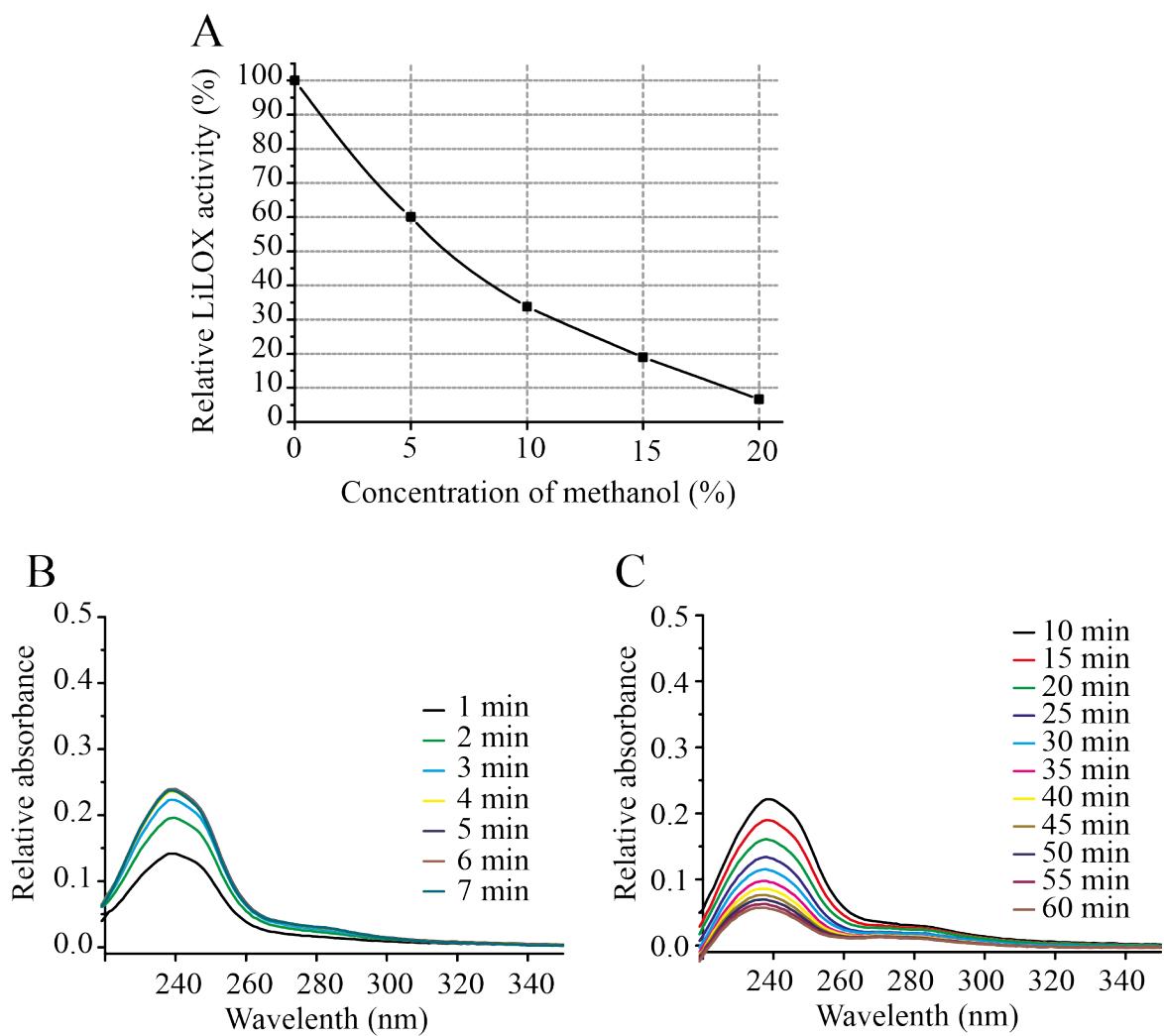
Supplemental Figure 7. Influence of methanol on the catalytic activity of LiLOX. 20 mM Bis-TRIS propane pH 7.5 was used as buffer, with different concentration of methanol (v/v). The FFA 18:2 (n-6) and LiMGDG derived from *L. incisa* were used as substrates. **A.** Spectroscopic assay measuring the initial reaction rate of LiLOX with 100 μM 18:2 (n-6) in presence of increasing concentrations of methanol (5 %, 10 %, 15 %, 20 %; v/v). **B.** LiLOX reaction with LiMGDG in presence of 10% (v/v) methanol (0 to 7 min). **C.** LiLOX reaction with LiMGDG in presence of 10 % (v/v) methanol (10 to 60 min). The baseline level is established after addition of LiLOX. All reactions were detected as changes in absorbance at 30 °C. Data shown represent a single experiment.
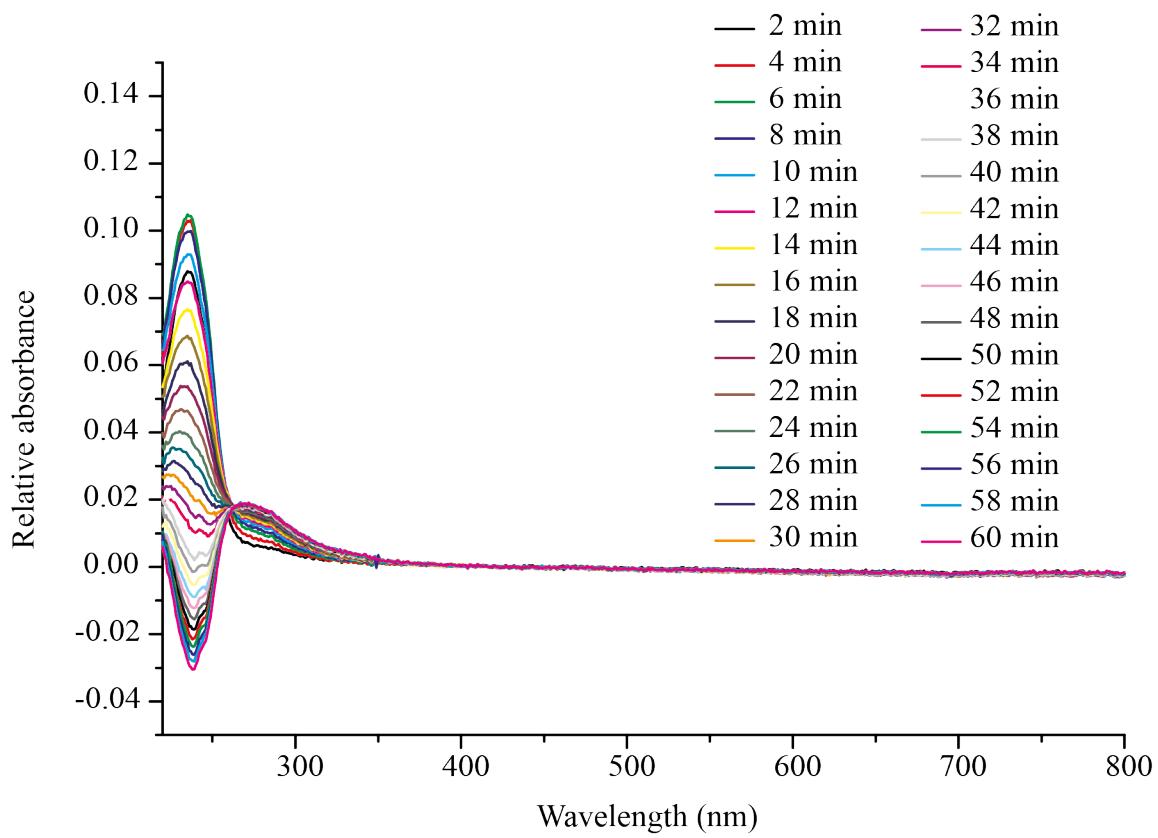
Supplemental Figure 8. Time course of *L. incisa* lipoxygenase (LiLOX) catalysis for monogalactosyldiacylglycerols from *L. incisa* (LiMGDG). LiMGDG was purified from *L. incisa* grown for 2 days in BG11 medium. After a total lipid extraction, lipid class separation by solid phase extraction (SPE) and thin layer chromatography (TLC). 20 mM Bis-TRIS propane pH 7.5 with 0.1 % sodium deoxycholate was used as buffer for LiLOX reaction with 100μM LiMGDG. The baseline level is established after addition of LiLOX. Data shown represent a single experiment.

```
                                            685        690        695
                                             |          |          |
 1. L. incisa LOX (13S)            L N V N S N A R Q Q L I N A G
 2. A. thaliana LOX2 (13S)         M E I N A R A R Q S L V N G G
 3. A. thaliana LOX3 (13S)         L E I N A L A R Q S L I S A D
 4. A. thaliana LOX4 (13S)         L E I N A V A R Q T L I S A D
 5. A. thaliana LOX6 (13S)         L E I N A R A R K S L I N G G
 6. O. sativa LOX (13S)            M E I N A L A R E S L I N A D
 7. O. sativa LOX2 (13S)           M E I N A Q A R G M L I N A N
 8. S. tuberosum LOX (13S)         M E I N A L A R E A L I N A N
 9. S. tuberosum LOX2 (13S)        L E I N G L A R Q S L I N A D
10. G. max LOX1 (13S)              M N I N A L A R Q S L I N A N
11. P. aeruginosa LOX (15S)        L F I N E G A A R I L L P S A
12. C. reinhardtii (13S)           L N I N R N A R A S L I N A G
13. N. punctiforme LOX1 (9R)       I F I N S S A V P K I I G S T
14. Cyanothece LOX1 (9R)           I N I N R R G D D L L V E P N
15. F. oxysporum LOX (13S)         L A L N D A A R K L L V P L V
16. G. graminis Mn-LOX (13R)       Y A I R P V G G A V L F N P G
17. M. oryzae Mn-LOX (9R)          Y A V R P L G E R V L F N K G
18. P. patens LOX1 (13S)           L E I N R Q A R A T L I A A G
19. P. patens LOX2 (13S)           L E I N R Q A R A T L I A A G
20. P. patens LOX7 (13S)           M E I N A A A R Q N L I A A G
21. G. max LOX4 (13S)              M N I N S L A R K A L V N A D
22. G. max LOX3 (9/13S)            M N I N G L A R L S L V N D G
23. G. max LOX2 (9/13S)            M N I N A L A R Q S L I N A D
24. A. thaliana LOX5 (9S)          M N I N A L A R H V L I N S D
25. A. thaliana LOX1 (9S)          M N I N A L A R Q I L I N G G
26. S. tuberosum LOX (9S)          M N I N A M A R Q I L I N A G
27. P. patens LOX5 (13S)           L D I N A A A R K A L I N A G
28. P. patens LOX6 (13S)           M D I N G A A R K A L I N A G
29. P. patens LOX3 (13S)           M D I N Q A A R K S L I N A G
30. P. patens LOX4 (13S)           M D I N Q S A R K S L I C A Q
31. G. fruticosa LOX (11R)         M A I N T L G R N D L I P T G
32. P. homomalla LOX (8R)          L A I D T I G R K E L I G S G
33. H. sapiens LOX (12S)           M E I N T R A R T Q L I S D G
34. H. sapiens LOX (15S)           L E I N V R A R T G L V S D M
35. H. sapiens LOX (5S)            I A I N T K A R E Q L I C E C
36. H. sapiens LOX2 (15S)          L H I N T L A R E L L I V P G
37. H. sapiens LOX (12R)           V Q I N S I G R A V L L N E G
38. Cyanothece LOX2 (9R/11R)       L A I N E L A R E Q L I S A G
39. N. punctiforme LOX2 (13S)      L A I N D A A Q R I L I A P G
40. B. thailandensis (13S)         L Y I N E L A A L T L L P P L
```

Supplemental figure 9. Alignment of amino acid residues from the arched helix in 40 LOXs, performed by the software Geneious, using Muscle alignment with the default parameters.

MELGLGARQAVLQPAAASRAPLGLLKAGHRAQQRRLPSVPSVSASASVTQGIPQT
SFLQKARDSVLPHGAPFTPTSKDSVQWTTTIYTTQLLRPEIHDLGFVEVLLASED
KEAVSERMTLKGFSRKPWTNLDGVPKWGAIFTGTLMLPAAMAKPAVMFININHPP
EGVQYFFANKIALDGPPGKTAHVDFVINSHVDSGPDAPRPFFTAQAYLPHAPMPD
YLAELREHELAILRGTAAAAKHERKGSERIYDYDVYNDLGTPTRSRPALGGDTLK
YPRRLRTGRRVVNGTEVAAKGKDWLPPDERFDDRKQENFDSRTLLATLPALSANL
LAALVPAGLQKLLRTPGSEFMSISDIEQLYSGNAAEDNEDNVLTNLVAPAAAPLA
AILGLLTQNSAQGNTPQKVFEQLSDFNKEVVNGALDALVVSLDDLGQSQRAAILH
ALSLTEKDFQEYAQAGTGRHEVHPVHANFVNLLQEVLHRLLHFSTPAVIREGREG
AWTTDEEWGREQLAGQNACMIHAIWNDAPIKDLPADSAITEAVLQGHLEGHSISQ
LLSGDKPRLFLIDYMKGFKDYAEKIAAAHPGNVMYAGRAVLYLRTDGELVPVAIE
LQAPRRKLEAFTSADSPTIWLLAKCIFSSIDAGYHQLISHFVRAHACTEPYIIAT
RRQLSVMHPVFKLLITHCRFTLNVNSNARQQLINAGGIIEGNFTPGRYAMELSSV
VYGLTWTFDSQALPHDLVNRGVARREKDGTLKLLMADYPYAADGLLVWDAFVEWF
DSYLRLYYDDEVDGKRVTDDPEITAWWTEIQEKGHPDIKEGWPQLQTIADLTQIL
TTIAWIASAHHAAINYGQYDYSGFMPNRSPMIRKAMPPKESDDFKTLAAQDAETA
ILPFLASPLQATQVMATLGLLSTHSENEEYINDLEHPYLMVGTEAYNKYKEFLSR
LKQAEDTIKKRNADSQGHVIRAGPDAIHYRLMNPSSITENGDVQRQGVTMSGIPT
SVSM

Supplemental Figure 10. LiLOX amino acid sequence. The parts highlighted in red represent the peptides found in the proteomics data, performed by Dr. Heike Siegler. The part highlighted in green represent the putative signal peptide, predicted using the server ChloroP1.1 (Emanuelsson *et al.*, 1999). Data shown represent a single experiment.
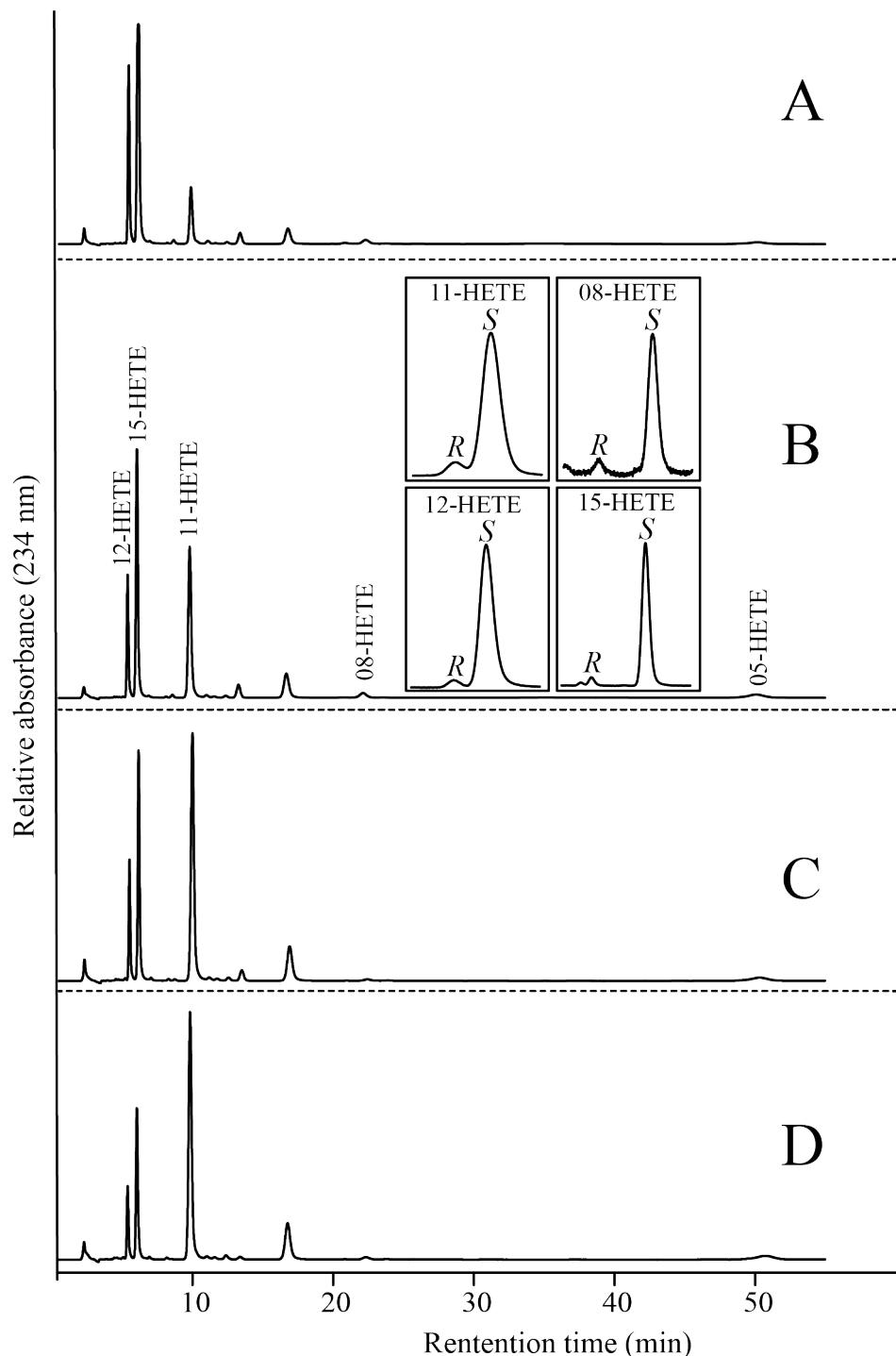
Supplemental Figure 11. Comparison of 20:4 (n-6) oxidation products of LiLOX N702T/F703V mutant at different pH. **A-D.** Regioisomers separated by SP-HPLC in n-hexanes:isopropanol:TFA 100:1:0.1 (v/v/v). 20 mM Bis-TRIS propane was used as buffer with 100 μM of 20:4 (n-6). Reaction happened at pH **A.** 8.0. **B.** 7.5. **C.** 7.0. **D.** 6.5. Chromatograms of CP-HPLC in n-hexanes:isopropanol:TFA 100:2:0.1 (v/v/v) is given for all 4 HETEs obtained after reaction at pH7.5 in each corresponding box.

Affidavit

I hereby declare that I wrote this dissertation on my own and with no other sources and aids than quoted.

Benjamin Djian

Göttingen, April 2017

Curriculum vitae

Name	Djian Benjamin
Date of birth	22.11.1989
Place of birth	Marseille
Nationality	French

Scientific education

Since 08/2013   PhD thesis entitled "Fatty acid oxidizing enzymes in *Lobosphaera incisa*" in the department of plant biochemistry, Georg-August-University, Goettingen, Germany. Under supervision of Prof. Dr. Ivo Feussner within the Program Biometals of the IRTG1422.

09/2011 – 06/2012   Master Thesis entitled "Planarian *Dugesia japonica*: A new model to study host-pathogen interactions" in the department URMITE, Faculté de Médecine, Marseille, France. Under supervision of Dr. Eric Ghigo

2012   Master of Science (M. Sc.) with honors, *Transmissible Disease and Tropical Pathology*, Aix-Marseille Université, Marseille, France

2010   Bachelor of Science (B. Sc.) with honors, *Physiology and Gene Biology*, Aix-Marseille Université, Marseille, France

2007   Higher education entrance qualification (Baccalauréat) with honors, Lycée Marie Curie, Marseille, France

Research internships

06/2015 – 07/2015   Internship at the Vanderbilt University School of Medicine, Nashville, USA, in the Department of Pharmacology, under supervision of Prof. Dr. Allan Brash

05/2009   Internship at the Aix-Marseille Université, in the center of research for neurobiology and neurophysiology, under supervision of Dr. Catherine Faivre Sarrailh

05/2008   Internship at the Aix-Marseille Université in the institute of biology and chemistry of proteins, under supervision of Dr. Christophe Grangeasse

Participation in summer schools and conferences

08/2015   Final Symposium of the IRTG1422 (Göttingen, Germany)

05/2014   Symposium Trends in Inorganic Chemistry (Lund, Sweden)

ACKNOWLEDGEMENTS

First I would like to thank Prof. Dr. Ivo Feussner for giving me the opportunity to work on this project. I am particularly grateful for the trust that he had in me throughout my stay in the department. Besides the trust, he always took the time to support, bring ideas to the project, and discuss it when it was needed.

Dr. Ellen Hornung is a person that I will never thank enough. Her scientific help in the lab was precious on so many aspects. Inputs that she gave me were determinant, and she was very helpful with the correction of this thesis. She is such an essential member of the atmosphere in the lab that I cannot imagine a team spirit without her cakes and her good mood.

I am very grateful to Dr. Kirsten Feussner as well. Her scientific help in general, and with the lipidomics analysis in particular were primordial. She gave me precious help in the correction of this thesis, and her moral supported during the writing process was crucial.

I am very thankful to Dr. Julia Newie who initiated me to the protein purification and Lipoxygenases. Her professionalism was very inspiring for me throughout this work, and I know it will be in my future ambitions. Dr. Steffen Kawelke taught me a lot about protein purifications as well. He left a year after I arrived in the department, and he was missed ever since. I would like to acknowledge him in his own words: "*Scientific discussions with him were and still are fruitful, as well as our everyday conversations about other important topics*". PS: Kölle alaaf! Dr. Dan Yu is the 3rd member of the *First Floor Hard Workers*. You have the perfect ratio between cuteness and craziness, please never change that.

I want to thank Dr. Heike Siegler, for initiating me to the joys of Microalgae, and to *L. incisa* in particular. Thank you for your great moral support and your patience, even during my moments of stress. Many thanks Dr. Till Ischebeck for the great discussion we had, scientific or not. I know you enjoyed my company even though I'm a Franzecke. Too bad you have such bad music tastes otherwise we could have enjoyed more concerts and festivals together. I thank Dr. Florian Brodhun for his guidance on general biochemistry and enzymology in particular.

Ich möchte Sabine Freitag auf Deutsch danken. Vielen Dank für alles, Sabine! Du bist so wunderbar, du bist ein Traum! PS: Liebe Grüße an Zündi von mir!

I would like to thank all the members of the department of plant Biochemistry who were involved in team building, and made of this lab so much more than just the place we come to

work. You were definitely more than coworkers, you became friends and I am extremely grateful for that!

I am also grateful to all the flatmates I lived with: Jule, Paula, and Tabea, thank you for supporting me, despite my panics and some of my bad habits.

Merci à Julia, Antoine et Shama. Vous avoir rencontrés fait partie des meilleures choses qui me soient arrivées à Göttingen. Julia et Antoine, merci pour toutes les soirées/journées qu'on a passées ensemble à jouer et/ou à papoter. Shama, merci d'être une amie géniale, et la meilleur coloc' du monde ! Merci à Jasmin de m'avoir soutenu moralement dans cette aventure. Je sais que tu finiras la tienne avec brio ! Paul et Boris n'habitent pas à Göttingen, mais le soutien des Bobs dépasse les frontières !

Merci Papa, merci Maman, vous êtes des parents formidables et je vous remercie de m'avoir soutenu tous au long de mes études. Vous avez toujours été à l'écoute avec un esprit très ouvert, si ces qualités sont essentielles pour être de bons parents, elles font de vous des belles personnes avant tout. Bien sûr je remercie aussi le reste de ma famille, en particulier Bastien et Jacqueline (pour une fois qu'elle n'a pas à corriger mon mémoire). Mais aussi tous ceux qui m'ont soutenu au long de ces trois ans.